CR 132267

BARNES ENGINEERING COMPANY
30 COMMERCE ROAD
STAMFORD, CONNECTICUT

ACCURATE, RELIABLE PROTOTYPE EARTH HORIZON SENSOR HEAD

SUBMITTED TO NASA LANGLEY RESEARCH CENTER

CONTRACT NASI-10952

DATE OF REPORT: May 1973

PREPARED BY:

Frank Schwarz
FRANK SCHWARZ

Hyman Cohen
HYMAN COHEN

TABLE OF CONTENTS

LIST OF ILLUSTRATIONS

1. INTRODUCTION

This engineering report describes the design and performance of an Accurate and Reliable Prototype Earth Sensor Head (ARPESH) recently completed and evaluated by BEC under contract from NASA Langley Research Center. Fig. 1-1, 1-2 and 1-3 are photographs of the sensor. The ARPESH employs a detection logic "locator" concept and horizon sensor mechanization developed by NASA/LRC personnel which is believed will lead to high accuracy horizon sensing that is minimally degraded by spatial or temporal variations in sensing attitude from a satellite in orbit around the earth at altitudes in the 500Km environ [1,2]. An accuracy of horizon location to within 0.7Km has been predicted, independent of meteorological conditions. This corresponds to an error of 0.015° at 500Km altitude. Laboratory evaluation of the sensor indicates that this accuracy is achieved. We will first describe the basic operating principles of ARPESH, next present detailed design and construction data and then report on performance of the sensor under laboratory conditions in which the sensor is installed in a simulator that permits it to scan over a blackbody source against background representing the earth space interface for various equivalent planet temperatures. The ARPESH sensor will be known as Model 13-311.

2.1 PRINCIPLE OF OPERATION OF ARPESH

The principle of the ARPESH locator technique is illustrated in Figure 2-1. Two radiometric fields of view (A and B) filtered to the 14 - 16μ CO_2 absorption band are caused to scan linearly across

1. TN D-6616, Conceptual Design and Analysis of an Infrared Horizon Sensor with Compensation for Atmospheric Variability by Antony Jalink, Jr., Richard E. Davis, & John A. Dodgen
2. Patent #3,714,432, Infrared Horizon Locator By Antony Jalink, Jr.

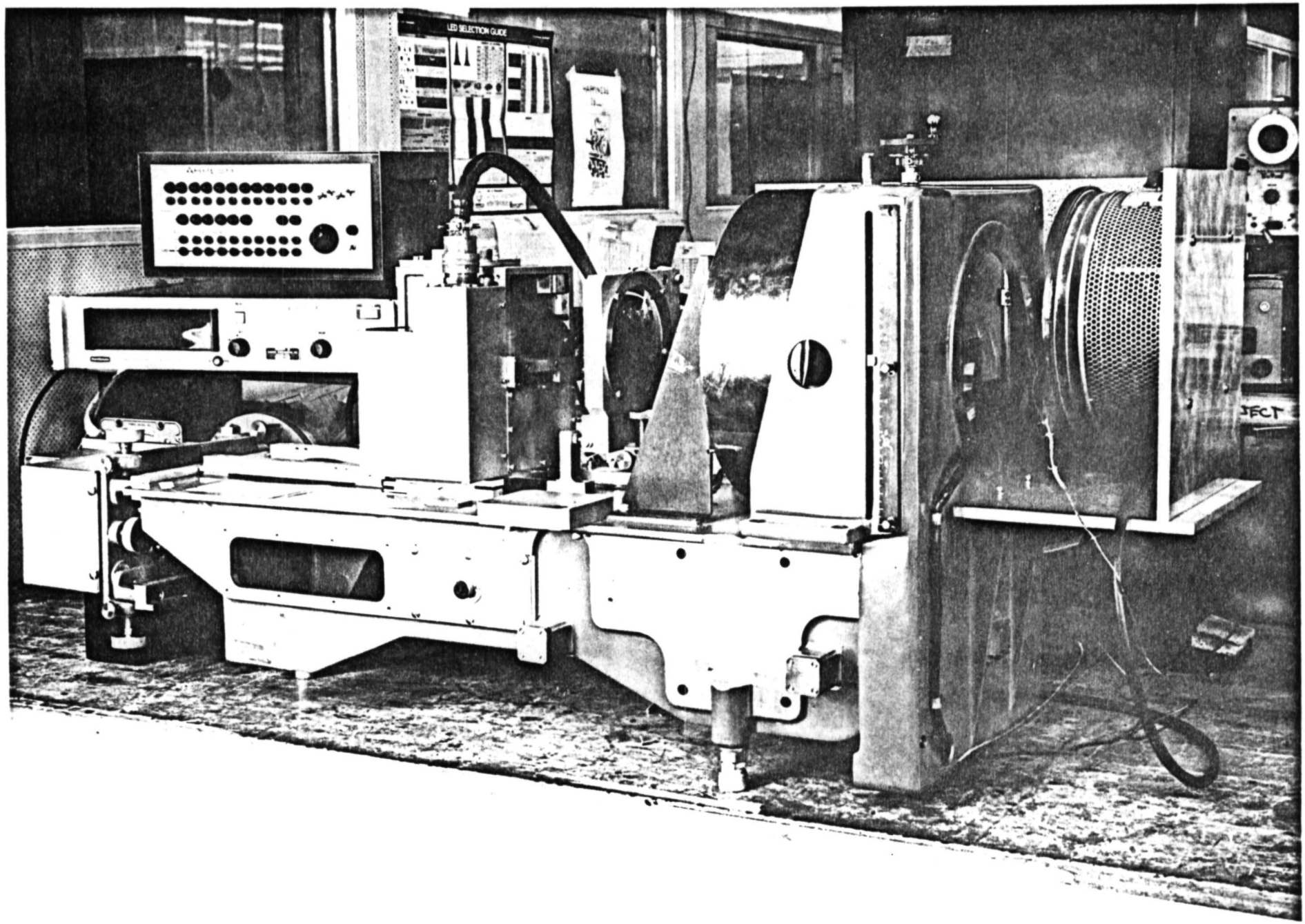

FIG. 1-1 ARPESH Sensor Head, Front View, with Auxiliary Unit, in Test Set-up

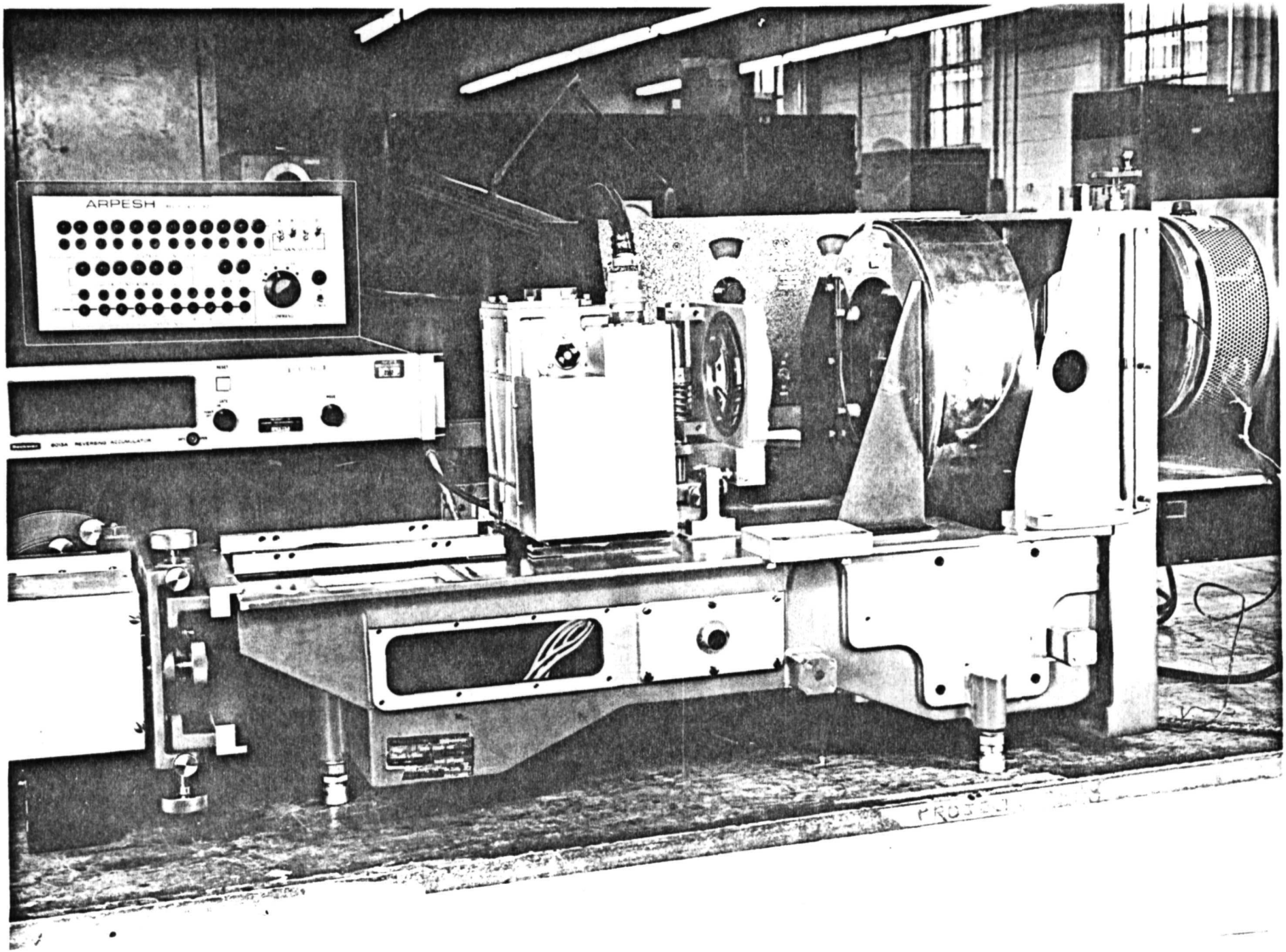

FIG.1-2 ARPESH Sensor Head, Rear View, with Auxiliary Unit, in Test Set-up

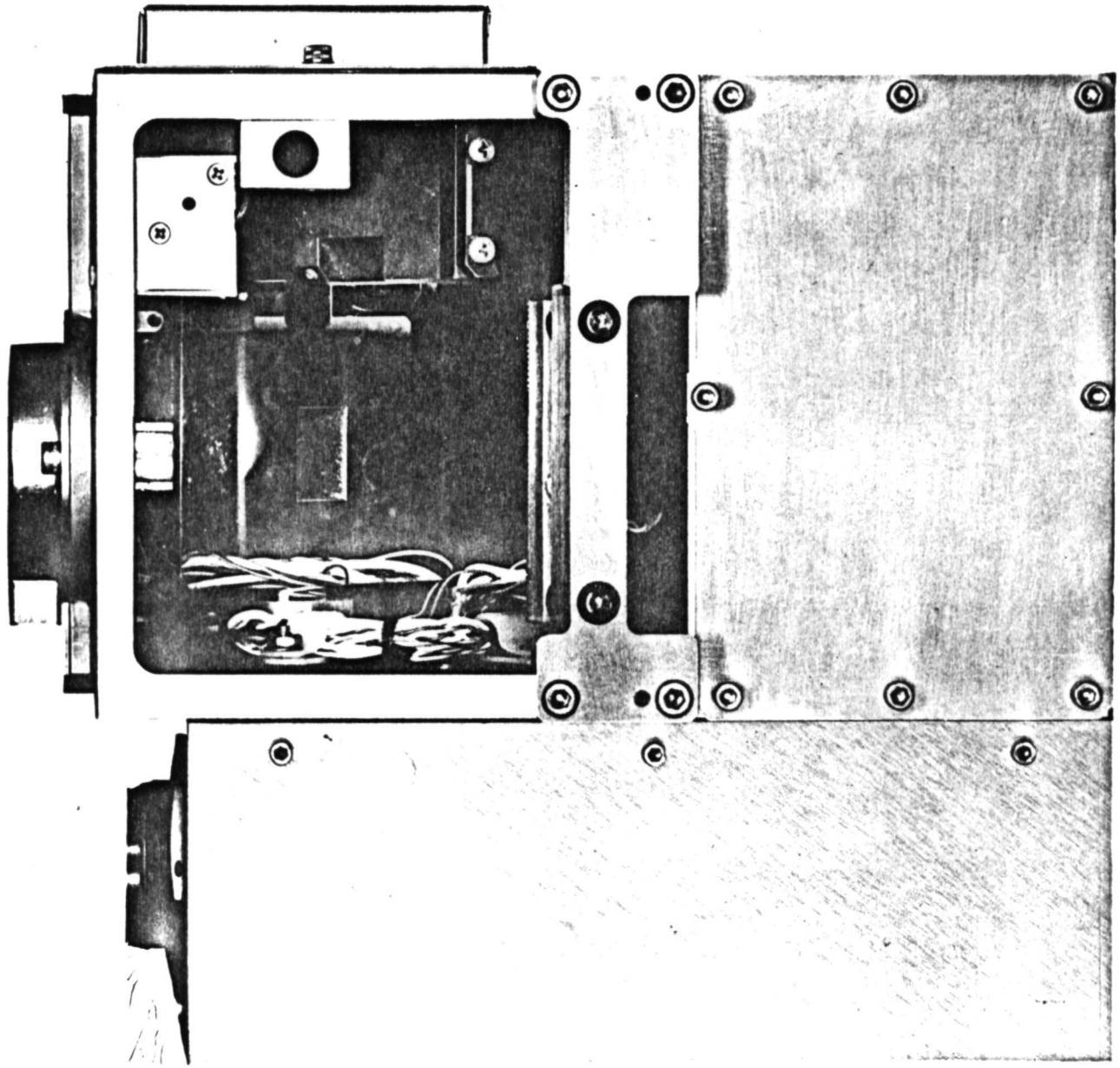

FIG. 1-3 ARPESH Sensor Head, Front View

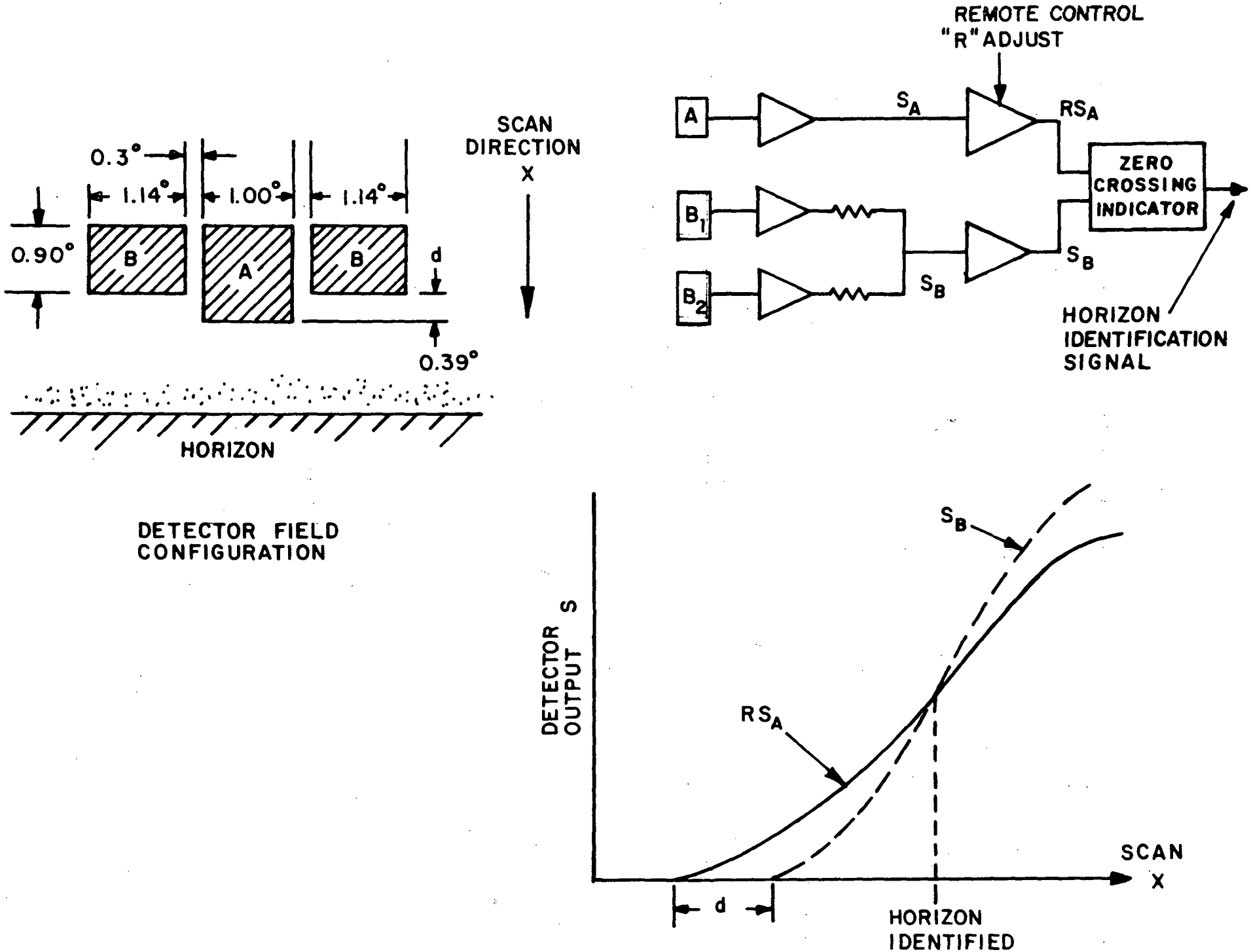

FIG. 2-1 ARPESH Locator Technique

the horizon. The two fields are displaced in the direction of the scan by a small amount "d" such that field A is leading B. The B field is divided into two equal elements located on each side of the A field in order to compensate for horizontal gradients or cross-coupling from the other axis. Separate detectors are used for the two B elements but they are electrically added and subsequently treated as a single output.

As the two fields scan into the horizon profile, they produce signals, S_A and S_B which are the integrals of the profile radiance with respect to altitude. Actually, they only integrate up to the point where the trailing edge of the detector fields of view reach the beginning of the profile, but the horizon identification takes place well before this so the signals can be considered true integrals in the region of interest. If the detector responsivities and amplifier gains of the two channels are equal, the signals will be identical, but S_B will lag S_A in time because of the physical displacement "d" of the two fields, and at any given time S_B will always be less than S_A. However, if the A channel is attenuated by a factor R with respect to the B channel, S_B will gradually catch up and eventually become greater than S_A. This crossover point identifies the horizon and is sensed by a comparator circuit. The gain ratio "R" determines the crossover point and is remotely adjustable.

The significance of this processing is that with the proper field displacement "d" and gain ratio R, this crossover point is always a constant altitude above the true "hard horizon" independently of climatic conditions to within 0.7Km. The parameter "d" is actually an angular displacement of the two fields in the sensor, which corresponds to a fixed altitude above the horizon,

and therefore is dependent upon the satellite altitude. However, it has been found that adjusting the gain ratio R instead of "d" compensates for altitude equally well and is much easier to implement remotely.

2.2 DESCRIPTION OF ARPESH SENSOR

The complete system is comprised of three or more sensor heads, each of which continuously scans the horizon and determines the angle between the located horizon and a spacecraft (or sensor) reference axis. Each sensor head contains two subsystems:

1. The radiometric and locator subsystem
2. The scanner and angle readout subsystem

These two subsystems are relatively independent of each other and will be described in the following sections.

2.2.1 THE RADIOMETRIC AND LOCATOR SUBSYSTEM

A folded reflecting telescope employing a 48 mm X 56 mm rectangular 15.24 cm F.L. spherical objective mirror, images the horizon field onto a field mask containing three rectangular apertures having the angular dimensions shown in Figure 2-1. This field mask defines the A and B fields mentioned previously.

Three identical germanium immersed thermistor bolometers are mounted just behind the field mask, one viewing through each of the apertures. The immersion lenses are hyper-hemispheres with the sides ground flat so that they can be stacked closely together such that each collects all the energy passing through its respective field mask. These immersion lenses act as field lenses and image the common entrance aperture of the system onto the thermistor elements, which are 0.5 X 0.5 mm square. The entire detector assembly is thermostated at 10°C, when ambient falls

below this value, to reduce the range of detector temperature variations. An optical bandpass filter transmitting between 14 and 16 microns is located just in front of the field mask. The detector-field mask arrangement is illustrated in Figure 2.2 and the entire radiometric optical system is seen in the layout drawing of the sensor head (Figure 2-3).

This IR telescope is directed into a plane scanning mirror which causes its field to linearly scan across the horizon. Each detector has its own preamplifier with gain adjustment to compensate for differences in detector responsivity. The outer pair of detectors comprise the B field, and their signals are added after preamplification. The remainder of the radiometric and locator processing is shown schematically in Figure 2-4. The final output of this subsystem is a signal commanding readout of the scanning mirror position at the time when the horizon crossing is identified by means of the locator logic described previously.

2.2.2 SCANNING AND POSITION READOUT SUBSYSTEM

The field of the radiometric telescope is caused to scan through a 7-1/2° angle with a quick return at a rate of one scan per second by means of the plane scanning mirror. This requires that the plane mirror scan 3.75°. In addition, the scan mirror can be driven on command through a reverse angle of 8° from the scan start position which directs the radiometer field onto a temperature monitored plate for detector calibration purposes. The scanning mirror is mounted on flexural pivots and driven by an intergral torquer which eliminates all the lubrication and wear problems that are associated with ball bearings and gears. Because of the small scan angle and low speed, the flexural pivots have a very long life and negligible hysteresis. The linearity of the scan is maintained by a tachometer mounted on the same shaft as the

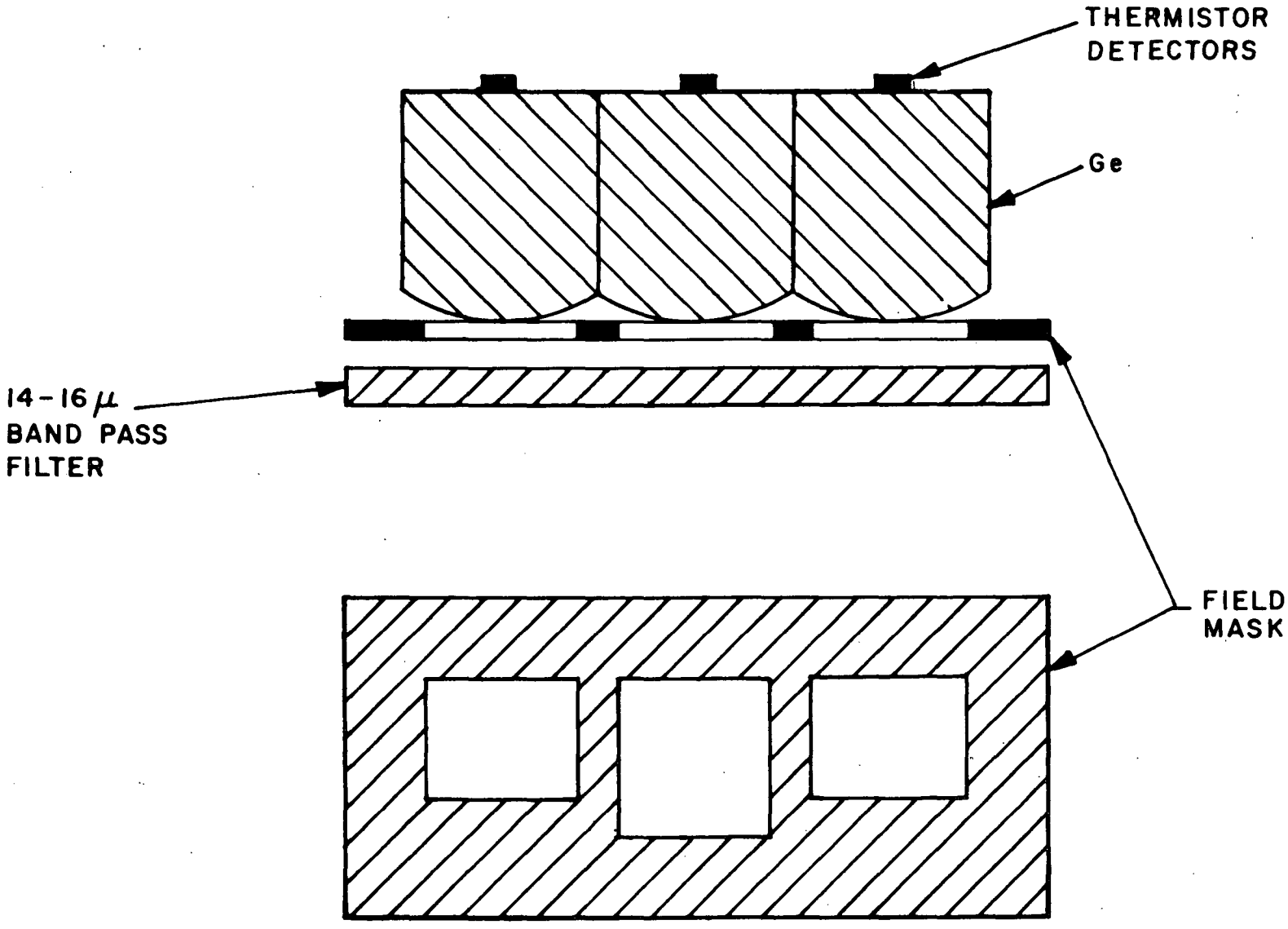

FIG. 2-2 Detector - Field Mask Configuration

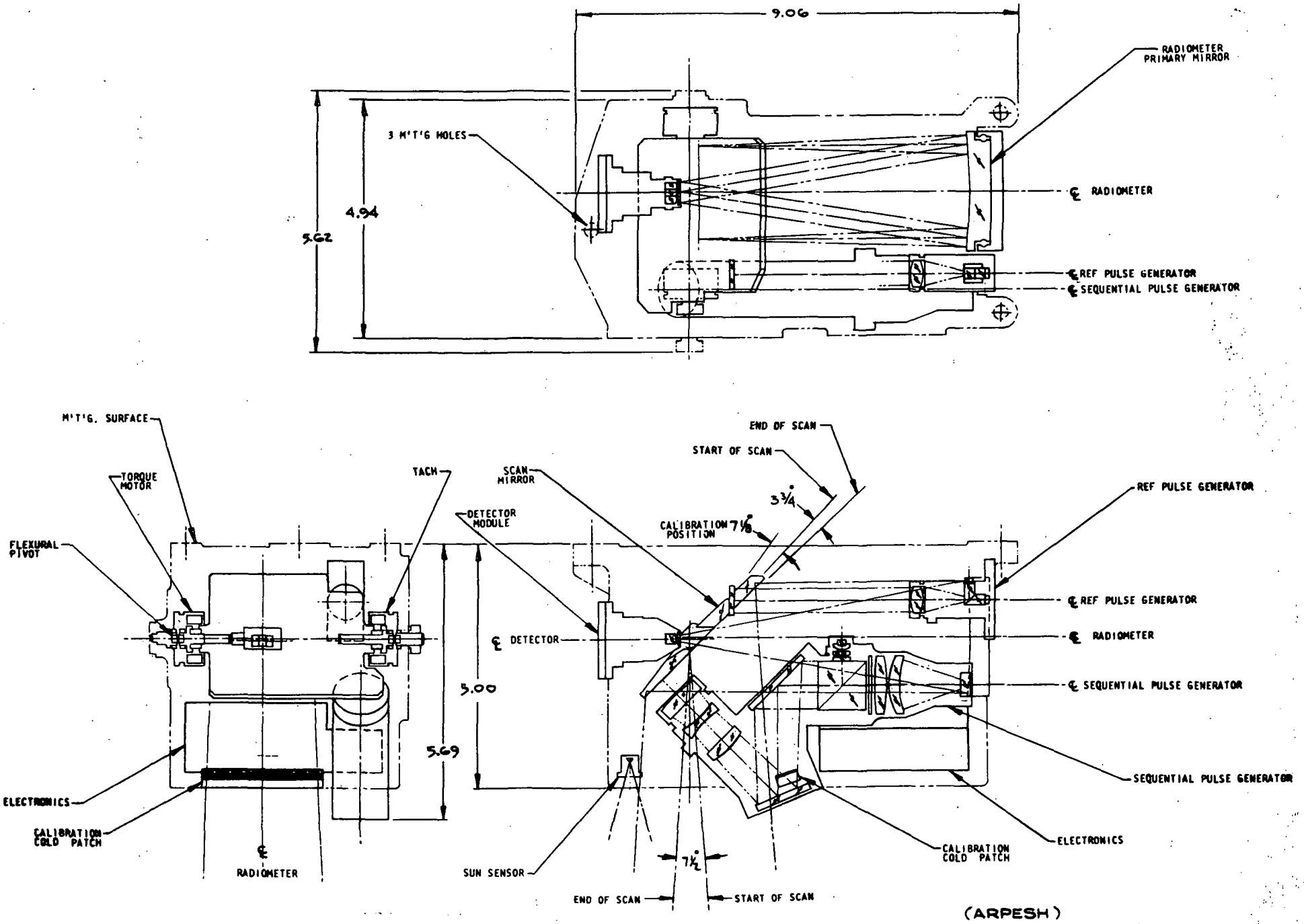

(ARPESH)
HORIZON SENSOR

FIGURE 2.3

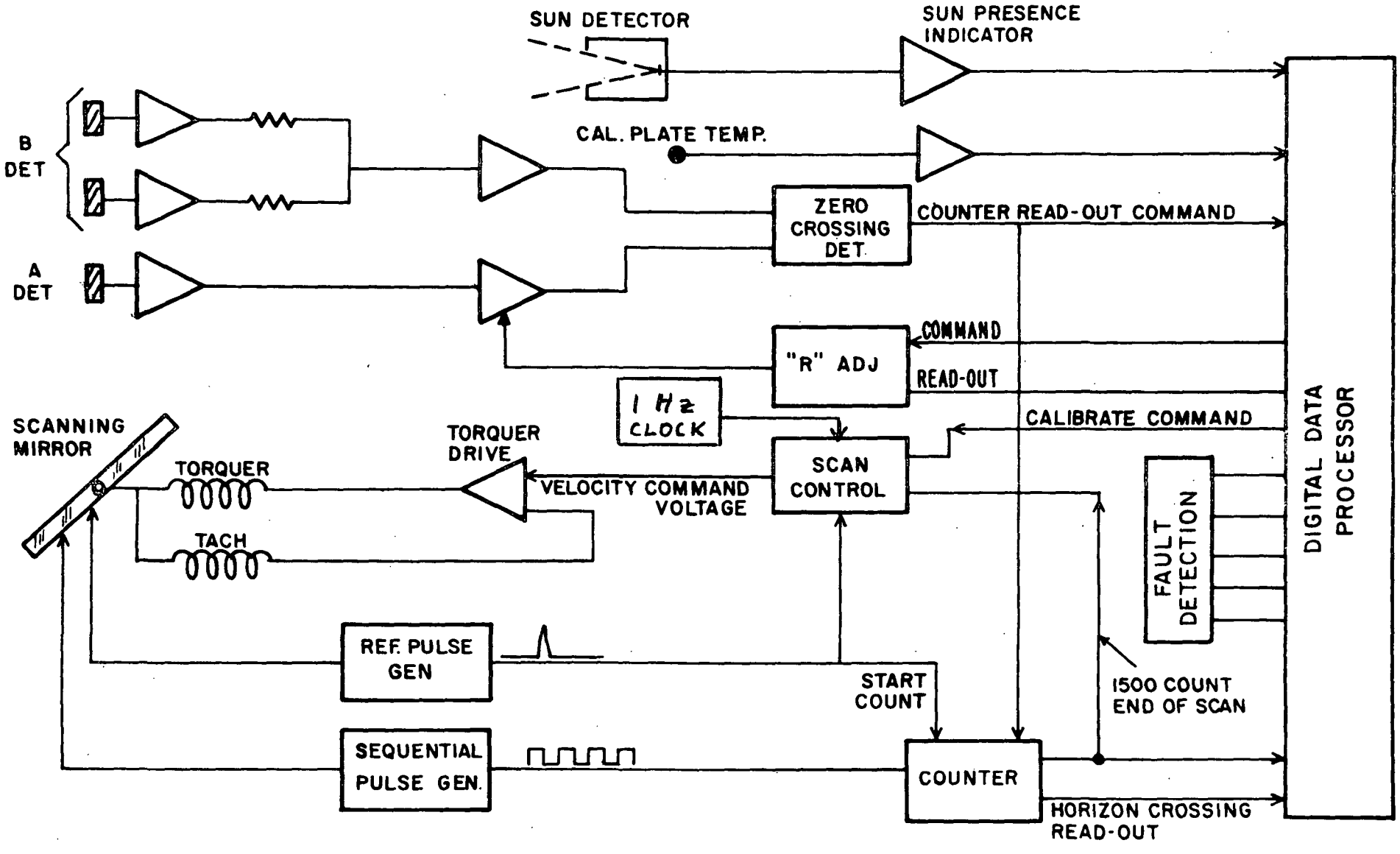

Figure 2.4 ARPESH SYSTEM BLOCK DIAGRAM

scanning mirror and used to control the torquer in a velocity servo circuit.

In order to benefit from the accuracy of this sophisticated horizon locator technique, it is necessary to determine the angular position of the scan mirror with respect to a sensor reference frame at the time of the read-out command from the locator logic, to an accuracy of better than 0.01°. This is done by means of two separate electro-optical sensors, one produces a reference or fiducial pulse at the start of the scan and the second produces a sequence of pulses, one for each 0.005° motion of the scanning mirror. The angular position of the horizon with respect to the reference axis is then determined by counting the number of pulses put out by the sequence pulse generator between the time of the reference pulse and the command signal from the locator logic.

Both of these position signals are obtained by reflecting light beams from a small auxiliary mirror attached to the plane scanning mirror. In the case of the sequential pulse generator, the collimated image of a very finely spaced Ronchi grating is reflected from the scanning mirror and then reimaged onto a similar, although longer, grating in the receiver. As the image of the reflected grating passes over the receiver grating, a series of pulses is generated, one for every movement of one line pair of the grating. The optical arrangement is shown in Figure 2-5. The gratings have a spatial frequency of 1000 lines and spaces per inch. Since the pulse is generated from the total signal from many grating lines, any slight irregularities in line spacings are averaged out.

The reference pulse generator is similar, except, instead of gratings a single line reticle is used. The light sources for

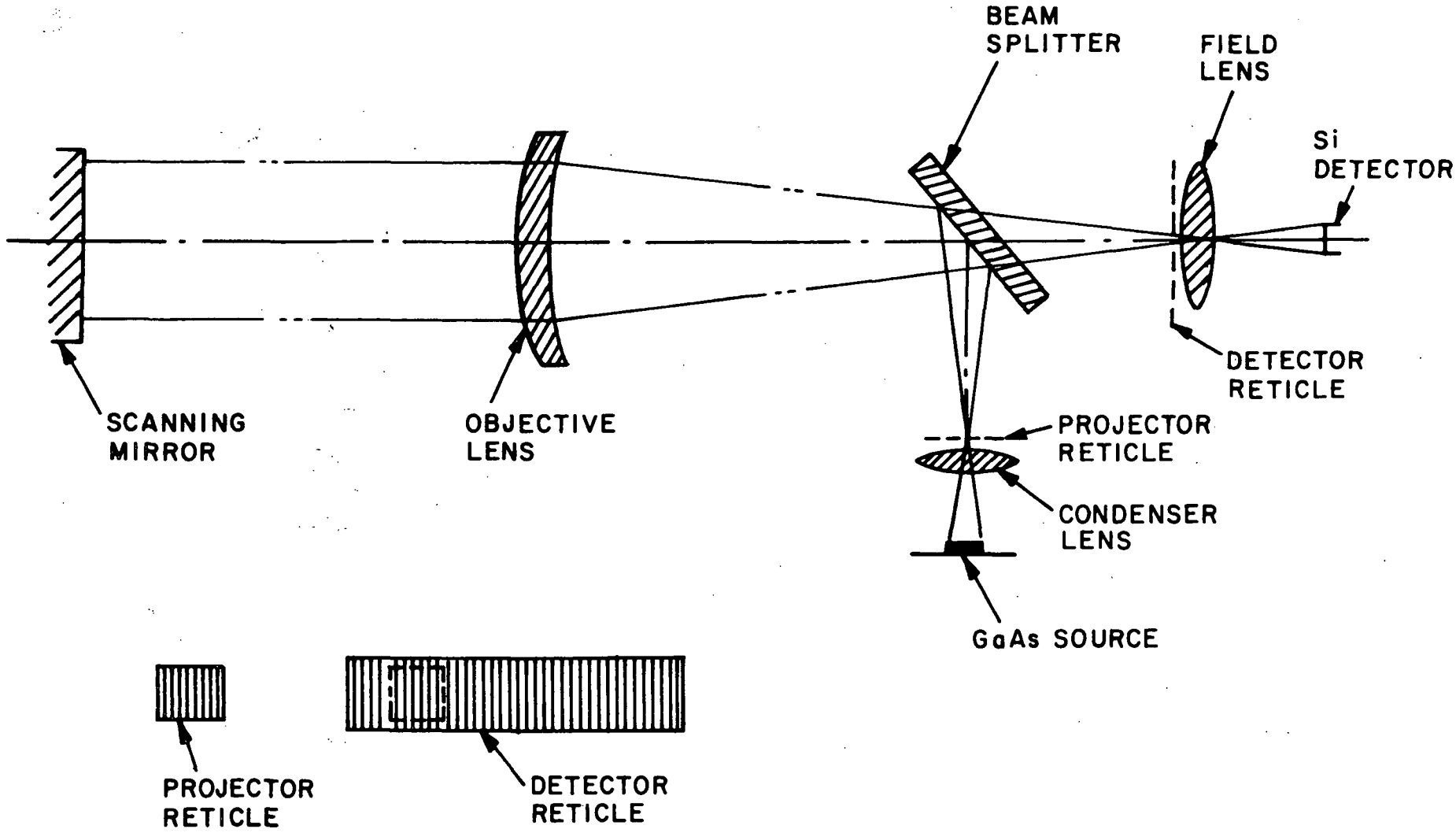

Figure 2.5 SEQUENTIAL PULSE GENERATOR

both systems are Light Emitting Diodes (LED) and the receivers use silicon detectors.

An advantage of this position readout system is that it eliminates all errors from non-linearities in the scan or drifts in the start position of the scan which could be caused by hysteresis in the flexural pivots.

2.3 OVERALL SYSTEM OPERATION

A block diagram of the ARPESH system is shown in Figure 2-4. A 1Hz clock establishes the time base of the system and causes the servo system and scanning mirror to start its forward scan. The scanning mirror executes the forward scan in 0.75 seconds. Thereafter the servo drives the mirror back to the origin in less than 250 m sec. There the servo awaits a new clock pulse to commence a second scan cycle. The drive is produced by voltages of the proper magnitude and polarity presented to the torquer velocity servo by the scan control circuit. Shortly after the start of the forward scan, the reference pulse appears from the reference pulse generator. This gates a counter which starts counting the pulses from the sequential pulse generator. When the horizon is located the output of the sequential pulse generator is stored. This count is a measure of the angle between the sensor reference and the horizon.

The counter continues to count the sequential pulse generator pulses until a count of 1535 is reached which occurs when the scanning mirror has scanned 7-1/2° (of field) beyond the reference position. At this point the counter sends a signal to the scan control circuit to reverse the scan motion at a high speed. The reference pulse produced during the retrace, signals the scan control circuit to hold at a rest position.

There is some overshoot while the motion reverses, and therefore another reference pulse occurs shortly after the forward scan begins. This pulse clears and restarts the sequential pulse counter to begin a new cycle. Whether the reference pulse is coming from a forward or reverse scan is recognized by means of the polarity of the torquer drive command voltage.

There are four input commands to the servo system:

1. Scan off which places the scan mirror in its steady rest position.
2. Normal scan at a 1-Hz rate as described above.
3. Cage position where the mirror is held, by its torquer, against a semi-hard stop during launch to lock the mirror in place.
4. Calibration command causing the mirror to scan to a position 8° from the neutral and allowing the detectors to scan over a high emissivity copper plate whose temperature is accurately monitored to provide a radiometric reference in contrast with the zero of space.

A static sun presence sensor views an 8-1/2° high by 4-1/2° wide field which overlaps the entire scanned field of the radiometric channel. If the sun appears anywhere within this field, a sun presence signal is produced.

The horizon location, as well as a number of other parameters are encoded in the digital data processor in the form of binary registers which can be read out in parallel or ultimately put in serial form. The following readouts are available in the auxiliary electronics unit:

1. Horizon Location (12 Bits)
2. Confirmation of Horizon Crossing (1 Bit)
3. "R" Value (4 Bits)
4. Sun Presence (1 Bit)
5. 4 Commands: OFF, SCAN, CAL., CAGE
6. Fault Detection and Identification Signals (6 Bits)
7 Spare (1 Bit)

SUMMARY OF ARPESH SYSTEM CHARACTERISTICS

Instantaneous Field of View	Approximately 1° Vertical 4° Horizontal
Scan Angle	7-1/2°
Scan Rate	1 scan/second
Resolution of Readout	0.005° of Field Position
Accuracy	0.02° at 500Km Altitude for 220°K Planet
Size (per sensor head)	20.3 x 12.7 x 11.43 cm (8" x 5" x 4-1/2")
Weight (sensor head)	5 Kg

In the sections which follow we will cover in more detail various design, construction and performance aspects of the ARPESH.

3. SENSOR DESIGN CHARACTERISTICS

In this section we will describe, in some detail, the design features of the Accurate Reliable Prototype Earth Sensor Head. Included in this discussion will be the design and properties of the block of three immersed thermistor detectors, the optics, processing electronics, both analog and digital, and the mechanical design of the system. Also described is the design of the auxiliary electronics unit and the interfaces, such as input power requirements and command inputs, and the waveforms and format of the data generated by the sensors.

3.1 DETECTOR

The detector used in the ARPESH is a trio of Germanium-Mylar immersed thermistors, the active flakes have dimensions of 0.5 x 0.5 mm. The thermistors are immersed in germanium hyperhemisphere lenses that are stacked one against the other, the lenses have flats ground on the sides where they join. By thus joining the lenses it is possible to make the fields of view of adjacent detectors essentially contiguous even though the tiny detectors immersed on a mylar base onto the germanium are separated and can thus be conveniently mounted in the center of the lens, and electrodes attached to the sides of the flakes. Figure 3.1-1, shows the detector housing and layout and Figure 3.1-2 lists some of its properties. With this arrangement we also achieve a very high optical speed with the result that the detector is small and the sensitivity is the highest that can be achieved with a thermistor detector. The field of view of the system is defined by the dimensions of a mask placed in the focal plane of the objective mirror, just in front of the trio of immersion lenses. (See Figure 3.1-3). The thermistor flake size is 0.5 mm on a side. The A detector subtends an angle of 1.392° in the direction of scan. The effective focal length for the system can be computed from these parameters as;

$$\text{e.f.l.} = \frac{0.5 \text{ mm}}{1.392^\circ \times .0175 \text{ mr/Deg.}} \approx 20 \text{ mm}$$

Since objective lens is about 57 mm on a side (2.2") the effective speed of the optics is

$$f/\# = \frac{\text{e.f.l.}}{\text{lens Ht.}} \doteq \frac{20}{57} \approx 0.36$$

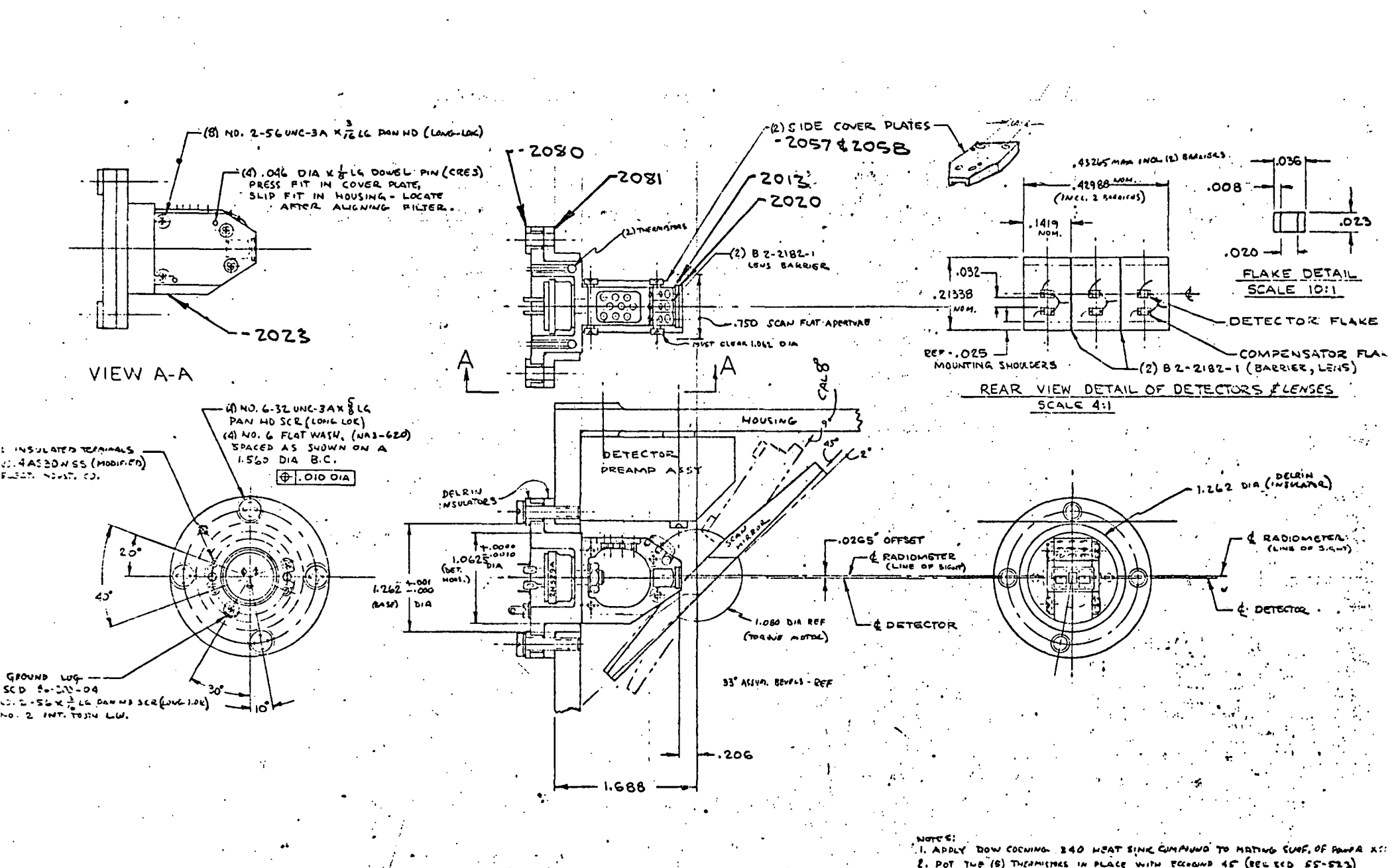

(1) NO. 8-32 SOCK. BUTTON HEX NUT-CRES
(1) NO. 8 INT. TOOTH LOCK WASH.-CRES
(1) SCREW #8-32 - CRES
(6) TERMINAL, INSULATED, FOR THERMISTORS - USE MODIFIED E.I. NO. 7AS17W SS
(9) FEED THRUS (ELECTRICAL INDUSTRIES No. 7AS17W SS)
(1) POWER TRANSISTOR ~~EUSM~~ 2N5005
(1) THERMOSTAT - NOT REQD
(5) THERMISTERS - USE G. SEC SCD 24-112-001
(4) TERMINAL, INSULATED, MODIFIED E.I. NO. 4AS30W SS

NOTES:
1. APPLY DOW CORNING 340 HEAT SINK COMPOUND TO MATING SURF. OF PARTS X
2. POT TUB (6) THERMISTORS IN PLACE WITH ECCOBOND 45 (REF SCD 55-523)
3. USE SOLDERING & BONDING TECHNIQUES OUTLINED IN DWGS # PLS D255001-1004.

FIG 3-1.1 LAYOUT - DETECTOR

FULL SIZE

B 206201-4008

FIG. 3.1-2 Detector Housing

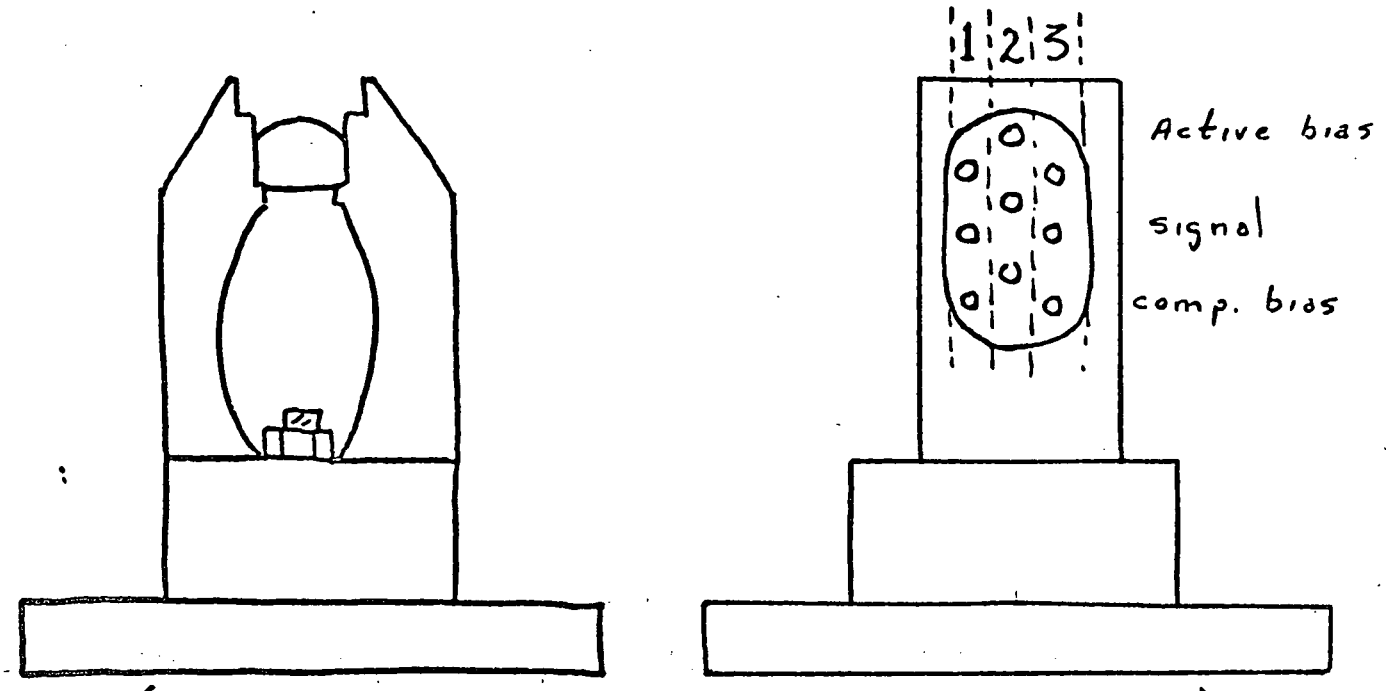

(Diagram not to scale, reference only)

Flake		Lens	
Length	0.50 mm	Length	3.60 mm
width	0.58 mm	width	5.40 mm
Area	0.29 mm^2		

	1	2	3
Resist., Act.	206 KΩ	208 KΩ	209 KΩ
Resist., comp.	209 KΩ	205 KΩ	207 KΩ
Peak voltage, Act.	117 V.	117 V.	115 V.
Peak voltage, comp.	116 V.	115 V.	113 V.
Signal (470, 15, 2-100)	4000 μV	9200 μV	4300 μV
Time const. (470, 15, 2-1000)	1.9 ms	1.9 ms	2.0 ms
Noise figure	1.37	1.35	1.35
Recommended bias	66 V/flake	66 V/flake	66 V/flake

FIG. 3.1-3 Detector Mask Dimensions and Fields of View

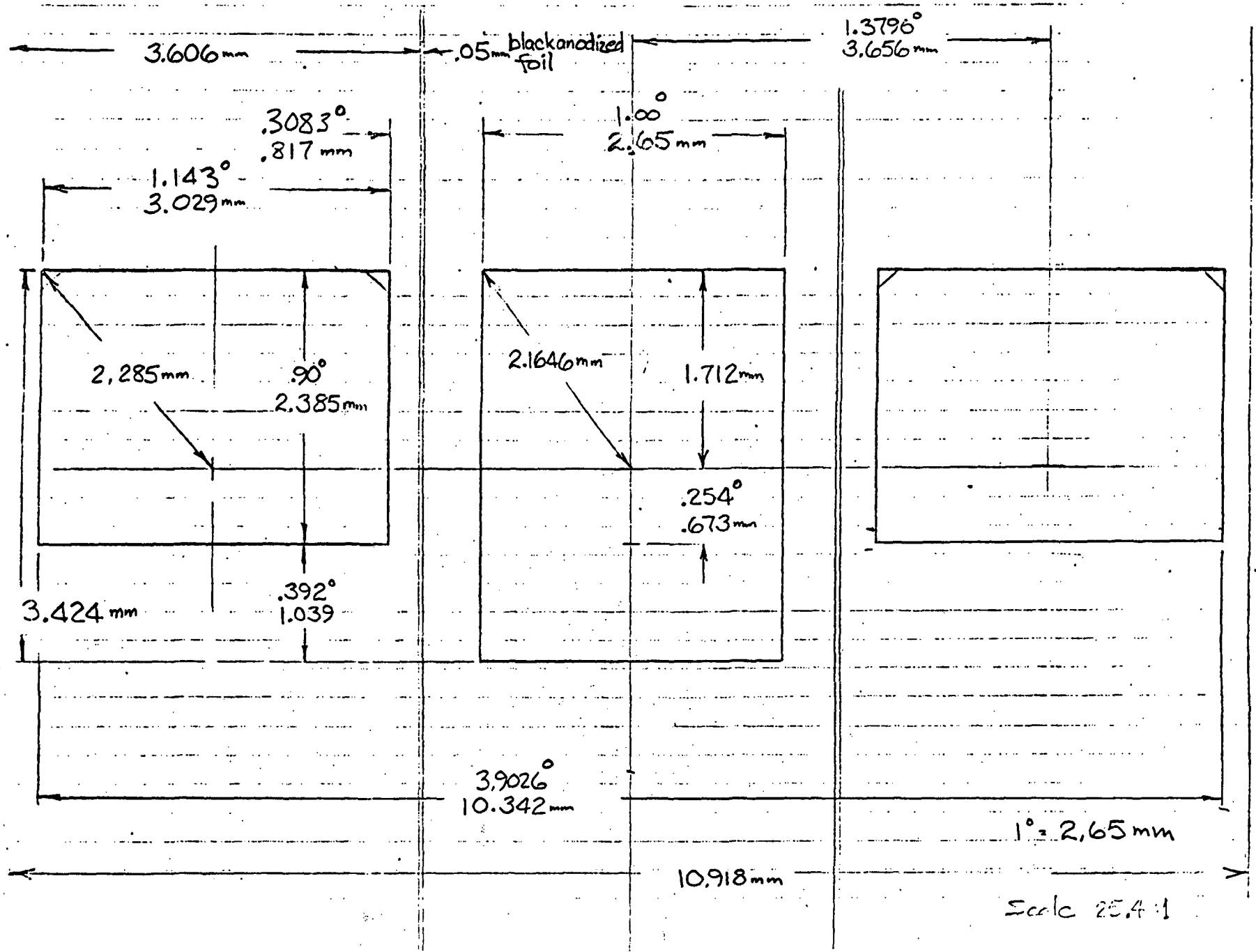

Summarized below are the principal parameters of the three detectors:

Responsivity at normal bias	$\mathcal{R} \approx 170$ V/W
Resistance of each flake	$R \approx 200$ K
Time constant	$T_{th} \approx 2$ msec.
Noise 1-100 Hz at normal bias	$Vn = 0.75\mu V$
Bias voltage	V_B = 180 Volts for active & compensator flakes in series

3.1.1 DETECTOR-NOISE CONSIDERATIONS

As indicated in Section 3.1 above the noise of the detector measured in a bandwidth of 1 - 100 Hz was $\approx 0.8\mu V$ RMS. We can compare this measured value with values calculated from basic parameters.

The noise characteristic of a thermistor detector can be approximated by the curve sketched below in a solid line with three frequency regions including a flat (white) Johnson noise region (f_3 and greater), a region from f_2 to f_3 with a 1/f low frequency noise characteristic and a very low frequency region f_1 to f_2 in which noise appears to increase at a rate $1/f^2$. (Figure 3.1-4 shows typical low frequency noise characteristics of thermistor detectors.)

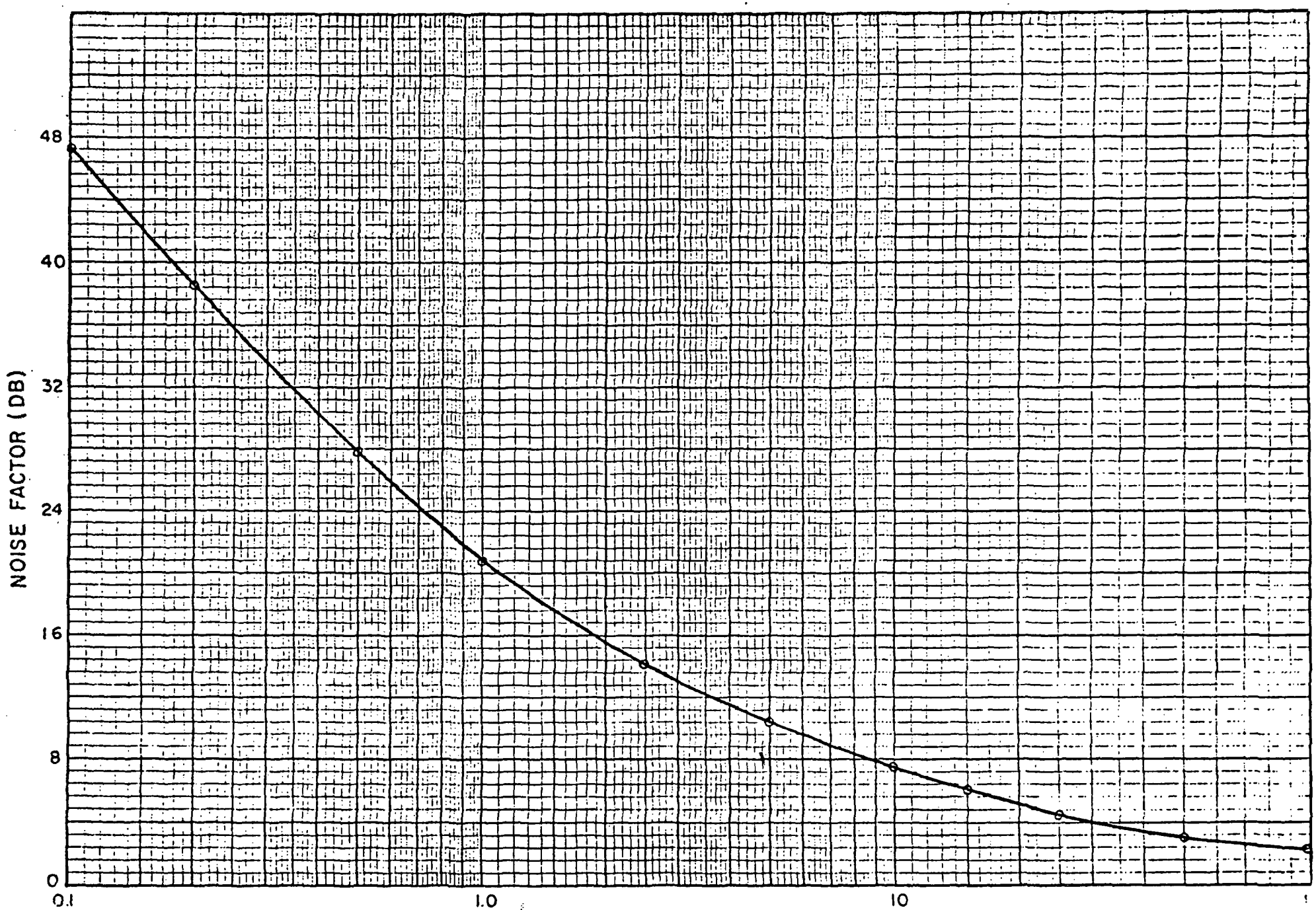

FIG. 3.1-4 Typical Thermistor Noise

The preamplifier will have a frequency response that will roll off at very low frequencies and will include a boost network starting at f_4 where the detector frequency response begins to fall and up to f_5, the high frequency cut-off for the system. Beyond f_5 the amplifier provides a 12 db per octave roll off.

To determine the degradation in noise due to the inclusion of the low frequency excess noise and the boosted high frequency Johnson noise, we can develop an expression for spot noise as a function of frequency.

$$V_T^2 = V_n^2 \left[\frac{f_3}{f_2} \int_{f_1}^{f_2} \left(\frac{f_2}{f}\right)^2 df + \int_{f_2}^{f_3} \frac{f_3}{f}\, df + \int_{f_3}^{f_4} df \right.$$

$$\left. + \int_{f_4}^{f_5} \left(\frac{f}{f_4}\right)^2 df + \left(\frac{f_5}{f_4}\right)^2 \int_{f_5}^{f_6} \left(\frac{f_5}{f}\right)^4 df \right]$$

For the sensor design, with a 750 msec forward sweep of the scanner the following break points have been established:

V_T = Total Noise

V_n = Johnson noise at the reference level

f_1 = 1.7 Hz

f_2 = 5 Hz

f_3 = 50 Hz

f_4 = 60 Hz

f_5 = 96 Hz as specified high frequency corner

f_6 = 173 Hz

$$V_T^2 = Vn^2 \left[\frac{50}{5} \int_{f_1}^{f_2} \left(\frac{5}{f}\right)^2 df + \int_{f_2}^{f_3} \frac{50}{f} df + \int_{f_3}^{f_4} df \right.$$

$$\left. + \int_{f_4}^{f_5} \left(\frac{f}{60}\right)^2 df + \left(\frac{96}{60}\right)^2 \int_{f_5}^{f_6} \left(\frac{96}{f}\right)^4 df \right]$$

$V_T^2 = Vn^2$ 280.6 and the loss is $\sqrt{280.6/96} = 1.7$

$$V_n = \sqrt{4kTR\Delta f} = \sqrt{4kT \times 10^5 \times 96}$$

where

R = resistance of bolometer bridge ≈ 100 kΩ

ΔF = bandwidth = 96 Hz

$V_n \approx .45\mu V$

With the degradation factor of 1.7 the total noise input will be 0.76μV, very nearly the value measured.

3.1.2 IMMERSED THERMISTOR DETECTOR OPTICAL PROPERTIES IN THE 14-16 MICRON BAND

Germanium immersed thermistors have been used extensively in radiometric measurements of atmospheric CO_2 in the 15 micron spectrum. These detectors have certain response deficiencies in this region of the spectrum due to a combination of 1) absorption in the germanium immersion lens, 2) absorption in the optical cementing layer, and 3) semitransparency of the thermistor flake. The spectral response characteristics of the germanium-Selenium glass and the germanium-Mylar film immersed thermistors are treated in the 13 to 17 micron.

3.1.2.1 MEASURED PROPERTIES OF DETECTOR COMPONENTS

Figure 3.1.5 plots the transmission of plane, polished, parallel-faced, high purity ($\rho \doteq 40$ ohm-cm) germanium in several thicknesses. From top-to-bottom in Figure 3.1.6, is 1) the measured transmission of sintered #2 thermistor material in an equivalent electrical thickness (standard) of 250 K Ω per square at 25°C, 2) measured transmission of this flake permeated with cured Bakelite resin (cement used to paste flake on the Mylar film), and 3) the total hemispherical reflectance of a thick opaque sintered #2 thermistor.

In Figure 3.1.5 we see that germanium has appreciable absorption in the CO_2 region. In Figure 3.1.6, the bare thermistor flake (top) goes from semitransparency at 14 microns to near-opacity at 15 microns. Permeated with Bakelite cement, broad absorption in the latter reduces the flake transparency.

FIGURE 3.1.5 TRANSMITTANCE OF HIGH PURITY GERMANIUM AT 25° C

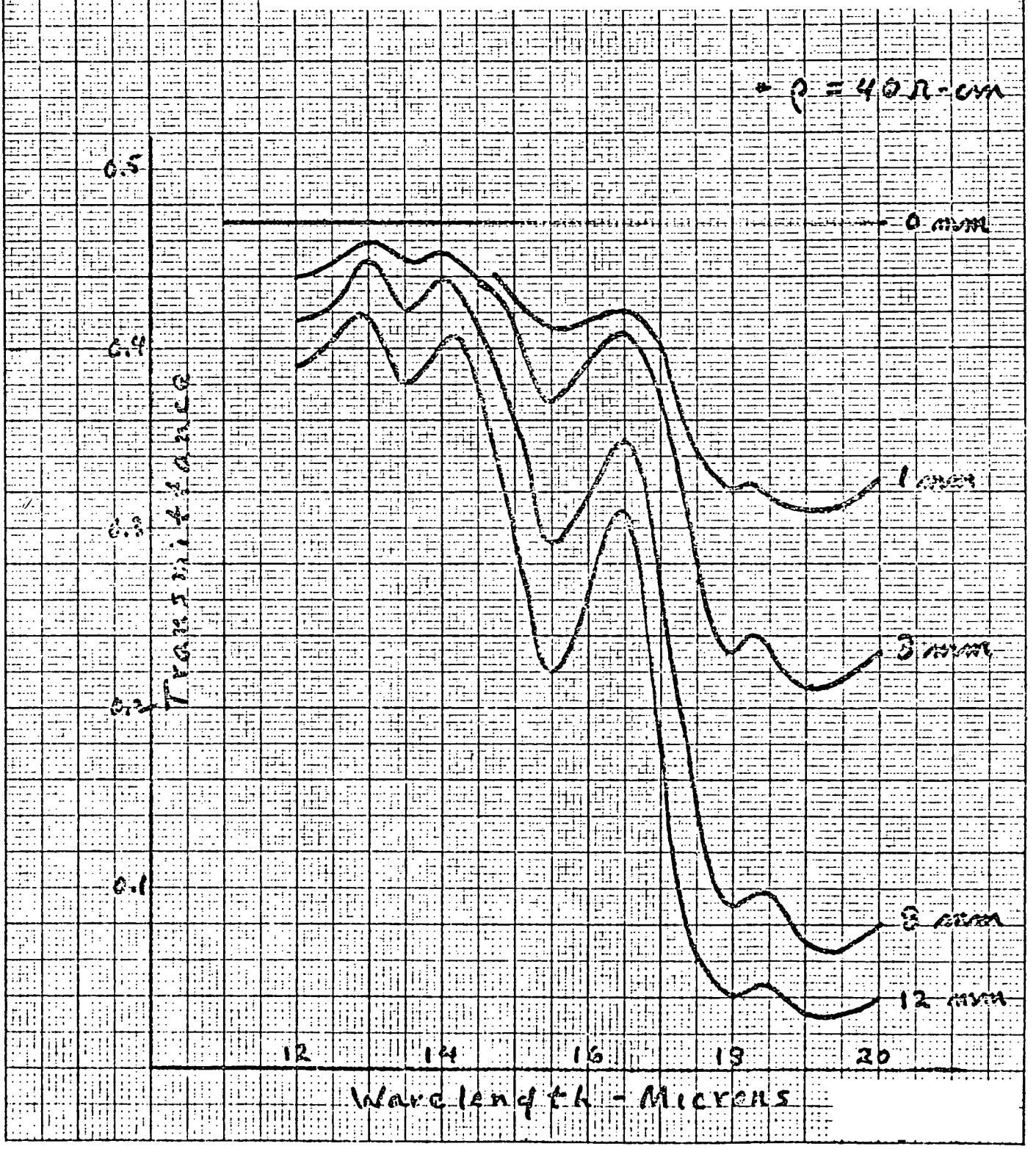

FIGURE 3.1.6 SPECTRAL TRANSMITTANCE AND REFLECTANCE OF THERMISTOR FLAKES

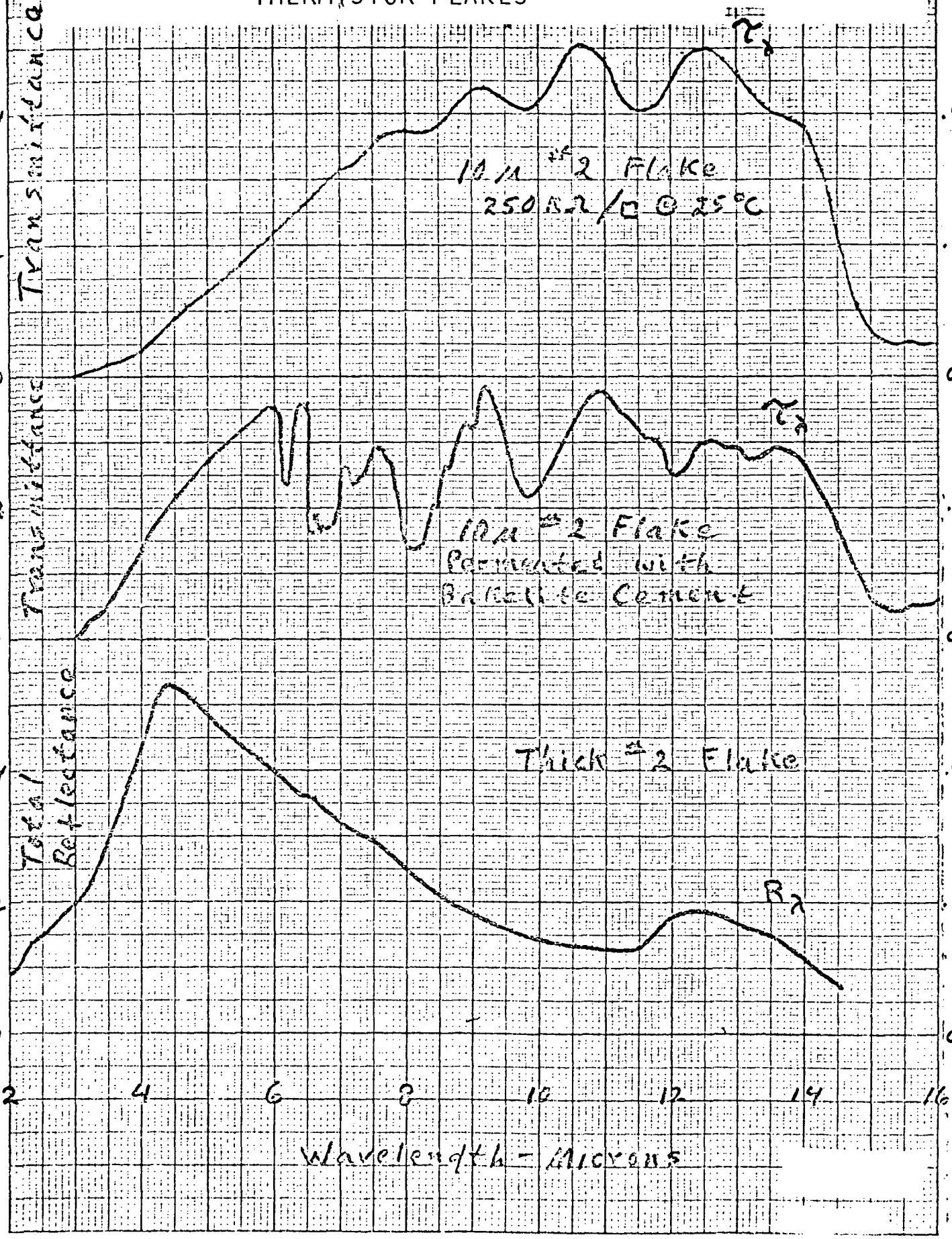

3.1.2.2 SIMPLIFIED THERMO-OPTICAL MODEL

In order to formulate an expression for the steady-state spectral response of the immersed thermistor, it is helpful to sort out the optical and thermal effects in the several layers. With the use of the model in Figure 3.1.7, this is done in a manner which considers each layer as an optical and thermal entity, neglecting thermal gradients and multiple reflections within the layers. The construction is that of the germanium-Selenium glass immersed type. The anti-reflection coating on the germanium is purposely omitted since it can easily be added later to adjust the spectral response of the detector.

We will assume that all energy absorbed in the bottom three layers of the stack, namely: The flake, the glass overcoat, and the black coating all contribute to heating the flake. Also, we will assume that all energy absorbed in the germanium and glass immersion layer does not heat the flake. Considering the high thermal conductivity and heat capacity of the relatively large germanium lens, and the high thermal impedance of the glass immersion layer, these assumptions are valid.

3.1.2.3 SPECTRAL RESPONSE CALCULATIONS

On this basis we can write for relative spectral response,

$$\mathcal{R}_\lambda = (1-r_1)(1-r_2)(1-r_3)(1-A_{Ge})\ (1-A_{Se})(A_{f,Se,B}) \qquad \text{(Eq. 1)}$$

where, r_1, r_2, r_3 are first surface reflectivity values at the interfaces labelled in Figure 3.1.7 and A_{Ge}, A_{Se} and $A_{f,\ Se,\ B}$ are the absorptivity in, respectively, germanium, selenium glass

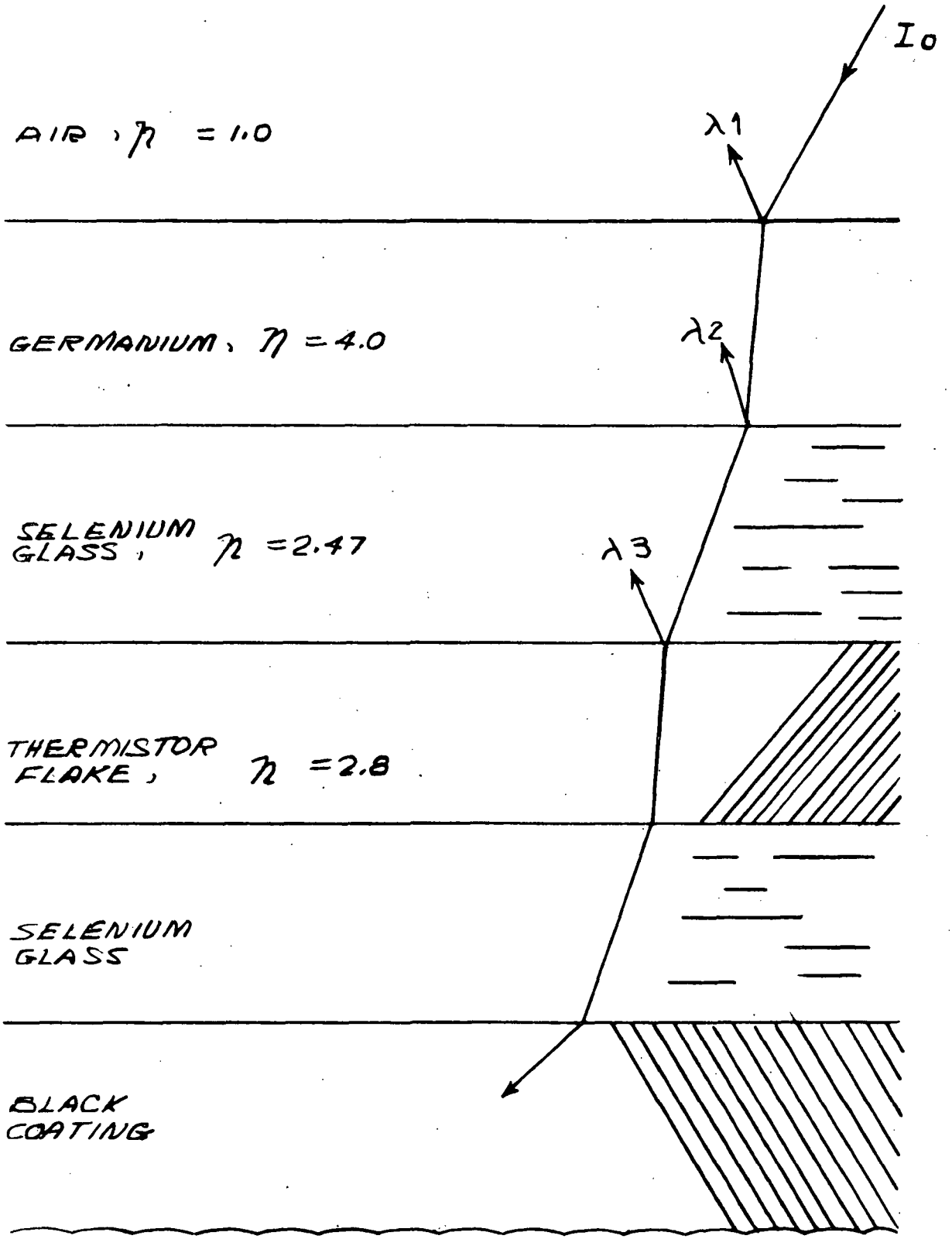

FIGURE 3.1.7 **GERMANIUM-SELENIUM GLASS IMMERSION**

and stack comprised of the flake, the glass and the black.

It has been shown[1] that the "true" transmissivity (τ_λ) of a plane polished parallel-sided slab is related to the measured transmissivity (τ_λ^*) by,

$$\tau_\lambda^* = \frac{\tau_\lambda (1-r_\lambda)^2}{1-r_\lambda^2 \tau_\lambda^2} \qquad \text{(Eq. 2)}$$

where

r_λ is the first surface reflectivity, namely,

$$r_\lambda = \frac{(n_1-n_2)^2}{n_1+n_2} \qquad \text{(Eq. 3)}$$

The absorptivity is then,

$$A_\lambda = 1-\tau_\lambda \qquad \text{(Eq. 4)}$$

We have measured values for the transmissivity (τ_λ^*) of germanium (Figure 3.1.5) and the flake (Figure 3.1.6) in air. Reflectivity from Equation 3 can be considered quite accurate for the case of polished germanium samples, but there can be some question about its validity for the flake. However, specular reflectivity measurements on thick flakes indicate it approaches a "polished" behavior at wavelengths longer than about 15 microns.

In evaluating the spectral response using Equation 1, the absorptivity in the selenium glass (A_{Se}) is assumed to be zero, and that in the black coating (A_B) unity. Values for refractive indices used were,

(1) McMahon, H.O., JOSA, 40, p.376, 1950

Material	Index
Germanium	4.0
Selenium Glass	2.47
Flake	2.8

Spectral absorptivity for two thicknesses of germanium are plotted in Figure 3.1.8, and for a standard thickness thermistor flake in the top of Figure 3.1.9. The former points up the large losses in pure germanium lattice absorption near 15.5 microns, and the latter shows the steep absorption gradient in the flake in the 14 to 15 micron interval. The dashed portion of the flake absorptivity curve signifies some doubt about the data.

3.1.2.4 GERMANIUM-SELENIUM GLASS IMMERSION

Spectral response for two germanium lens thicknesses (3 and 12 mm) are shown in Figures 3.1.10 and 3.1.11, with and without an opaque coating of black applied to the flake. Depending upon the spectal interval involved in radiometric sampling of CO_2 the black coating on the flake can be important. At wavelengths greater than 15μ the black adds nothing to the response, while in the 14 to 15μ interval it can make a difference of as much as two times. Also important relative to the black is that a good (opaque) coat may increase the time constant of the flake by 50%. Hence, if fast response is required for 14 to 15 micron radiation, a delicate trade-off between higher DC response (more black) and faster response time (less black) is called for.

3.1.2.5 GERMANIUM-MYLAR IMMERSION

The germanium-Mylar immersed thermistor has been used extensively in applications where the detector is exposed to

FIGURE 3.1.8 ABSORPTIVITY IN HIGH PURITY GERMANIUM AT 25° C

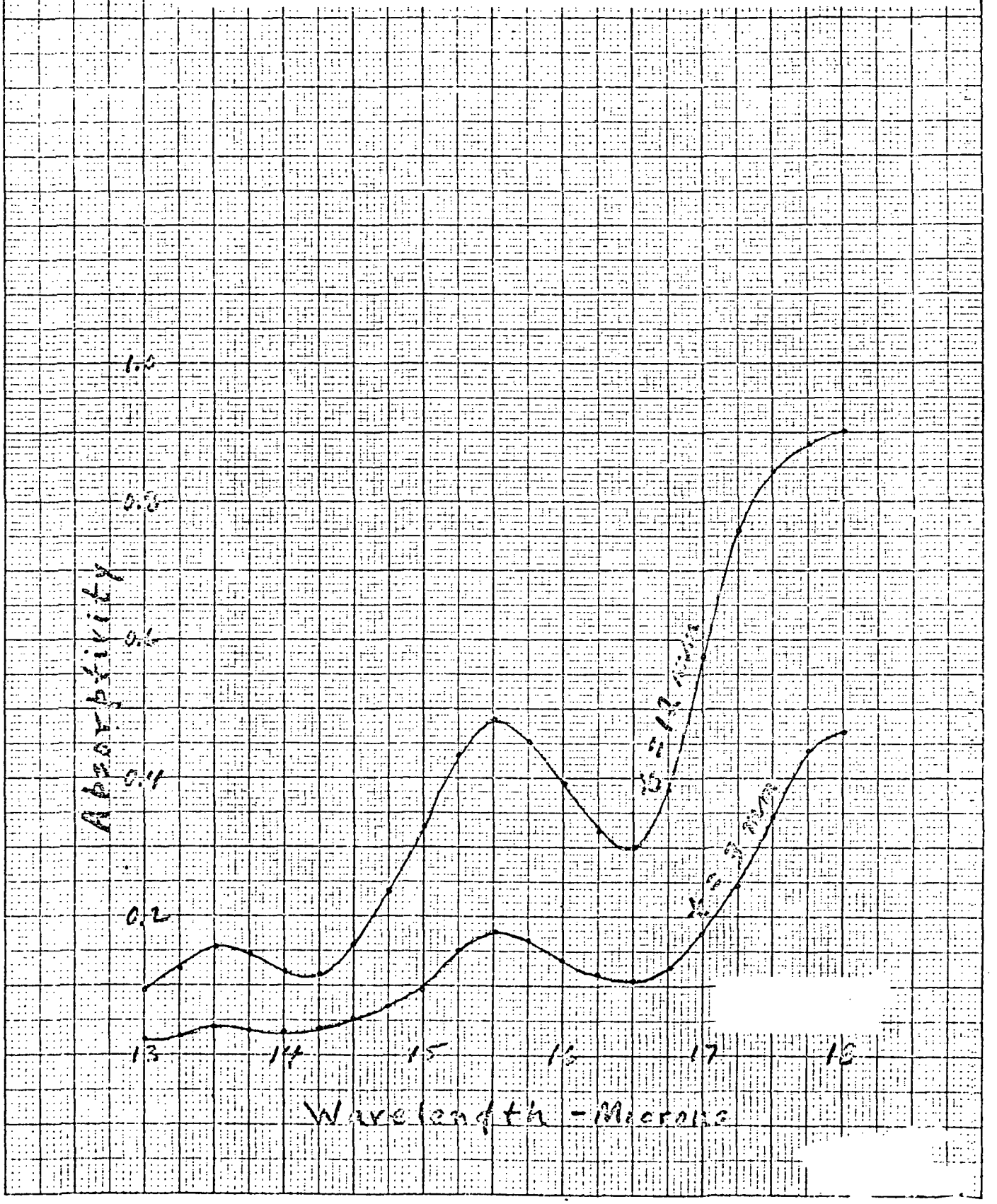

FIGURE 3.1.9 ABSORPTIVITY IN THERMISTOR FLAKE

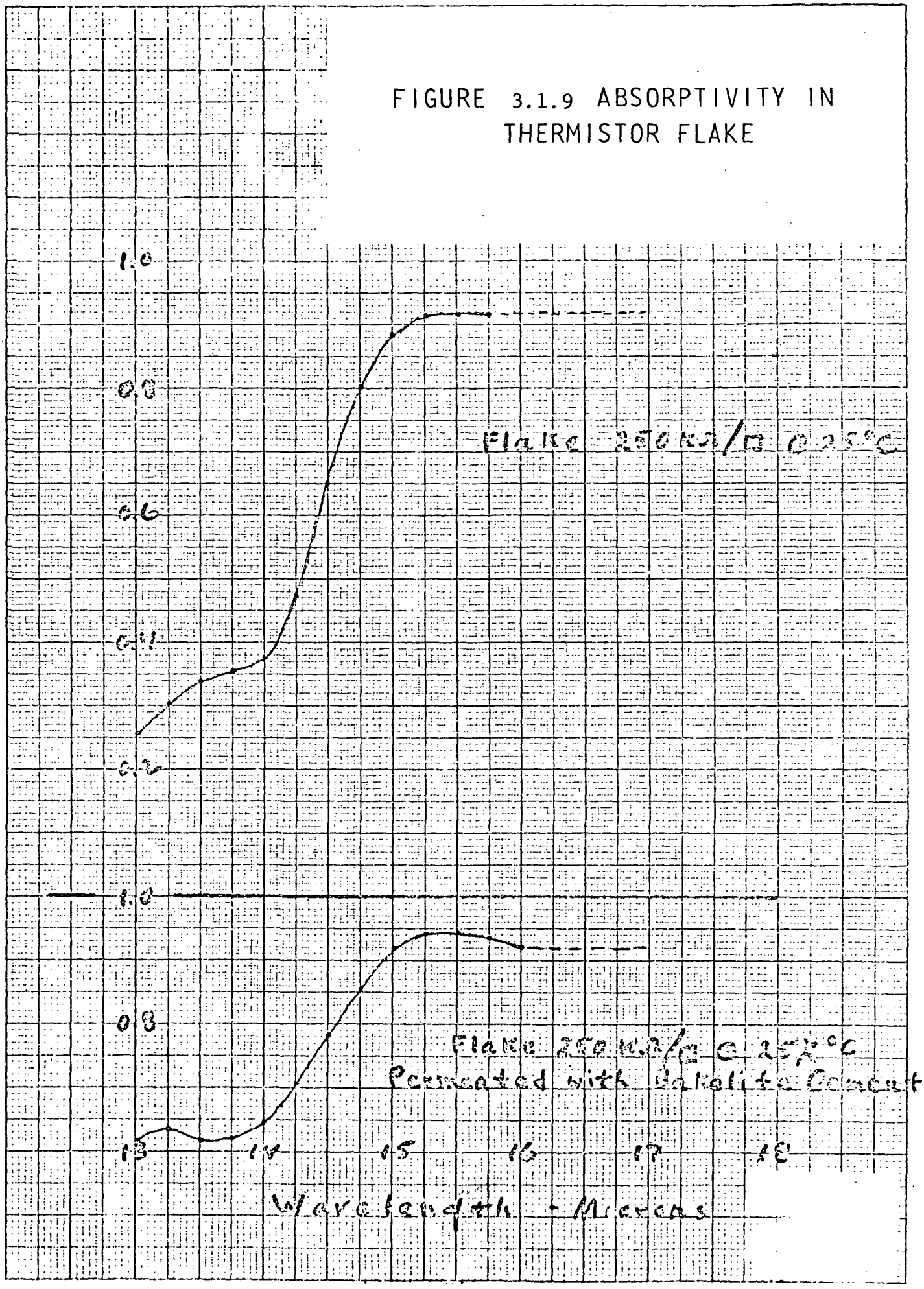

FIGURE 3.1.10 SPECTRAL RESPONSE OF GERMANIUM - SELENIUM GLASS IMMERSED THERMISTOR

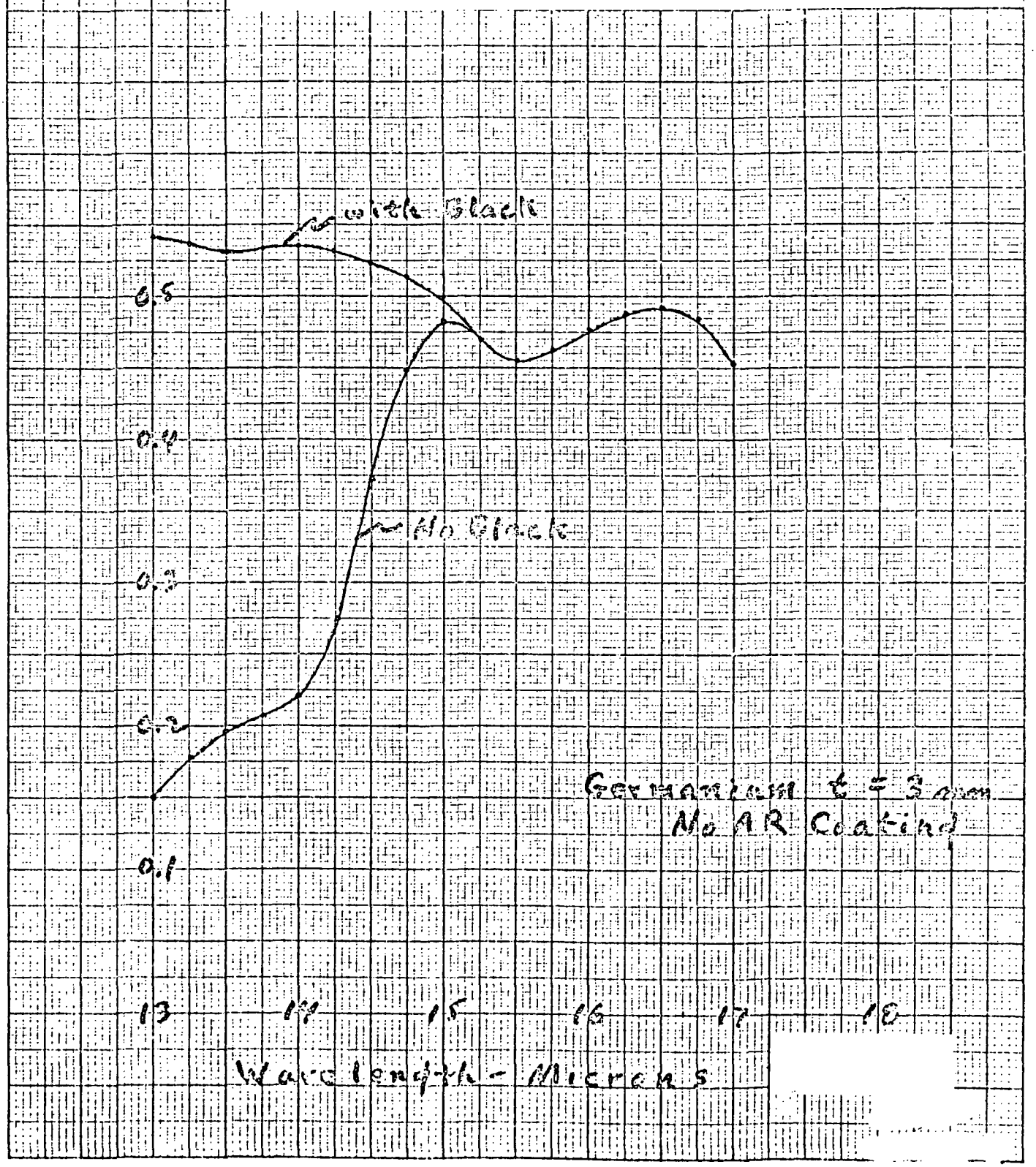

FIGURE 3.1.11 SPECTRAL RESPONSE OF GERMANIUM - SELENIUM GLASS IMMERSED THERMISTOR

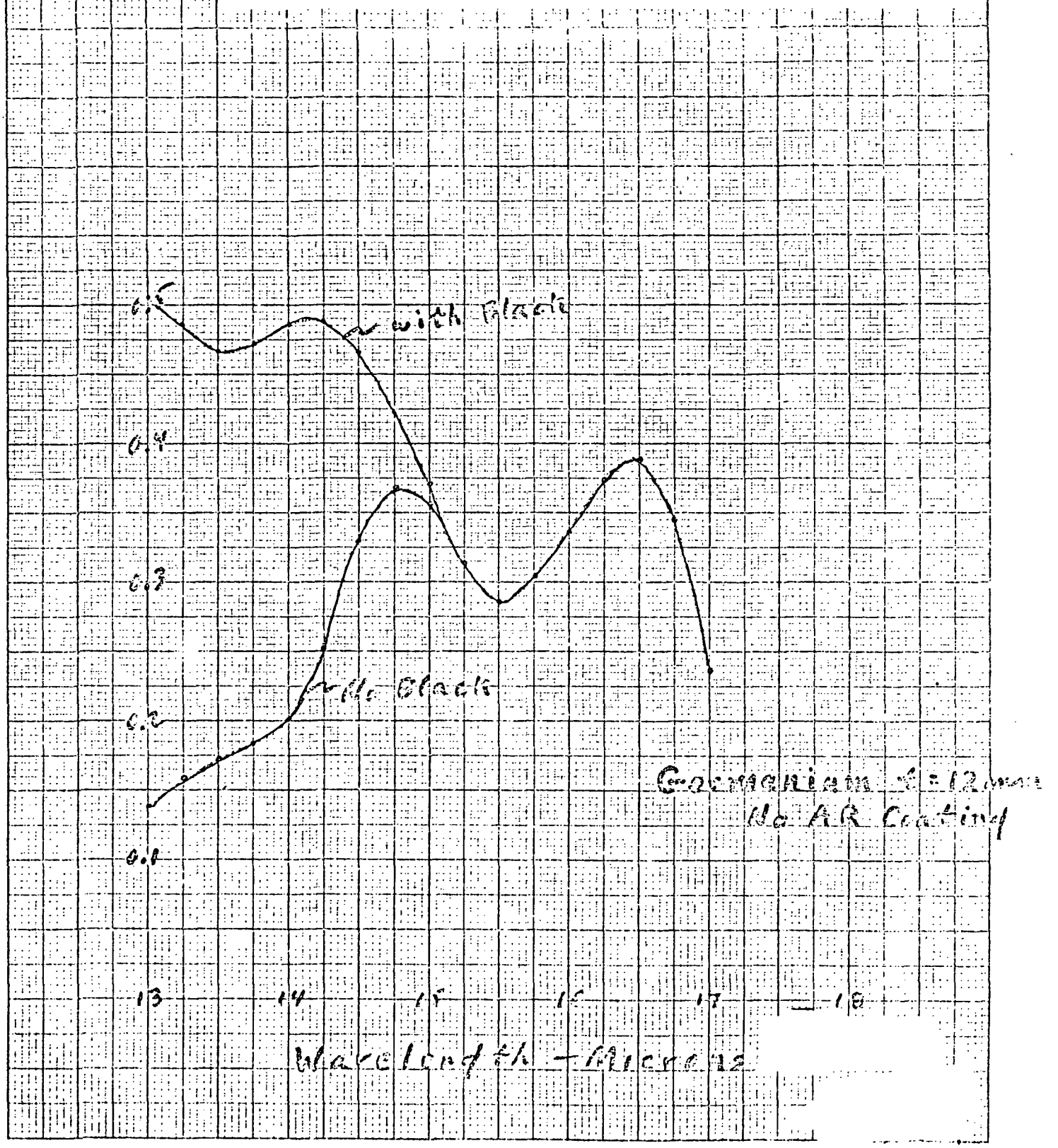

elevated temperatures (> 55 to 60°C) which can degrade both the electrical (noise) and optical properties of the selenium (arsenic modified) glass. The layers in the stack for this design are identified in Figure 3.1.12.

Deficiencies in this design are two-fold. The low refractive index of the cement (ca 1.5) at the germanium interface reduces the critical angle from 37 degrees for the selenium glass case to 21 degrees for that of mylar. This reduces the effective speed of the optical system one can employ with the immersed thermistor and hence limits the responsivity gain afforded by germanium immersion. The other factor involves radiation loss in a strong absorption band in Mylar centered at 13.7 and to a smaller extent due to spectrally broad absorption in the Bakelite resin layer which cements the mylar to the germanium. (This layer is usually very thin and because the resin has no strong bands in the 15 μ CO_2 region, its absorption losses are neglected here.)

With this design, where the immersion layer (Mylar) has significant absorption, the premise of lumped thermal behavior is less valid than for the selenium glass (non-absorbing) design. This is so because radiation dissipated in the Mylar absorption band can transfer part of its heat to the flake.

The spectral transmission (τ_m*) of Mylar in the several thicknesses which have been used in this detector design are given in Figure 3.1.13. The film thickness is varied to control the detector time constant (unblackened) nominally as follows,

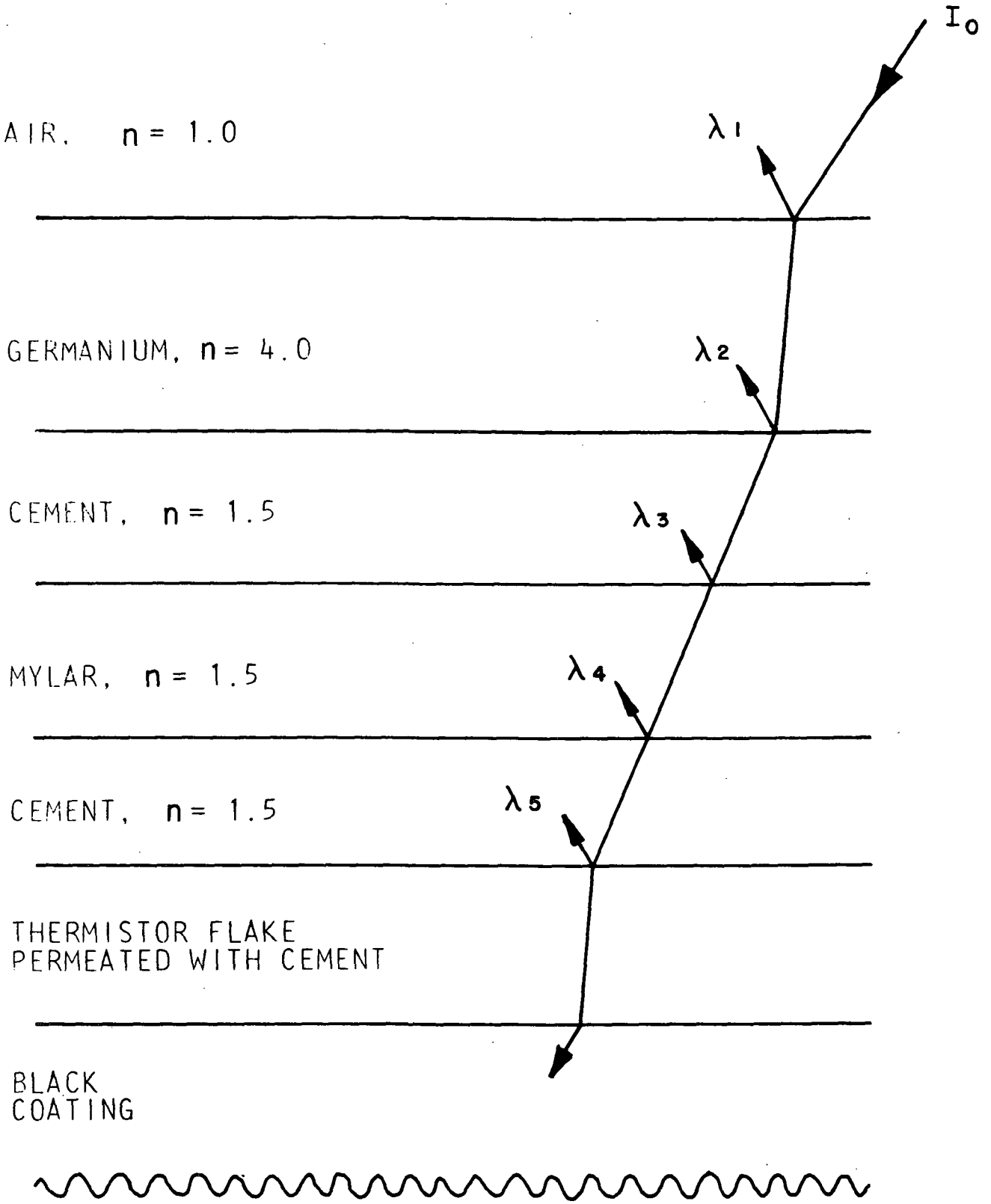

Figure 3.1.12

GERMANIUM - MYLAR IMMERSION

FIGURE 3.1.13 SPECTRAL TRANSMISSION OF MYLAR FILM

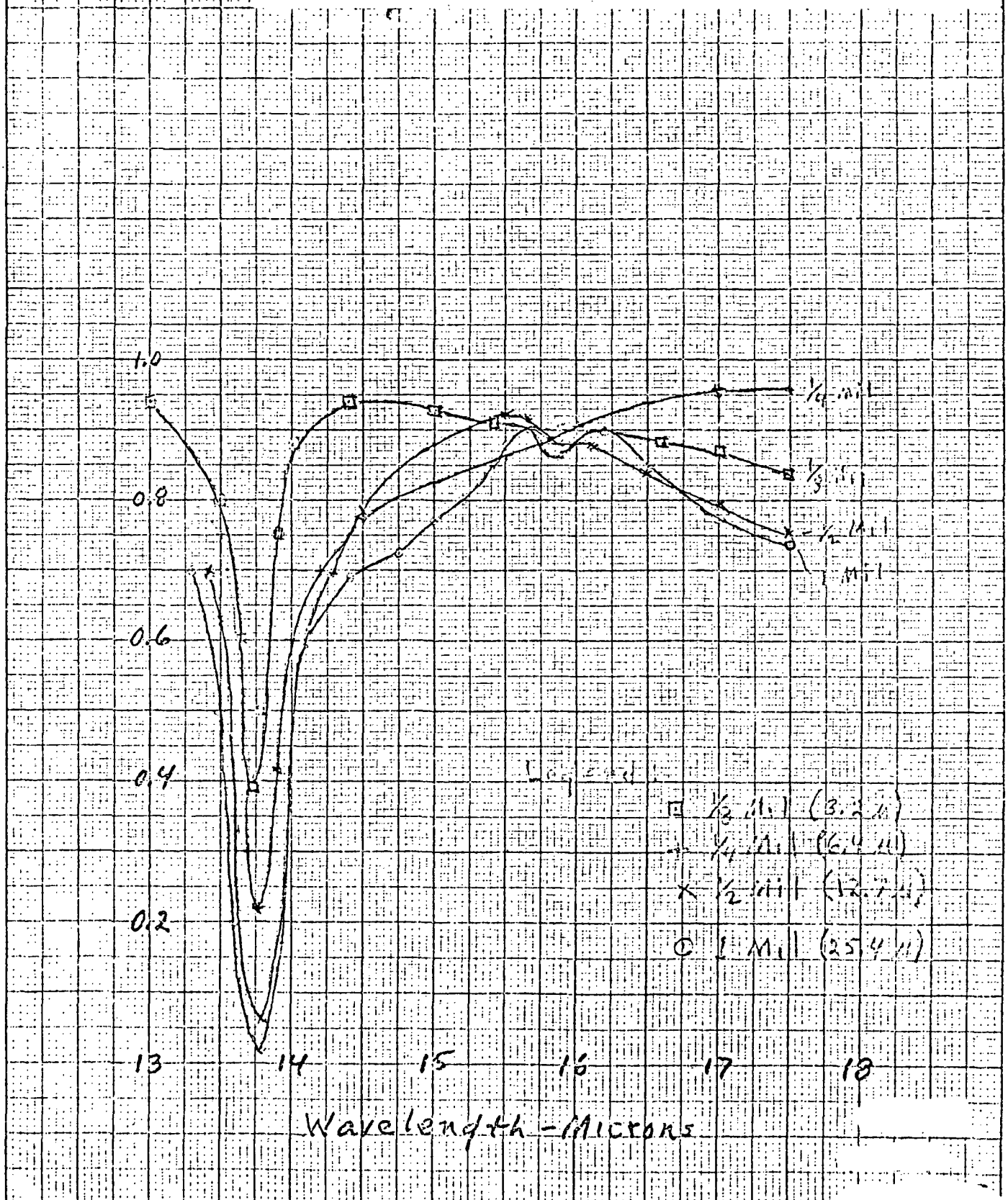

MYLAR THICKNESS		TIME CONSTANT
1000th Inches	Microns	Milliseconds
1/8	3.2	1.3 - 1.8
1/4	6.4	2 - 2.5
1/2	12.7	4 - 5
1	25.4	8 - 9

In this design absorption in the unblackened flake is different from that of the germanium-selenium glass detector because the Bakelite cement permeates the porous flake and hence contributes to absorption and flake heating. The spectral transmission (τ^*_{f+c}) of the cement permeated flake was shown in Figure 3.1-6.

Referring to the detector stack construction of Figure 3.1-12, and neglecting multiple reflections in the layers as well as the thermal spread from absorption in the 15.5 μ Mylar band, the relative spectral response of the germanium-Mylar immersed thermistor is,

$$\mathcal{R}_\lambda = (1-r_1)(1-r_2)(1-r_3)(1-r_4)(1-r_5)(1-A_{Ge})(1-A_m)(A_{f+c,B}) \quad \text{(Eq.5)}$$

The refractive indices of the materials in the stack, from which reflectivity at the several interfaces is computed are,

Material	Index
Germanium	4.0
Bakelite Cement	1.5
Mylar	1.5
Flake	2.8

Since the cement and mylar indices are equal, Equation 5 becomes,

$$\mathcal{R}_\lambda = (1-r_1)(1-r_2)(1-r_3)(1-r_4)(1-r_5)(1-A_{Ge})(1-A_m)(A_{f+c,B}) \quad \text{(Eq.6)}$$

Figures 3.1-14 and 3.1-15 plot the solution of Equation 6 for 3 and 12 mm thick germanium and 1/8 mil (3.2 μ) Mylar film. Absorptivity values for germanium (A_{Ge}), Mylar (A_m), and the cement permeated flake (A_{f+c}) are found using Equations 2,3 and 4 and the measured transmission of these components.

In the final illustration (Figure 3.1-16, the theoretical spectral response of a germanium-Mylar immersed assembly is compared with the measured spectral response of an immersed detector of similar design.

As observed in Figure 3.1-15, the greatest uniformity is achieved without blackening of the flake. In Figure 3.1-15c, we have superimposed the spectral band limits on the detector spectral response. The result appears to be an average throughput of 0.27 without benefit of AR coatings. The peak deviations from the average transmission would be approximately .035 or 11% maximum deviation. This is the first evaluation of spectral uniformity over the spectral interval and requires better definition of the achievable spectral uniformity of the bandpass filter.

FIGURE 3.1-14 SPECTRAL RESPONSE OF GERMANIUM - MYLAR IMMERSED THERMISTOR

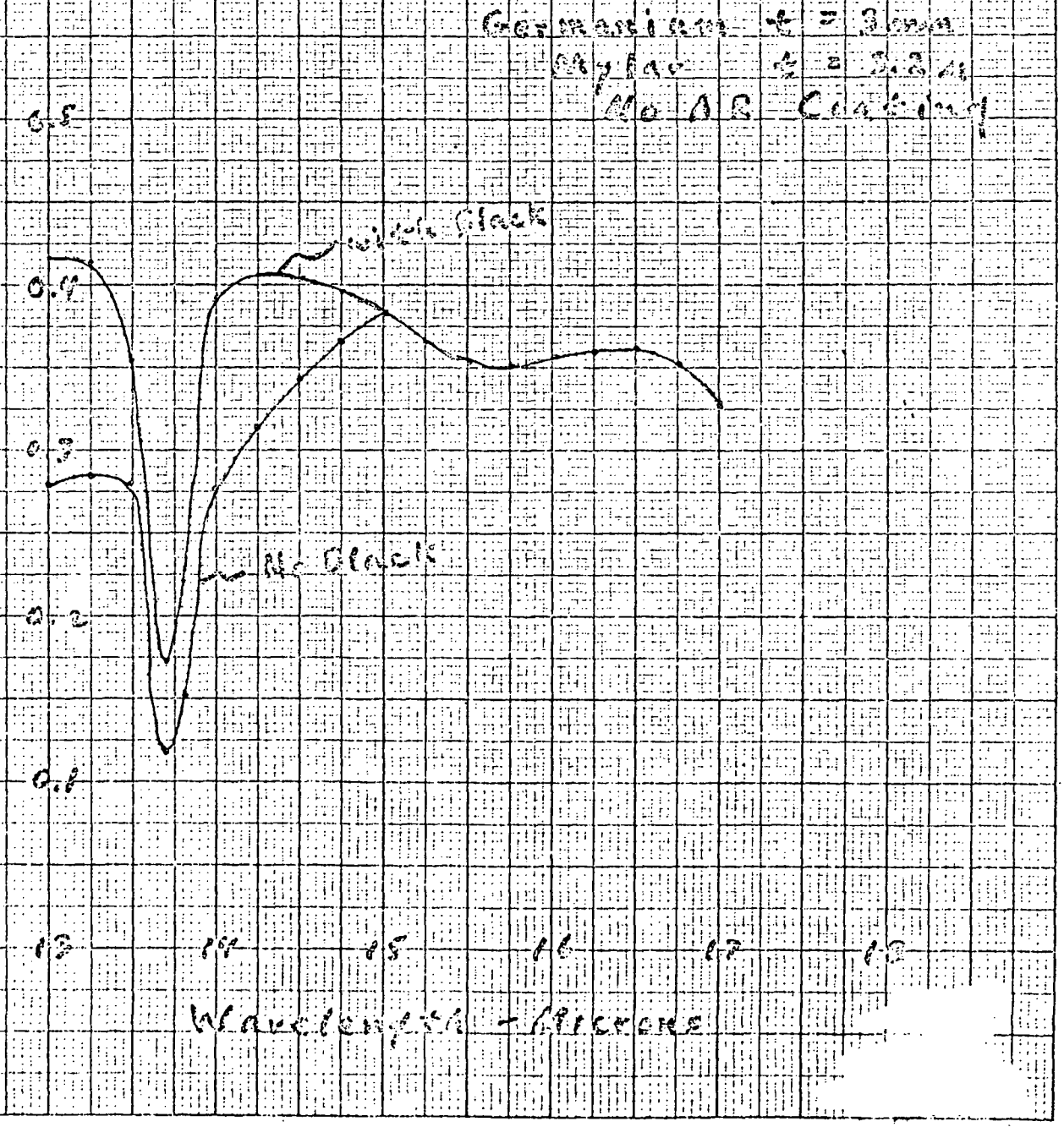

FIGURE 3.1-15 SPECTRAL RESPONSE OF GERMANIUM - MYLAR IMMERSED THERMISTOR

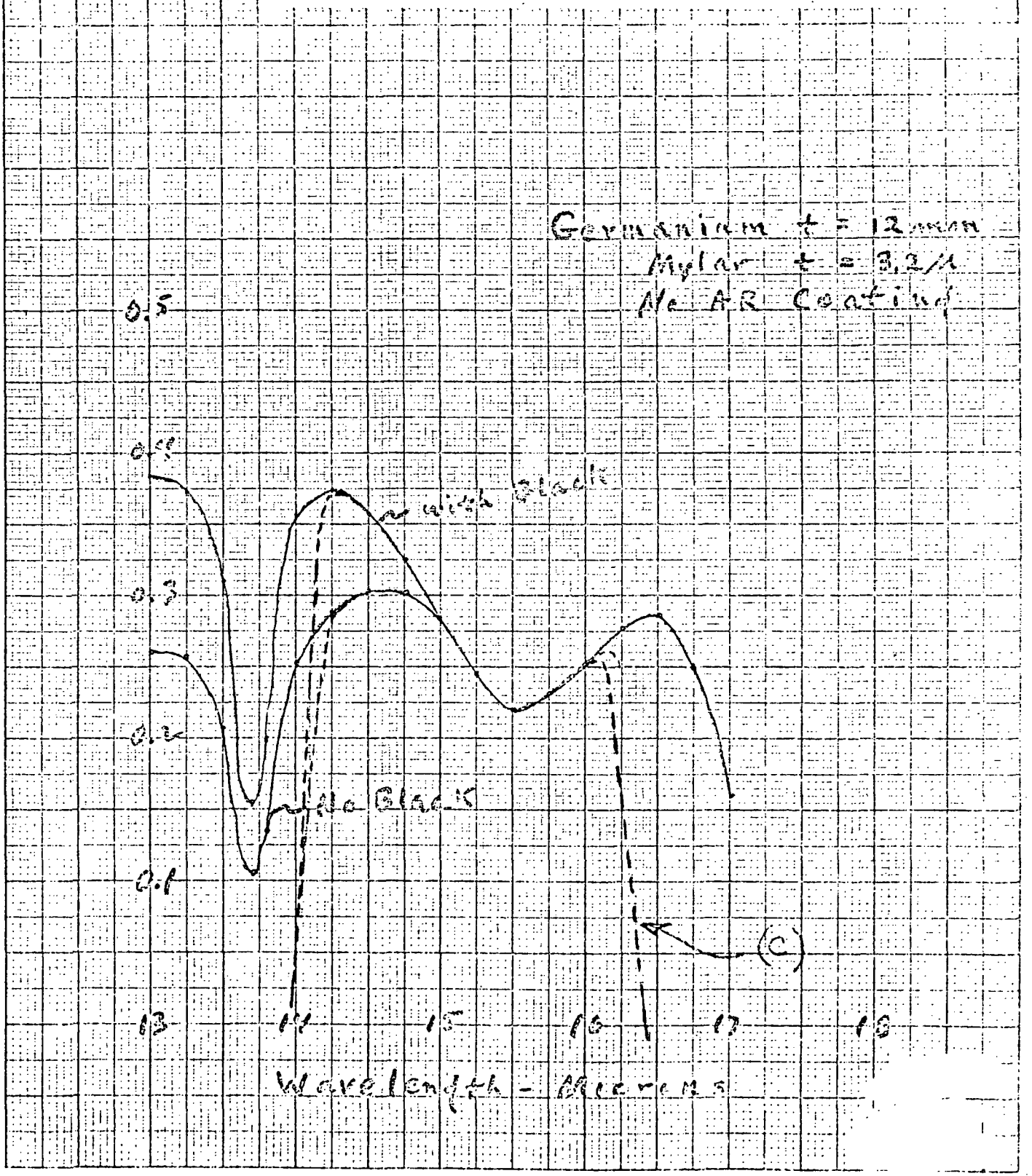

FIGURE 3.1-16 RELATIVE SPECTRAL RESPONSE OF GERMANIUM - MYLAR IMMERSED THERMISTOR

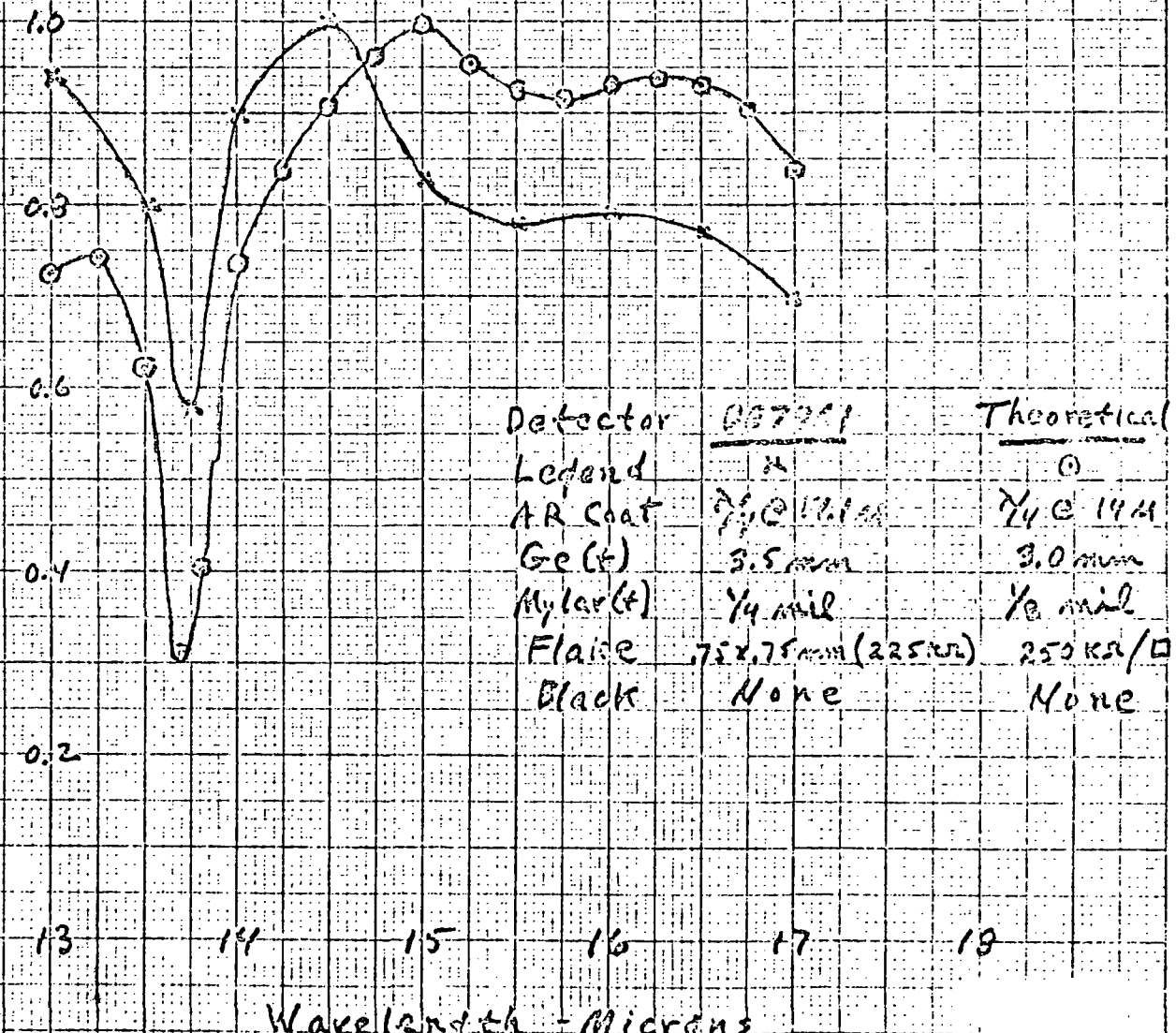

3.1.3 DETECTOR HISTORY

Various problems were encountered in connection with the detector fabrication and the 1000 hour burn-in required by the contract. As a result of several failures - a number of occasions when detectors became noisy and one instance in which a detector was burned out - it was necessary to rebuild the detectors a number of times. The last occasion for such re-building occurred after an apparently satisfactory set had been built and about 1/4 of the burn-in testing was done. One of the detectors became noisy and it was necessary to rebuild the set once again and carry out the 1000 hour burn-in once again.

One recurring problem was excessive noise that could be attributed to contamination of feed-through pins, usually due to humidity. This type noise would usually disappear after thorough cleaning and bake-out to boil off the moisture.

Even after successful completion of the burn-in one more failure occurred that could not be associated with contamination. For reasons not fully confirmed (but believed to be due to a possible temporary wiring short circuit across the active detector B_1), the compensator flake appears to have lifted away from its base. Evidence to this effect is the fact that the bias voltage across this flake is abnormally low indicating excessive compensator flake heating when bias is applied. Without bias the resistance is the normal value, about 200KΩ. Time and cost considerations dictated a simple remedy short of rebuilding the entire detector system. The remedy was to install a substitute compensating thermistor flake on the detector housing in good thermal contact with the detector block and thus at the same temperature as the principal detector. Performance of this detector is not measurably different than that of the others.

3.1.3.1 AUXILIARY CIRCUITS ASSOCIATED WITH DETECTORS

The detector mounting base is provided with a temperature controller that heats the detector block to, and maintains it at 10°C if the ambient temperature falls below this value.

The detectors are compensated for ambient temperature variations through use of a quasi - constant current bias source to maintain a bias level that results as nearly as possible in an optimum bias level. In addition, to maintain a responsivity that is nearly independent of ambient temperature variations a separate thermistor is supplied with each signal channel, mounted on the detector block. The function of these thermistors is to correct the gain of the electronics to maintain constant output voltage levels (for a given irradiance) independent of the ambient temperature.

3.2 OPTICS

The optics of ARPESH includes a telecentric radiometric optical system with a rectangular reflecting primary, a multipulse generator with Ronchi grating for generating pulses to serve as an incremental position encoder and a single pulse generator that provides a precise position reference (fiducial pulse) to define the start position of the active forward mirror scan.

3.2.1 RADIOMETRIC OPTICS

The design of the infrared radiometer optical subsystems closely follows the design described in the various progress reports submitted. An original design which was based on a refracting system had to be abandoned because the index of refraction changed too much over the temperature range. A reflecting telecentric optical system is used with a 6" focal length spherical curvature reflector of rectangular shape with dimensions of 48 mm x 56 mm.

The field of view for each detector in this optical configuration is defined by the dimensions of the field mask located in the focal plane of the optical system. The field of view and relative position of the detectors is shown in Figure 3.1-3.

3.2.1.1 CONSIDERATIONS LEADING TO CHOICE OF SPHERICAL REFLECTING OPTICS FOR RADIOMETER SYSTEM

The originally proposed design was based on use of a germanium objective lens for the ARPESH radiometric optics.

A determination of the defocusing produced by the wide temperature range indicated a serious problem in the radiometer optical system if one uses a refracting system (e.g. germanium

lens).

Using the data of Cardona et al (J. Phys. Chem. Solids, 8, 204-6, 1959) for $dn/n\ dT = 6.9 \times 10^{-5}/°C$, we find that the +55°C temperature excursion from ambient produces a shortening of the focal length of 0.5 percent, or 0.038 inches.

The extension of the focal length due to increase in radius of curvature and thickness is only 0.002 inches, so the net effect is that the focal point moves toward the lens by 0.036 inches.

If the objective lens and detector are separated by any material having a positive temperature coefficient, the effect of the latter increases the malfocus between the two. Aluminum, for example, produces an added displacement of 0.009 inches, for a total relative focal shift of 0.045 inches. With an f/3 system, the "smear" due to this effect is 0.015 inches, or 2 milliradians. This corresponds to nearly four times the allowable spot size.

In view of the fact that no direct information was found to conclusively indicate what the temperature coefficient of the refractive index for germanium is at 15 microns we solicited help in this area from NASA/LRC personnel. A literature search showed that no direct and reliable data is available for $\frac{dn}{ndT}$ of germanium at 15 microns. (It would probably be a good thing to initiate a program to conduct the necessary measurements.) There is considerable disagreement in $\frac{dn}{ndT}$ among the measurements reported by researchers such as Cardona, Lukes, Rank, Collins and others, most of whom made their measurements in the 2 - 5 micron region. If we used the Collins

data, the only program that shows dn/ndT figures to 12.35 microns dn/ndT = 12 x 10^{-5}/°K our results would be even worse than reported above for the Cardona figure of 6.9 x 10^{-5}/°K. With these parameters the degradation in blur circle over the temperature extremes considered would be as shown in the attached Figure 3.2.0.1 This is clearly an unacceptable blue circle degradation.

A number of compensating means were explored, including bimetal construction, "oil can" mechanism, etc. The solution finally settled on, however, as being the more reliable was to use a spherical mirror for producing the horizon image. If this mirror is made of the same metal as that used to separate it from the field mask-detector assembly, the system is completely self-compensating with respect to temperature.

The attached spot diagrams indicate that the image quality obtained with the spherical mirror is well within the allowable dimension. (Figures 3.2.0.2 to 3.2.0.6)

The change from a refracting to a reflecting system has several effects, which can be enumerated as follows:

a. The entrance pupil of the system remains in the vicinity of the scanning mirror, although the mirror is moved to opposite ends of the instrument.

b. The field mask-detector assembly is also as close as feasible to the scanning mirror, and requires that the latter be perforated. Therefore, there is a small obscuration in the center of the pupil.

c. The (three) exit pupils of the system are at the detectors, and the entrance pupil is defined by their three (coincident) images formed by the field lenses and imaging mirror.

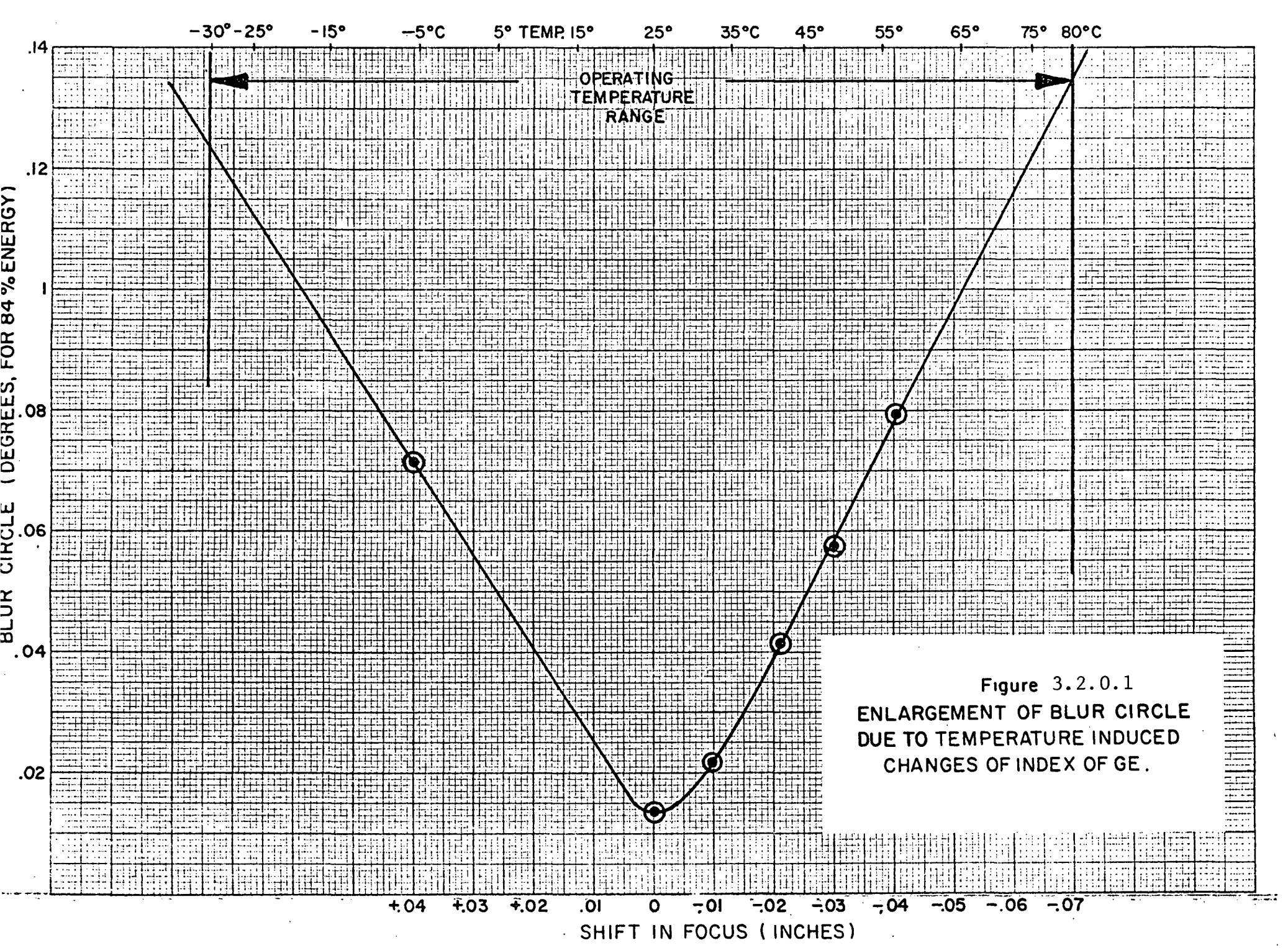

Figure 3.2.0.1

ENLARGEMENT OF BLUR CIRCLE DUE TO TEMPERATURE INDUCED CHANGES OF INDEX OF GE.

FIGURE 3.2.0-2 RADIOMETER - OPTICS

KNIFE EDGE SPOT DIAGRAM

206 rays

12 x 12 mm obscuration

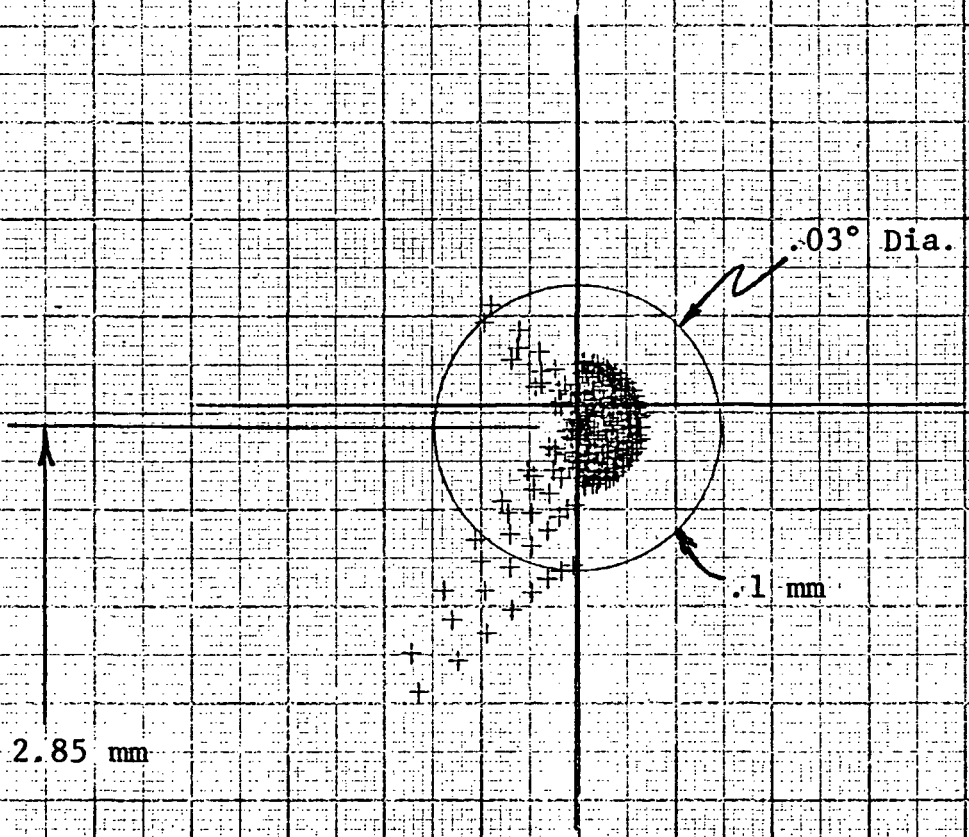

EFL = 190.00 mm

BFL = 190.12 mm

θ = .015 rad. = .857°

CHIEF RAY HEIGHT -2.8568 mm

FOCUS SHIFT 0.000000

1 INCH = 0.066500 mm = .02°

FIGURE 3.2.0.3

RADIOMETER - OPTICS

KNIFE EDGE SPOT DIAGRAM

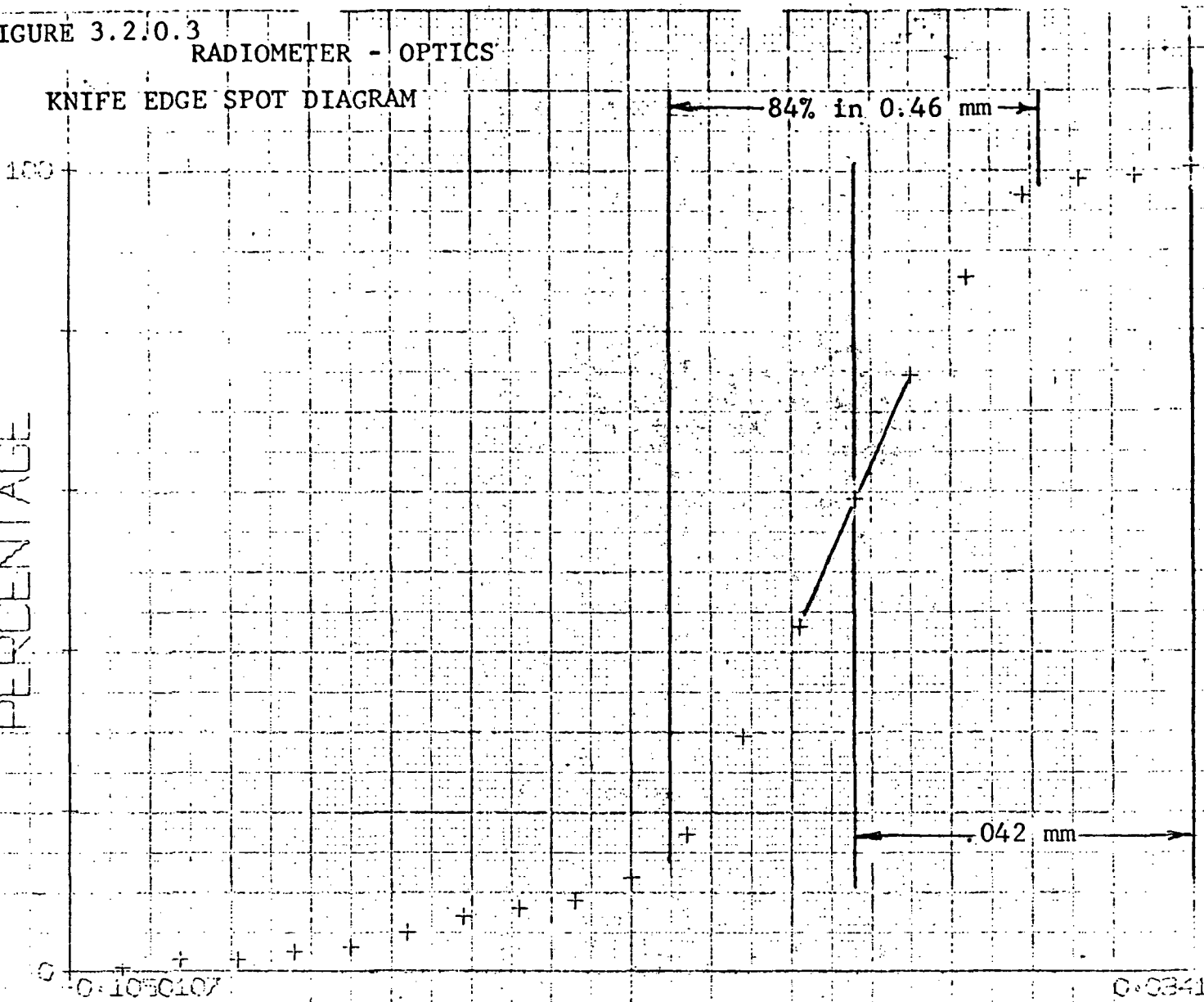

θ = .015 rad.

CHIEF RAY HEIGHT	-2.85568
FOCUS SHIFT	0.000000
ORIENTATION ANGLE	0.0

FIGURE 3.2.0.4 RADIOMETER - OPTICS

KNIFE EDGE SPOT DIAGRAM

206 Rays

12 x 12 mm Obscuration

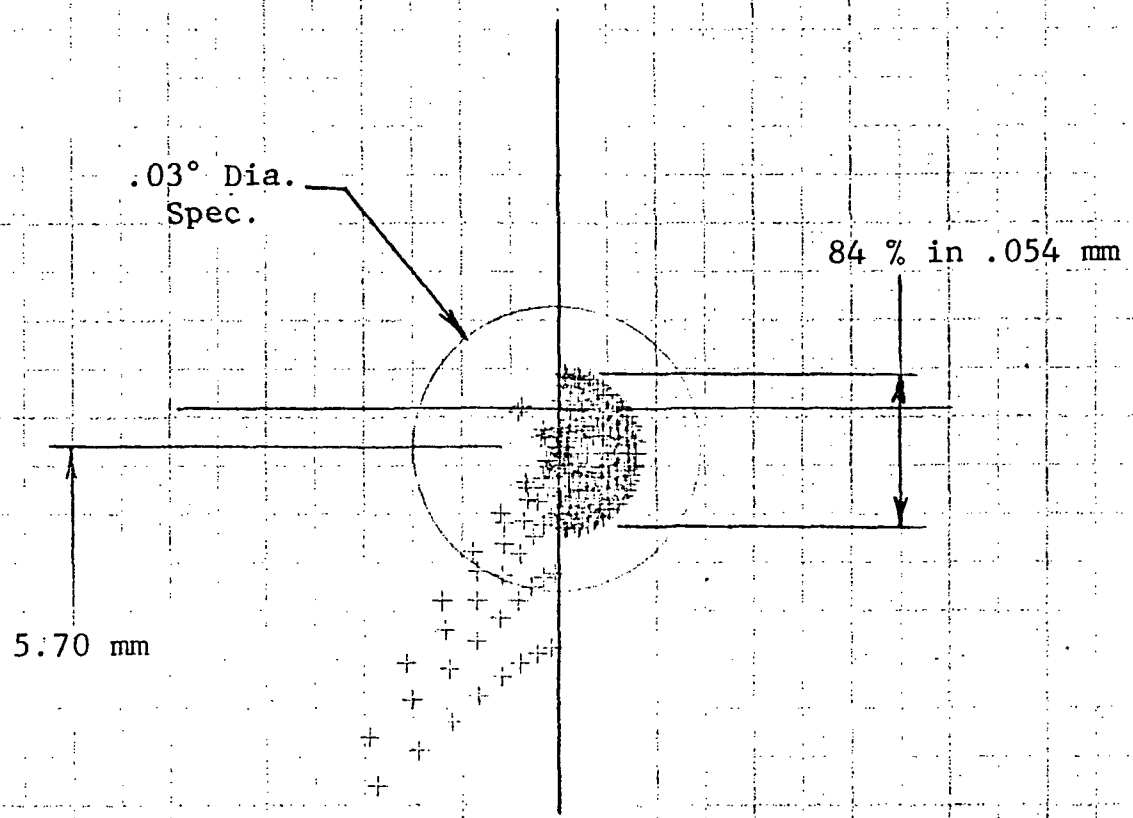

EFL = 190.00 mm
BFL = 190.12 mm
θ = .03 rad. = 1.71°

CHIEF RAY HEIGHT -5.7122 mm

FOCUS SHIFT 0.000000

1 INCH = 0.066500 mm = .02°

FIGURE 3.2.0.5
RADIOMETER - OPTICS
SPOT DIAGRAM
EDGE - "B" FIELD

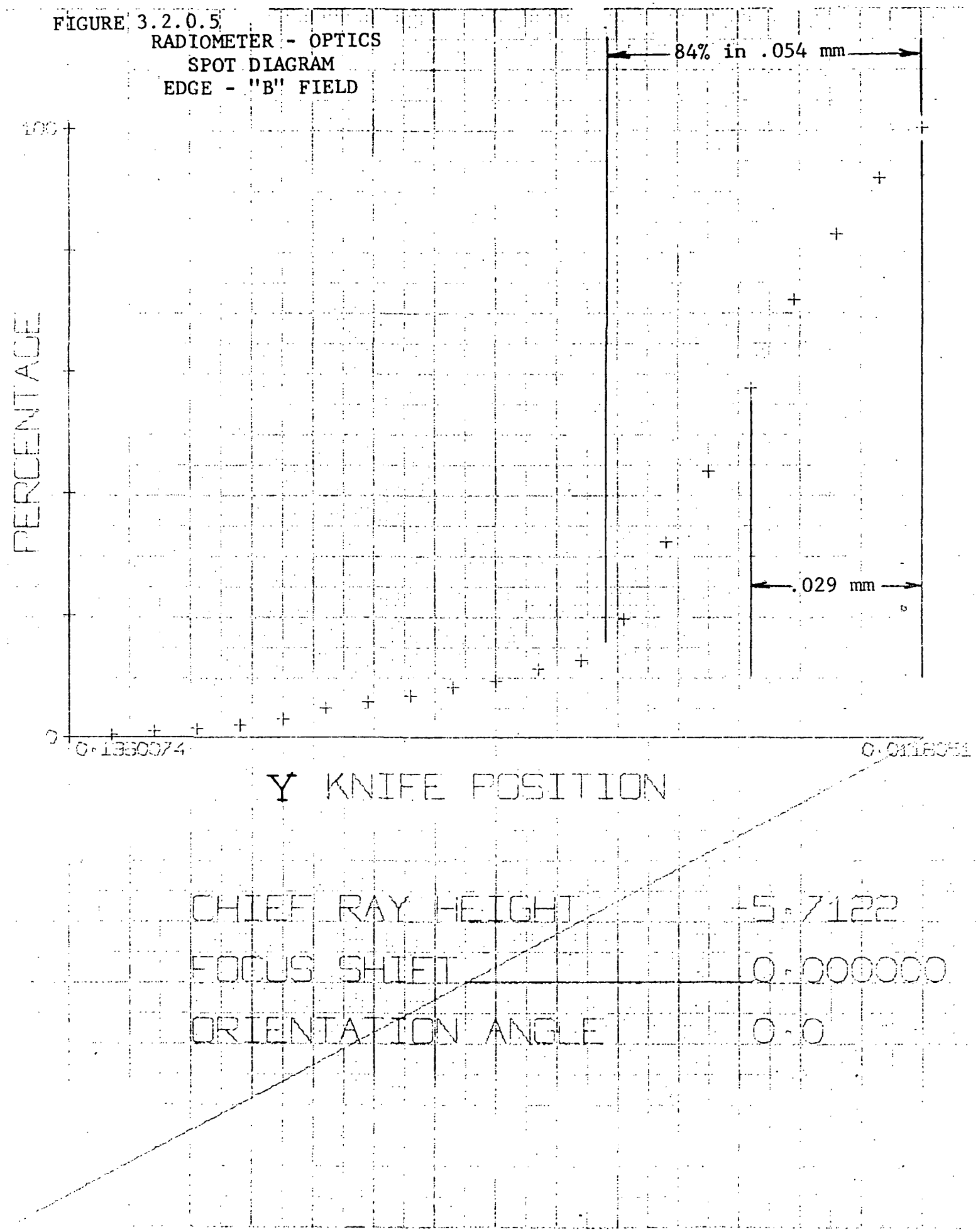

FIGURE 3.2.0.6

RADIOMETER - OPTICS
SPOT DIAGRAM
EDGE - "B" FIELD

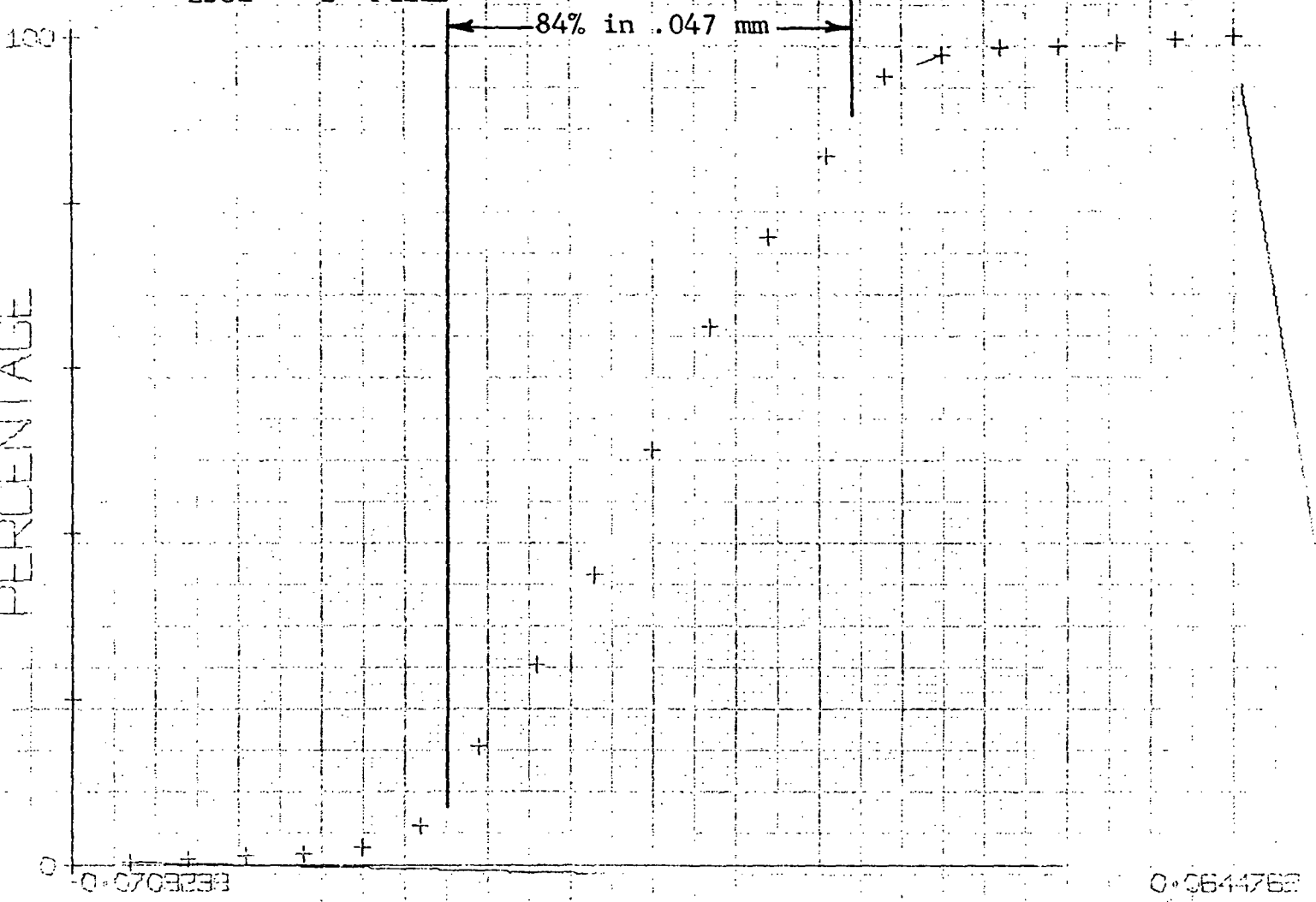

X KNIFE POSITION

CHIEF RAY HEIGHT +5.7122

FOCUS SHIFT 0.000000

ORIENTATION ANGLE 0.0

d. Since the entrace pupil as "seen" by the three field lenses is effectively at infinity (as imaged by the imaging mirror) it is no longer necessary for the field lenses to be tapered. This will result in a simpler construction for both the lenses and their housing.

e. The elimination of the objective lens reduces the total thickness of germanium in the system, thus increasing and "flattening" the transmittance.

f. The new configuration permits a mounting arrangement for the single-pulse generator which is self-compensating with respect to misalignments between the radiometer fields of view and the timing of the start pulse. This is discussed more fully in a later section.

g. The spot diagrams reveal that the image quality at the edges of the field of view is essentially the same as on axis, even in a flat focal plane. Therefore, the field mask will consist of a single flat mask in the focal plane. It will be in contact with the front surface of the filter.

For all of these reasons, it is felt that the mirror system represents an appreciably better system than the refracting one.

3.2.1.2 OPTICAL THROUGHPUT

The CO_2 band filter is located just in front of the field defining mask and has a spectral transmission as shown in Figure 3-2.2.

The total optical throughput was originally estimated to be 0.3. Actual measurements show somewhat poorer performance, mainly due to the CO_2 band filter itself, resulting in a total throughput of approximately 0.22.

The various contributors to the total optical throughput are tabulated in Section 3.2.2.

FIG. 3-2.1 Optical System Data Sheet

SYSTEM DESCRIPTION: HORIZON SENSOR

DATE 11-23-71

SURF NO.	mm. RADIUS & TOL in.	CC or CX	mm. CLEAR APER in.	mm. THK & TOL in.	MATERIAL	SURF. CODE	IRREG (fr.)	COATING TYPE	COATING THK	COATING λ(μ)
			X Y							
1	SCANNING FLAT (PUPIL)	-	48.00 × 56.00 (1.89 × 2.205)			80-50	4	Au		
				141.00 NOM (5.551)	air					
2	303.00 ± 1.00 (11.929)	CC	59.50 × 58.40 (2.343 × 2.299)			80-50	4	Au		
				151.07 ★ (5.947) NOM	air					
3	ALL FIELD MASKS ∞	-	4.57 (.180) ★★			80-20	20	FILTER		15
				1.00 (.0394)	Ge FILTER SUBSTRATE					
4	∞	-	4.67 (.184)			80-20	20	FILTER		15
				.50 (.020)	air					
5	4.64 ± .03 (.18268)	CX	5.10 ★★★ (.201)			80-20	10	AR	-	15
				6.07 ± .03 (.239)	Ge 30 Ω CM					
6	∞ ±10 FR	-	.77 (.030)			50-20	10	-	-	-
				—	MYLAR					
7	DETECTOR		.50 × .58 (.020 × .023)					-	-	-
8										

REMARKS: ★ SHIM PRIMARY TO ±.12 MM FOR FOCUSING

★★ 3.029 FOR X, 3.424 FOR Y DIRECTION

★★★ 3.606 " 4.08 " "

SURFACE 5 thru 7 IS FOR ONE OF THREE ADJACENT LENSES WITH PARALLEL AXEES, SPACED 3.656 (.14394) ON CENTERS

Fig 3-2.2
Spectral Response of CO_2 Band Filter

OCLI OPTICAL COATING LABORATORY, INC.

2789 Giffen Avenue
Santa Rosa, California
Telephone (707) 545-6440

SPECTRAL PERFORMANCE

DATA IDENTIFICATION

OCLI W/O 14-5800-760
Run No. 4RS-543-086

Serial No. P/N 20.6201-2013-1-B

SAMPLE IDENTIFICATION

Filter Type BANDPASS
Material GERMANIUM

Configuration 1" X 0.040"
WITNESS

INST. OPERATING PARAMETERS

5-37

- [x] CARY 90
- [ ] CARY 14
- [ ] IR-12
- [ ] IR-4

Resolution 1.5 cm⁻¹ SH.T.
Scan Speed 0.3 cm⁻¹/SEC.
Response 0.3
Aperture 0.8"
Expansion 0-100

- [x] Percent Transmission
- [ ] Percent Reflection
- [ ]

TEST CONDITIONS

Temp. ≈25°C Angle 0°

Analyst DKG Date 4-12-72

PAGE ..... of .....

- [x] Wavenumber
- [ ] Wavelength in cm⁻¹

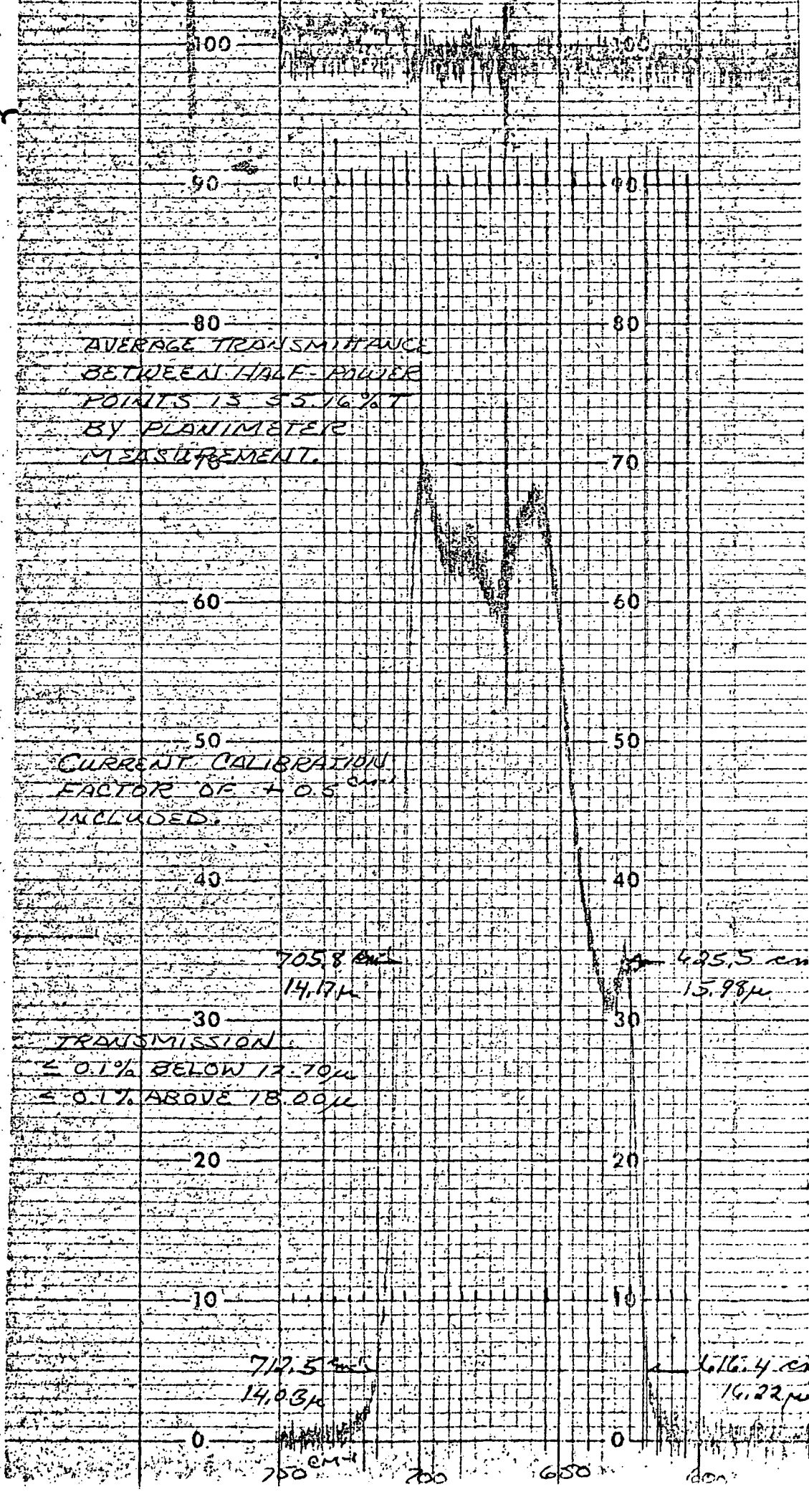

3.2.1.3 FILTER CHARACTERISTICS

The filter transmittance is shown in Figure 3-2.2. The values of transmittance vs wavenumber were tabulated from the curve, shown in Figure 3-2.2, and key points were compared with the specification. These key features, with the specified and measured values, are listed in Table 1.

TABLE 1

Item	Spec.	Measured
Peak Transmittance	$\geqq$ 65% absolute	69%
Ave. Trans. between half-power points	$\geqq$ 55% absolute	55.6%
Cut-on λ, 50% of peak	14.23 ± 0.14μ	14.13μ
Cut-on λ, 5% absolute	50% λ-0.10 to 0.30μ	50% λ-0.17μ
Cut-off λ, 50%of peak	16.08 ± 0.16μ	15.97μ
Cut-off λ, 5% absolute	50% λ+0.08 to 0.31μ	50% λ+0.23μ

The data for even-valued intervals of wavelength were derived by interpolation between the wavenumber values and are recorded in Table 2.

3.2.1.4 FIELD LENS TRANSMITTANCE

The field lenses were coated at BEC and a monitor sample was coated at the same time and its transmittance measured. Since the monitor sample was 2.54 mm thick, compared with the 6.00 mm average thickness of the field lenses, it was necessary to extrapolate from the measured data to allow for the added absorption in the field lenses. This was done graphically on

semi-log paper, using the zero thickness and 2.54 mm values to extrapolate to 6 mm. The extrapolated values are also listed in Table 2.

An additional modification needs to be made to allow for the fact that the monitor sample had one Ge/air interface, at which a reflection loss of 36% can be assumed. The actual reflection losses between the germanium and the detector occur at the Ge/Mylar and the Mylar/detector interfaces.

At an average angle of incidence of 15° at the Ge/Mylar interface, the calculated reflection loss for unpolarized radiation is 21% at the first surface and 10% at the second. (This is based on indices as indicated in the Design Report.) Net transmittance at the second surface is then 0.71, compared with 0.64 at the Ge/air interface on the monitor sample. A gain of 1.11 can, therefore, be anticipated.

Absorption in the 0.125 mil Mylar is represented in the third column of Table 2.

Finally, the reflectance of the scanning and focusing mirrors is predicted to be 0.98 throughout the region 14 to 16 microns.

Overall transmittance up to the detector, therefore, can be expressed as:

$$T = 0.98^2 \times 1.11 \int_{14}^{16} F\lambda \; G\lambda \; M\lambda \; d\lambda$$

Where $F\lambda$ = spectral transmittance of filter.

$G\lambda$ = spectral transmittance of monitor sample extra-polated to field lens thickness.

$M\lambda$ = spectral transmittance of 0.125 mil Mylar

Values of the above functions are included in the table from 13.7 to 16.3 microns for completeness, but integration is carried out only over the interval 14.0 to 16.0.

TABLE 2

λ	Fλ	Gλ	Mλ	PRODUCT
13.7	.005	.534	0.400	.0011
.8	.011	.542	0.440	.0026
.9	.025	.555	0.750	.0104
14.0	.066	.550	0.880	.0319
.1	.250	.559	0.900	.1258
.2	.580	.557	0.920	.2972
.3	.680	.552	0.930	.3491
.4	.655	.550	0.940	.3386
.5	.635	.541	0.940	.3229
.6	.640	.526	0.940	.3164
.7	.631	.504	0.940	.2989
.8	.625	.494	0.940	.2902
.9	.609	.480	0.930	.2719
15.0	.645	.433	0.925	.2583
.1	.660	.440	0.920	.2672
.2	.665	.442	0.920	.2704
.3	.626	.425	0.915	.2434
.4	.550	.400	0.910	.2002
.5	.455	.393	0.910	.1627
.6	.375	.395	0.905	.1341
.7	.330	.402	0.900	.1194
.8	.320	.410	0.900	.1181
.9	.335	.415	0.900	.1251
16.0	.310	.430	0.900	.1200
.1	.115	.432	0.900	.0447
.2	.050	.440	0.895	.0197
.3	.015	.448	0.895	.0060

$F\lambda G\lambda M\lambda = 4.581$

Ave. $= 4.581/20 = 0.229$

T $= 1.023.0229 = 0.234$

The integral in the expression for T was evaluated using Simpson's rule, with the result that average transmittance between 14.0 and 16.0 microns is found to be 23.4 percent.

Absorption by the detector, which was discussed in the design report, is not considered in the above calculation.

3.2.2 MULTI-PULSE GENERATOR OPTICS

In order to permit precise determination of the angle of the scanning mirror at the position where the horizon has been located, an optical system was designed as an incremental encoder. A series of pulses are generated as the scan mirror movement causes a bar pattern generated by a Light Emitting Diode in conjunction with a Ronchi reticle to be swept across a stationary reticle and detected by a silicon photocell. The collimated image of the Ronchi grating (reticle) reflected from the edge of the scanning mirror is reimaged on another grating located in front of an optical system associated with the silicon detector. The image of the reflected bar pattern moves across the grating at the detector; as it does so the detector generates a series of pulses that are later converted into an accumulated count for readout of the angle at which the horizon is located. The optical components of the Multi-pulse generator are described below and are best understood in conjunction with Figure 3-2.3.

3.2.2.1 OBJECTIVE LENS

A choice of grating spacing of 1000 lines per inch indicated a focal length of 14.55 cm in order to generate a pulse every 0.01 degrees. An aperture diameter of 1.91 cm was selected as a good compromise between aberration correction and diffraction limitation. A three-element design was generated,

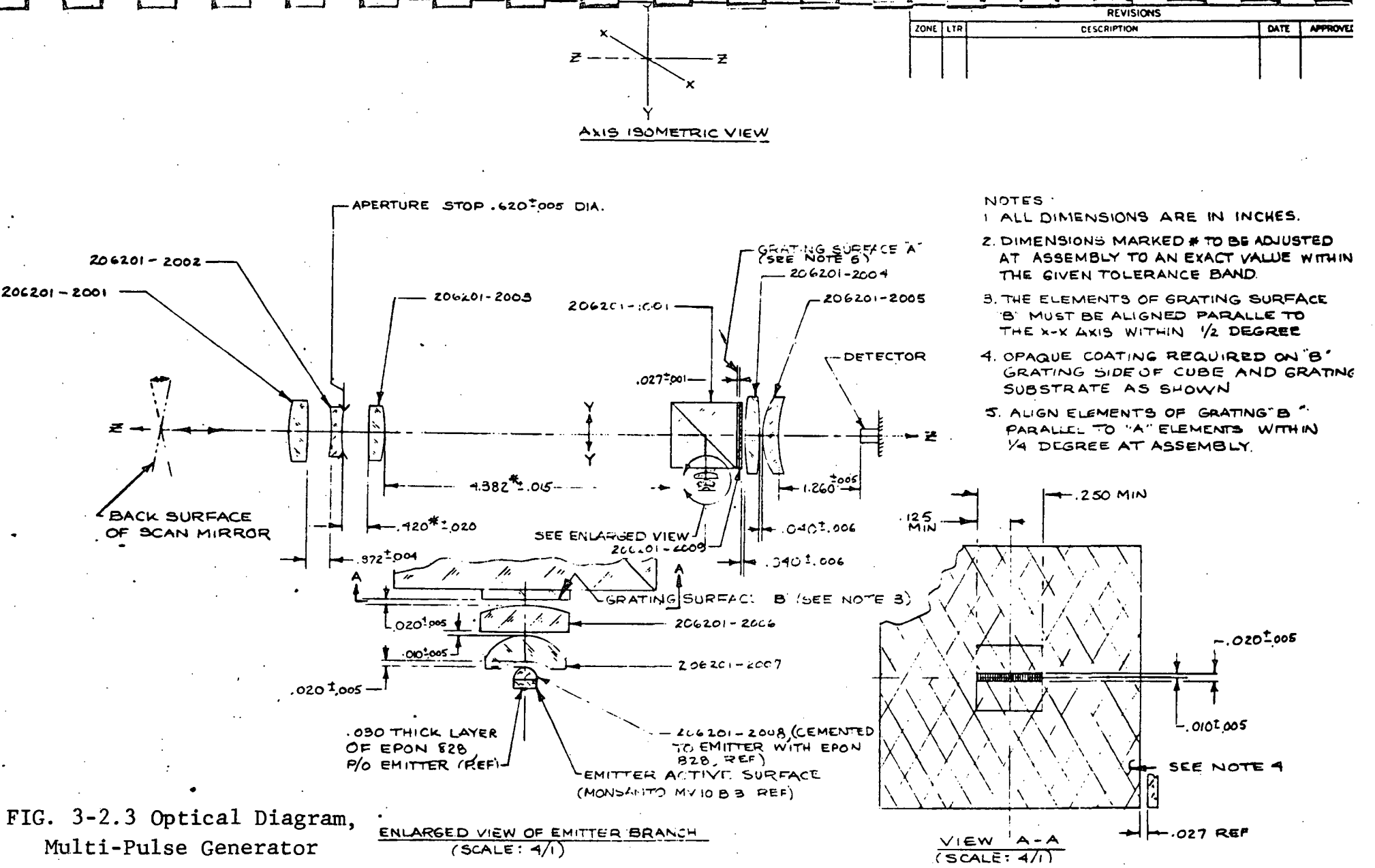

FIG. 3-2.3 Optical Diagram, Multi-Pulse Generator

which is diffraction limited. It is documented on the Optical Data Sheet, shown as Figure 3-2.1. The parameters were obtained by a computer analysis based on spherical and chromatic aberrations, astigmatism and distortion. All aberrations were reduced to one-fourth wavelength or less (double passage) and the predicted modulation in the image is 25-30% after allowing a reasonable tolerance for degradation due to imperfect surfaces and other errors. The lens curvatures were adjusted slightly to conform to existing tooling for economy in manufacture.

3.2.2.2 CONDENSER LENS

After reviewing available light-emitting diodes for illuminating the source grating a Monsanto type MV 10 B3 LED was selected, partly on the basis of past experience with these and related sources. This source is provided with a polymer lens to concentrate the emitted light into a lobe of restricted angular spread. Such plastic lenses have a poorly controlled shape, so that the light distribution is subject to considerable variation. A practice and method has been developed of sawing off this lens and replacing it with a glass lens of more precisely defined characteristics. The condensing system, which spreads the light uniformly over the reticle and images the source on the objective lens, uses existing tooling to a maximum degree. The Optical Data Sheet records the design parameters. It was found to be impossible to illuminate the corners of a reticle 0.635 cm square, given the other parameters such as source size and objective lens aperture, so a circular area 0.635 cm in diameter was used instead. Calculations have been made (see Section 3.3.1.5.1)of light intensity at the detector, indicating a background-to-noise ratio of approximately 10^4, using this circular reticle area. Later considerations indicated the

importance of rotationally aligning the source reticle so that the bars in its image are parallel to those in the detector reticle. This alignment is less critical if the line images are relatively short. It was decided, therefore, to limit their length to 0.051 cm, decreasing the light by about one order of magnitude, which still allows an adequate signal-to-noise ratio.

3.2.2.3 FIELD LENS SYSTEM

In view of the availability of detectors large enough to cover the entire one-inch span of the detector reticle, some effort was directed at deciding between a large detector mounted directly behind the reticle vs a smaller detector using a field lens to concentrate the light. The larger detectors, commercially readily available, are of the Schottky barrier type, in contrast to the diffused barrier type. Consideration of the required temperature span indicates that the Schottky barrier type is unsuitable. The diffused barrier type is not available in the large size required for focal plane mounting. A tentative spec was developed, therefore, for a diffused barrier detector based, to as large an extent as possible, on a commercially available type, viz. United Detector Technology type PIN-6D. A field lens system was designed for coupling the 2.54 x 0.635 cm area with such a detector; this is recorded in a third Optical Data Sheet. The lens design is also based on existing tooling and test plates.

3.2.2.4 THERMAL ANALYSIS

The most significant requirement for satisfactory function of the multi-pulse generator is the need of maintaining focus to assure the required modulation. For this reason, an analysis of the objective lens design was made to indicate the defocusing

caused by temperature excursions and by the absence of air in the optical path in the vacuum environment of space. The temperature effects result from dimensional and refractive index changes in the glass, and the pressure effect from difference in the refractive index between air and vacuum. The results of this study indicated that adequate focus can be maintained over the entire temperature range by using either fused quartz or Invar for the spacers between the objective lens cell and the focal-plane assembly. The focal shift induced by the loss of air is in excess of the tolerance, however, and some compensating means or procedure must be provided.

The multi-pulse generator layout is seen in detail in Figure 3.2.3.1. (Drawing B206201-4010)

The lens labeled as 2001 is normally focused optimally under standard pressure conditions. For operation in vacuum it is necessary to shorten the focal length, or screw the lens inward by 0.0061" for optimal focus in vacuum. An alternate procedure would be to fabricate a spacer and a shim of 0.0061" the total thickness being that required between the 2001 lens cell and the housing. In that case the lens would be screwed in completely for proper focus in air. For operation in vacuum the 0.0061" shim would be removed. However, such a shim was not made and the present procedure requires measurement of the lens cell position with respect to the housing and resetting for vacuum.

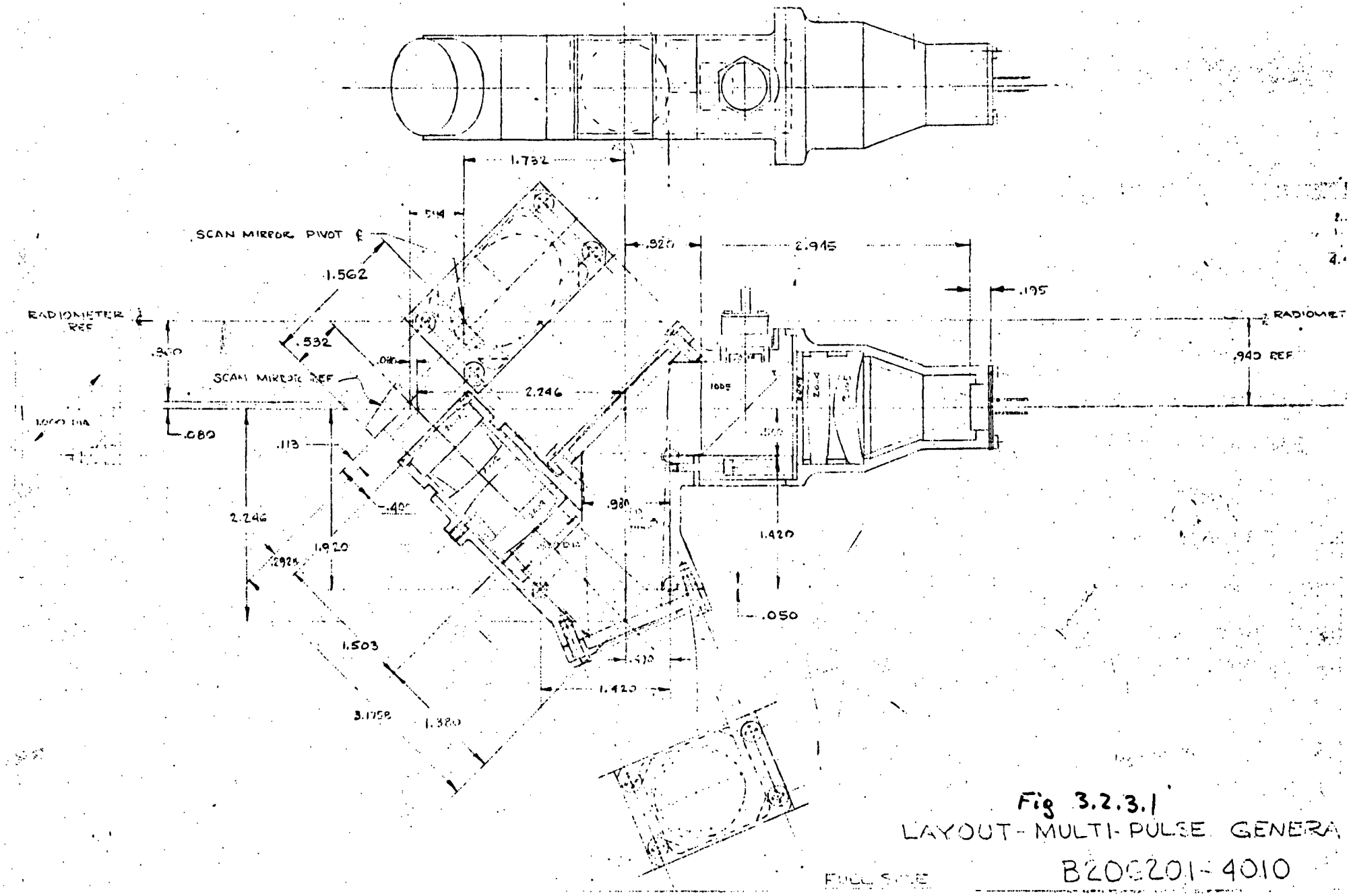

Fig 3.2.3.1
LAYOUT - MULTI-PULSE GENERA

FULL SIZE B20C201-4010

3.2.3 SINGLE PULSE GENERATOR OPTICS

An optical single pulse generator has been designed and built to provide a precisely defined mark (fiducial pulse) at the start of the forward movement of the scanning mirror. The design used is a modification of a miniature electric auto collimator made by Barnes Engineering Company, a description of this device is given in a brochure shown as Appendix A. Figure 3.2.4, shows a layout of the single pulse generator for the sensor head.

NOTES:

1. BOND MODIFIED LED & SILICON DETECTOR WITH ADHESIVE & TO BE SYMMETRICAL ABOUT PRISM SURFACE WITHIN .010. SEE OPTICAL DATA SHEET B206201-3003 FOR PROPER ORIENTATION

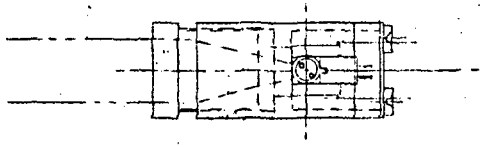

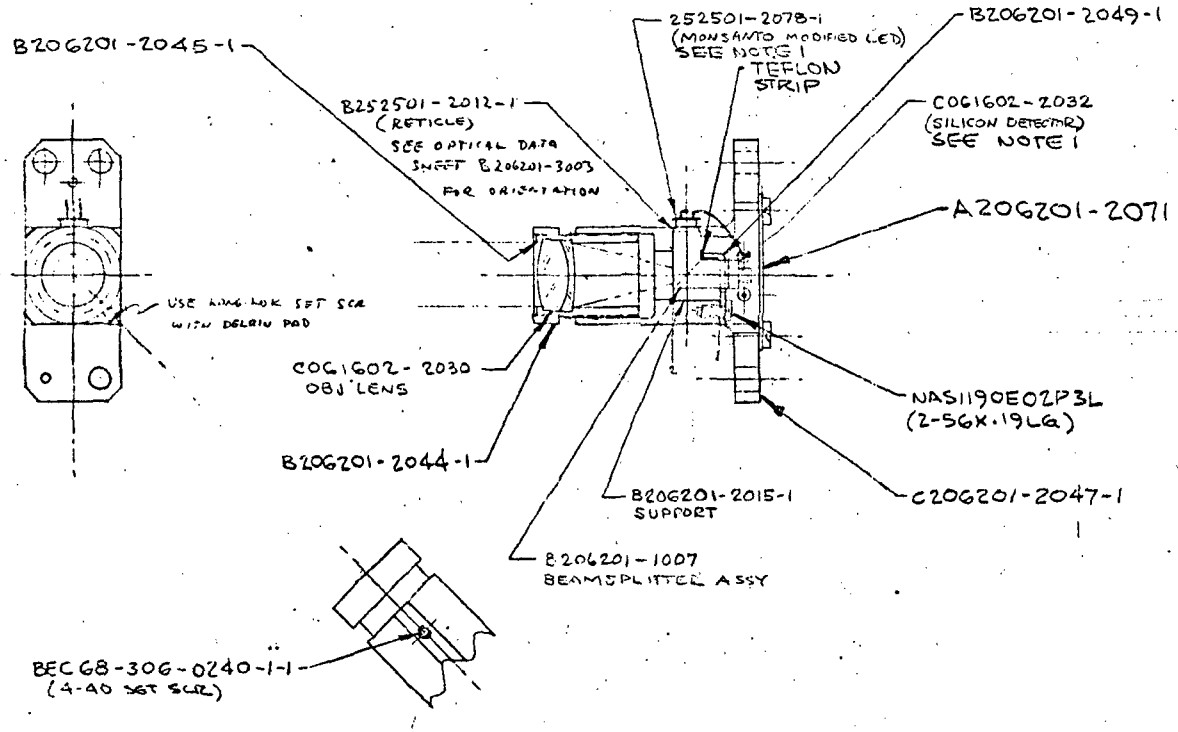

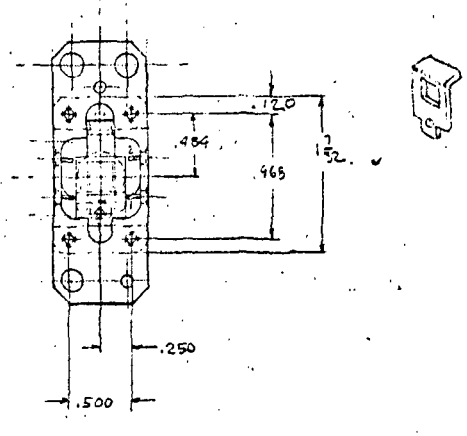

FIG 3-2.4 LAYOUT- SINGLE PULSE GENERATOR

SCALE 1:1

3-24-72

3.3 SYSTEMS ELECTRONICS, OVERALL SYSTEM

The horizon sensor system was built as two separate units: the sensor head and the auxiliary electronics package. The former includes all the circuitry needed to process signals representing target acquisition and scan mirror position determination at time of horizon crossing (locator) for a single head. The auxiliary electronics unit contains those circuits which would normally service 2, 3 or 4 heads used in a spacecraft attitude determination system. These circuits include the command inputs to the system (gain adjustments etc.), power supplies, scan synchronization drive, system condition-failure indicator, and locator angle position readout.

We will first describe the function of the principal modules or building blocks of the sensor and then discuss the interface and output data format.

3.3.1 SENSOR HEAD ELECTRONICS

Principal modules of the sensor head are:

1. Servo drive for scan mirror
2. Detector analog signal processing.
3. Zero crossing circuitry.
4. Single pulse generator
5. Multi-pulse generator
6. Auxiliary circuits such as:
    a) Sun Sensor
    b) Ambient Temperature Monitors
    c) Detector Temperature Controller
    d) Detector Bias Supply
    e) Fault Detection Circuits

3.3.1.1 SERVO DRIVE (NORMAL SCAN, CALIBRATE AND CAGE)

A 1-Hz generator located in the auxiliary electronics unit serves as a timing generator for driving the scanning mirror of the sensor head. The servo drive system causes the torquer to drive the motor forward linearly at a rate established by the current flowing through the torquer, and its physical properties. Thus driven, the mirror movement in the normal forward scan direction causes the single pulse generator to generate a fiducial pulse that also starts the counting of the multi-pulse generator which produces a chain of pulses accumulated up to a count of 1535 in about 750 msec of forward scan (7-1/2 degrees). The count is accumulated in a binary counter, which when it reaches a count of 1535, commands the return of the scan mirror rapidly to the opposite extreme scan position (in less than 250 msec). The torquer remains in this attitude until a new 1 Hz pulse is introduced whereupon it starts a new forward sweep. In this manner a continuous scan pattern is produced with a 750 msec forward sweep, a quick return to a negative position, about 2° mechanical below the neutral, unenergized position.

With the scan command in "off" position the 1 Hz signal is not introduced to the torquer drive and the scan mirror remains in a neutral position. On applying a "cage" command a constant positive signal is introduced in the servo drive. This results in the torquer driving the mirror to an extreme reverse position where the mirror comes to rest on a nylon pin stop that locks it in place and reduces the possibility of mirror vibration axially or laterally and thus prevents possible damage caused by possible high vibration levels during the spacecraft launch.

With the scan command in the "calibrate" position a constant negative signal is applied to the servo amplifier and torquer. This has the effect of driving the scan mirror forward for a total of +8° past a "space look" and onto a high emissivity copper reference block, whose temperature is monitored and which serves as a reference calibration radiance source. The analog outputs of channels A, B_1, and B_2, which are available on the panel of the auxiliary electronics will produce a pulse when the FOV's are scanned over the calibration plate to check the performance of the optics, detectors and analog electronics.

3.3.1.1.1 ANALYSIS OF SCAN SYSTEM

The scan mirror normally rotates through a relatively small angle (approximately 4 degrees). Therefore a very satisfactory method for supporting the scan mirror is by means of flexural pivots. These pivots are ideal for space application because they eliminate the lubrication problems associated with ball bearing type pivots. In addition, for this particular application they have an indefinite life with negligible hysteresis.

Their selection was based on the maximum launch shock vibration environment which was 100 g's @ .5 msec sinusoidal pulse and 12 g's sinusoidal vibration and 10 g's RMS random vibration. From past experience it has been estimated that in the worst case the mirror will "see" about 50 g's. Each of the flexural pivots will take about 1/2 of this dynamic load which is 50 x weight of the scan mirror (0.1 lb) or 1/2 x 50 x .1 = 2.5 lbs.

A preliminary selection was the 5006-800 Bendix flexural pivot 3/16" size, with a load capability of 2.6 lb.

In an effort to keep the weight low the scan mirror was made of aluminum.

The scan mirror center shift that can be attributed to the flexural pivot rotation presents no readout or pointing error. The readouts as well as the infrared optical system reflect collimated beams and are not influenced by the center shift.

During the launch phase and the vibration test (per MIL-STD-810), the scan mirror mechanism will be caged to insure the scan mechanism against possible damage and misalignment. The caging will be accomplished by energizing the torquer such that it drives the mirror against the nylon stop. The amount of power required to cage the scan mirror is approximately 1 watt.

3.3.1.1.2 SCAN DRIVE

The scan cycle consists of 3.75° of scan motion @ 5°/sec followed by retrace. The total cycle time is 1 sec with 750 msec alloted for scan and 250 msec alloted for retrace. Figure 3.3.1.1, a computer output, shows this sequence.

SCAN CYCLE DESCRIPTION

The scan cycle starts with the servo controlled scan motion from some angular position just before the angular position (called 0°) that corresponds to the start of the scan. A servo system assures that the mirror will achieve uniform angular velocity of 5°/sec by the time it reaches 0° and will remain at that value until the mirror passes through the 3.75° position which corresponds to the end of scan. An end of scan pulse signals the beginning of retrace motion. It disables the servo control system and delivers a 150 msec voltage pulse (to the mirror drive) of predetermined amplitude which reverses the mirror with minimal undershoot of the 0° position. Following this motion, the output of an "and" logic circuit enables the servo system, thus completing the cycle. The inputs to this "and" circuit are one signal indi-

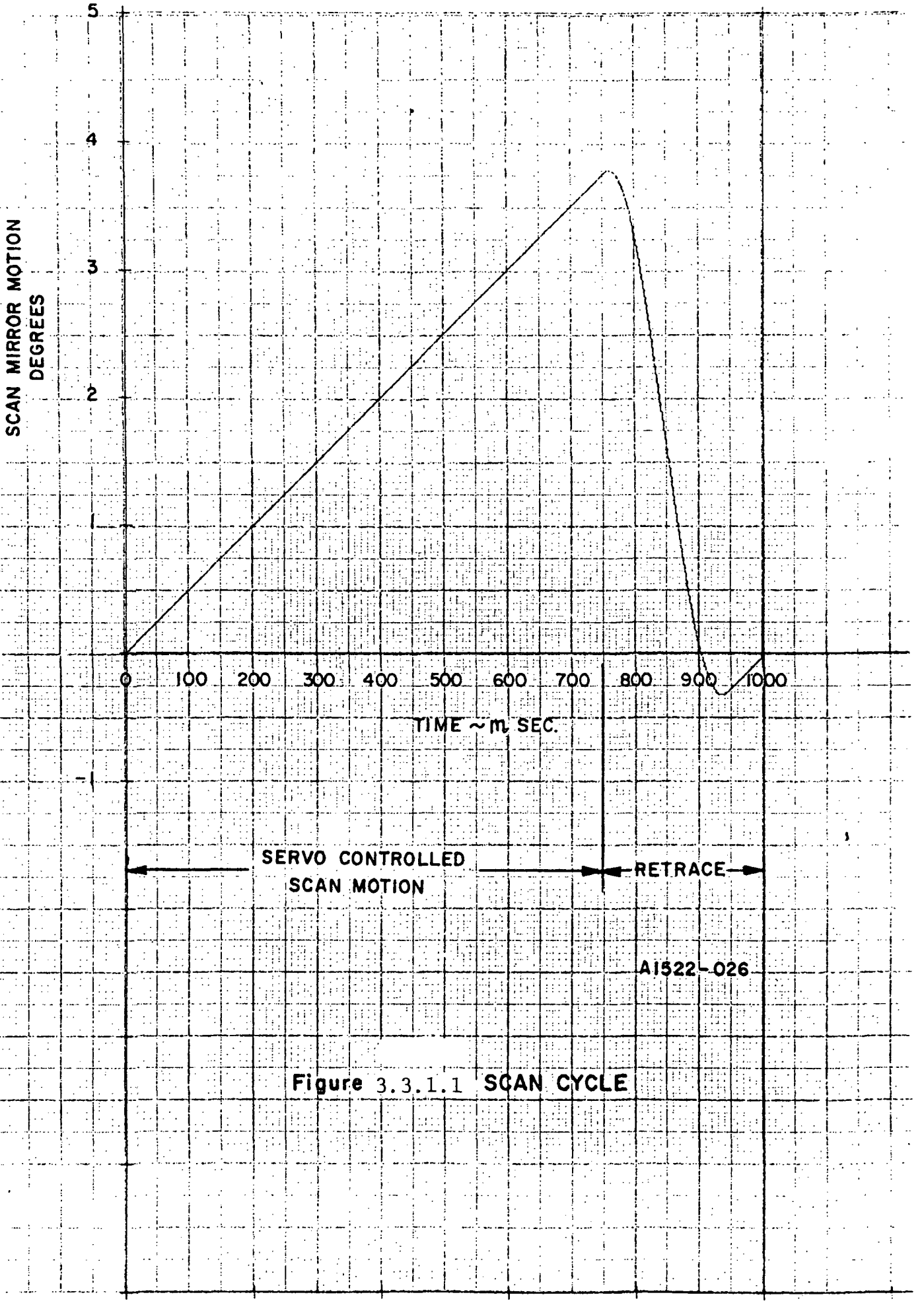

Figure 3.3.1.1 SCAN CYCLE

cating that the 150 msec pulse has been delivered and the remaining signal indicating that the mirror has undershot the 0° position. The transient start-up (i.e., starting the system from rest) is accomplished by a start-up pulse which enables the servo system taking one cycle to reach the proper position - time sequence.

SCAN DRIVE AND CONTROLS

SCAN SERVO SYSTEM

The scan motion is uniform in angular velocity and is controlled in a feedback loop as shown in the block diagram,

2.3-5

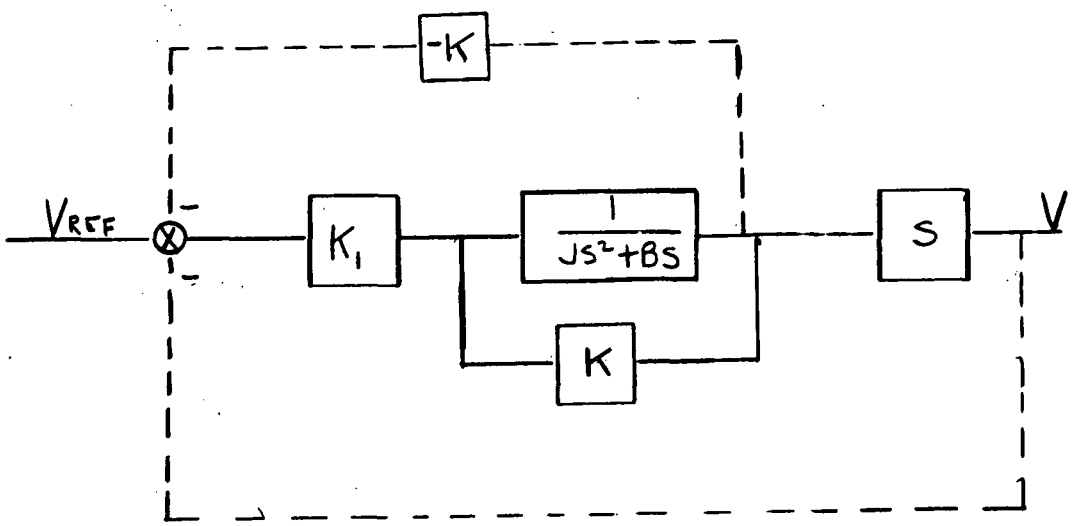

where the solid inner loop is due to the second degree dynamic system and

V = scan mirror velocity

Vref = reference velocity

J = inertia

B = viscous and electrodynamic damping

K = spring gradient of flexural pivots

The dotted signal flow lines and the blocks to which they are attached are the control functions. It should be noted that positive feedback (Kθ) is employed to negate the spring torque.

The overall transfer function is approximately

$$V/Vref = \frac{K1}{JS + B + K1}$$

and the steady state velocity is

$$V_{ss} = \frac{K1}{K1 + B} Vref$$

The time constant is

$$\tau = \frac{J}{B + K1}$$

A reasonable value for τ is 0.1 msec which gives ample velocity response with no stability or noise problems.

RETRACE DYNAMICS

The dynamics of the retrace are governed by the second order equation

(1) $$J\ddot{\theta} + B\dot{\theta} + K(\theta-\theta_o) = T$$

A typical torque deflection curve is shown in Figure 3.3.1.2 where J, B, and K have previously been defined and

T = torque

θ_o = quiescent scan mirror position

W_n^2 = K/J

For the system under consideration $B=10^{-3}$ inch-oz/rad/sec K=1.28 in-oz/radian, and J=.004 in-oz-sec^2. Division of (1) by J and ignoring the negligible effect of damping yields

$$\ddot{\theta} + W_n^2 (\theta-\theta_o) = T/J$$

$$\ddot{\theta} + W_n^2 (\theta-\theta_o + T/K) = 0$$

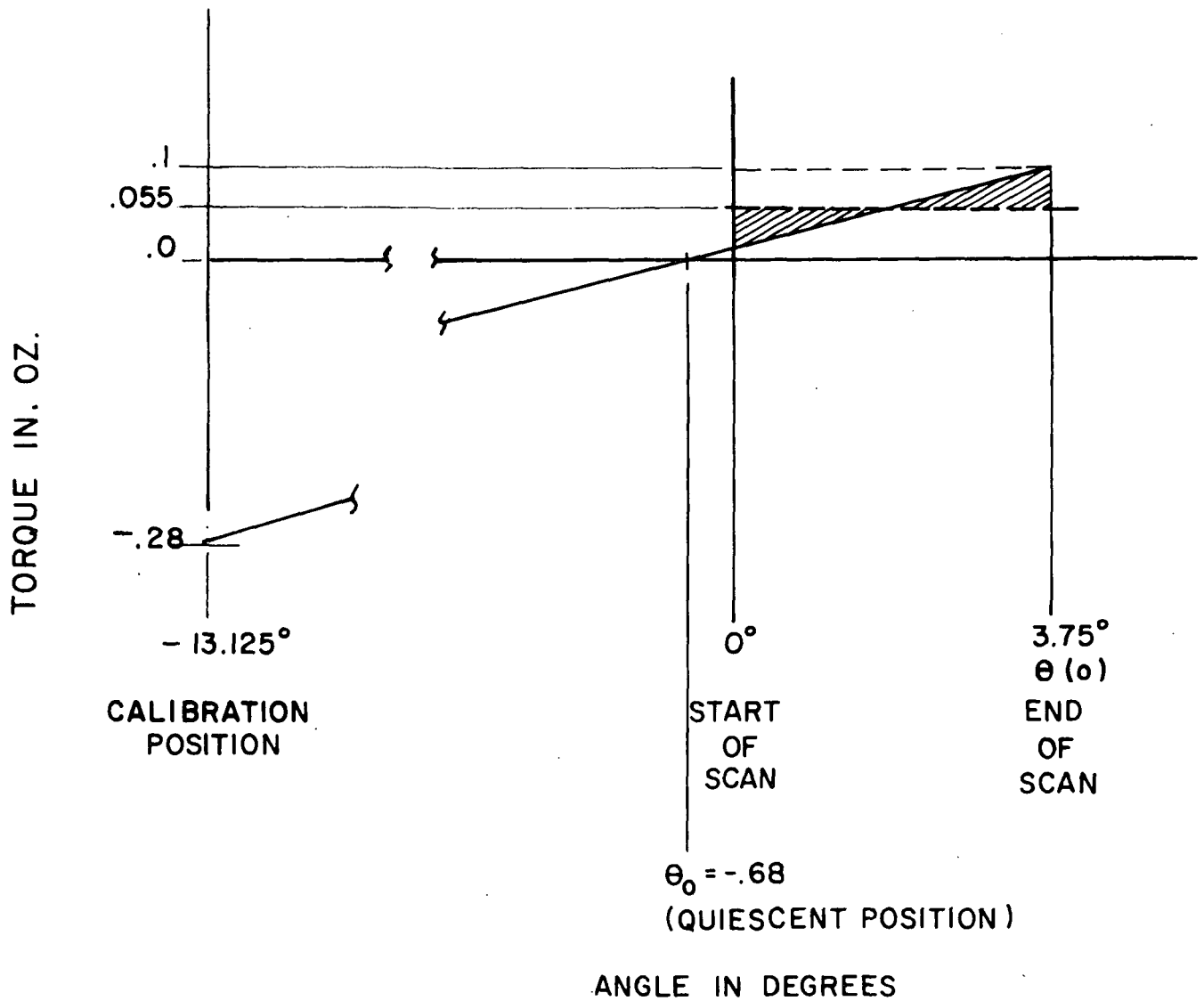

FIGURE 3.3.1.2 - SCAN MIRROR TORQUE / DISPLACEMENT CURVE

The solution to this equation for constant T, initial angle $\theta = \theta^{(\circ)}$ and angular velocity $\dot{\theta} = \dot{\theta}^{(\circ)}$

$$(\theta - \theta_\circ - T/K) = \frac{\theta^{(\circ)}}{\omega_n} \sin \omega_n t + (\theta^{(\circ)} - \theta_\circ - T/K) \cos \omega_n t$$

Where time = 0 corresponds with the end of the scan $\theta^{(\circ)} = .066$.

Figure 3.3.1.1 shows a more exact computer solution for the system. The ideal amplitude for T/K was determined to be .03 - $\theta_\circ$ corresponding to

$$T = 1.28\ (.03 \pm \theta_\circ) = .0484 \text{ in-oz} - 1.28\ \theta_\circ$$

Referring back to Figure 3.3.1.2, it is seen that during about 1/2 of the return motion the spring torque exceeds T and during the remainder T exceeds the spring torque. The crosshatched areas shown are the energies delivered to and from the system. In view of the low forward velocity these areas are almost equal.

It is desirable to make $\theta_\circ$ some small negative angle (i.e., make the rest position of the scan mirror somewhat less than the starting angular position) so that in the event of failure of the retrace power pulse, the system would naturally undershoot the 0° position, thus assuring that the controlled

scan motion can be accomplished with a penalty of increased cycle time. A value of θ = -.012 radian = -.68 degrees was selected which corresponds to a peak forward torque (at end of scan) of approximately

$$T = K\ (\theta(o) - \theta_o) = 1.28\ \left[.066 - (-.012)\right] = 0.1 \text{ in-oz}$$

Power - Torque Requirements

The average torque required during scan is approximately

$$Tav = K\ \left[\frac{\theta(o)}{2} - \theta_o\right] = \left[\frac{.066}{2} - (-.012)\right] 1.28 = .058 \text{ in-oz}$$

The retrace torque is (from above)

$$T = .0484 - 1.28\ (-.012) = .055 \text{ in-oz}$$

The overall average is about .057in-oz

The average power is proportional to T^2

Therefore

$$P = \frac{.057}{.33} \times 1400 = 42 \text{ mW}$$

Where .33 in-oz and 1400 mW correspond to the torque - power for the tentative torquer (TQSW-1P - Aeroflex), the peak torque requirement occurs during calibration which occurs about once per month when the scan mirror is rotated negative from 0° position to - 13 1/8°

The total torque is

$$T_{rev} = 1.28\ \frac{(13.125 - .68)}{57.3} = .28 \text{ in-oz}$$

The corresponding power is

$$P = \left(\frac{.28}{.33}\right)^2 \times \frac{1400}{1000} = 1.0 \text{ watt}$$

3.3.1.2 DETECTOR ANALOG SIGNAL PROCESSING

The signal processing channels include a low noise pre-amplifier, post-amplifier with frequency compensation (boost of high frequencies) and an active clamp circuit that clamps the analog signal to zero volts during retrace and at the scan mirror rest interval. The clamp is released when the forward scan is executed.

Summing inputs to a second post amplifier allows the B_1 and B_2 detector output signals to be combined into a single channel with a gain nominally 4-1/2 times greater (this represents the ratio "R" of the locator) than the gain of channel A to permit a zero crossover to occur for Channels A, and B_1 and B_2 at the desired "locator" position.

The gain of Channel B is 10,000 including a pre-amplifier gain of 100. Since two B channels are summed, the output of the B Channel is effectively raised by a factor of 20,000. Channel A has a gain that is nominally 4600. The gain of channel A is variable, and is established by the selection of the "R" gain ratio value to be discussed later.

3.3.1.3 ZERO CROSSING CIRCUITRY

The zero crossing circuit provides the timing pulse that holds the angle readout where the "locator" position has been identified. It consists first of an "allow" pulse that presages the advent of a zero crossing and next a voltage comparator that switches state upon receipt of two identical amplitude inputs and, finally, gating circuits that store and hold the count of the multi-pulse generator counter output to allow readout of the angle at which crossover was achieved.

The "allow" pulse is obtained by monitoring the output of detector A channel and generating a gating pulse when its value exceeds a preset threshold level indicating that detector A has encountered the earth's horizon. The "allow" pulse is used to enable a summing amplifier whose inputs are the analog signals of Channels A, B_1, and B_2. The resultant waveform is then applied to an input of the zero crossing voltage comparator, the output of which shows that a zero crossing has occurred at an appropriate location. (The "allow" pulse is included to prevent premature or false indications of a horizon crossing as in retrace, or during forward scan before the actual horizon crossing due to an identical noise output of the two channel amplitudes being compared.) The gated output pulse is used along with commands from the fiducial pulse generator to hold, and subsequently release, the count representing the "locator" angle.

3.3.1.4 SINGLE PULSE GENERATOR

The single pulse generator produces a fiducial pulse at the start of the forward movement of the scan mirror. The device is essentially a miniature electric autocollimator. A light beam created by a Light Emitting Diode (LED) is reflected

from a small reflecting surface attached to the scanning mirror and is received by a special dual silicon photo-diode equipped with a reticle that defines, with high precision, the position at which the returned LED beam crosses the photo-detector. The single pulse generator produces a pulse that serves as the reference or fiducial pulse, which signifies the start of the forward scan of the scanning system. A pulse is generated both in the forward and return portion of the scan, however, the photo-diode detector is made up of a series connected pair of diodes that generate oppositely phased pulses when a beam of light crosses each photo-diode in turn. This phase information is used to gate in only the pulse representing the correct "forwarding" fiducial pulse.

A departure was made from the planned 10KHz operated LED described in the proposal and the design report. In the final design the LED's are operated with DC excitation. It was felt that this approach is simpler and leads to fewer components which are also more dependable. The only justification for using a carrier type system would be to avoid possible stray ambient light problems. However, it was felt that the sensor housing serves as a shield and the pulse generators are almost fully enclosed so that stray light would not present any problems. In the completed unit this was proven to be indeed the case.

3.3.1.5 MULTI-PULSE GENERATOR

A scan angle readout system has been designed that employs an optical incremental pulse generation system. The optical system with its scanned Ronchi reticle was described in Section 3.2. The electronics processing must filter, amplify and limit the pulses generated by the silicon detector to produce a pulse train with individual pulses of constant amplitude and width as the scan mirror rotates.

The amplifier employs shunt voltage feedback. With a 5.6 meg Ω feedback resistor and a current responsivity of 0.5 A/watts for the silicon detector, together with the preamp we obtain a voltage responsivity of 2.8×10^6 volts/watt. The corner frequencies of the electrical filter are 800 and 1200 Hz, to pass the nominal pulse frequency which is 1000 Hz. The post amplifier has a gain of 500.

The signal level expected from the silicon detector, when it is illuminated by the modulated return beam from the LED, is calculated below.

3.3.1.5.1 CALCULATION OF SIGNAL LEVEL FOR MULTI-PULSE GENERATOR

The illuminance, E in the image plane = $\pi BT \sin^2 \theta'$

Where B = luminance of source

T = transmittance of system

θ' = half-angle of cone of beam converging on image. The irradiance,

$H = \pi NT \sin^2 \theta'$, where N = radiance

From Monsanto catalog, for MV10B3

L = 1000 ft. - lamberts

= 1000/930 lumens/cm^2 = 1.075 ℓ/cm^2

Since the source emits at 6700°A, where luminous efficiency = 0.032,

1.075 ℓ/cm^2 = 1.075/680 x 0.032

= 0.049 w/cm^2

If we assume source is Lambertian,

$N = 0.049/\pi$ w/cm^2 ster

For an aperture of 0.75 cm^2 and efl = 5.73 sin θ' =0.0654 We will calculate the energy on the detector after estimating optical losses.

Calculated below are the expected losses:

Assuming 24 air glass surfaces, coated so that the transmission at each interface is Tg = 0.995

Three mirror reflections @ R = 0.97

One beam-splitter, RT = 0.15

Then the transmission of the optical train is

$$T = 0.995^{24} \times 0.97^3 \times 0.15 = 0.12$$

and the irradiance,

$$H = \pi \frac{0.049}{\pi} \times 0.12 \ (0.0654)^2 = 2.5 \times 10^{-5} W/cm^2$$

Area of image = $(0.635 \text{ cm})^2 = 0.4 \text{ cm}^2$

Image is 50% blocked by source reticle, so

$$P = 2.5 \times 10^{-5} \times 0.40 \times 0.5$$

$$= 5 \times 10^{-6} \text{ watts}$$

Allowing for smearing of image, assume 3×10^{-6} watts is transmitted to detector

Assume Si detector, irradiated by ± 30° cone - then from n'y' sin θ = n'y' sin θ' (semi-diagonal)

$$\text{Or } y' = \frac{0.75 \times 0.093}{0.5}$$

$$= 0.14 \text{ in.}$$

$$= 3.6 \text{ mm}$$

$$a = (0.36 \text{ cm})^2 = 0.13 \text{ cm}^2$$

Assume the detectivity of the detector is

$D^* = 5 \times 10^{11}$ cm $Hz^{1/2}$ $watt^{-1}$ @ 0.9μ at shorter wavelength there is a degradation such that we can expect a lower $D^* = 0.83 \times 5 \times 10^{11}$ @ 0.67μ

$$D^* \approx 4 \times 10^{11} \text{ cm } Hz^{1/2} \text{ watt}^{-1}$$

Let $\Delta f = 2500$ Hz then the Noise Equivalent Power is found to be:

$$NEP = \sqrt{\frac{0.13 \times 2500}{4 \times 10^{11}}} = 4.5 \times 10^{-11} \text{ Watts}$$

And $S/N = \frac{3 \times 10^{-6}}{4.5 \times 10^{-11}} \approx 7 \times 10^{4}$

This is the expected Signal to Noise ratio of the multi-pulse generator neglecting any possible losses due to the Ronchi grating.

At image plane, $H \approx 2.5 \times 10^{-5}$ cm, so if detector is placed there, the energy density would be the same.

If a field lens is used with a 3.0 mm square detector,

$a = 0.13\ cm^2$

$P = 5 \times 10^{-6}$

$H_d = 5 \times 10^{-6}/0.13 = 4 \times 10^{-5} W/cm^2$

If we illuminate only a circular area of the source reticle, the image will be reduced to

$A = \frac{\pi}{4} (0.635\ cm)^2 = 0.31\ cm^2$

$P = 2.5 \times 10^{-5} \times 0.31 \times 0.5 \approx 4 \times 10^{-6}$ watts

Allowing for smearing of image, assume 2×10^{-6} Watts reaches the detector.

Using PIN-6 D detector manufactured by United Detector Technology Corp.

$a = 0.203\ cm^2$

$D^* = 2 \times 10^{12}$

$\Delta f = 2500$ Hz

Then the noise equivalent power is

$$NEP = \frac{\sqrt{0.203} \times \sqrt{2500}}{2 \times 10^{12}} = 1.1 \times 10^{-11} \text{ Watts}$$

and the system Signal to Noise

$$S/N = \frac{P}{NEP} = \frac{2 \times 10^{-6}}{1.1 \times 10^{-11}} \approx 2 \times 10^{5}$$

In practice considerably lower signal to noise ratios were obtained, believed to be due to unwanted reflections from the metallic Ronchi reticle.

In this case it was necessary to add another amplifier and low and high frequency cut-off RC filters in order to extract a signal of sufficient amplitude and signal-to-noise ratio to generate the desired timing pulses. The 1KHz signal generated by the scan mirror sweeping over the Ronchi grating is frequency doubled by electronic circuitry to 2KHz. This is used as the angle readout signal to identify the position of the scan mirror at the time the horizon is located.

3.3.6 AUXILIARY CIRCUITS

3.3.6.1 Sun Sensor

The radiant intensity of the sun is very high, also highly sensitive detectors are available at the peak spectral wavelength of the sun, therefore the sun sensor subsystem of ARPESH could be made quite simple, and require only elementary optics.

A pinhole camera type system was designed. A silicon diode is the detector and a simple mask in front of the detector defines the field of view to be sensed.

The sun sensor is located at the front edge of the sensor head, near the scanning mirror, as shown in the layout drawing, Figure 1-3. The field defining mask (see Figure 3-3.1) is located 12.5 mm behind the pinhole aperture and has dimensions of 2 mm x 1.25mm, so that the sensor subtends a field of view of about 9.5° x 5.8°. This covers a field of view about one degree larger on all sides than the infrared sensor field, and thereby warns of possible sensor errors due to the sun in the sensor field.

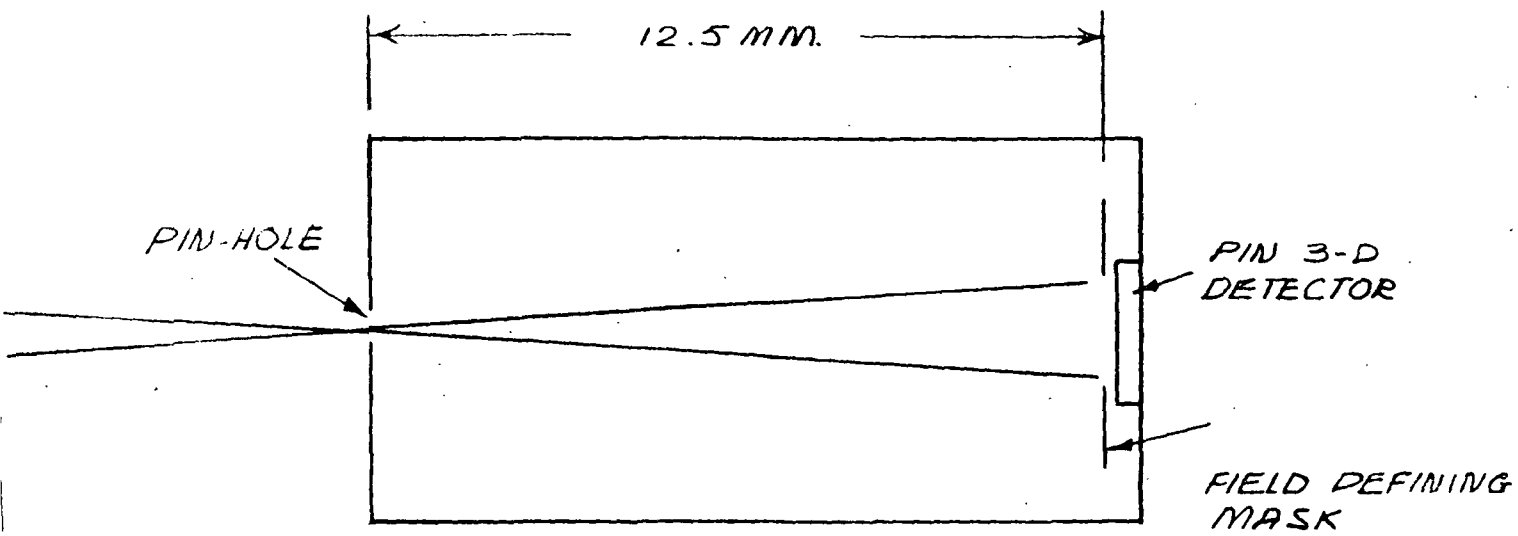

Figure 3-3.1 Sun Sensor Detector Diagram

The detector used is a United Detector Technology PIN 3D which has a 2.5 mm diameter. The pinhole is 1/2 mm in diameter.

The PIN 3D detector output feeds an LM 108 op-amp. Feedback sets the detector operating point near zero bias and lets the detector operate in current-mode. This results in linear operation and is most favorable for minimum responsivity variation over the wide operating temperature range.

The output of the sun sensor preamp feeds a voltage comparator lamp driver. A lamp on the front panel of Auxiliary Unit provides the logic output signifying presence or absence of the sun in the sensor's field of view.

3.3.6.2 Ambient and Calibration Patch Temperature Monitors

Identical circuits are used to monitor the ambient temperature of the low level electronics and the calibration patch. Each circuit consists of a single low-power operational amplifier, seven resistors, 2 small capacitors and a miniature precision thermistor.

Over the temperature of interest (-30°C to +80°C) the thermistor (RT) experiences a 90 to 1 change in resistance. As ambient temperature decreases, the thermistor resistance increases, supplying greater negative current to the summing junction of the amplifier. This causes greater positive current to flow through feedback resistor and drives the output positive. If ambient temperature increases, negative current to the summing junction decreases and the output of the amplifier becomes less positive.

Figure 3-3.2 shows the circuitry used for the temperature monitor circuits and Figure 3-3.3 is a calculated curve of voltage output as a function of temperature.

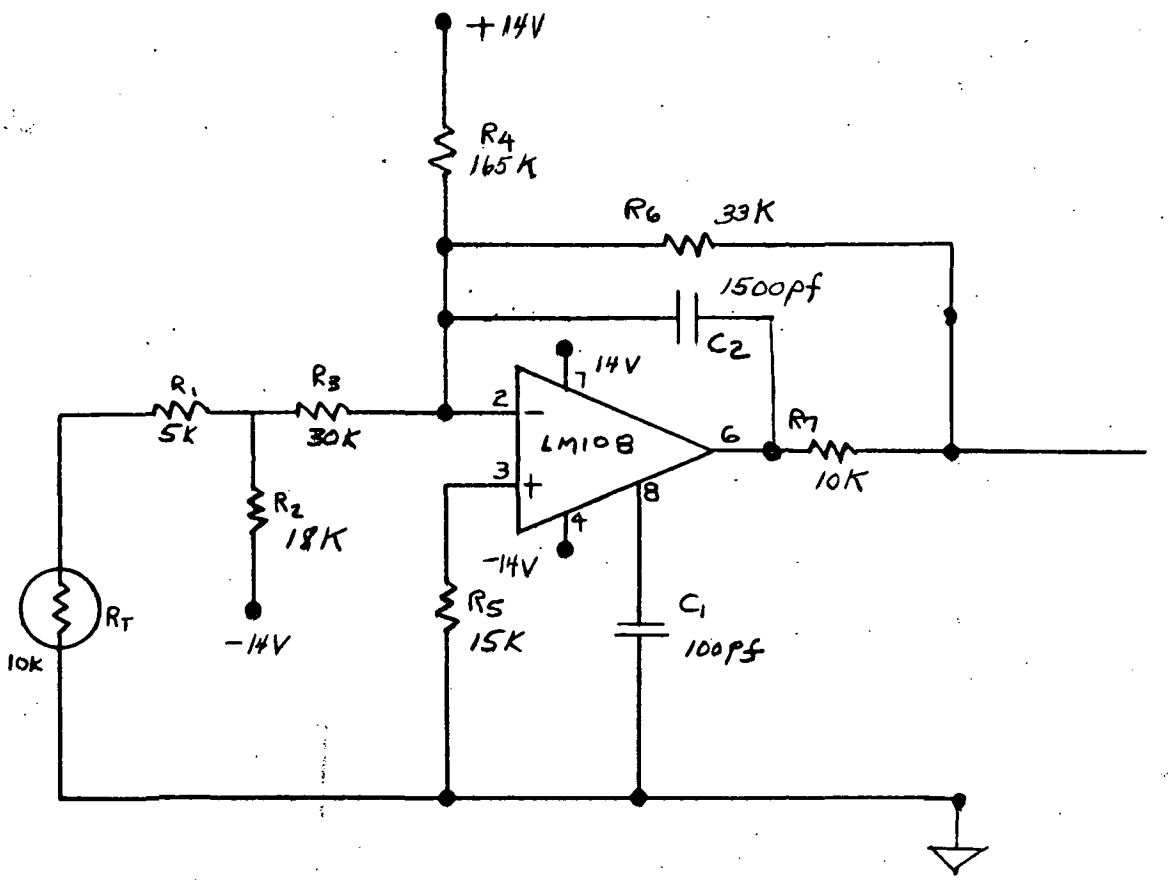

A23358

Figure 3-3.2 Temperature Monitor Circuit

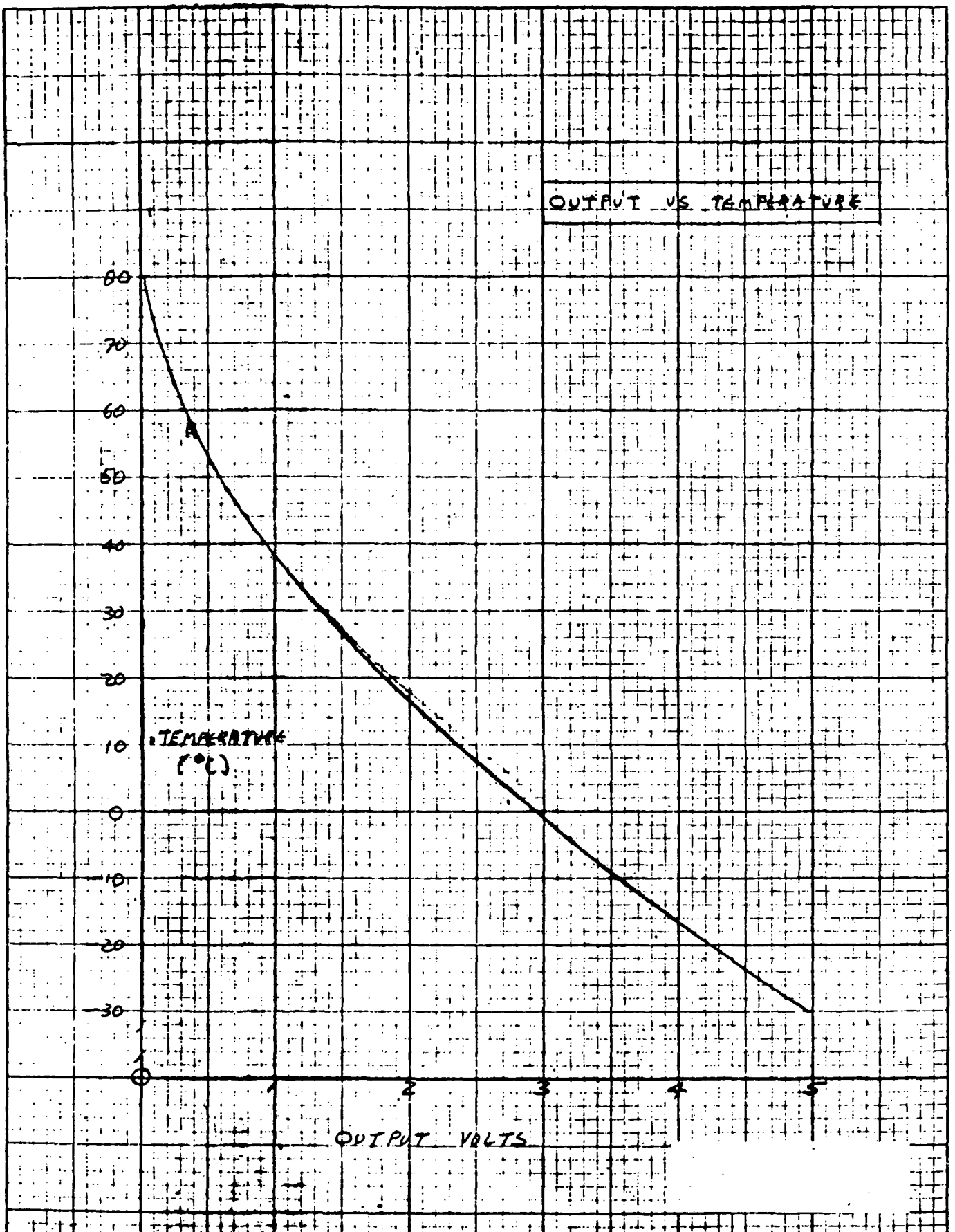

FIGURE 3-3.3 CALCULATED CURVE OF AMBIENT AND PATCH TEMPERATURE MONITOR

3.3.6.3 DETECTOR TEMPERATURE CONTROLLER

In order to minimize detector responsivity variation with temperature the detector assembly is heated whenever the ambient temperature drops below 10°C. This is accomplished by applying a current to a transistor, the case of which is in thermal contact with the detector assembly. The increased dissipation in the transistor provides the thermal energy to heat the detectors.

Ambient temperature changes are sensed by a precision thermistor. The output of the thermistor network is fed to an operational amplifier which provides the drive for the heating transistor. When the temperature drops below 10°C, the detector assembly is maintained at this temperature by the closed loop system formed by the heating transistor and thermistor.

3.3.6.4 DETECTOR BIAS SUPPLY

The detector bias supply provides a high voltage low-noise power source for the detectors. In the present system the 1200 V DC is obtained from a commercial regulated power supply, the output of which is coupled to two sections of active filtering for each detector.

A circuit diagram of Section 1 of the bias filters is shown in Figure 3-3.4. The filter is composed of a field effect transistor and a bipolar transistor which are used as pass transistors for the regulator dc current. The field effect transistor provides negligible loading for the high-impedance RC filter and a low impedance output to the bipolar transistor. The bipolar transistor supplies the current to drive three additional filter circuits in Section 2, for further filtering.

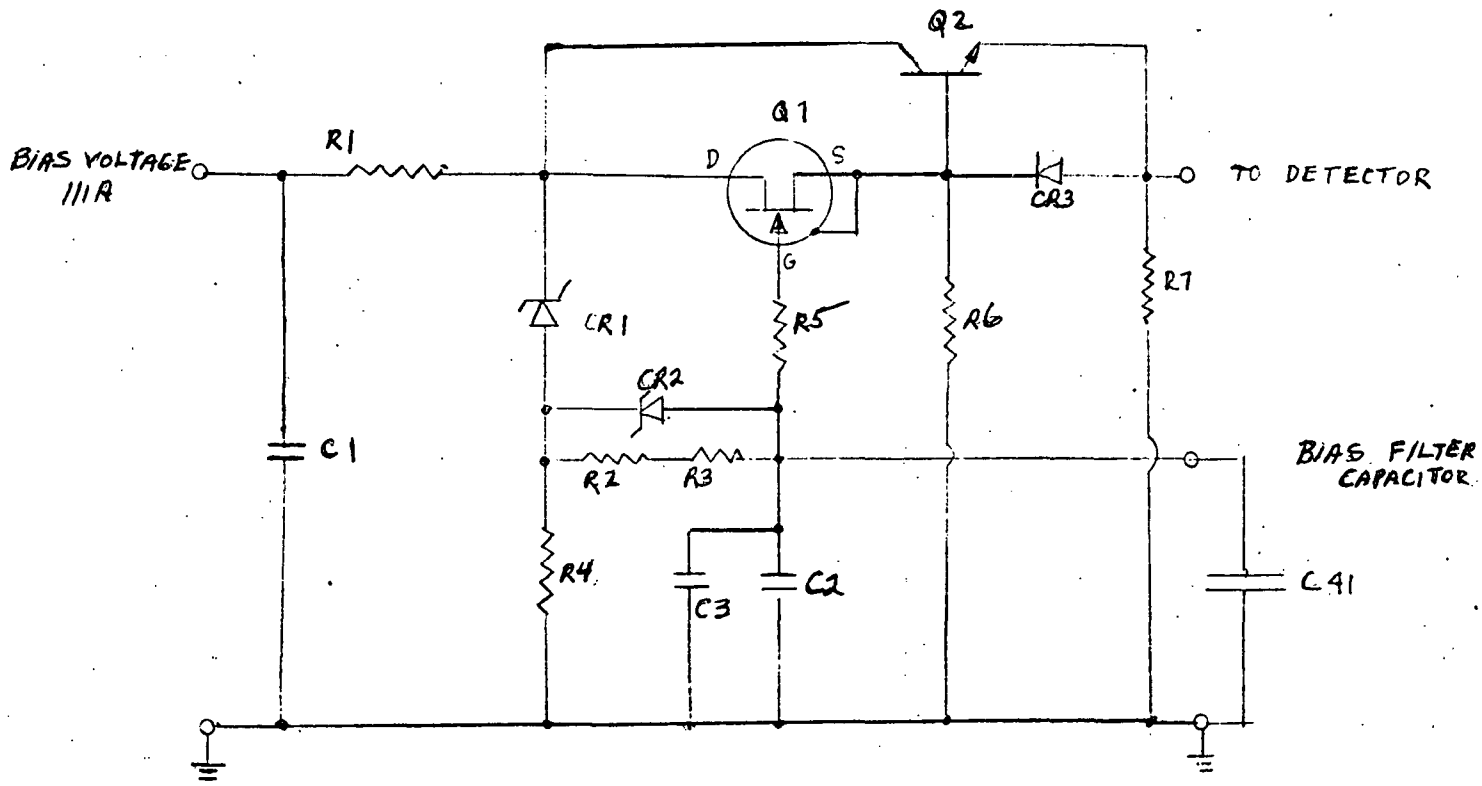

PRELIMINARY ELECTRICAL & ELECTRONIC SCHEMATIC DIAGRAM	DES. ENG. _____ DATE _____ SUPV. ENG. _____ DATE _____ PROJ. ENG. _____ DATE _____ REL. ENG. _____ DATE _____	CUSTOMERS SPEC. NO.	NAME OF UNIT OR SYSTEM BIAS FILTER, SECTION 1
Barnes Engineering Company Stamford, Connecticut		PROJECT NO. 2062 PARTS LIST NO.	DWG. NO. FIG. 3-3.4 SCHEMATIC DETECTOR BIAS FILTER SHEET 1 OF 2

The second section of the bias filters consists of three parallel active filters, each used to provide bias to a detector. The circuit operation is similar to that described above except that the extra current capability of the bipolar transistor is not needed and a series dropping resistor is located at the input to the filter. The dropping resistor allows a bias voltage inversely proportional to load to be supplied to the detector and stabilizes the responsivity of the detector over the temperature range by adjustment of the bias voltage.

3.3.6.5 FAULT DETECTION CIRCUITS

The fault detection and indicating circuits are located in the Auxiliary Unit. The signals which have been selected for fault detection are as follows:

1. Channel A Noise
2. Channel B Noise
3. Detector Bias Voltage
4. Multipulse Generator Output
5. Single Pulse Generator Output
6. Scan Drive

These signals are fed to the Auxiliary Unit from the Sensor Head. A failure of any one of the systems monitored by these signals would result in a malfunction of the Sensor Head. The failure is indicated by a light on the front panel of the Auxiliary Unit. Test jacks are also located on the front panel to provide the capability to monitor the above signals during system operation.

The input circuits used to detect excessive channel A and Channel B noise are precision half wave rectifiers and filters. The resultant dc level is applied to a threshold circuit, the output of which is a logic 1 when excessive noise appears at the input. This level is used to turn on an indicator light on the front panel. To determine if excess noise is present, the system command switch is turned to OFF. In the normal SCAN mode, the radiance signal will cause the light to turn on because signals may be generated when the horizon is crossed.

The detector Bias dc level is fed into an operational amplifier threshold circuit. If the bias level fails, the output of the circuit goes to a logic 1 and lights a lamp on the

front panel.

The Multipulse Generator, Single Pulse Generator, and Scan Drive signals each are fed into a rectifier, filter, and threshold circuit. Failure of these signals causes the particular threshold circuit to go to a logic 1 and light the appropriate lamp on the front panel of the Auxiliary Unit.

3.4 MECHANICAL DESIGN

A mechanical design was worked out that would provide good support for the optical components allowing them to perform optimally under severe environmental conditions such as the temperature extremes, -30°C to +80°C, and the possible high vibration and acceleration level to be encountered during launch. This required somewhat different approaches in the design of the main housing and the various optical subsystems such as the multi-pulse and single-pulse generators. These will be described in more detail below and can be best understood in conjunction with Figure 1-3.

3.4.1 STRUCTURE

The support structure is basically a box-shaped aluminum block with substantial central cross members. The housing has been machined out of a solid aluminum block. A section plane perpendicular to the long axis would show an "H" shaped form, with the radiometer and single-pulse optics mounted under the cross member, and the multi-pulse optics and the electronics mounted above it. Reinforcement is provided across the top of the casing, and locally, in order to strengthen the areas for mounting the sensor head to the spacecraft. Wall thickness, which is generally a .317cm(1/8") nominal, is locally increased for heat sink and mounting rigidity purposes at such points as the primary mirror and the multi-pulse housing attachment points.

3.4.2 LAYOUT OF MAJOR SUB-ASSEMBLIES

(a) Radiometer Optics: This system is an in-line reflective system, omitting any error-susceptible "folds" in the optics. Provision is made for focus adjustment, and for correction of alignment errors between the radiometer optical path and the

boresight by movement of the scanner mirror and/or the detector assembly as may prove necessary. Alignment within the radiometer (scanner to spherical reflector to detector) is accomplished by these same adjustments. Both the spherical mirror and the detector assembly are mounted to reinforced portions of the housing in order to provide rigidity.

(b) Single-pulse optics: These optics are mounted on the spherical mirror, with the single-pulse mirror mounted on the radiometer scanner. This orientation minimizes any divergence of these optical paths due to thermal or other distortion of the housing, since any movement of the scanner or primary mirror will be exactly followed by the mirror and generator of the single-pulse system. The generator assembly can be adjusted for focus, and for correction of alignment errors at the final assembly level.

(c) Multi-pulse generator: The multi-pulse optics are independently packaged in an Invar housing to prevent unwanted thermal expansion. The shape of the optical path, including the penta-mirror fold was dictated by volume limitations and by the necessity of making the reflected surface one piece with the scanner mirror. Use of an in-line optical path for the long focal length of the multi-pulse systems would result in an awkward configuration with considerable wasted volume. Provision has been made to adjust the orientation of the complete multi-pulse package to correct for alignment errors. This is accomplished by loosening and resetting bolts (using Allen wrenches) at the side of the housing which supports the Invar housing.

(d) Scanner Mirror: The scanner mirror assembly consists of the scanner itself, the mirrors serving the single-pulse and

multi-pulse generators, the scanner-driving torque motor, the feed-back tachometer, the flexural pivot bearings, and the adapters to mount the assembly to the main housing. Difficulty of mounting all the scanner parts at final assembly has led to the development of this major sub-assembly, in addition an access opening in one side of the main housing was provided. The design provides for rotational positioning of the scanner, and also for adjustment to eliminate any objectionable slewing of the scanner axis due to tolerance build-up.

(e) Detector Assembly (Radiometer): The detector sub-assembly consists of the 3-detector array and masks, the copper housing containing a power transistor to heat up the block and a thermal insulating mounting adapter. This sub-assembly is flange mounted and is capable of movement perpendicular to the optical axis as an alignment adjustment. Provision has also been made for focus adjustment.

(f) Electronics: Packaging of the electronics has been done in a functional form, placing low signal level circuits in the most favorable location near the detectors they service while high level circuitry has been packaged as a grouping of four large boards mounted at the side of the sensor head. Thus the three thermistor detector preamplifiers plus bias decoupling and filtering networks are built as printed circuit boards which are near and part of the detector subassembly. Likewise the pre-amplifiers for the single-pulse and multi-pulse generators and the sun sensor are built as small printed circuit boards nested in with the silicon photo-detectors with which they are associated.

The four large P.C. boards measuring 10 x 12.7cm are sandwiched together with stand-off separators and mounted to the side of the sensor. A sheet metal cover encloses and shields these boards. Cables to the boards are led through holes in the side of the sensor head frame and draped along the inside walls with clamp supports.

3.4.3 MATERIALS SELECTION

All materials have been selected in a trade-off process among the following criteria:

(a) Effects on possible thermal distortion and resulting impact on the maintenance of optical accuracy

(b) Ease and practicability of fabrication

(c) Weight

(d) Strength characteristics

Item (a) is the prime area of concern, since the total allowable error is only 0.01 degree. Therefore, the thermal expansion and thermal conductivity characteristics of each material have been first considerations in satisfying the severe temperature range of -30°C to +80°C.

Material weight density, and the resulting "g" loads, have been carefully considered in view of the specifications of vibration and shock environment. In some cases, density has been of major importance due to resulting inertia values and power consumption levels.

3.4.4 HOUSING - COMPLETE ASSEMBLY

Aluminum was selected for the following reasons:

(a) Compatibility with the parent assembly at the mounting interface.

(b) Good thermal conductivity

(c) Light weight

(d) Readily fabricates as machined assembly or ultimately as a casting.

The high thermal conductivity of aluminum is of prime importance, since it will tend to minimize thermal gradient throughout the structure. Since the interrelated optical elements are all

mounted on this structure, distortion due to temperature differentials, and the corresponding variations in thermal expansion, would destroy the optical precision of the assembly. While it is true that aluminum has a higher coefficient of expansion than some other structural materials, the control of temperature gradients is more critical to the maintenance of dimensional stability than a proportionate change of dimensions due to temperature variations.

3.4.5 MULTI-PULSE OPTICS HOUSING

The exceptional sensitivity of the multi-pulse system to dimensional change has dictated the use of a material with a very low coefficient of expansion for all elements to which multi-pulse optics are mounted. Invar was selected as the best material for the multi-pulse generator housing to maintain the allowable focal length tolerance of 0.0076 cm .

Although Invar has a very low thermal conductivity, the overriding need in this instance is for a material with very low thermal expansion.

Provision has been made to absorb the resulting differential expansion between the Invar and the main aluminum housing at the mounting interface.

3.4.6 SINGLE-PULSE OPTICS HOUSING

In this instance, the prime purpose was to use a material which closely matched the optical elements in the single-pulse generator in its thermal expansion. The material selected was a "300 series" stainless steel, with a coefficient of thermal expansion of 17.3×10^{-6} cm/cm/°C. The high weight of the steel is not a significant factor due to the small size of this assembly - approximately 1.9 cm diameter by 3.8 cm long. The method of

mounting this assembly to the overall housing, and its orientation relative to the radiometer optics, make its expansion compared with the aluminum non-damaging.

3.4.7 RADIOMETER OPTICS

Both the flat scanner mirror and the spherical primary mirror were made aluminum, primarily to maintain thermal expansion compatibility with the overall housing to which they are mounted. Stresses induced in these mirrors due to differential expansion could be appreciable, since dimensions over 7.6 cm are involved. Resulting distortion would seriously degrade optical performance. In addition, the aluminum provides the high conductivity necessary to minimize thermal gradients. Used with suitable optically finished plating, aluminum is an entirely acceptable mirror substrate material.

3.4.8 RADIOMETER DETECTOR MOUNTING

The detector array is mounted in a copper housing, to provide a very high degree of thermal conductivity, and consequent temperature uniformity among the three detectors. Since a heater (power transistor) is used to provide temperature controls of this housing, it must be thermally isolated from the power-consuming heat sinks of the overall housing. The material used between the main housing and the detector mount is Delrin. Delrin is a good compromise in that it provides a very low thermal conductivity, adequate strength and dimensional stability.

3.4.9 PACKAGE SIZE AND WEIGHT

3.4.9.1 Volume

The total volume, allowing for irregularities in the envelope, is estimated as:

$3{,}200\ cm^3$

3.4.9.2 ENVELOPE

The envelope dimensions of the package are as follows:

24.64 cm long x 14.22 cm high x 12.7 deep

3.4.9.3 PACKAGE WEIGHT

The weight of the optomechanical package, including all electronics which are mounted in the stated volume as weighed upon completion was 5 Kg.

4. TEST INSTRUMENTATION

A test program had been planned and submitted to NASA/LRC for review early in the program. Due to budgetary and time constraints not all the tests and procedures outlined in the test plan were followed. However, the principal ones demonstrating performance capabilities of the ARPESH were carried out, using simulation equipment and instrumentation appropriate for this purpose. The test plan is appended to this section as a guide to possible future testing that may be performed.

4.1 TEST EQUIPMENT FOR FIELD OF VIEW DEFINITION AND FOCUSING

To find the best focus for the sensor and allow plotting the field of view of the three detectors the sensor was installed on a test stand equipped with a collimator (a 11.43 cm germanium doublet coated for maximum throughput at 15 microns) and with a blackbody source that could be maintained at a conveniently high temperature (200°C) so that a field of view plot of good definition could be obtained, with signals considerably larger than system noise. The test stand and instrumentation used for these tests is shown as Fig. 4-1. In these tests the sensor scan mirror is kept in a fixed position and a chopper (modulation at 15Hz) is placed in front of the slit through which the sensor sees the blackbody source.

4.2 TEST EQUIPMENT FOR HORIZON SCANNING

To perform zero crossing repeatability tests at various equivalent earth temperatures the sensor is installed on the test stand, as described above, this time with the scan mirror driven at the normal 1Hz rate. In place of the slit and chopper the sensor is allowed to scan over the space (ambient simulator temperature as reflected from the mirror surface vane) to earth

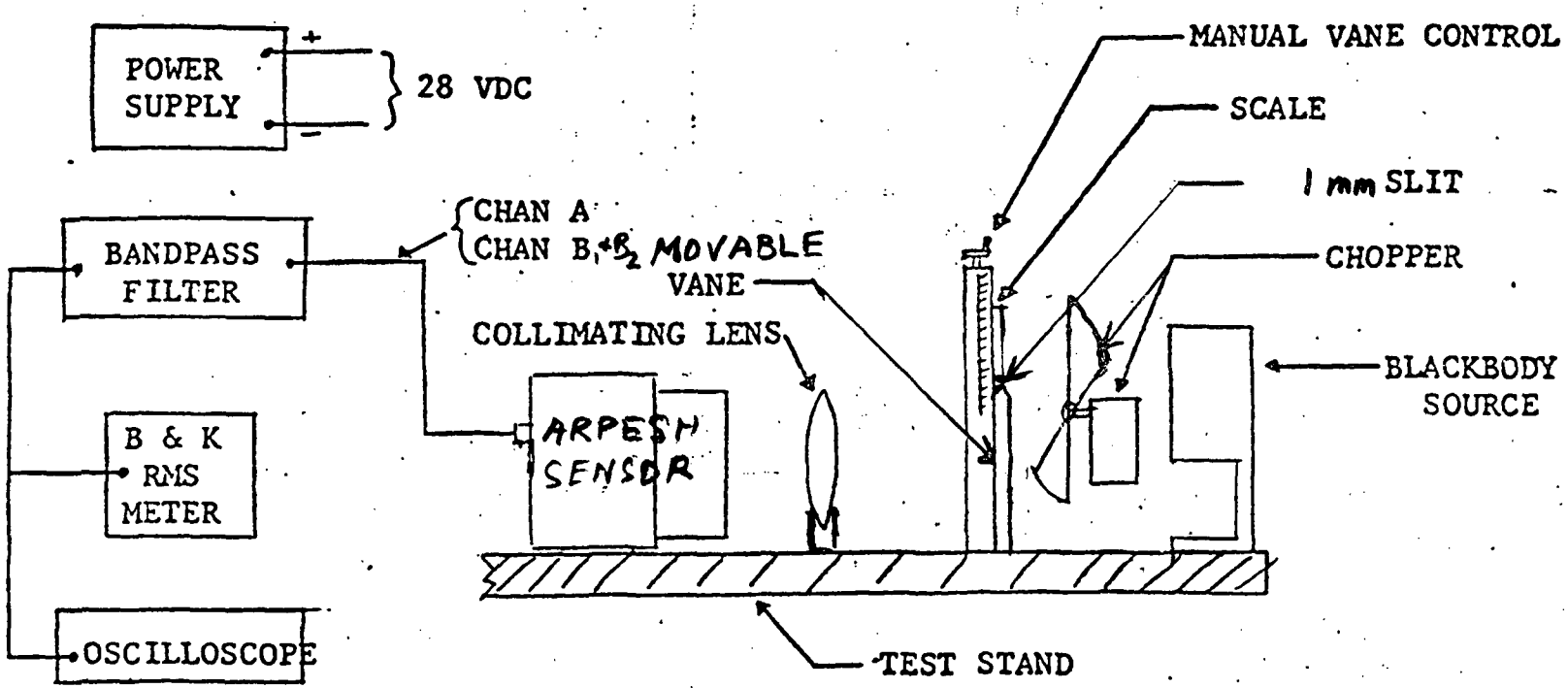

FIG. 4-1 Instrumentation for Field of View Measurement

(blackbody source) interface. The installation and test equipment is as shown in Fig. 4-2.

4.3 EQUIVALENT EARTH TEMPERATURES

The simulator employs a doublet germanium collimating lens with a transmission of approximately 50% in the 14-16 micron spectral range. Careful calculations were made of radiance at the aperture of a sensor placed in front of the collimator, for various blackbody temperatures. This radiance can then be expressed in an equivalent earth temperature (with no collimator lens used). With the knowledge of the collimator optical throughput a curve was plotted that shows the equivalence of earth temperature and simulator blackbody temperature for various possible ambient temperatures. This is shown as Fig. 4-3. However, one must also take into account the blackbody source emissivity which will influence the irradiance of the sensor.

In our tests we used a blackbody source whose emissivity is estimated to be 0.85. The irradiance of the sensor aperture must therefore be multiplied by 0.85 to account for the imperfect "blackbody" source surface.

4.4 ACCEPTANCE TEST PLAN FOR ARPESH

1.1 SCOPE

This document establishes the test methods and procedures to be followed for the acceptance testing of the ARPESH.

1.2 APPLICABLE DOCUMENTS

The following documents form a part of this document to the extent required and specified herein:

a) Statement of Work NASA/LRC L-15-1787, Exhibit A
b) BEC Proposal P-1522
c) MIL-STD 461A
d) MIL-STD 462
e) MIL-STD 810B
f) MIL-STD 202D

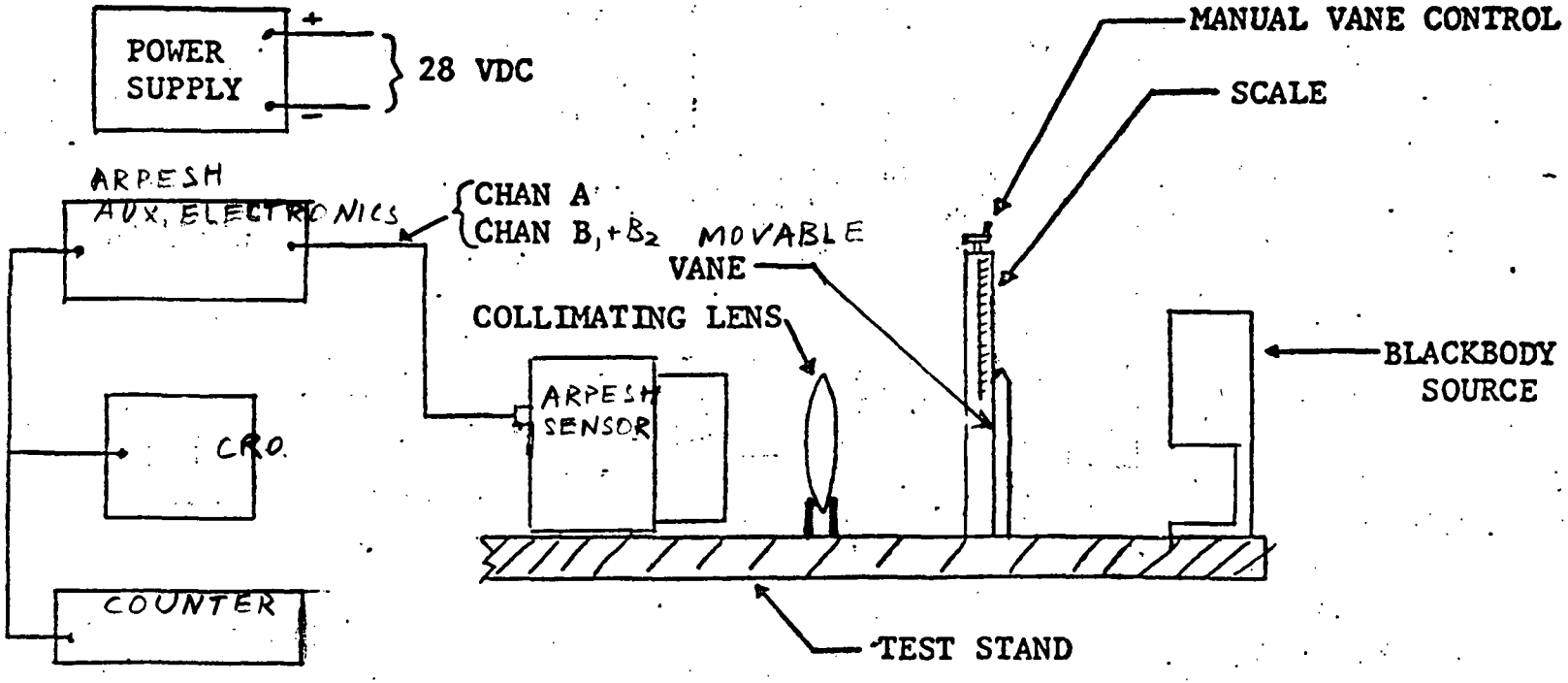

FIGURE 4-2 INSTRUMENTATION FOR HORIZON ACQUISITION TESTS

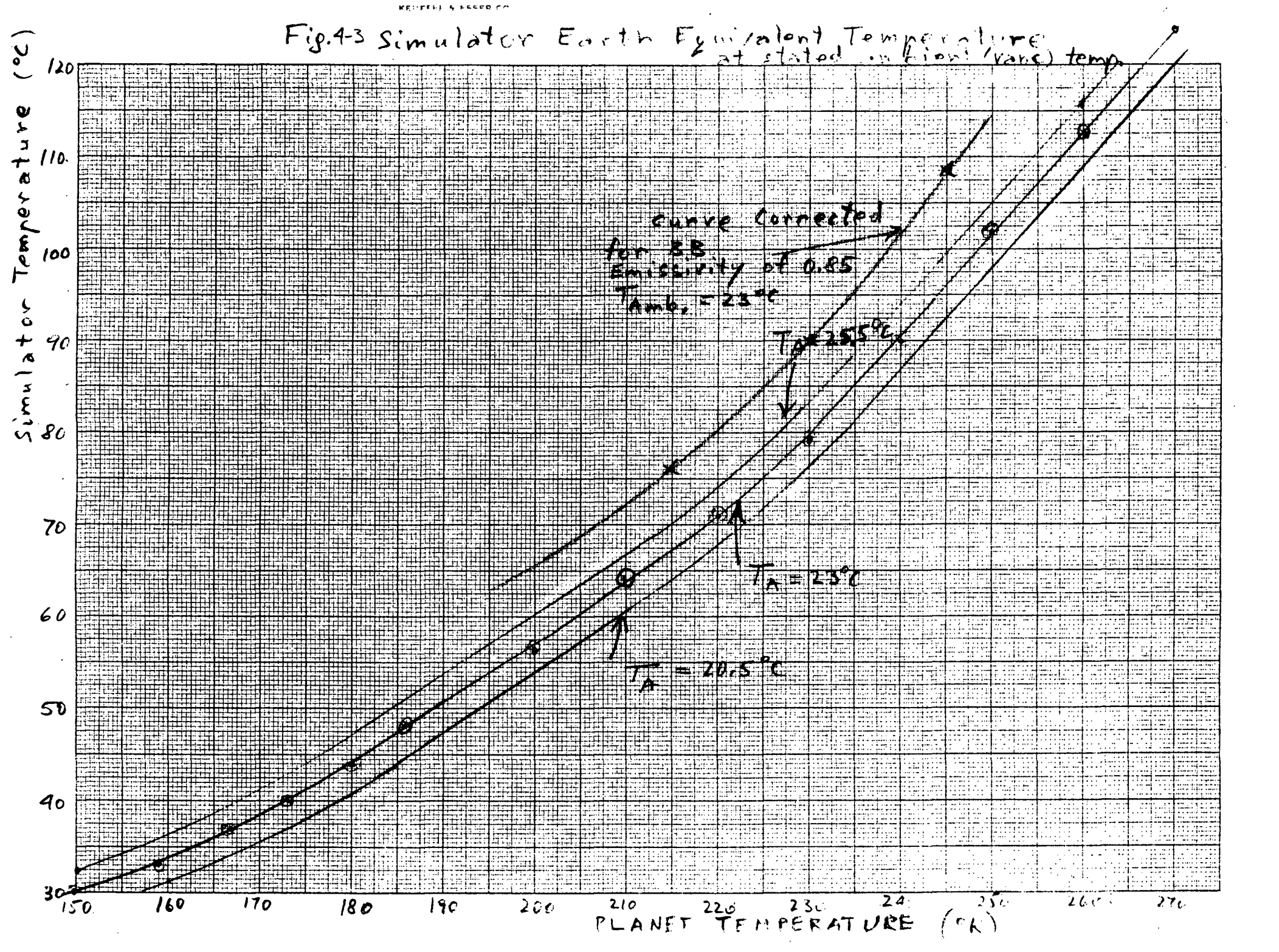
Fig. 4-3 Simulator Earth Equivalent Temperature at stated ambient (vars) temp.
Simulator Temperature (°C)
PLANET TEMPERATURE (°K)
120
110
100
90
80
70
60
50
40
30
150
160
170
180
190
200
210
220
230
240
250
260
270
Curve Corrected for BB Emissivity of 0.85
$T_{Amb.} = 23°C$
$T_A = 25.5°C$
$T_A = 23°C$
$T_A = 20.5°C$

1.3 PURPOSE OF TEST PROGRAM

The test program is designed to demonstrate compliance of ARPESH with contractual requirements and specifications called for in the Statement of Work when subjected to the tests called for in this ATP.

1.4 IN-PROCESS TESTS

Some tests cannot readily be verified in the completed assembled instrument and are considered to be tests to be performed on subsystems prior to final assembly of the system. These include spectral response measurements to be performed on the detectors and the optical filter prior to system tests. Also included are independent performance measurements of each detector and noise and frequency response measurements performed on each amplifier. Data showing the results of these tests shall be supplied to NASA/LRC with the data package and shall conform with the specifications of Work.

1.5 TEST FACILITY REQUIREMENTS

The testing is to be conducted at Barnes Engineering Company

It is expected that the test facility will include a simulator (test stand 203950-1001) that will be borrowed from other programs and suitably modified and equipped to perform the tests specified by this ATP. The relative vane position settings on the collimator shall be known to better than 0.010". A variable speed chopper will be used for response time and other measurements. Also to be used for these tests is a 6" diameter off-axis collimator with an autocollimating microscope attachment for alignment of the IR and visual fields of view. Environmental Laboratory facilities and outside facilities will be used in conducting EMI, vibration and other tests.

1.6 TEST EQUIPMENT TO BE USED FOR TESTS

The *following standard test equipment (or their equivalents)* will be required for performance of the specified tests.

a) Beckman 1455 Printer
b) Beckman 60 13A Accumulator
c) Beckman Counter (E put meter)
d) Cathode Ray Oscilloscope Tektronix 502
e) Digital Voltmeter HP 3440A
f) Multimeter, Simpson 260 (including ammeter)
g) RMS Meter, Bruel Kjaer 2417
h) VTVM Hewlett Packard 412
i) Chart Recorder Sanborn 152
j) Wave Analyzer HP 302
k) Blackbody source of adjustable temperature with temperature readout (e.g., BEC RS-12)
l) Krohn-Hite filter or lock-in amplifier for low frequency noise measurements.

1.7 PERFORMANCE TESTS

The following tests will be performed to confirm that the sensor meets the requirements of the contract and Statement of Work.

1.) Optical and Mechanical Alignment

a) Field of View - horizontal
b) Field of View - vertical, static
c) Field of View - vertical, scan range
d) Boresighting of visual and IR field

2.) Radiometric System

a) Signal transfer function - all channels
b) Frequency response - all channels
c) Noise response - all channels
d) Sensitivity and NEP - analog of all channels

3.) Scan System Performance

a) Scan angle measurement
b) Rate of scan - record of time position
c) Linearity of scan velocity
d) Cage mode operation
e) Calibration command

4.) Sensor Locator Acquisition

a) Locator position identification as a function of simulated planet temperature.

b) Repeatability of locator acquisition at low, medium and high equivalent planet temperature.

c) Checkout of locator position at other values of "R" settings.

5.) Tests of Auxiliary Systems

a) Sun Sensor
b) Failure detection system
c) Loss of track indicator

6.) Sensor Physical Characteristics

a) Measurement of size and weight
b) Measurement of power requirements

7.) Environmental Tests

a) Operating temperatures -7°C to +70°C
b) Shock, vibration, acceleration
c) EMI tests

1.8 MALFUNCTIONS

Any malfunction of the ARPESH or the test equipment which may occur during any test will be immediately analyzed to determine its cause. The test in process will cease and resume after the cause of the malfunction has been identified and corrected. Prior tests that may have been affected by the malfunction will be repeated. Data from prior tests will be examined and accepted only if it is established that it has not been affected by the malfunction.

1.9 OPTICAL AND MECHANICAL ALIGNMENT

1.9.1 Field-of-View - Horizontal

The sensor is mounted in a vertical position on the simulator test stand. (90° from the normal position). A slit subtending 0.1° is installed in front of blackbody source at the adjustable

position vane and a chopper is placed behind the slit. Blackbody is set to 200°C. Sensor scan command is in neutral position. Move vane from lowest to highest position where signals are detected. Plot analog outputs of Channels A, B & B_2 (read on HP 302 wave analyzer) with a minimum of 15 points for each channel. 1/2 power points shall be within 10% of specified field-of-view. (Figure 2 of Statement of Work).

1.9.1a Field-of-View - Vertical

Install sensor on test stand in the normal orientation. Move vane and register and plot analog outputs of Channels A, B & B_2 for each of at least 11 positions between the 50% points and at the 10% and 2% field-of-view edges for each channel. 1/2 power points shall be within 10% of specified fields (Figure 2 of Statement of Work).

1.9.1.b Field-of-View - Vertical Scan Range

Set up as in 1.9.a, above, except with chopper removed. Turn scan command to normal scan. Record output waveforms (on Sanborn recorder) with vane (slit) moved to extreme positions at which the signal is just detected at both scan extreme positions. Note position of vane. The range of the scan system shall be greater than 7-1/2°.

1.9.2 Radiometric System

a) Frequency Response

Set up sensor and test stand as in Section 1.9.1. Set blackbody source to a temperature of 200°C. Chopper is operated over a wide range of frequencies. Measure outputs of Channels A, B_1, B_2 on HP 302 wave analyzer at 20 frequencies from 0.1 to 150 Hz. Plot response of all channels.

b) Noise of Sensor

With simulator chopper stopped and scanner off, measure noise of Channels A, B_1 and B_2 at the analog output monitor points using the RMS voltmeter (Bruel & Kjaer). Also record wide band noise output on recorder (Sanborn). Repeat this measurement with the detector bias turned off.

c) Transfer Function Measurements

With sensor mounted on the simulator and scanner operating set blackbody source (earth simulator less chopper and narrow field slit), succesively, to five temperature simulating earth temperature of 210°K to 270°K. Record signal outputs (on Sanborn Recorder) at Channel A, B_1 and B_2 analog output terminals. (The equivalent blackbody temperatures are given in Figure 4-3). Record a minimum of ten scans that totally expose the field of view of the detectors to radiation from the blackbody source.

d) Calculate Signal to Noise ratio at all equivalent earth temperatures after averaging ten or more samples of signal for each channel and using the corresponding noise as measured with the voltmeter.

e) Calibration Test

BEC shall supply a calibration curve of calibration monitor thermistor temperature vs. output voltage. In this test, the outputs of Channel A, B_1 & B_2 will be recorded during calibrate command with device placed in front of the aperture and the calibration patch temperature measured on VTVM.

1.9.3 Scan System Performance

1.9.3a Scan Angle Measurement

The simulator is equipped with a variable position vane, in the focal plane of the collimator that permits precise measurement of the edge position of the simulated earth, to an accuracy of 0.01°. Turn on sensor scan system and record analog outputs of Channel A (on Sanborn) with the vane set at the extreme positions where the edge of the earth is first detected and results in an output of one volt (for 240°K earth). Note span of simulator vane position. The span shall be greater than 7-1/2°.

1.9.3b Rate of Scan

At a fixed position of the simulator vane (approximately in the center of the span), repeat all above for at least ten scans recorded on the oscillograph recorder. Use timing marker on recorder as a check of the recorder speed accuracy. Measure duration of each scan, repeat at a fixed level (one volt). Average out the time span for at least ten traces. The scan rate shall be 1/sec±10%.

1.9.3c Scan Velocity Linearity

The velocity of the forward scan is tested by recording the waveform of the output of the tachometer (voltage across emitter driver series resistor) on the chart recorder as a function of time. The slope can be measured in the central 7-1/2° of the scan pattern. No linearity has been specified. However, it is possible to demonstrate that the linearity is considerably better than 10%.

1.9.3d Cage Mode Operation

This test merely established the position of the scan mirror during "cage". (Effectiveness of caging is established in vibration and shock tests.)

Place scan command switch in "cage" position. With chopper and slit aperture installed in the simulator, move vane to position where detectors A, B_1 & B_2 analog outputs commence. Note vane position.

1.9.3e Calibration Command

This test, like 1.9.3d, checks the position of the component in question - the calibration patch. With the vane slit and chopper installed in the simulator, record a number of traces when the scan command is repeatedly switched to and out of "Calibrate". Find the vane position just at the edge of the calibration patch before the analog signal in Channel A fades out. Note angular position of vane. Record the temperature of the patch and the output of the calibration pulse from each channel.

1.9.3f Repeat the above chopper-vane-slit position measurement with the scan command in neutral or off position.

1.9.4 Sensor Locator Acquisition

1.9.4a Locator Position Identification

Sensor is set up on test stand in the normal manner, and the vane is set approximately to the center of the field-of-view. The "R" value is set to mid-range. The blackbody source is set to a temperature equivalent to a cold earth (220°K, see Fig. 4-3, for calibration curve). Set scan command to normal scan. Record angular position output data (at zero crossing point) using counter and printer. Register a minimum of one hundred consecutive acquisitions (zero crossing). During this time, the Sanborn recorder is to record the analog outputs of Channels A & (B_1 & B_2). RSS the printed-out position values. Their spread shall be less than 0.01° (3σ) error.

Repeat 1.9.4a with the vane (or sensor) moved through steps of 1/2 degree over the total 7-1/2° range, using 25 readings per step.

1.9.4b Repeatability at Medium and High Equivalent Earth Temperature

Repeat 1.7.4a for a 240°K equivalent earth temperature. The same criteria applies to the error interpretation. Also repeat the 260°K equivalent earth temperature.

1.9.4c Minimum "R" Setting

Repeat 1.7.4a and b with "R" gain setting at minimum position.

1.9.4d Maximum "R" Setting

Repeat 1.9.4c for maximum "R" setting.

1.9.4e Measure and Record the vane position dial readings versus position reference using an autocollimator or height gage.

1.9.5 Tests of Auxiliary System

1.9.5a Sun Sensor

A pilot light is placed in front of the sun sensor aperture hole. The sun output indicator shall go to a "One" position.

1.9.5b Failure Detection

Check operation at failure detection circuits by deliberate temporary failure simulation and show that failure indicators go to a "One" position. For the various circuits, this is done by removing the appropriate signal such as detector bias, scan operation, etc.

The single pulse and multipulse operation may be inhibited by blocking the light emitting diodes. Excess noise in Channels A and B are checked (during prolonged "Cal") by

feeding in a source of A_1, (e.g., 60 Hz) via a capacitor, to the detector output leads of Channels A and B.

1.9.5c Loss of Track

The loss of track indicator output shall go to "One" when the sensor aperture is blocked during normal scan mode operation.

1.9.6 Sensor Physical Characteristics

Measure size, weight and power consumption (of sensor head, not power supply input drain) and establish that these are within values specified in the Statement of Work.

1.9.7 Environmental Tests

Environmental tests shall be conducted in accordance with the appropriate specifications and MIL Standard listed in Section 1.2.

5. TESTS OF HORIZON SENSOR

Upon completion of assembly, wiring and trouble-shooting, the horizon sensor was installed on a test stand. The stand is equipped with a 4" dia. germanium collimator lens, a blackbody source for simulating various earth temperatures, and a variable position vane that permits precisely measured movement of the simulated earth-space interface. With this simulation input to the sensor head and an electronic counter connected to SH output terminals readout measurements were obtained that permit determination of horizon sensor precision to detect the horizon acquisition (zero crossing). This allows measurement of the sensor's accuracy for various simulated earth equivalent temperatures. Also measured with the test stand were other significant sensor head system parameters, including field of view of the three detector channels and scan angle limits. The simulator blackbody temperatures required to simulate various earth temperatures are given in Figure 4-3 along with simulation equipment description provided in Section 4.3 of this report.

Unfortunately due to budget and time limitations only preliminary tests could be performed. However, the fundamental sensor head characteristics that prove the viability of the concept and system design have been done; they show the sensor in a favorable light. The tests included optimum focusing, plotting of the sensor's fields of view and zero crossing repeatability under a variety of simulated earth temperatures. The results of these measurements are presented below:

5.1. Focusing and Field of View Definition

For this test a narrow slit aperture is used in the focal plane of the test stand collimator. The slit

is located in a position parallel to the earth-space interface, the radiation through the slit is chopped at 15Hz. The slit can be moved up and down with the vane on the simulator. A plot of the field of view of the individual detector channels was obtained at various focus settings. The plot with the steepest field edges (slopes) represents the best sensor focus. After a number of trial runs on both sides of the optimum focus point a best position was established. The fields of view of detectors A, B_1 and B_2 obtained at the location of best focus are shown as Figures 5.1, 5.2 and 5.3.

5. 2. Repeatability of Zero Crossing

The principal function of the sensor head is to provide a high accuracy angular readout signal to indicate the attitude of the spacecraft in which it is used with respect to the earth. The spacecraft will be orbiting the earth. This is an important test that will establish the sensor's sensitivity and accuracy. Readouts were obtained in three forms.

a. The zero crossing pulses were displayed on a cathode ray oscilloscope (CRO). In this test the location of the initial pulse edge was compared with respect to a CRO time reference for a large number of scans (the oscilloscope sweep generator was triggered by the sensor head fiducial pulse reference position time marker).

FIG 5-1 FIELD OF VIEW, CHANNEL H

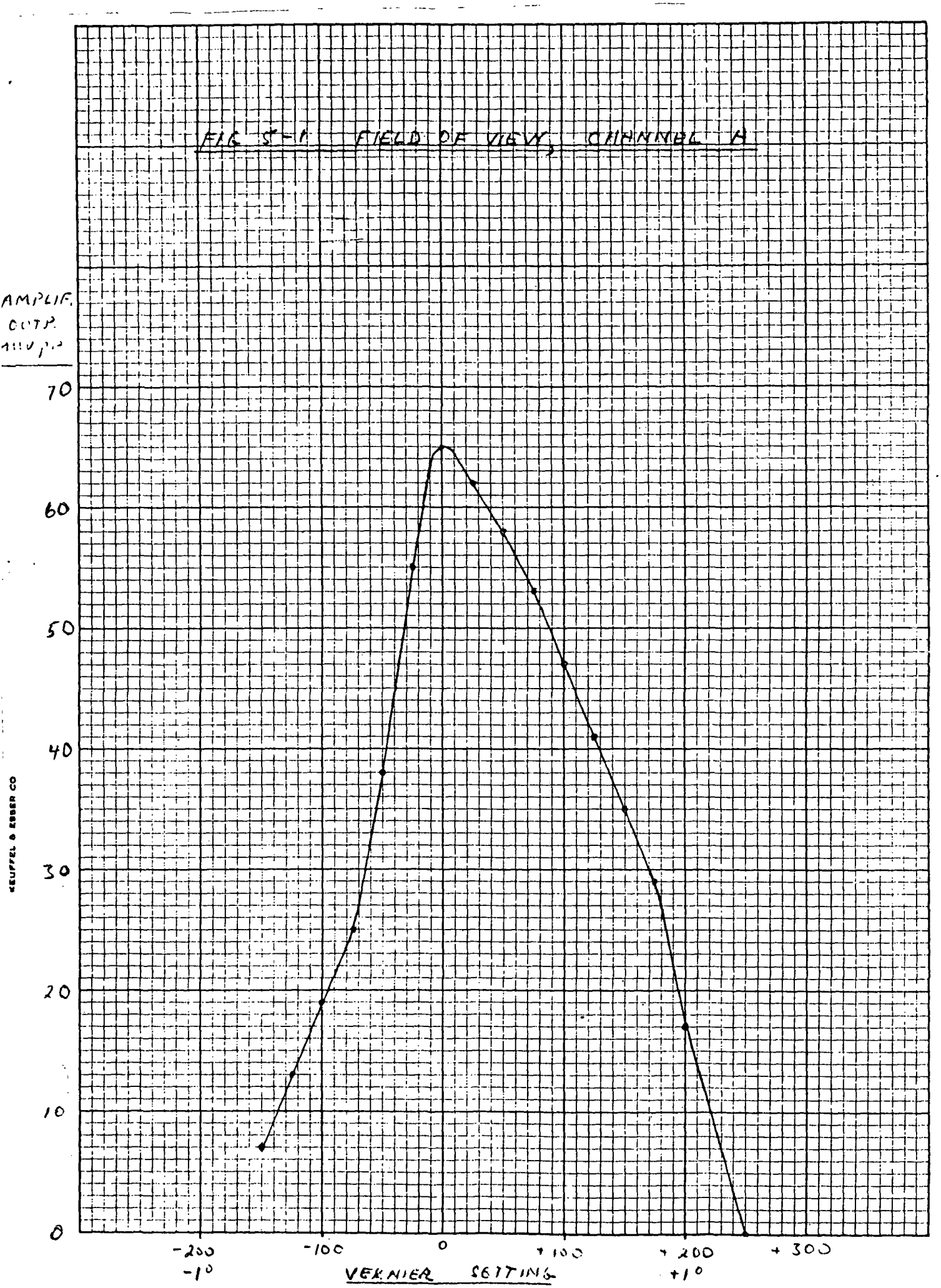

KEUFFEL & ESSER CO

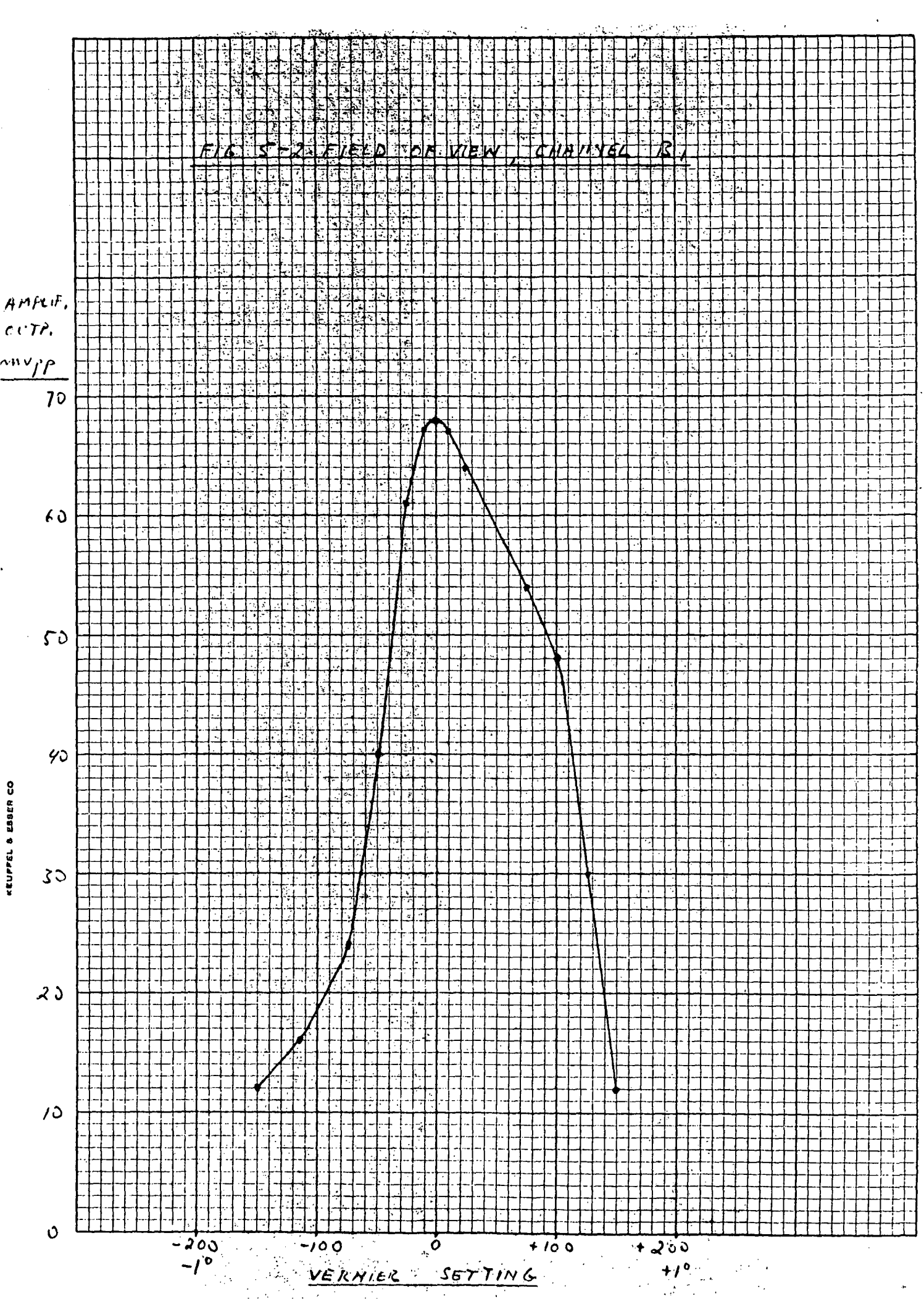
FIG 5-2 FIELD OF VIEW, CHANNEL B1
AMPLIF. OUTP. mV/pp
70
60
50
40
30
20
10
0
-200
-1°
-100
0
+100
+200
+1°
VERNIER SETTING
KEUFFEL & ESSER CO

FIG 5-3 FIELD OF VIEW, CHANNEL B2

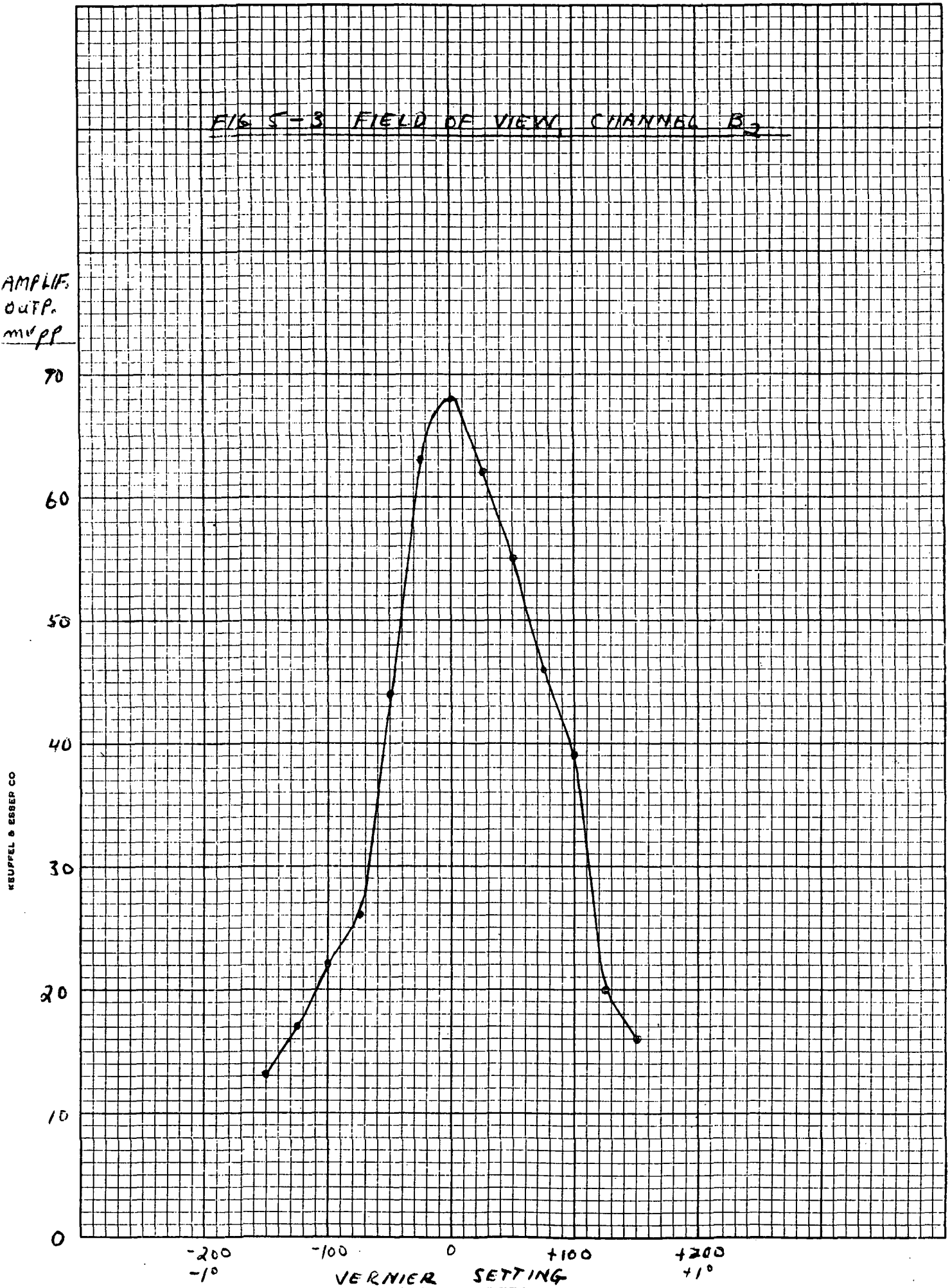

KEUFFEL & ESSER CO

b. A binary parallel readout in the sensor head auxiliary electronics unit. The horizon angle appears as a binary code on a series of lights configured in a 12 digit readout.

c. A decimal counter readout that registers the incremental encoder pulse accumulation at the time of zero crossing. Each horizon scan produces a count which represents the horizon angle. The count is displayed until the start of the next scan cycle.

This last type of presentation is the most useful, inasmuch as it is easily tabulated, it produces continuously repeated readout angle, which shows the variation of the zero crossing angle from scan to scan. This output allows computation of the error with which the sensor head establishes the horizon position. The other two methods of displaying the sensor head position determination at zero crossing are less flexible but they are not without merit and will be discussed first.

5.2.1 a.) CRO readouts as described in Section 5.2a were obtained, they are a means of determining position readout error in the form of jitter of the horizon zero crossing with respect to a CRO sweep that is synchronized to the scan mirror position. Figure 5.4 is a photograph of one zero crossing. Figure 5.5 is a time exposure showing ten superimposed zero crossings. From this, and a knowledge of the time between peak to peak variations of zero crossing, one can obtain the peak to peak error. In the photographs one division corresponds to 1 msec which, in turn corresponds to 0.01° scan angle.

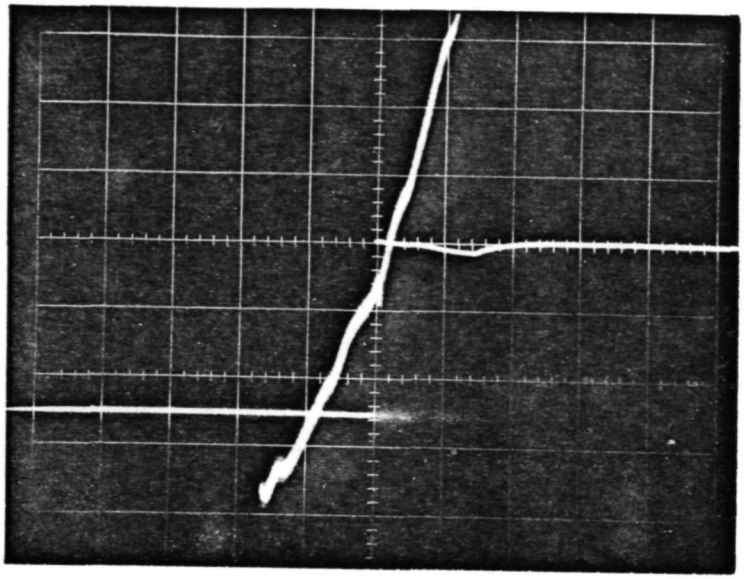

Crossover Detector Input:

V =100mv/cm, H=10ms/cm

Detector Output:

V=5v/cm, H=10ms/cm

FIG. 5-4 Scope Photograph of Zero Crossing Signal and Null Indicator Output

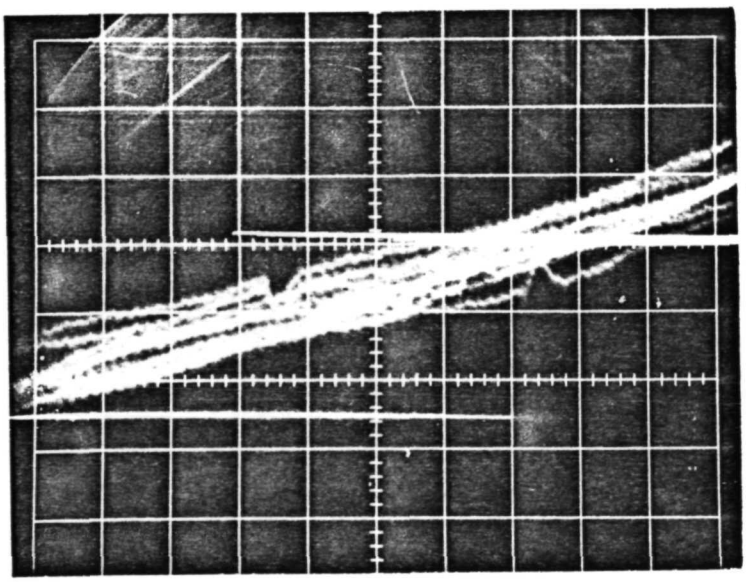

Crossover Detector Input:

V=100 mv/cm, H=1 ms/cm

Detector Output:

V=5v/cm, H=1 ms/cm

FIG. 5-5 Time Exposure of 10 Zero Crossings

A spread of 4 msec in noise indicates a peak to peak noise of 0.04° of attitude error.

5.2.2 b. The second method of reading output angles is by observing the parallel binary lamp display. To do this effectively requires some familiarization in rapid binary to decimal conversion, speed of observation is important inasmuch as readings have to be noted in about 1/4 second since new readings are obtained once a second. With some practice one can fairly well establish the maximum error and approximate the one sigma variation of the sensor head position readout.

5.2.3 c. The principal mode of readout of zero crossing position employs an electronic counter (accumulator) which is programmed to determine and hold the pulse count of the incremental position encoder that indicates the angle of the zero crossing command. At the beginning of a new scan the counter is automatically cleared and reset for display of the next horizon crossing.

For a sequence of numbers displayed (in the tests run, 100 samples were used) at a given simulated horizon condition the accuracy of the sensor was established. Readings were taken for conditions that included cold earth (215°K), warm earth (245°K), and moderate earth temperatures (230°K). The electronic counter used for these tests is a Beckman 6013A Reversing Accumulator.

The readings obtained are tabulated below, both as a group of numbers noted and as a bar graph distribution curve. The 1σ errors for the three simulator blackbody settings, to be interpreted in more detail in the section which follows, are:

Equivalent Earth Temperature	1σ Count Deviation	1σ Angular Error, Degrees
245°K	1.55	±.0077
230°K	2.2	± .011
215°K	2.8	± .014

The readings obtained under the measurement conditions cited are given in Tables V-1 through V-3a

The distribution curves (bars) are shown as Figures 5.6, 5.7, and 5.8.

5.3 ANALYSIS OF TEST RESULTS

It was stated in the previous section that the 1σ sensor head error for a simulated earth temperature of 215°K is 2.8 counts (or0.014°). To obtain this RMS error the average reading of 100 samples of the accumulated count was determined. The deviation of each of the 100 readings from the average was recorded, and subsequently the square root of the sum of the squares of these deviations was calculated. In this process the conversion factor needed is the relationship between count number and the sensor head scan angle. The incremental counter counts to 1535 over the full scan of 7-1/2° of the field of view. Therefore, one count corresponds to $\frac{7.5}{1535} \approx \frac{1}{200}$ Degree, and one

TABLE V-1

ZERO CROSSING ANGLE READOUT REPEATABILITY
FOR 245°K EQUIVALENT EARTH TEMPERATURE

960	957	958	960
964	960	959	955
961	960	957	962
957	957	959	958
957	957	957	960
960	960	958	962
959	959	962	960
959	958	961	960
960	960	958	958
960	960	959	962
959	957	958	958
960	959	959	959
958	961	958	960
960	956	960	959
961	957	958	959
959	958	960	959
960	960	958	958
958	962	957	959
957	959	961	959
958	957	960	959
957	959	960	959
955	959	956	958
958	960	959	959
959	962	960	960
960	960	958	959

TABLE V-1a ERROR DATA FOR 245°K PLANET

```
   ?V
ØN-LINE SYSTEMS  V1-3

1651     4-30-73
USER NUMBER?..3700,10,2413NC
BØØØ
ALL BATCH USERS RUN NEWS*
SYSTEM?..
.TEL
TELCØMP III VERSIØN 7.04C

>LØAD NC
>TYPE ALL

  1.1 DEMAND NMIN, NMAX
  1.2 DEMAND B[R] FØR R=NMIN:1:NMAX
  1.3 T=SUM(B[R] FØR R=NMIN:1:NMAX)
  1.4 S=SUM(B[R]*R FØR R=NMIN:1:NMAX)
  1.5 A=S/T
  1.6 P=SUM(((R-A)↑2)*B[R] FØR R=NMIN:1:NMAX)
  1.7 SIGMA = SQRT(P/T)
  1.8 TYPE T,S,A,P,SIGMA


XØØ PART A
>DØ PART 1
        NMIN=5619,
J I DØN'T CØMPLETELY UNDERSTAND YØU
        NMIN=46YJDG
 NAME TØØ LØNG (MØRE THAN SIX CHARACTERS)
        NMIN=55
        NMAX=64
       B[55]=2
       B[56]=1
       B[57]=13
       B[58]=21
       B[59]=24
       B[60]=27
       B[61]=5
       B[62]=6
       B[63]=0
       B[64]=1
           T=     100
           S=    5902
           A=      59.02
           P=     239.96
       SIGMA=       1.54906423
>LØGØUT
 CP UNITS     3.5

 CØNNECT TIME  00:05
```

Source temp = 115°C

TABLE V-2

ZERO CROSSING ANGLE READOUT REPEATABILITY

FOR 230°K EQUIVALENT EARTH TEMPERATURE

959	956	956	968
961	963	963	961
960	961	961	962
956	957	962	958
963	960	962	961
963	965	962	959
965	965	963	962
963	961	960	958
964	966	961	964
961	961	962	960
960	963	963	964
962	958	964	961
962	962	960	958
962	964	963	962
963	961	963	960
964	961	960	958
961	963	962	966
962	963	961	962
962	961	962	965
962	962	966	963
961	963	960	961
961	965	961	961
966	963	958	962
960	958	961	962
961	963	967	964

TABLE V-2a ERROR DATA FOR 230°K PLANET

```
  LØAD NC
 >DØ PART 1
          NMIN=56
          NMAX=66
         B[56]=

  INTERRUPTED AT STEP 1.2
 >

 >DØ PART 1
          NMIN=56
          NMAX=67
         B[56]=3
         B[57]=1
         B[58]=7
         B[59]=2
         B[60]=10
         B[61]=22
         B[62]=21
         B[63]=17
         B[64]=6
         B[65]=6
         B[66]=3
         B[67]=1
              T=      99
              S=    6103
              A=      61.6464646
              P=     480.626263
         SIGMA=       2.2033635
 >SEND 12                                    SOURCE TEMP = 94°C

 >
```

TABLE V-3

ZERO CROSSING ANGLE READOUT REPEATABILITY

FOR 215°K EQUIVALENT EARTH TEMPERATURE

970	968	965	966
965	966	966	973
963	965	967	966
968	964	971	970
965	968	966	966
973	968	966	968
964	970	968	968
964	961	961	964
969	965	966	965
966	966	966	963
966	970	970	963
964	965	967	961
965	966	961	968
969	967	964	963
967	967	969	969
962	967	967	972
970	964	963	966
971	964	963	960
963	962	968	966
964	966	963	969
966	966	970	965
967	971	968	970
967	968	964	967
966	964	970	972
963	965	966	969

TABLE V-3a ERROR DATA FOR 215°K PLANET

```
  SEND 7 FOR I- 1 TO 20
               ↑
  = MISSING
 >
  SEND 7 FOR I- 1 TO 20
↑             =
  SEND 7 FOR =- 1 TO 20
↑             I=
  SEND 7 FOR I= 1 TO 20
↑
 >SEND 7
 >LOGOUT


  CP UNITS     5.1

  CONNECT TIME  00:11


\PWJGO.,6XX# %?X22-
                    29YJXDVY3XXCXC
 ON-LINE SYSTEMS  V1-11

 1622     4-30-73
 USER NUMBER?..3700,10,2413PJ
 BBDDR
 ALL BATCH USERS RUN NEWS*
 SYSTEM?..
 .TEL
 TELCOMP III VERSION 7.04C

 >DO PART 1
  THERE IS NO PART 1
 >@
  ↑
  THAT'S NOT A TELCOMP COMMAND
 >LOAD NC
 >DO PART 1
          NMIN=60
          NMAX=73
         B[60]=1
         B[61]=4
         B[62]=2
         B[63]=9
         B[64]=11
         B[65]=10
         B[66]=20
         B[67]=10
         B[68]=11
         B[69]=6
         B[70]=9
         B[71]=3
         B[72]=2
         B[73]=2
             T=     100
             S=    6634
             A=      66.34
             P=     788.44
       SIGMA=       2.80791738
```

SOURCE TEMP = 71°C

FIG. 5-6 Bar Graph of Crossover Data T source = 75°C

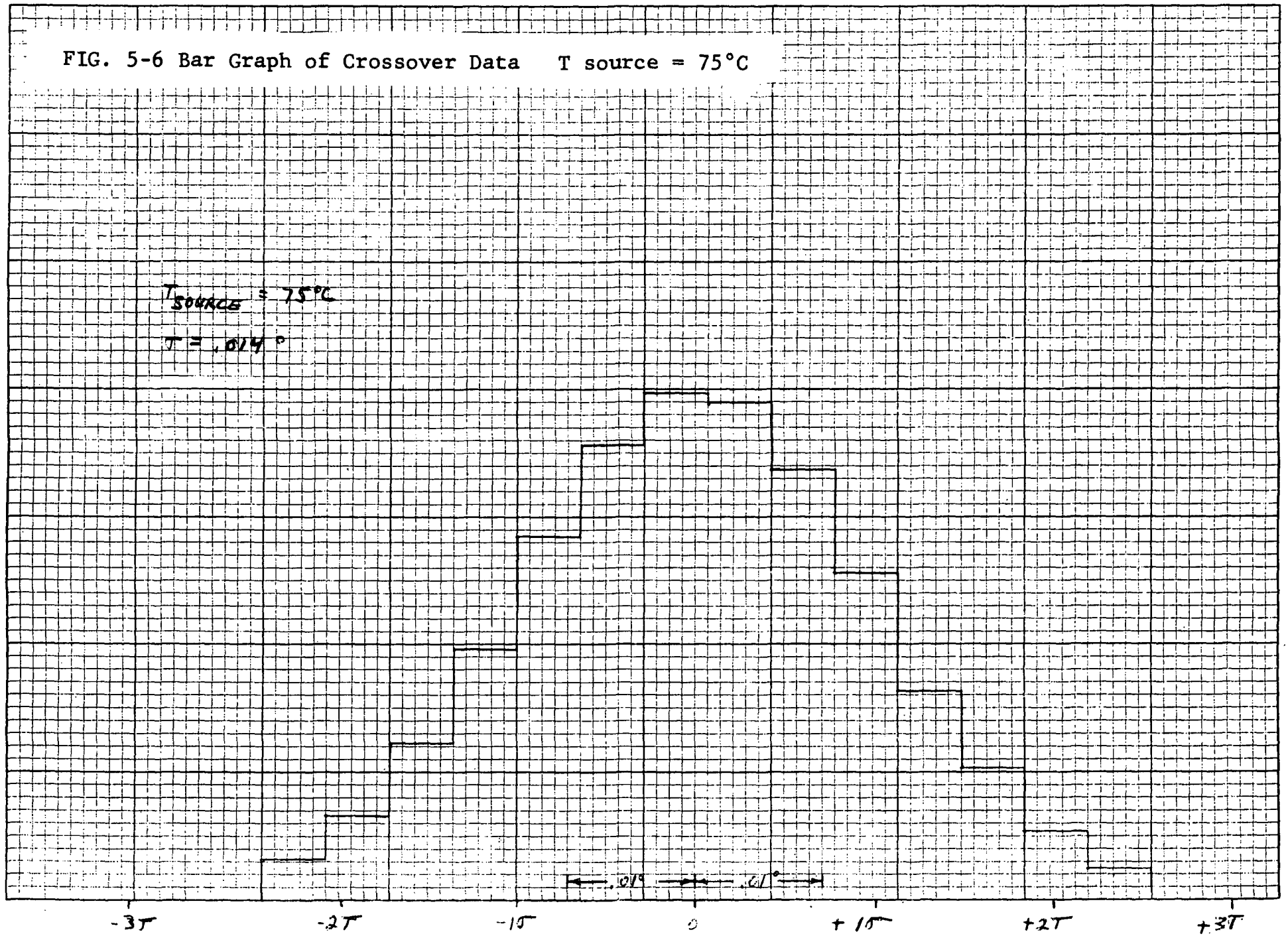

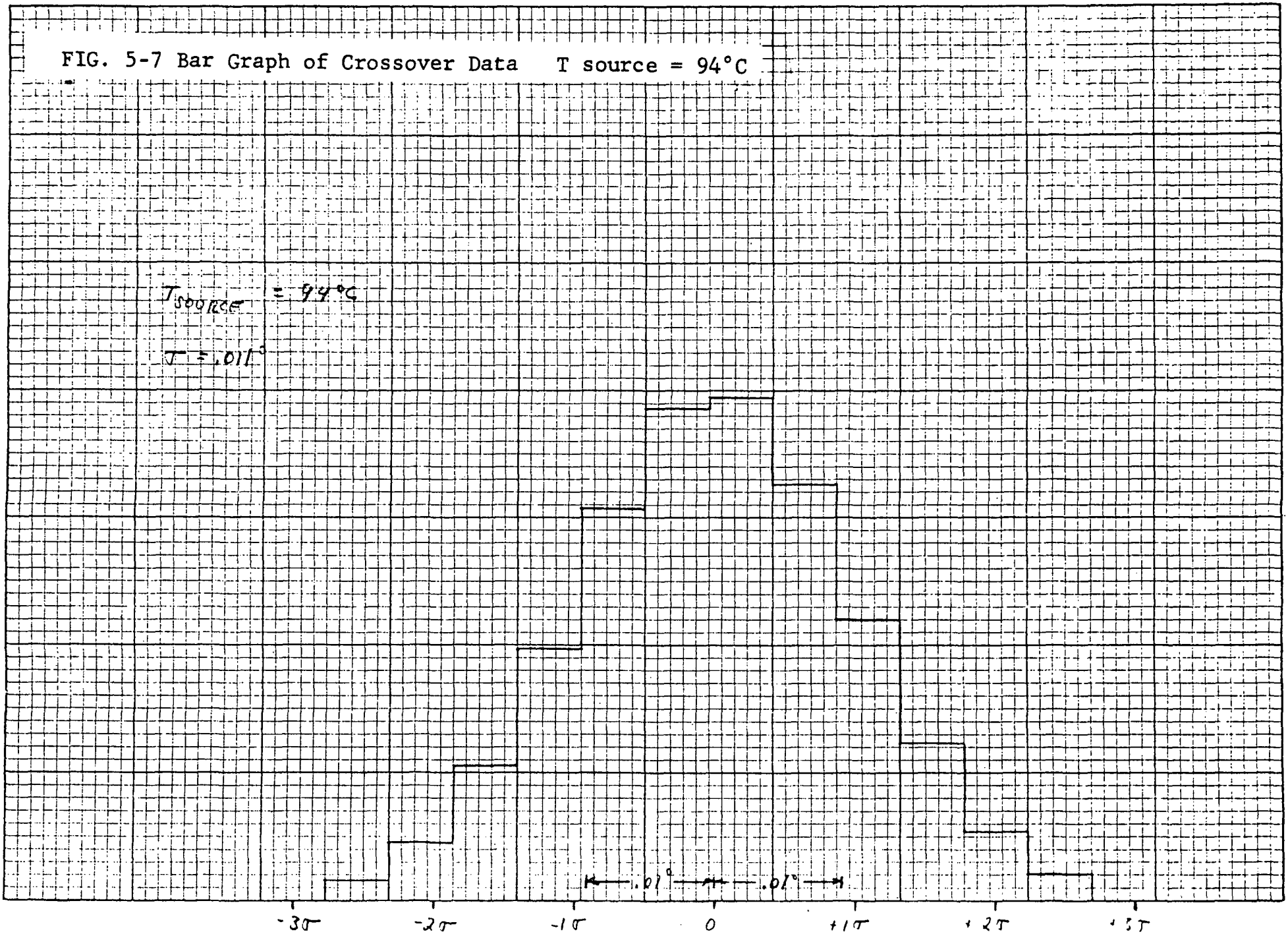

FIG. 5-8 Bar Graph of Crossover Data T source = 110°C

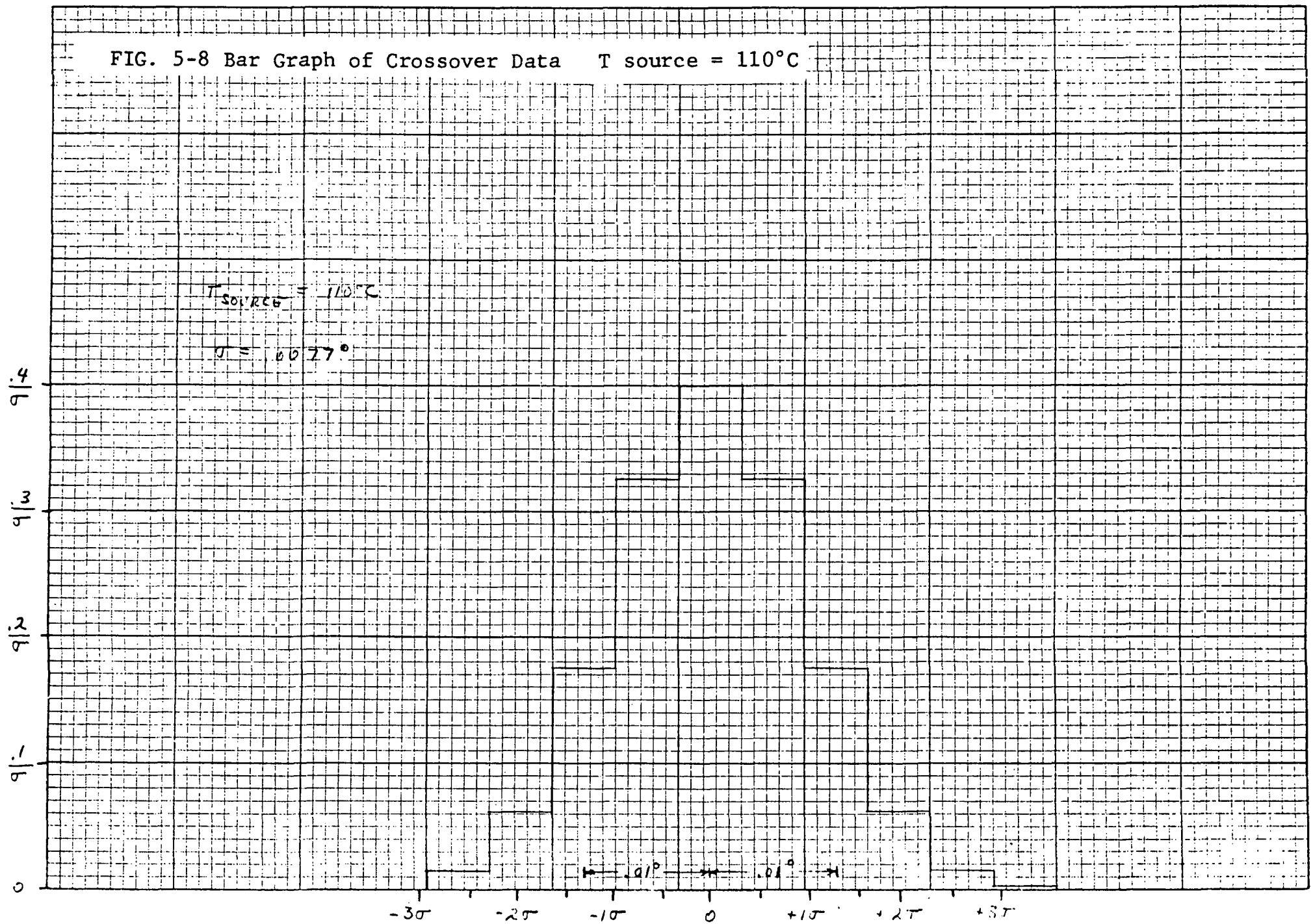

count = 0.005 degrees. A 1σ count error of 2.8 (for Arctic winter conditions) corresponds to an RMS angular error of 2.8 counts x0.005°/count = 0.014°. This error is very close to that predicted for the system. It will be instructive to compare the performance measured with the predicted and calculated parameters of the various components of the system.

Figures 5-9 and 5-10 show typical horizon radiance profiles. From these profiles we can compute the power incident on each detector at various scan positions, particularly near the normal zero crossing position. The computations are based on spacecraft altitude of 500Km. At the locator positions shown (i.e. 27Km for channel A and 43 Km for channels B_1 and B_2) the integrated irradiance of the detectors is:

For channel A:

$$N_{eff\ A} = 1.6 \times 10^{-4}\ W\text{-}cm^{-2}\text{-}\ ster^{-1}$$

and For channel B:

$$N_{eff\ B} = 4.5 \times 10^{-5}\ W\text{-}cm^{-2}\text{-}\ ster^{-1}$$

The solid angle covered by detector A at this position is:

$$\omega_A = .65 \times .0175 \times 1 \times .0175 = 2 \times 10^{-9}\ ster.$$

For detectors B the solid FOV is:

$$\omega_{B_1+B_2} = .5 \times .0175 \times 2 \times .0175 = 3 \times 10^{-4}\ ster$$

Next the power on each detector is computed.

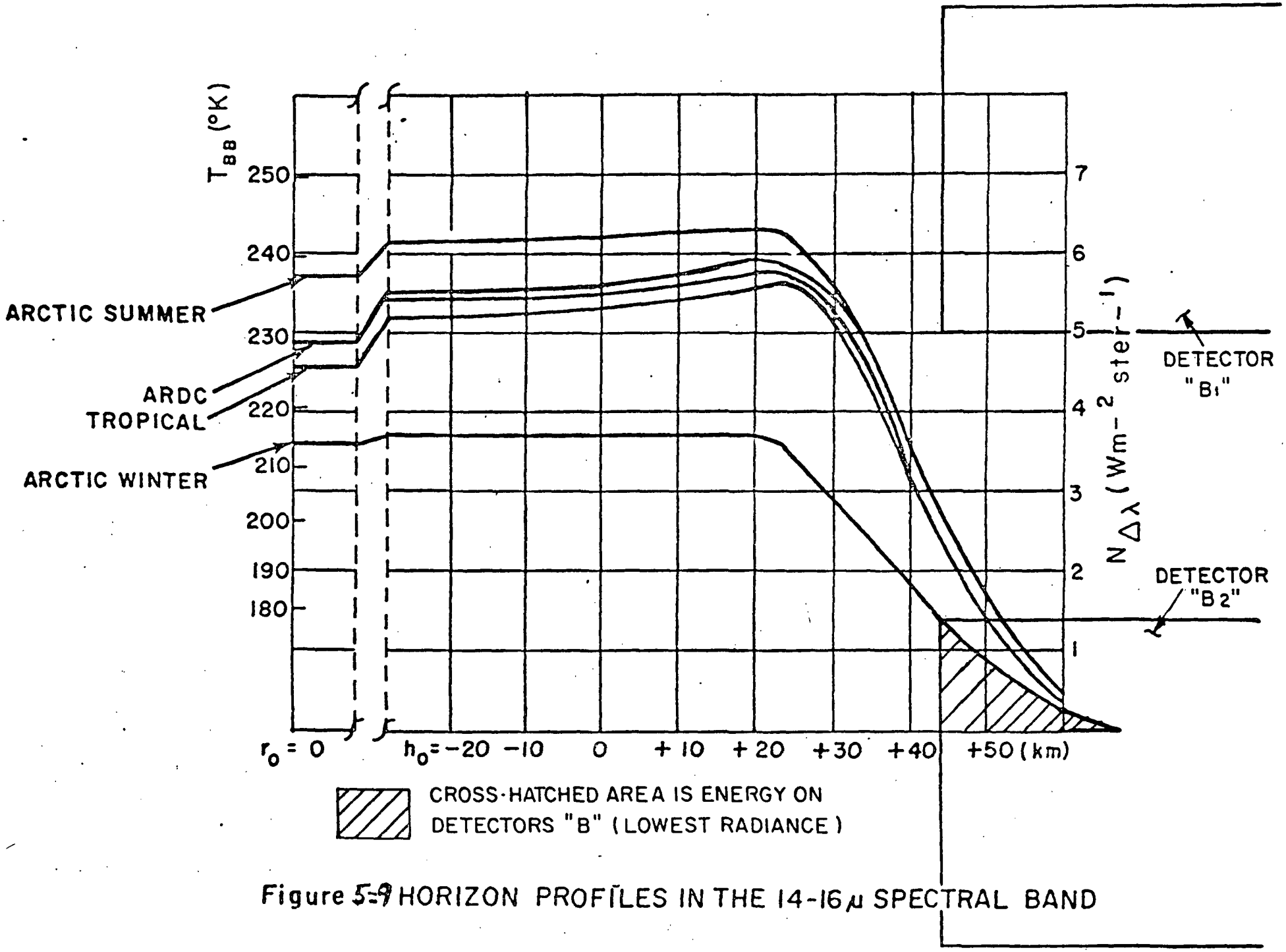

Figure 5-9 HORIZON PROFILES IN THE 14-16 μ SPECTRAL BAND

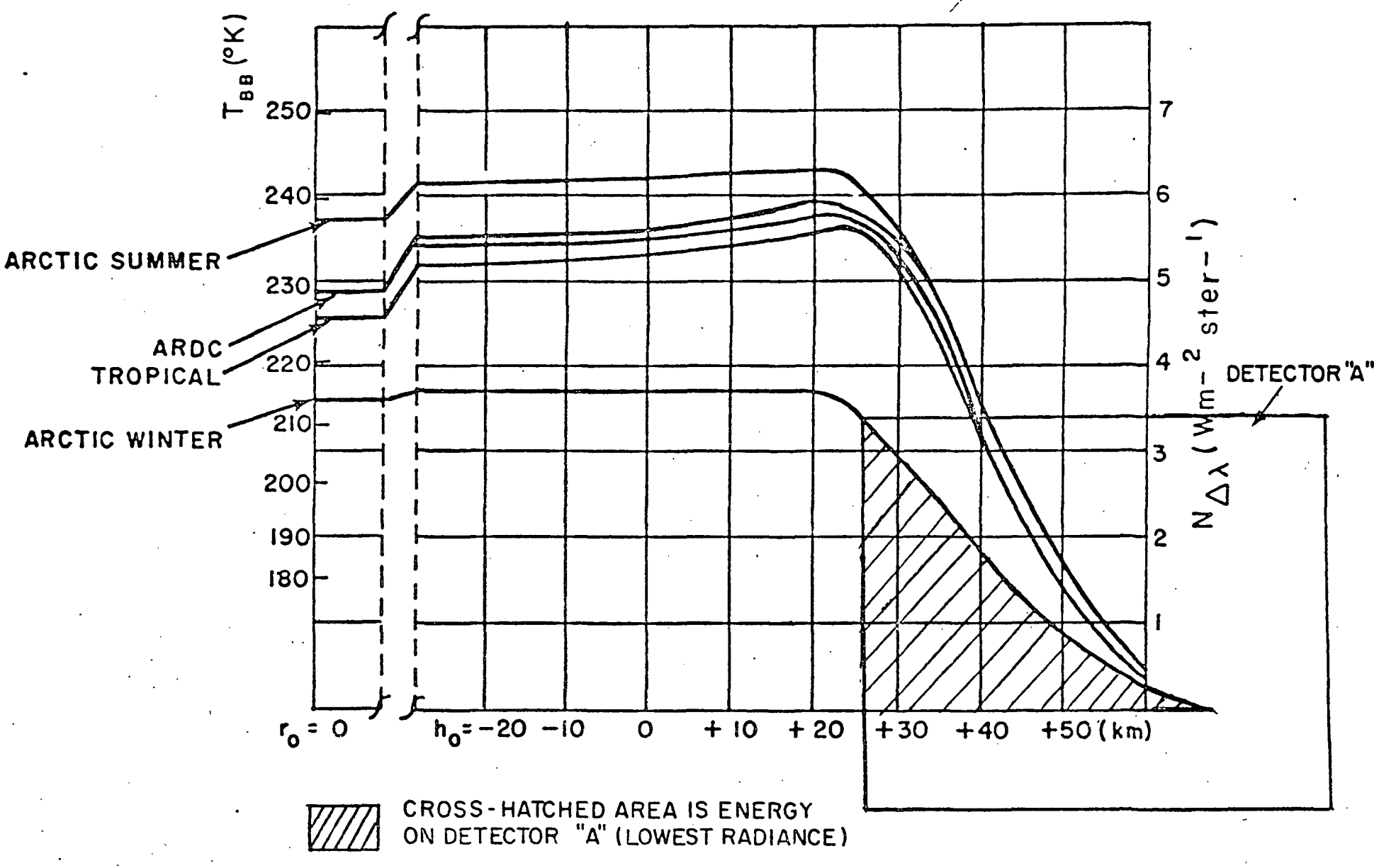

Figure 5-10 HORIZON PROFILES IN THE 14-16 μ SPECTRAL BAND

For channel A:

$$P_{D_A} = N_{eff\ A}\ \omega_A A_o \eta = 1.6 \times 10^{-4} \times 2 \times 10^{-4} \times 26 \times 0.22$$

$$= 1.8 \times 10^{-7} \text{ Watts}$$

Where A_o = clear aperture of sensor = 26 cm^2

η = efficiency of optical system estimated to be 0.22 (see Discussion of Optics)

For channels $B_1 + B_2$

$$P_{D_{B_1+B_2}} = N_{eff\ B}\ \omega_{B_1+B_2}\ A_o \eta$$

$$= 4.5 \times 10^{-5} \times 3 \times 10^{-4} \times 26 \times 0.22 = 8 \times 10^{-8} \text{ Watts}$$

Calculated values of responsivity and noise, at room temperature were: $\mathcal{R}$ = 170 V/W.*

It can be shown by calculation that detector noise is expected to be 1.3μV RMS.** By employing a sawtooth scan pattern the bandwidth requirement was reduced to under 100Hz which reduces the noise by a factor of ≈ 1.5 to 0.87μV RMS.

* Note, Appendix B shows the predicted responsivity of this detector.

** Calculations in Appendix C lead to the expectation that noise in this bandwidth referred to the detector level, should be 1.3 μV.

Since two B detector channels are operated in parallel the effective noise of Channel $B_1 + B_2$ is $0.87\mu V \times \sqrt{2} = 1.22\mu V$, so that the Noise Equivalent Power (NEP) of the B channel is:

$$NEP_{B_1+B_2} = \frac{V_n}{\mathcal{R}_B}_{B_1+B_2} = \frac{1.22 \times 10^{-6}}{170} = 7 \times 10^{-9} \text{ Watts RMS}$$

From this result and the power on the detector the position error for channel B and for the combination of channels A and B is obtained as:

For channel B:

$$\frac{S}{N_{RMS_B}} \frac{P_{D_{B_1+B_2}}}{NEP_{B_1+B_2}} = \frac{8 \times 10^{-8}}{7 \times 10^{-9}} = 11.4$$

Channel A has a considerably higher S/N:

$$\frac{S}{N_{RMS_A}} \frac{P_{D_A}}{\frac{V_{n_A}}{\mathcal{R}_A}} = \frac{1.8 \times 10^{-7}}{\frac{0.87 \times 10^{-6}}{170}} \approx 35.4$$

The total RMS value for the three detector system is then; $\frac{S}{N_{tot}} = 10.8$, for a cold planet.

The noise equivalent angular error for a cold planet is then, $\frac{0.34^\circ}{10.8} = 0.0315^\circ$ or $\pm\ 0.0157^\circ$, where 0.34° is the amount by which the FOV covers the earth.

It appears that the sensor head yields a measured repeatability that is slightly better than the value predicted by calulation.

5.4 MEASUREMENTS AT ANALOG AMPLIFIER OUTPUTS

Measurements were made of signal and noise at each of the analog amplifier outputs to determine how closely predicted performance figures match the measured results.

With the scanning-mirror drive turned off the wide band noise for channel A is 17 mV peak to peak, (3.4 mV RMS was measured). The gain from detector output to the point of measurement (test point on the auxiliary electronics unit) is 4600. Therefore the noise referred to detector level is: $\frac{3.4}{4600} = 0.75\ \mu V$, this is just slightly less than the predicted 0.87 μVolts.

The signal at the amplifier output for a 230°K equivalent planet temperature, with the detector scanned fully across the target was measured as 0.8 Volts. The signal at the detector is therefore, $V_D = \frac{0.8}{4600} = 174\ \mu V$ peak.

The power on the detector flake for a 230°K planet temperature and full illumination of the detector is found from

$$P_{D_A} = N_{\Delta\lambda}\ \omega_A\ A_o$$

where

$N_{\Delta\lambda} = 5 \times 10^{-4} W\ cm^{-2}\ ster$

$\omega_A = 1.292 \times 0.0175 \times 1 \times 0.0175 = 4 \times 10^{-4}\ ster$

$A_o = 26\ cm^2$

$\eta = 0.22$

$P_{D_A} = 5 \times 10^{-4} \times 4 \times 10^{-4} \times 26 \times .22 = 1.14\ \mu W$

The measured value of responsivity (152) is just under the expected level (170) and the measured noise is somewhat less than the predicted value.

The Noise Equivalent Power (NEP) is:

$$\text{NEP } (14\text{-}16\mu,\ 1\text{-}100) = \frac{P_D}{S/N} = \frac{1.14 \times 10^{-6}}{174\ \mu V/.75\ \mu V} = 4.9 \times 10^{-9} \text{ Watts}$$

This compares closely with the predicted value of 5×10^{-9} Watts.

6.0 INSTRUCTIONS FOR OPERATING THE ARPESH SYSTEM

The Arpesh System consists of two units, the sensor head and the auxiliary electronics unit, interconnected by means of a single cable (see Figure 1 - 1).

Set the head up on a suitable test stand that may be used for testing for horizon acquisition and repeatability of horizon location. The normal attitude of the sensor head is that shown in Figure 1 - 1 with the connector and cable emerging at the top of the sensor head. The auxiliary electronics may be placed in any convenient location. Connect the cable from the rear of the auxiliary electronics unit to the top of the sensor head.

Next connect the power input at the rear of the auxiliary electronics to a power supply, leaving power switch on electronics panel in "off" position. With the power supply set for 28 volts (use a supply capable of furnishing 2 Amps), connect the red lead to the +28 Volt terminal and the black lead to the Zero volt terminal. Note, the power pilot light will go on when prime power is applied even though the front panel power switch is still off.

With the power supply power "on", the various power supplies in the auxiliary electronics are connected to the 28 Volt input and power will be drawn and some of the lamps on the panel will be "on". (Much of the primary power drawn is used for the lamps.) Place the command switch in the Off-position and turn power switch "On". For normal scanning to obtain target acquisition and horizon location (assuming a blackbody, BB, source simulating the earth is heated to the appropriate temperature - see Section 4 for typical simulator system and simulator BB temperatures), turn command switch to "scan".

The outputs from the auxiliary electronics include the lamp status conditions (lights On or Off) for binary position readout, acquisition, sun presence, possible failures, etc. Also,

available are: a) a 1Hz clock pulse (BNC connector) for CRO synchronization, b) a pulse count output for readout of angular position on an accumulator, c) a reset pulse for accumulator discharge.

Figure 6 - 1 shows the front panel layout of the auxiliary electronics unit. This serves to identify the various indicator lamps, controls and test points. The waveforms and amplitudes at the various interconnections of greatest interest are sketched in Figure 6 - 2.

The gain values for the various combinations of switch position of the four "R" adjust command toggle switches are listed below (corrected for detector area factor):

Switches				
1	2	3	4	Gain Ratio 'R'
0	0	0	0	4.017
0	0	0	1	3.974
0	0	1	0	3.930
0	0	1	1	3.886
0	1	0	0	3.842
0	1	0	1	3.799
0	1	1	0	3.755
0	1	1	1	3.712
1	0	0	0	3.688
1	0	0	1	3.624
1	0	1	0	3.581
1	0	1	1	3.537
1	1	0	0	3.493
1	1	0	1	3.450
1	1	1	0	3.406
1	1	1	1	3.362

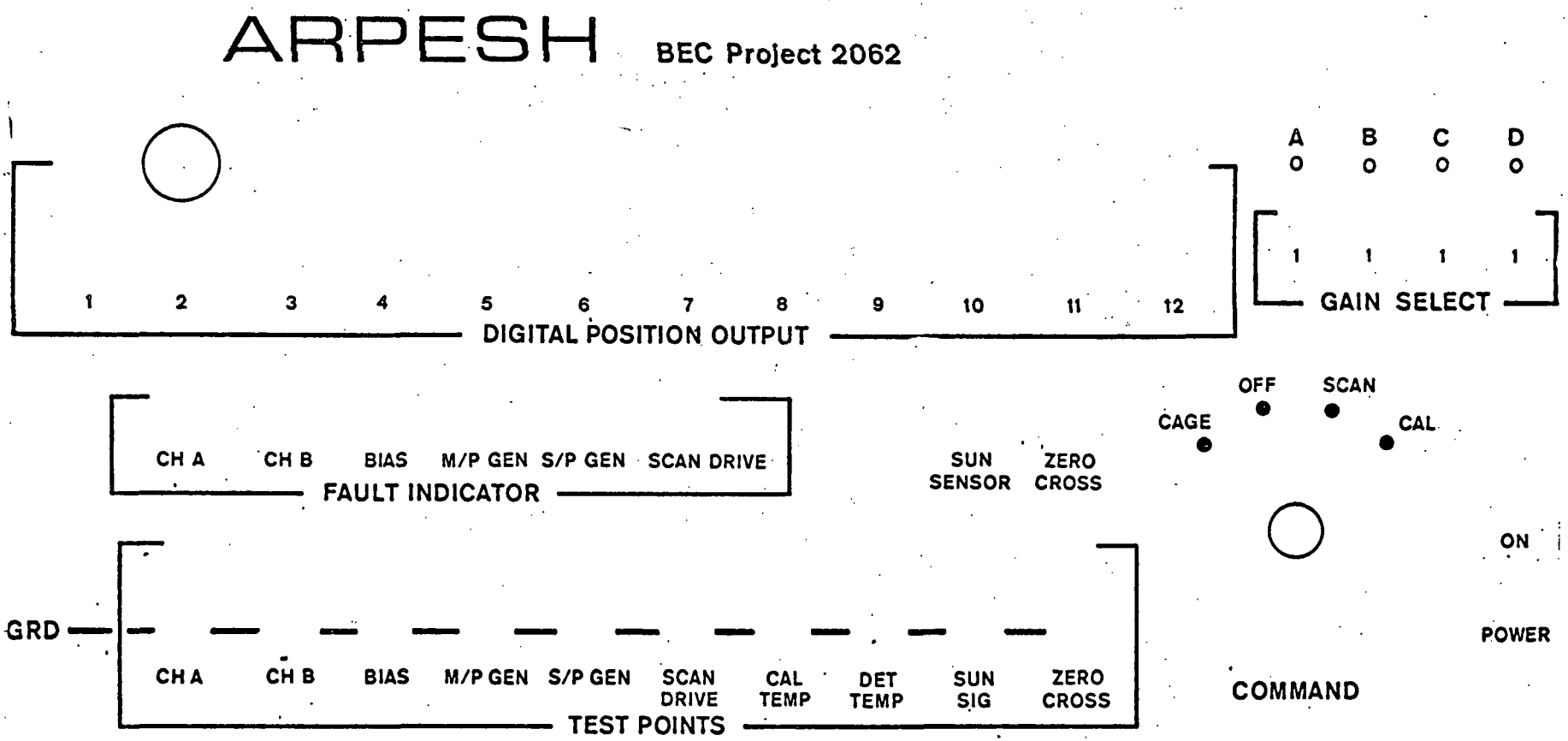

FIG. 6-1 Front Panel Layout, Auxiliary Electronics Unit.

Figure 6-2 TYPICAL WAVEFORMS AT AUXILIARY ELECTRONICS TEST POINTS

FRONT PANEL (L TO R)

1. Channel A (CH-A)

2. Channel B (CH-B)

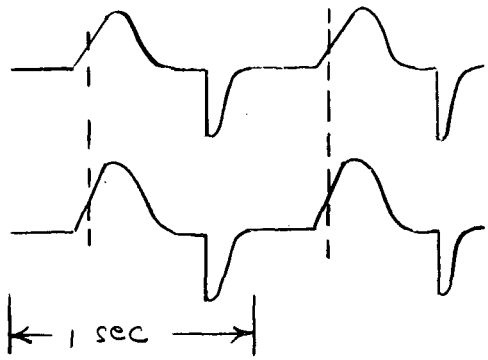

3. Detector Bias (BIAS)

4. Multipulse Gen. (M/P GEN)

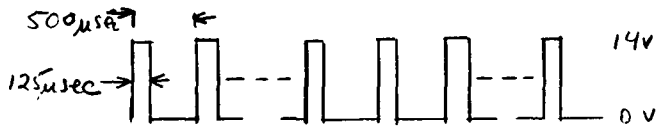

5. Single Pulse Gen (S/P GEN)

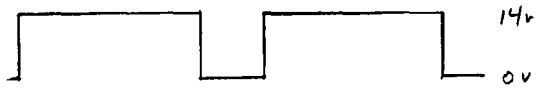

6. Scan Drive (SCAN DRIVE)

7. Cal. Patch Temp. (CAL TEMP) DC Output as per Fig. 3-3.3
8. Detector Temp. (DET. TEMP) DC Output as per Fig. 3-3.3
9. Sun Signal (SUN SIG) +14V (and light) indicates sun presence

10. Zero Crossing Indic. (ZERO CROSS)

11. 1 Hz Clock (BNC) (rear)

12. Serial Null Count (G-R Jack)

13. Accumulator Reset (G-R Jack)

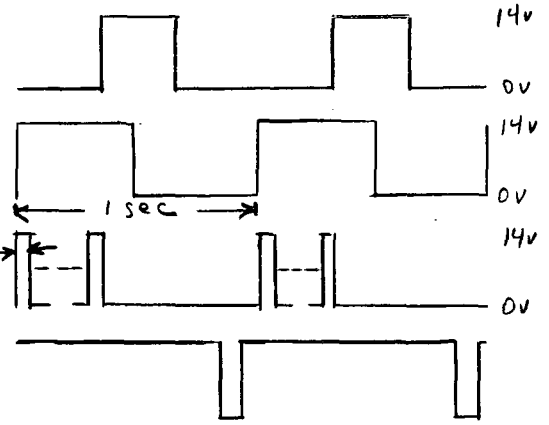

Mirror Scan Pattern (for reference only)

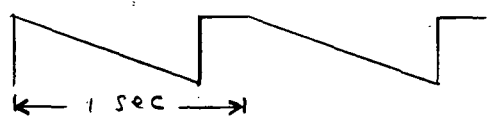

The lamp readouts, in binary code, are listed below for convenience; their sum representing the Ronchi pulse count:

LIGHT	BITE											
	1	2	3	4	5	6	7	8	9	10	11	12
ON	1	2	4	8	16	32	64	128	256	512	1024	2048
OFF	0	0	0	0	0	0	0	0	0	0	0	0

The thermistor temperature readout is in analog form. Figure 3-3.3, shows the equivalent temperatures for given DC voltage readouts.

Note that while the fault detection system shows a simple light "ON" condition indicating a fault in the various critical systems, there is one exception to this. The noise measurement and excess noise fault circuitry is not able to differentiate between excess noise and a possible target presence signal that will normally be larger than normal noise. Therefore, in normal scan mode, it will be noticed that the Channel A and B noise fault lamps will flicker when the detectors see radiance variations. To use the Channel A and B noise fault detection system, it is necessary to command the scanner to stop its movement. This is done by switching the mode switch preferably to the off-position.

6.1 SENSOR HEAD ELECTRONICS CIRCUIT TEST POINTS

The main electronics section of the Sensor Head is comprised of four printed circuit boards located on the side of the unit. Standoff terminals on the boards are used as junction points for wire-to-pc board connections and are also used as test points at which circuit waveforms may be obtained. The location of these test points and signal waveforms are shown in Figures 6-3, 6-4, 6-5, and 6-6. Circles with numbers are inputs to or outputs from circuits on the board. Circles without numbers are interconnection terminals near the edges of the board and are used as an aid in location of test points.

The circuits on the boards are as follows:

1. Board No. 1 - Processing circuits
2. Board No. 2 - Scan Drive Generator & Section of Servo Circuit
3. Board No. 3 - Servo Motor Drive Circuit
   Single Pulse Generator
   Multipulse Generator
   Preamplifier Low Voltage Regulators
4. Board No. 4 - Bias filter Section 1
   Multipulse Generator Post Amp
   Detector Heater Amplifier
   Decoupling Networks

(19) NULL INDICATED OUTP.

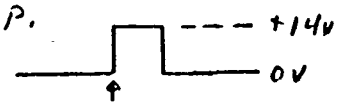

(18) FOV B OUTP.

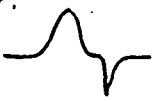

GND (12)

CHAN B_2 INP. (11)

BOARD # 1

(1ST FROM TOP)

RT_3 INP. (9)

GND (10)

GND (8)

CHAN B_1 INP (7)

(20) ALLOW NULL

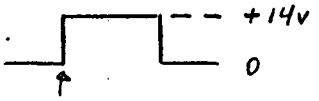

RT_2 INP. (5)

GND (6)

FOV A OUTP.

GND (4)

(21)

(17) CLAMP GATE

CHAN A INP. (3)

+14VDC

(22)

(16) R CONTR. D

(23) (24) -14VDC

(15) (14) R CONTR. B

R CONTR. C

GND (2)

RT_1 INP. (1)

(13) R CONTROL A

FIGURE 6-3 TEST POINTS & WAVEFORMS

BOARD # 2

(2ND FROM TOP)

1 HZ CLOCK. INP. (3)

(2)

TACH. GND

(7)

SERVO

(14) INTEGRATOR OUTP.

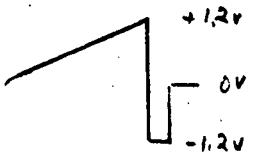

END OF SCAN (1)

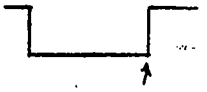

-14v

(22)

(21)

+14v

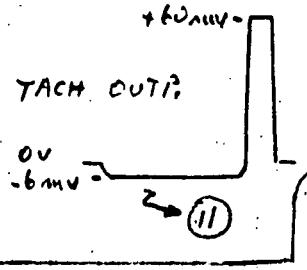

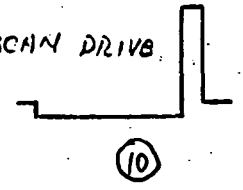

FIGURE 6-1 TEST POINTS & WAVEFORMS

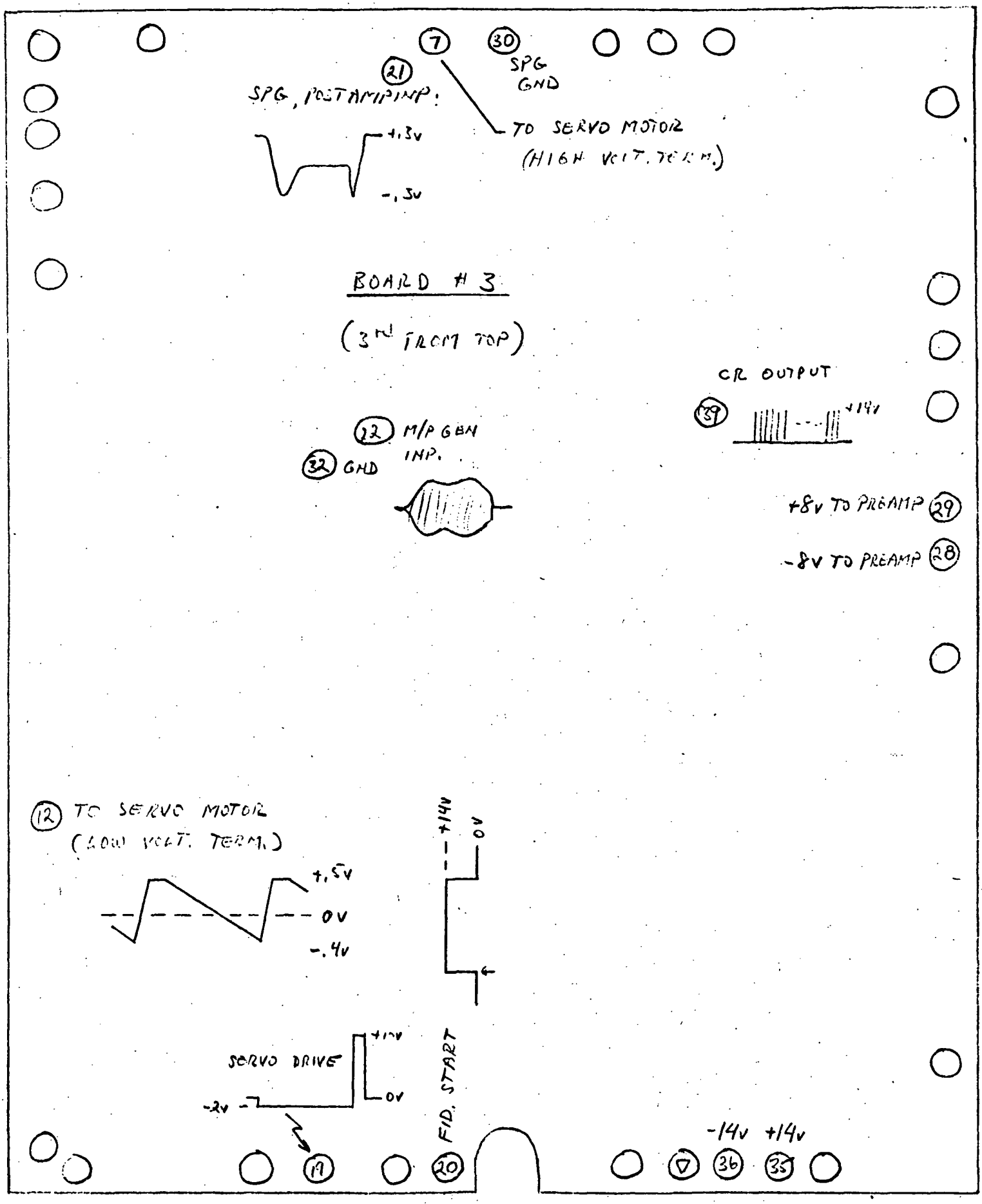

FIGURE 6-5 TEST POINTS & WAVEFORMS

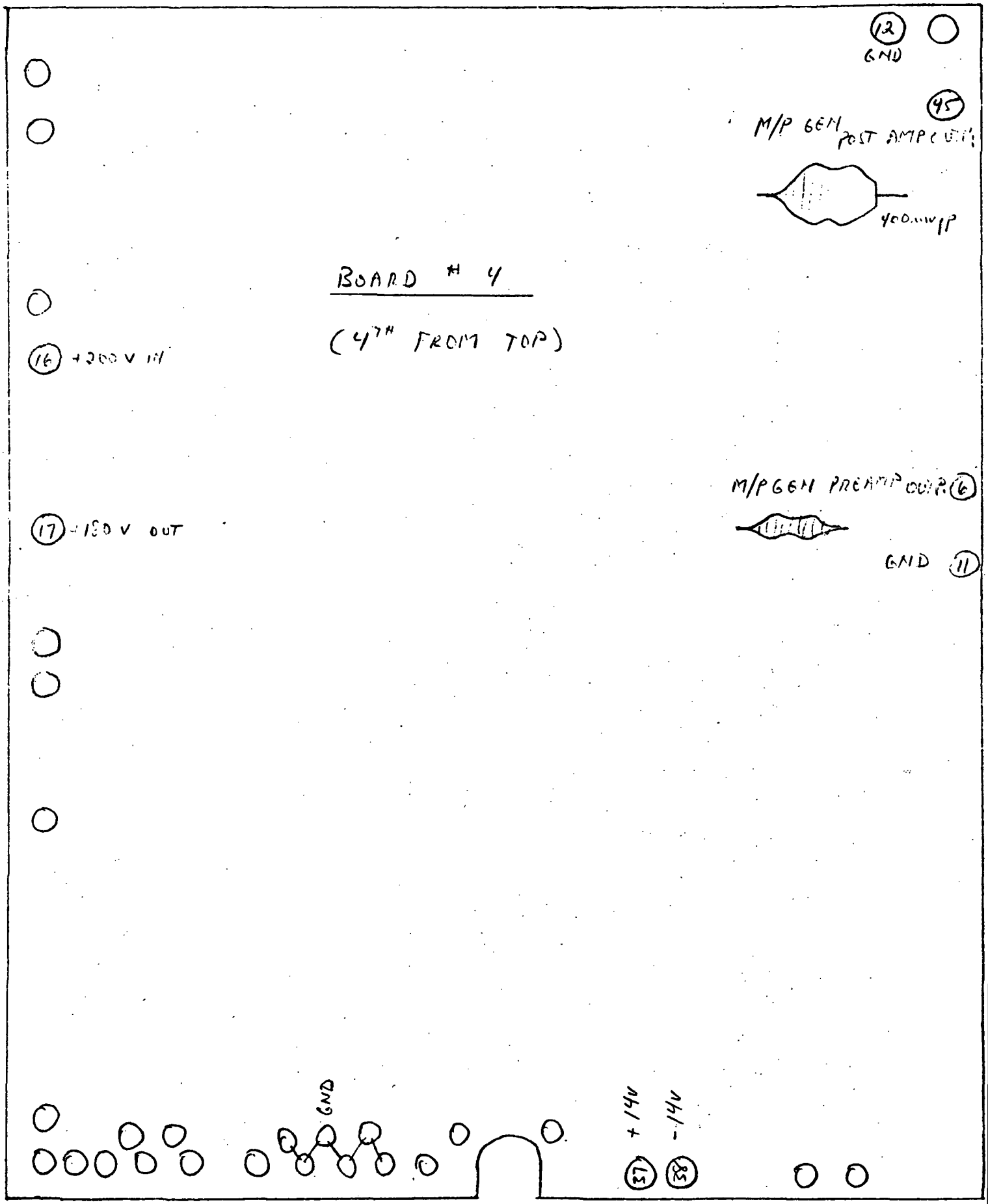

FIGURE 6-6 TEST POINTS & WAVEFORMS

7. CONCLUSIONS

The ARPESH program just concluded has advanced the state of the art of infrared horizon sensors in a number of areas. The horizon sensor system was conceived by NASA/LRC and was designed and constructed by BEC. This unique horizon sensor is capable of providing what is probably the highest accuracy achieved by this technique to date.

The system employs only one moving part (scanning mirror) that is supported by flexural pivots stressed minimally, thus having virtually unlimited life. By avoiding use of components such as bearings that require lubrication, there are no parts that wear out with the results that a high reliability is achieved. The system design incorporates some unique features that are responsible for the high accuracy achieved. These include a novel "locator" concept developed by NASA/LRC that produces a highly repeatable null crossing, nearly independent of radiance variations on the horizon, when a detector produces a signal (representing the integrated radiance over a segment of the horizon) that is equal in amplitude to a signal produced by a second detector channel (with higher gain) and whose field of view is so located that it trails that of the first channel.

This "locator" system with parameters of the sensor design has been exercised through computer calculations at NASA/LRC using a large variety of radiance profiles and was found to yield a horizon crossing definition with a variation of less than 0.7 Km at an altitude of 500 Km.

The horizon sensor built was tested in the laboratory with simulation equipment that permits the sensor performance to

be estimated for various equivalent earth horizon temperatures.

By monitoring the sensor output (scanner angle at which the horizon is located), angle errors were recorded as follows:

For 245°K equivalent earth temperature = .0077° (1σ)

For 230°K earth = .011° (1σ) and

For 210°K earth = .014° (1σ)

Among the novel design features used in this horizon sensor are: a scan angle measurement system that creates a large number of pulses (1500 counts for a 7-1/2 degree scan field) optically, by illuminating a Ronchi reticle with a light emitting diode (LED) and sensing the modulation produced when the bar pattern is reflected from the scan mirror and an interference pattern is detected by a silicon photo diode. By counting pulses from the start of the scan to the point of zero crossing (horizon location), an angle readout is obtained as a digital number (representing the angle scanned to the locator or in the form of a binary code). The resolution of the angle readout system is 0.005°.

A second precise optical position location system is used for accurately indicating the start position of the scanning mirror. This start position (or fiducial mark) is generated by a technique similar to that used in an electrical auto-collimator in which an LED light beam is reflected from another portion of the rear of the scan mirror and intercepted at a point on a fine reticle in front of a dual silicon photo cell. The repeatability of this fiducial reference mark can be established to a tenth of an arc-second.

The design of all systems(detector, optics, electronics mechanical parts) has been carried out so as to insure operation under stringent operating conditions including an operating temperature range -20°C to +75°C and a high vibration and acceleration environment.

The feasibility and system accuracy have been established as part of the present program. A sensor has been built with high grade components, that at least have MIL Spec equivalents, and with drawing and workmanship standards suitable for space instruments. Not all tests could be performed as part of the present program.

Information and experience gained in carrying out the design and construction of the ARPESH indicate areas in which improvements and simplifications are possible. These include improvements in the detector, the multi-pulse generator used for angle readout, the scanner, and possible reductions in weight and power consumption.

APPENDIX A

SOLID STATE ELECTRO-OPTICAL ALIGNMENT INSTRUMENTS

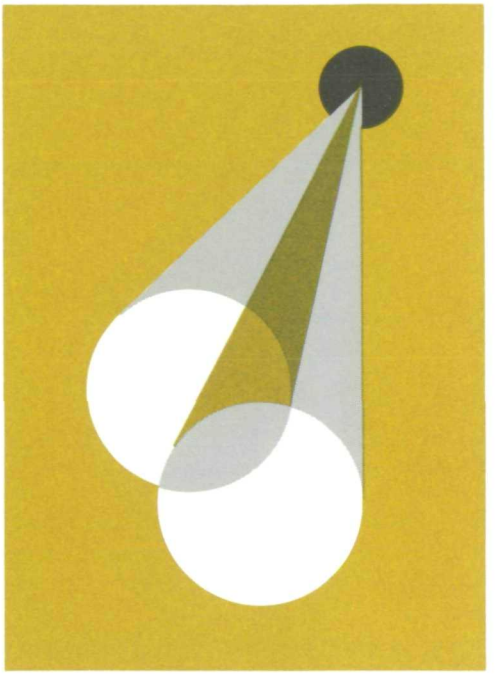

MINEAC®

MINIATURE ELECTRONIC AUTOCOLLIMATOR SYSTEM

For precise, non-contact measurement of angular position or deflection in either one or two axes

APPLICATIONS/ALIGNMENT & MONITORING

- ☐ Architectural Structures
- ☐ Missile Guidance Systems
- ☐ Antennas
- ☐ Space Vehicles and Airframes

APPLICATIONS/SPECIAL STUDIES

- ☐ Thermal Deformation
- ☐ Vacuum Testing
- ☐ Mechanical Loading and Vibration

GENERAL DESCRIPTION

The Miniature Electronic Autocollimator (MINEAC®) System provides highly sensitive and extremely reliable angular position measurements. The System will precisely and continuously monitor and control the attitude of a reflecting surface to within as little as 0.02 arc-second.

The MINEAC System consists of an all-solid-state angular position transducer (MINEAC) with a gallium arsenide light source and a rugged, lightweight MINEAC Amplifier-Demodulator (MAD) unit. The transducer weighs only 5.5 ounces. It has no moving parts, occupies 3.5 cubic inches of space, and consumes only 0.4 watt of power. The companion MAD unit supplies all operating voltage and output circuitry to provide dc analog data. A special, four-foot, flexible ribbon cable connects the two elements of the MINEAC System.

The MINEAC System is ideal for dynamic applications where the target being monitored is subject to changes in orientation. The MINEAC System does not make physical or electrical contact with the target under observation. Using projected and reflected light beams, the system generates electrical error signals directly proportional to the magnitude and direction of the target's angular deviation.

In a closed-loop servo system, these signals can be used to correct or maintain predetermined angular relationships between the MINEAC System and its monitored target.

The MINEAC System is capable of providing continuous, automatic monitoring from either immediately adjacent or reasonably remote locations. Absolute maximum working distance is five feet. As the distance between the MINEAC transducer and the target is increased from zero to 60 inches, scale factor, resolution, linearity, linear range and acquisition range are predictably reduced.

Other electronic autocollimators suitable for use at greater distances than five feet are also available from Barnes.

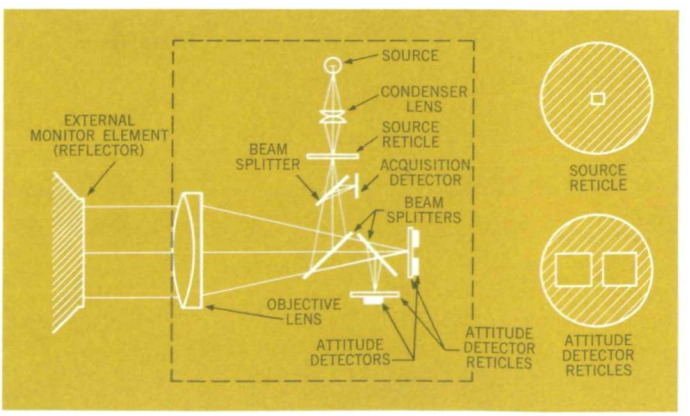

Figure 1. Optical System Schematic

BARNES ENGINEERING COMPANY

30 Commerce Road, Stamford, Connecticut 06904
Telephone (203) 348-5381 / TWX 710-474-3367

Bulletin 23-521C

Printed in U.S.A.

SYSTEM OPERATION

Basic elements of the MINEAC System are a pulsed, gallium arsenide diode "light" source (which emits in the near infrared region), an optical system, one or two independent pairs of measuring detectors for single or dual axis measurement, a confirmation detector, and three preamplifier channels.

The gallium arsenide source and its associated optics project a modulated, collimated light beam to the target's reflecting surface.

Upon receiving the reflected light beam from the target, the MINEAC System generates electrical signals which are directly related to the angular deviation between the projected and reflected beams. The magnitude of the angular deviation is represented by the output signal amplitude. The phase of the signal indicates the direction of movement. The ac signal generated by the preamplifiers is synchronously demodulated in the MINEAC Amplifier-Demodulator (MAD) unit to give a dc output whose polarity represents the direction of deviation.

If the reflected light beam is perfectly parallel to the outgoing beam, no signal will be generated by the MINEAC System. Thus, a null output normally indicates perfect alignment of the target.

However, if the plane of the reflecting surface has shifted by as little as 0.02 arc-second, a discrete error signal proportional to the deviation is produced.

To provide means for distinguishing between the null output condition and an ambiguous, out-of-field condition, an additional detector provides a separate confirmation signal whenever the target's reflecting surface is within approximately 10 arc-minutes of perfect alignment. In this condition, a green light appears on the front panel of the MAD unit, while the outputs of the measuring detectors are presented on panel meters.

Output jacks on the rear of the MAD unit provide means for recording attitude deviations. The confirmation signal is also available externally for lock-on functions or remote display.

OPTIONAL ACCESSORIES

Mounting Fixture: Mounting Fixture (Part No. 23 – 573) is adapted for mounting the MINEAC transducer to its upper surface, while the bottom plate is secured to the customer's equipment. The collimated light beam is projected through an aperture in this bottom plate. Two independent, fine-adjusting screws provide precise adjustment of the MINEAC transducer's pointing direction for convenience in initial alignment with the target's reflector. This Mounting Fixture also contains two mounting slots for insertion of the Optical Wedge to calibrate either axis.

Optical Wedge: Optical Wedge (Part No. 23 –574) is a glass deviation wedge mounted in a Delrin slide for insertion into the Mounting Fixture. It deviates the collimated light beam by a known amount, which is supplied as a calibration. Deviation values from 30 to 300 arc-seconds are available.

Alignment Mirror: A reference mirror facing in the opposite direction to the collimated light beam may be supplied for orienting the pointing direction of the MINEAC transducer to a predetermined direction. It is mounted inside the transducer case and is normally covered by a rotatable cap. Its pointing direction is within one arc-minute of that of the collimated light beam.

The alignment mirror must be installed in the MINEAC transducer at time of purchase.

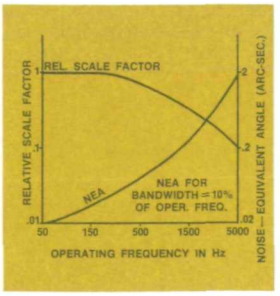

Figure 2. Frequency Response (typical)

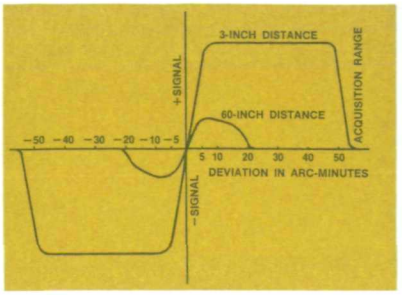

Figure 3. Transfer Functions (typical)

SPECIFICATIONS

*Linear Range	± 5 arc-minutes
*Linearity (over ± 5 arc-minutes)	15 percent
*Resolution (Noise Equivalent Angle)	0.02 arc-second (Note 1)
*Cross-coupling	2 percent
*Acquisition Range (measuring detectors)	± 54 arc-minutes
*Confirmation Detector Range	± 10 arc-minutes
Output Scale Factor (Note 2)	Adjustable, 10-1000 mv/arc-sec.
Operating Distance (Note 3)	0 to 60 inches
Operating Frequency (Note 3)	50 to 5000 Hz
Output Impedance	10K ohms
Power Requirements (Note 4)	117v, 50-400 Hz, 10W
Dimensions:	
MINEAC Transducer	1.88L x 1.56W x 1.25H (inches) 4.78L x 3.96W x 3.18H (centimeters)
MINEAC Amplifier-Demodulator (MAD)	10W x 5H x 10D (inches) 25.4W x 12.7H x 25.4D (centimeters)
Weight:	
MINEAC Transducer	5.5 ounces (165 grams)
MINEAC Amplifier-Demodulator (MAD)	11 pounds (5 kg.)

*For precise definitions of parameters preceded by an asterisk (*), please refer to the Table of Definitions.

NOTES

Note 1. 1 Hz bandwith

Note 2. Saturation will limit output to ± 8 volts.

Note 3. The performance specifications listed above apply to the MINEAC transducer mounted within three inches of the reflector, and operating at 60 Hz. (See Figures 2 & 3 for relative performance at 60 inches and at higher frequencies.)

Note 4. For operation at 50 to 400 Hz, the MINEAC Amplifier-Demodulator unit may be connected directly to a power supply having 10 watts capacity. As an alternative, this unit may be powered from a 50-60 Hz power supply and triggered up to 5 KHz by an auxiliary 10 ma input to the rear panel.

TABLE OF DEFINITIONS

(as they appear in Specifications)

Linear Range: The angular region on either side of the null position within which the signal is proportional to angular deviation.

Linearity: The maximum departure of indicated angle from a best-fit straight line drawn through data points from – 5 to + 5 arc-minutes, expressed in percent of true angle.

Resolution or Noise Equivalent Angle (NEA): The angle which generates a signal equal to the rms value of noise within a specified bandwidth at the output.

Cross-coupling: The spurious output from either channel when deviation occurs only in the other channel.

Acquisition Range: The angular range on either side of null over which a reading at least twice the noise level is obtained from the measuring detectors.

Confirmation Range: The angular range around null within which the confirmation detector circuit is operative.

APPENDIX B

THERMISTOR RESPONSIVITY

The responsivity of a thermistor detector of dimension 0.5 x 0.5 mm as used in ARPESH and its variation with ambient temperature is approximately as in the graph attached (A Thermistor). For the 0.5 x 0.5 mm detector, at room temperature, we expect $\mathcal{R}$ = 170 V/W.

Further data on thermistor detector characteristics is given in the attached paper and Bulletins 2-101 and 2-102.

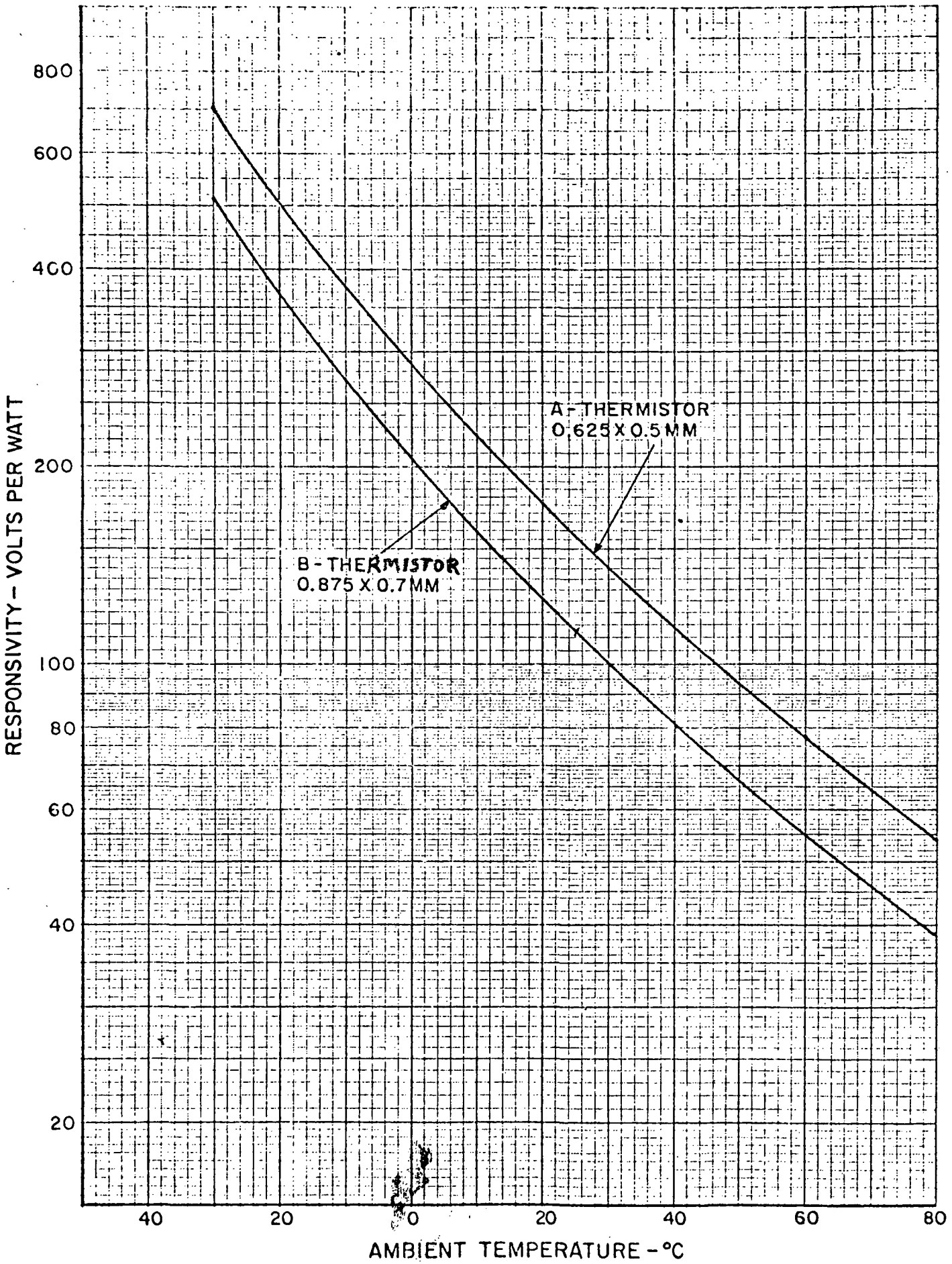

VARIATION OF BRIDGE RESPONSIVITY WITH AMBIENT TEMPERATURE AT 60% OF PEAK BIAS

THERMISTOR INFRARED DETECTORS

PART I

INTRODUCTION AND OPERATING PRINCIPLES

By Russell DeWaard and Eric M. Wormser
Barnes Engineering Company
Stamford, Connecticut

December, 1961

PROPRIETARY NOTICE

This document contains information proprietary to Barnes Engineering Company that is not to be divulged outside the Company without written permission.

PATENT NOTICE

This document contains information concerning items for which patents have been awarded to Barnes Engineering Company and items for which patent applications are pending.

FOREWORD

This is an incomplete draft of a paper prepared about one year ago for submission to the Journal of the Optical Society of America. Unfortunately the authors have been unable to find time to complete the paper. It is believed, however, worthwhile at this time to issue the material as a Company report for its educational value. Unfinished topics under Part I are listed in the table of contents.

One or two more Parts on the subject are intended for the near future, covering more definitive data on standard and immersed detectors as well as information and properties on specialized detectors such as "selective wavelength" types.

The authors intend to complete, revise, and edit Part I and to submit it for publication in Applied Optics early in 1962.

TABLE OF CONTENTS

LIST OF ILLUSTRATIONS

LIST OF TABLES

1. INTRODUCTION

Thermistors are thermally sensitive resistors which have a large negative temperature coefficient of resistivity. Employed as radiation detectors, thermistor elements are made in the form of small thin flakes and attached to good heat sinks to induce fast response. The thermistor element, or elements, comprise part of a simple electrical circuit. Resistance change in the thermistor due to temperature fluctuations produced by incident radiation causes a voltage change in the circuit. In a true sense, the thermistor element is not a transducer but operates by virtue of its temperature dependence to modulate a steady voltage applied to the detection circuit.

Thermistor detectors were developed by the Bell Telephone Laboratories in 1946 and reported in classified literature [1] [2]. One of the present authors* published [3] on their status and properties in 1952. Developments through 1958 are described in a Navy Department report [4]. The thermistor detectors described in the present papers refer to those developed by the Barnes Engineering Company, the work in part being supported by contract** from the Navy Bureau of Ordnance.

* Eric M. Wormser

** Contract Bu Ord. No. 14836

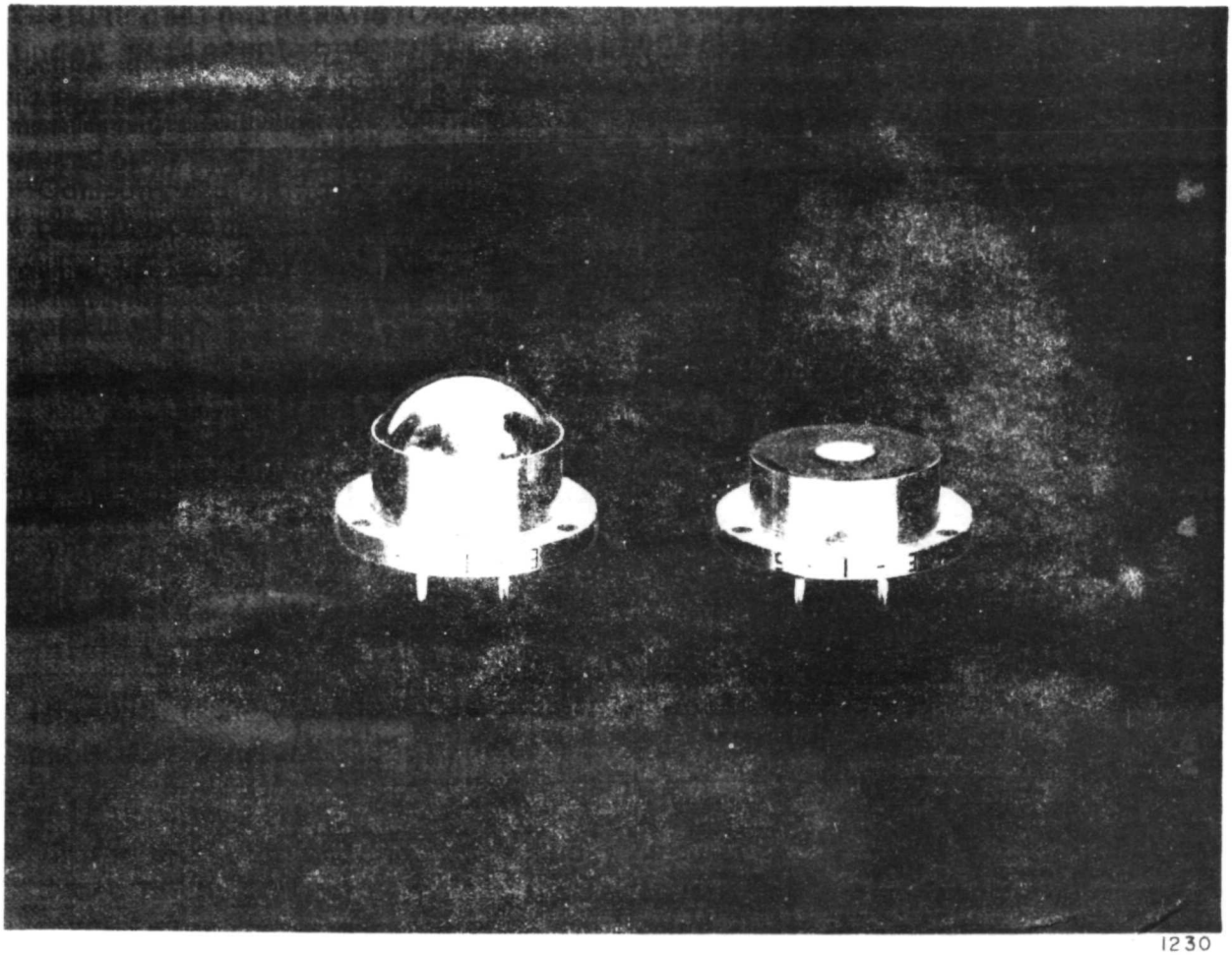

1230

Figure 1- TYPES OF THERMISTOR DETECTORS

2. THERMISTOR PROPERTIES

Two types of thermistor detectors are shown in Figure 1. In over-all size they are about 5/8" in diameter by 1/2" in length. One is an optically immersed detector, the dome shaped optical element being high purity germanium with an anti-reflection coating. The other is sealed with an infrared window material, such as KRS-5, silver chloride, germanium, silicon, or other infrared optical material depending upon the wavelength region of interest. The detector capsule may be sealed at normal pressure or evacuated.

Thermistor materials are metallic oxides, chiefly of manganese, nickel, and cobalt. They were originally developed in several compositions at the Bell Telephone Laboratories[5]. In sintered form they are semiconductors exhibiting a high negative temperature coefficient of resistance, about 4%/°C. In particular, two compositions designated as Material No. 1 and Material No. 2 are of chief interest because they permit the attainment of a desired detector impedance in a variety of geometric shapes. The electrical properties of these materials are listed in Table I.

TABLE I

	Material No. 1	Material No. 2
Resistivity (ohm-cm)	2500	250
Resistance- Megohms/square in 10 micron thickness	2.5	0.25
Material Constant - β (°K)	3800	3400
Temperature Coefficient of Resistance $-\alpha$ ($°C^{-1}$)	-.042*	-.038*

The two compositions differ principally in resistivity, Material No. 1 being 10 times that of No. 2. The former yields suitable resistance values in square or near square elements in the nominal thickness of 10 microns. Material No. 2 is employed for long-narrow thermistors or may also be used in short-wide configuration where low resistance is desired. Depending upon the length to width proportions, one or the other affords detector impedance in a suitable range for coupling to vacuum tube preamplifiers (1-10 megohms). Material No. 2 in short and wide configuration yields lower impedances(50K ohms) suitable for coupling to transistor type preamplifiers.

Thermistors obey the simple exponential law characteristic of intrinsic semiconductors, namely,

$$R = K\epsilon^{\beta/T} \quad \ldots\ldots\ldots\ldots\ldots\ldots\ldots\ldots (1)$$

*Values given for T = 300°K

R is resistance.

T is absolute temperature (°K).

K is a constant determined by the resistivity and geometry of the thermistor element.

Material constants (β) for Materials No. 1 and No. 2 are given in Table I, the former having a slightly higher value. Differentiating Equation (1) with respect to temperature yields the rate of change of thermistor resistance as a function of temperature (α)

$$\frac{1}{R}\frac{dR}{dT} = \frac{-\beta}{T^2} = \alpha \quad \ldots \ldots \ldots \ldots \ldots \ldots \quad (2)$$

At 300°K, which is the nominal operating temperature for thermistor detectors, α is slightly greater than 4%/°C for Material No. 1 and slightly less than this figure for Material No. 2. α is negative for both materials. Because thermistors used as radiation detecting elements fluctuate in temperature only very small amounts about a mean ambient value, α remains substantially constant and is a basic parameter in determining detector sensitivity.

In addition to the electrical characteristics of thermistor elements, their physical, optical, and thermal properties play an important role in use as detection elements. Sintered thermistors are spinel-like polycrystalline solids. Grain size, determined by electron photomicrography, is in the order of 1 micron. There is porosity in the body structure, estimated to total about 20% voids. The linear coefficient of thermal expansion is about 7 micro inches/inch/°C, making it compatible with common backing materials like quartz, sapphire, germanium, and some metals. The specific heat of the thermistor is approximately 0.18 calories/gram/°C.

From interference phenomena measured in transmission on thin thermistor films of known thickness, refractive index in the infrared (wavelengths 8-12 microns) has been estimated to be 2.8 to 3.

The absorption of radiant energy by thermistor elements in thicknesses employed in detector fabrication (5-10 microns) has been determined both in the infrared and visible portions of the spectrum. Spectral absorption is determined from transmission and reflectance measurements. Data are shown plotted in Figures 2 through 5. A Hardy spectrophotometer was employed for measurements from 400 to 700 millimicrons. In the infrared from 2 to 15 microns a Perkin-Elmer spectrophotometer was used for transmission data. An integrating cavity [6] [7] coupled with a double beam infrared monochromator was employed for total hemispherical reflectance measurements. From .4 to 15 microns absorption data are given for both uncoated 10 micron flakes and for the case where the flakes have been coated with a thin layer of a

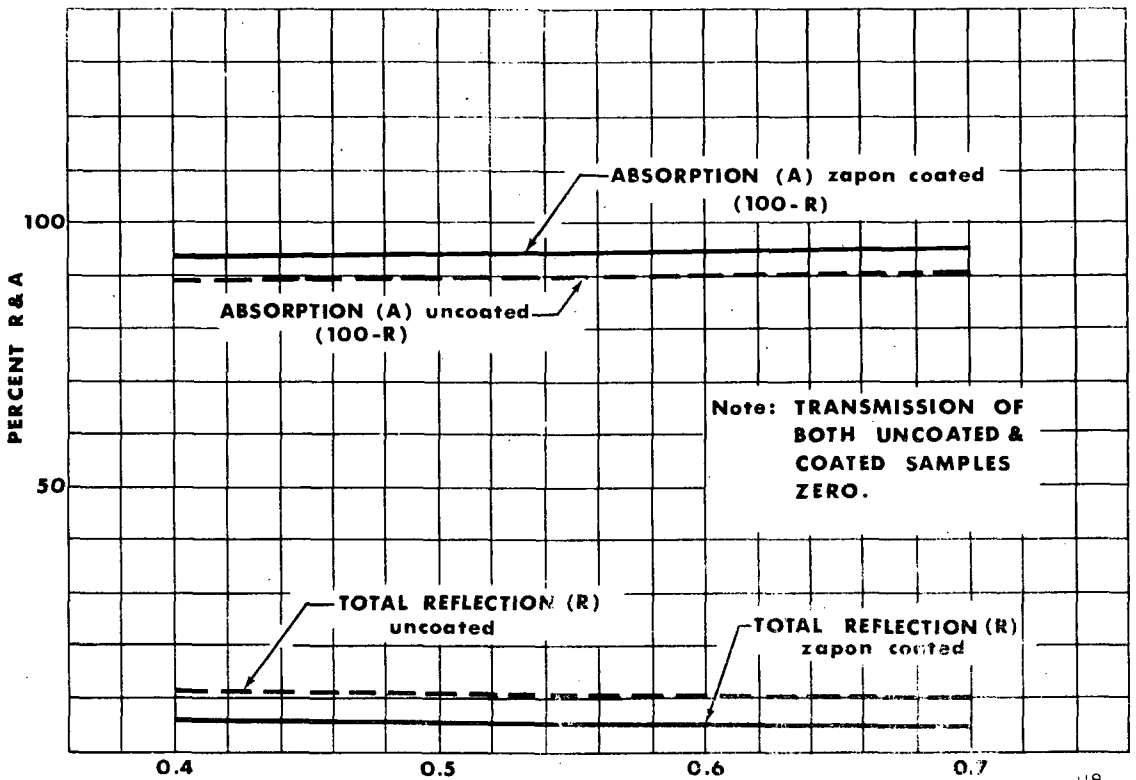

Figure 2 THERMISTOR- MATERIAL RAND A DATA IN THE VISIBLE SPECTRUM

118

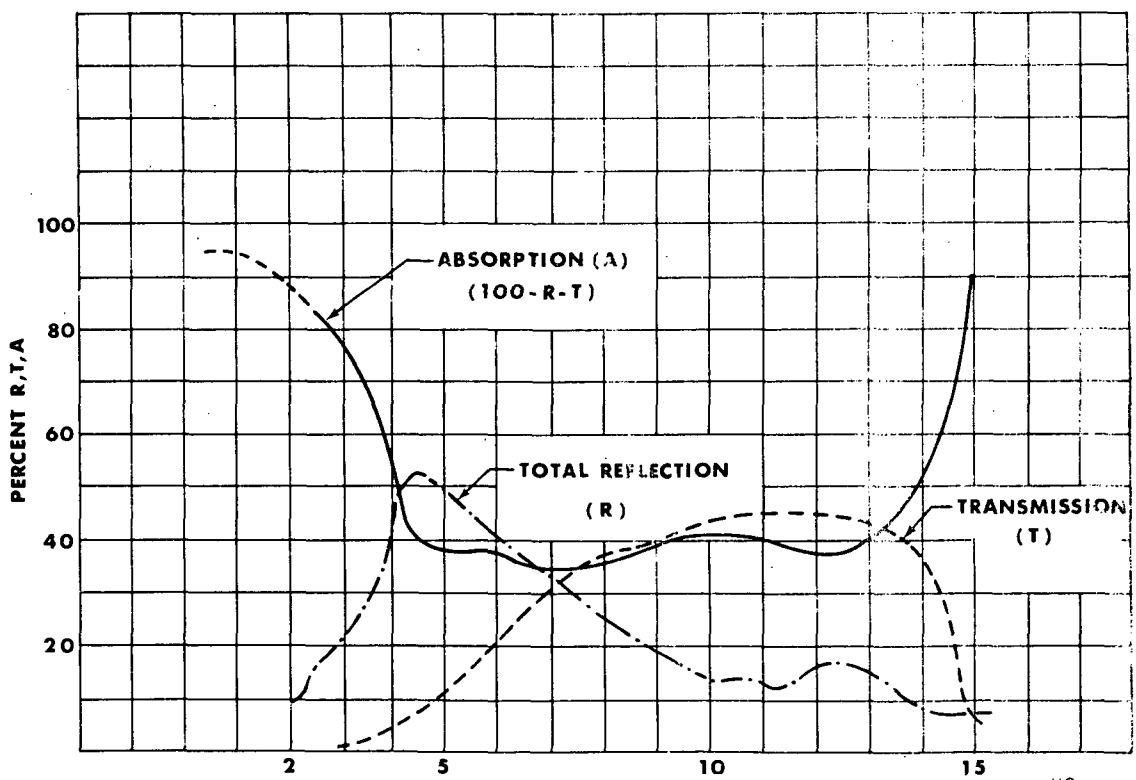

Figure 3 INFRARED R, T, AND A DATA ON UNCOATED THERMISTOR MATERIAL

119

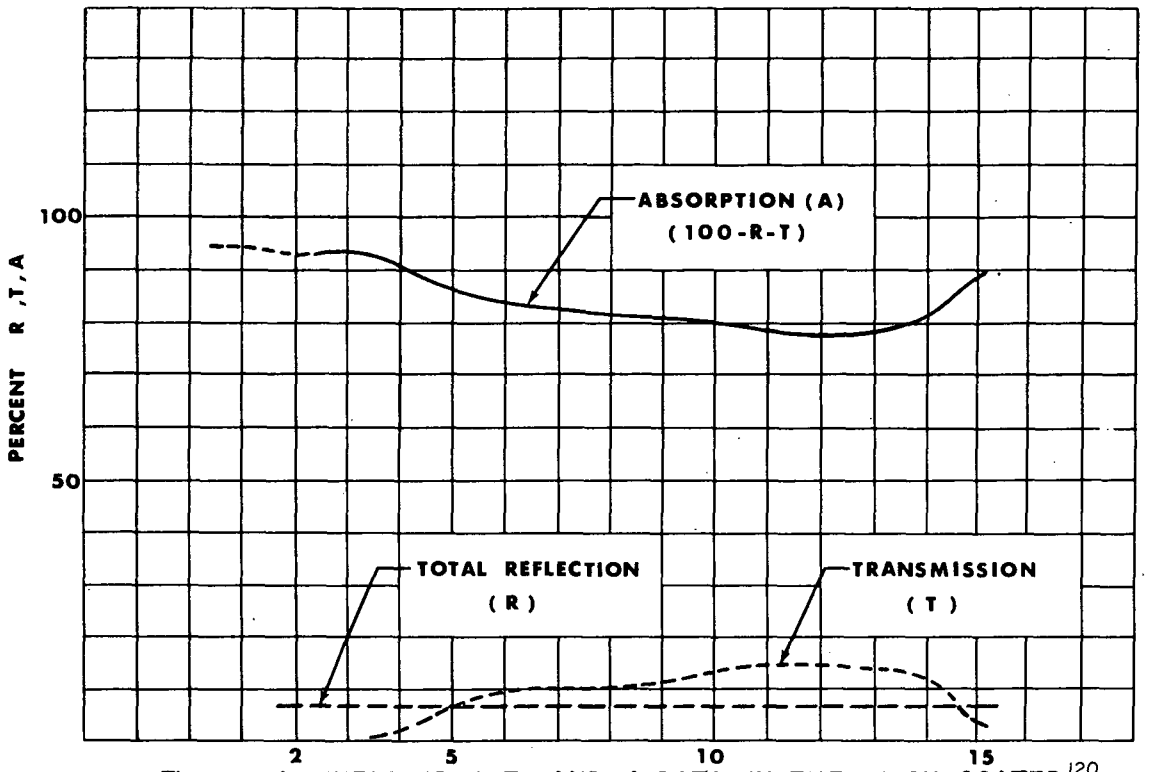

Figure 4 INFRARED R,T, AND A DATA IN THE V ON COATED[120] THERMISTOR MATERIAL

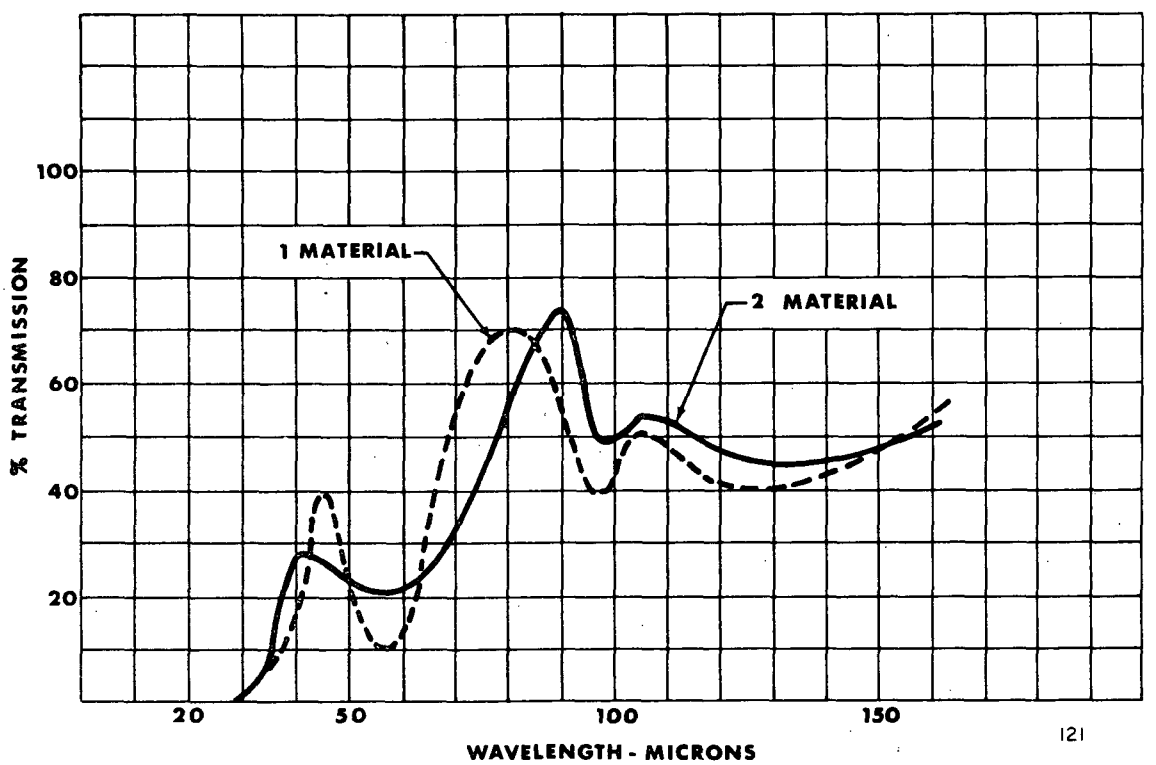

Figure 5 THERMISTOR-MATERIAL TRANSMISSION DATA ABOVE 15 MICRONS

black absorbing lacquer (Zapon black). Some information is available at wavelengths longer than 15 microns as shown in Figure 5. This, however, does not provide complete absorption information since reflectivity data are absent. Furthermore, no transmission measurements were taken with the black Zapon coating on the thermistor flakes.

3. OPERATING CHARACTERISTICS

(a) Solid-Backed Detector Construction

Up to this point we have not considered the thermistor element in the role of a radiation detection device. In order to make the sensing element respond rapidly to radiation changes, it is necessary that the thermistor flake be part of a fast thermal circuit. By this we mean that the heat capacity of the thermistor must be small and also capable of rapidly dissipating its thermal energy. The solid-backed detectors described in these papers are designed to conform with these operational parameters.

Figure 6 shows a simplified cross sectional diagram of the solid-backed construction. Radiant power (ΔP) incident on the thermistor surface is absorbed and heats the thermistor flake. This temperature increment (ΔT) produces a resistance drop (ΔR) which in turn modulates a steady stage voltage to produce a voltage increment (ΔV) proportional to the incident radiant power. It is clear that the ability of the thermistor flake to rise in temperature rapidly will be a direct function of the heat capacity and thermal conductivity of the thermistor. In order that the thermistor element may return to its ground thermal state and, hence, prepare for recurrent changes in radiant power, it is necessary to dissipate the thermal energy acquired from the first thermal pulse. As shown in Figure 6, a thin dielectric layer separates the thermistor flake from a relatively massive thermal sink. The latter may be metal or other good heat conducting solids. Important thermal properties of a number of thermistor backing materials are listed in Table II.

High conductivity and heat capacity are desirable. In general these are found in metals. Because the flake must be electrically insulated, however, good heat conducting dielectrics like sapphire, periclase, and beryllium oxide also make good backing materials. Poorer heat conductors like organic polymers and glass are listed by way of contrast.

(b) The Bolometer Bridge Circuit

Thermistor bolometric elements are usually used in a simple "bridge" arrangement as shown in Figure 7. One thermistor flake is exposed to radiation while an identical flake is shielded from radiation. Equal bias voltages of opposite polarity are applied to the two thermistor flakes, thus maintaining the signal junction S near ground potential independent of variations in ambient temperature. This condition minimizes microphonics, and possible noise from leakage current in the coupling capacitor. It also makes the signal output less dependent upon ambient temperature. The temperature compensating thermistor R_C maintains the same mean temperature as the active thermistor R_A because both are thermally attached to the relatively massive bolometer base. Exposed to chopped or modulated radiation, the active thermistor produces an a-c voltage at the junction S.

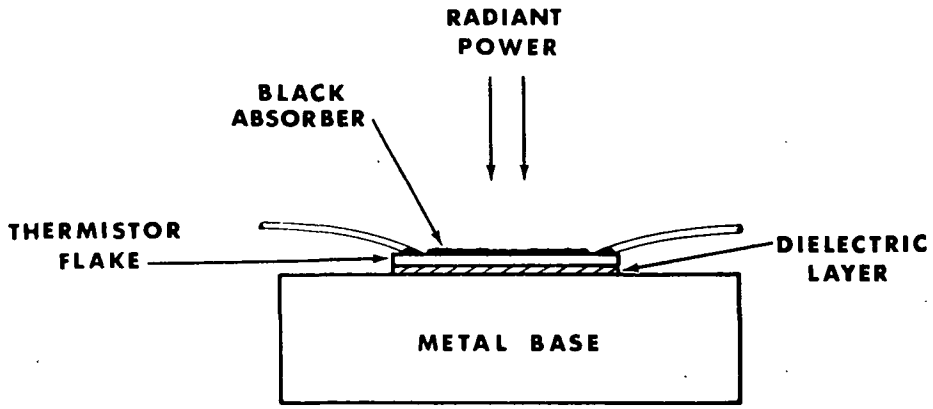

Figure 6 CROSS-SECTION OF SOLID BACKED DETECTOR

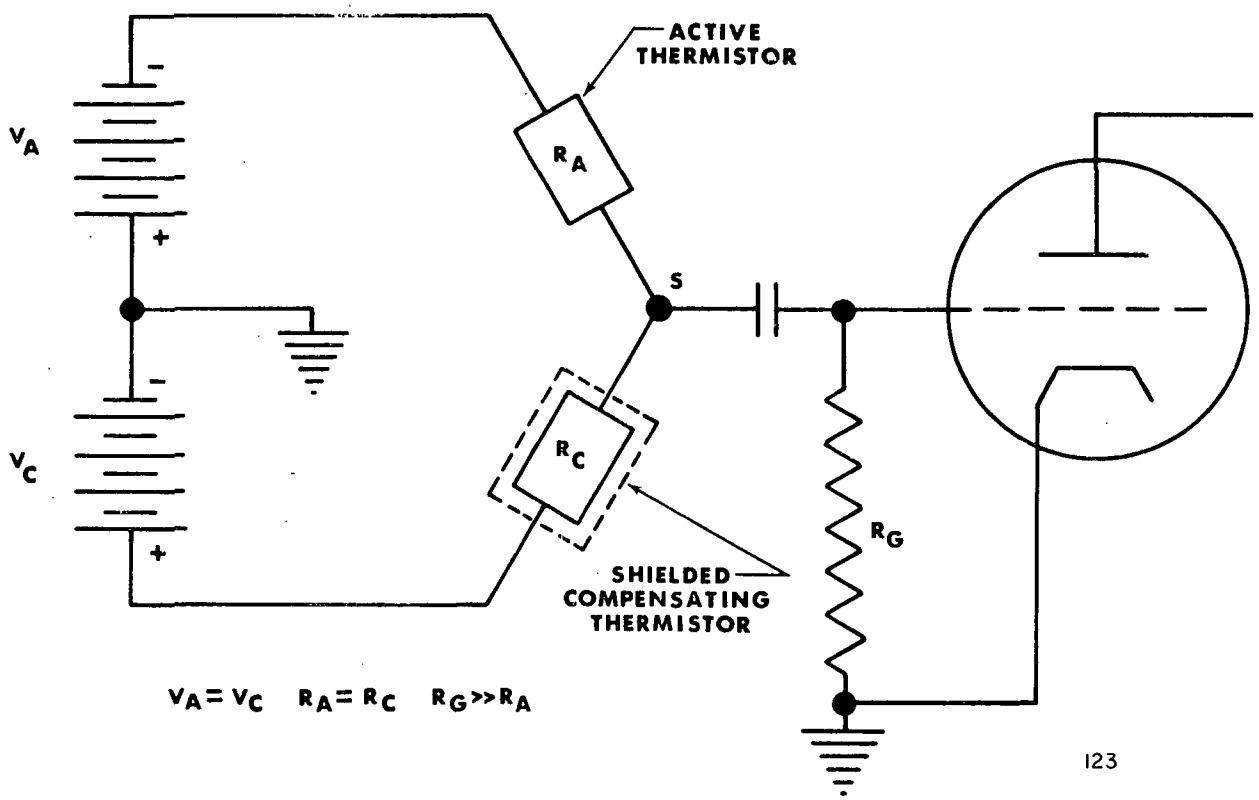

Figure 7 SIMPLE BOLOMETER BRIDGE CIRCUIT

(c) Bias Voltage Limitation

It is clear from the above discussion that the signal voltage derived from the bolometer bridge circuit will increase directly as the bias voltage. Due to the negative resistance-temperature coefficient of the thermistors, however, there is a practical limitation to the bias voltage which can be applied to the thermistor. Maximum voltage to which the thermistor can be subjected is determined by the rate at which electrical power dissipated in the thermistor can be conducted to the detector base. For small bias currents the thermistor approximates Ohm's law because it is not measurably heated. Departure from constant resistance conditions takes place with larger currents because the thermistor then heats and drops in resistance. As the bias current is increased, eventually a point is reached when an increase in current causes a decrease in voltage across the thermistor. If the current is not limited externally in some manner, the detector will "run away" and burn out at this point. This behavior is illustrated in Figure 8, which shows a plot of the voltage-current characteristics of the solid-backed detector. At peak voltage the thermistor flake rises about 30°C above the detector base for operation at 25°C. In practice the V-I curve is determined with a constant current source of voltage to prevent instantaneous burn-out which otherwise would occur at peak voltage.

Because the thermistor rises in temperature at higher bias voltages, there exists a bias voltage for a given detector which yields maximum signal response. In Figure 9 relative responsivity is plotted as a function of fractional peak voltage. Maximum response occurs at a bias voltage approximately 81% of peak. In practice, however, it has been found most advantageous to operate thermistor detectors at 60% of peak voltage. At this voltage level, the detectors can safely operate over a reasonable range in ambient temperature. At 60% of peak voltage the thermistor element operates at about 5°C above the base and detector responsivity is 86% of its maximum. In a later section effects of ambient temperature upon the performance characteristics of thermistor bolometers will be more thoroughly discussed.

(d) Idealized Detector Performance

The bolometer can be thought of as a simple thermal circuit comprised of a single heat capacity element (H, the thermistor flake), a thermal resistance element (Z, dielectric layer between flake and sink), and a thermal ground (sink). In Figure 10 the physical construction and equivalent thermal circuit of the solid-backed detector are illustrated. To determine transient response assume the thermistor is exposed to steady state radiant power (P_1 watts) of which a portion (αP_1) is absorbed depending upon the absorptivity (α) of the thermistor, and that this heats the latter to a steady temperature (T_1 °C). At this temperature the thermistor element will have an energy state (Q_1 joules) above that of the sink and we can write, $T_1 = \frac{Q}{H} + PZ$. If the radiant power is now suddenly removed, the thermistor temperature will decay to the sink temperature T_o.

MATERIAL	CONDUCTION COEFFICIENT - K	HEAT CAPACITY-C	DENSITY ρ	DIFFUSIVITY $\alpha = \frac{K}{C}$
Copper	0.92	0.093	8.9	1.11
Aluminum	0.48	0.21	2.7	0.85
Beryllium Oxide	0.40	0.26	3.0	0.51
Germanium	0.14	0.074	5.3	0.36
Periclase (MgO)	0.10	0.21	3.6	0.13
Sapphire	0.06	0.18	4.0	0.083
Quartz	0.03	0.19	2.6	0.061
Glass	0.0025	0.18	2.8	0.005
Polymers	0.0003	0.35	1.5	0.0006

K (cal/sec cm°C)
C (cal/gm°C)
ρ (gms/cc)

TABLE II

THERMAL PROPERTIES OF BACKING MATERIALS NEAR 300°K

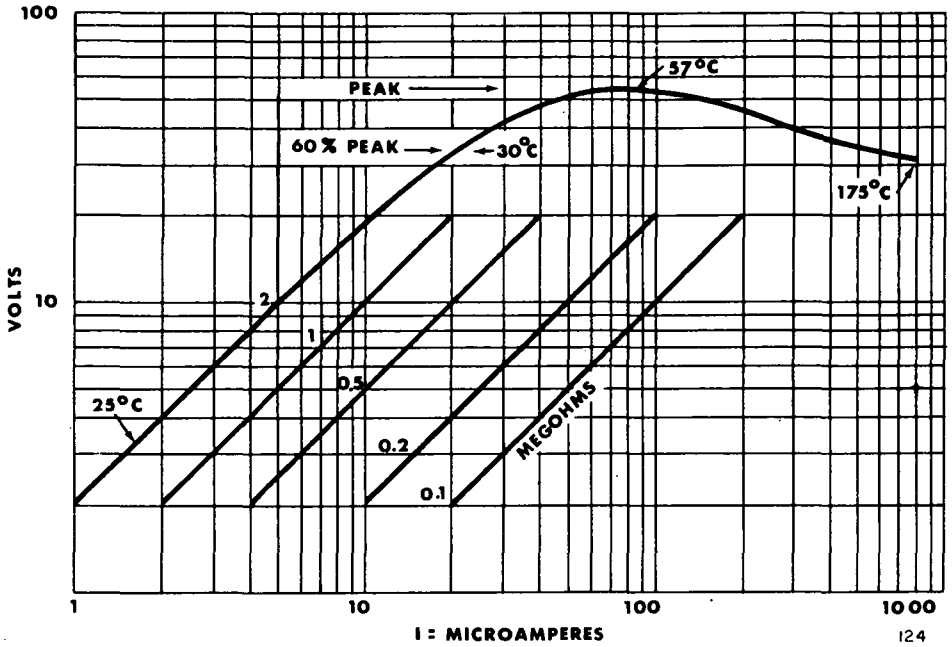

Figure 8 VOLTAGE-CURRENT CHARACTERISTICS OF THE SOLID-BACKED DETECTOR

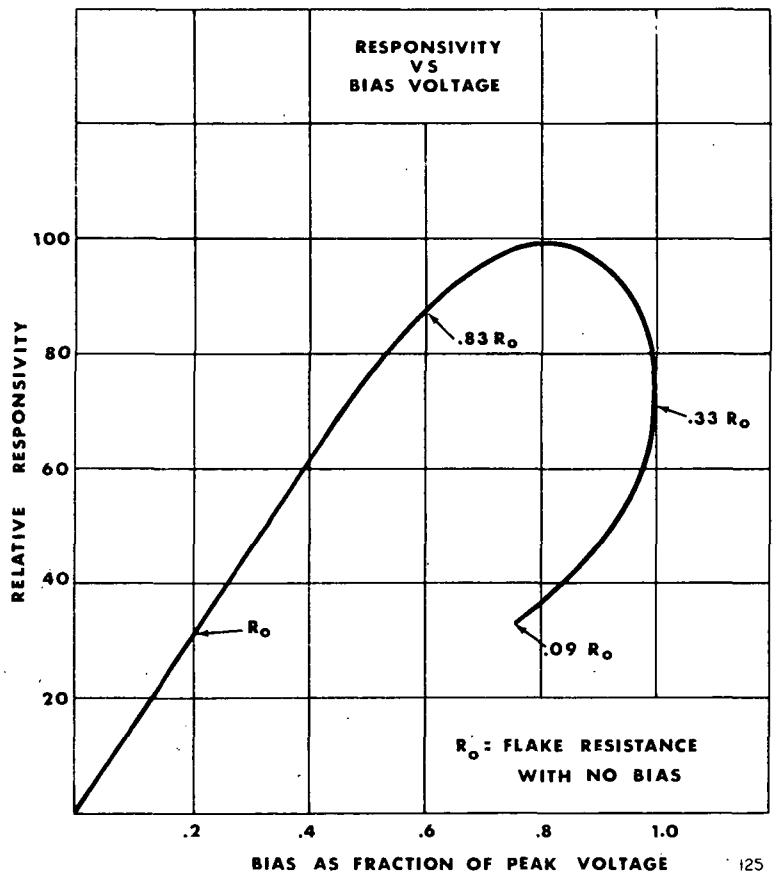

Figure 9 EFFECT OF BIAS VOLTAGE ON THERMISTOR RESPONSIVITY

differentiating with respect to time,

$$\frac{1}{H}\frac{dQ}{dt} = -Z\frac{dP}{dt}$$

or, since $P \approx \frac{dQ}{dt}$,

$$\int\frac{dP}{P} = \frac{1}{HZ}\int dt$$

whose solution is

$$P = \epsilon^{-t/HZ} + \text{constant}$$

or from $P = \alpha P_1$ when $t = 0$.

$$P = \alpha P_1 \epsilon^{-t/HZ} \quad \ldots\ldots\ldots\ldots\ldots \quad (3)$$

Also since $T = \frac{Q_1}{H} = T_1$ when $t = 0$ $\ldots\ldots\ldots\ldots$ (4)

$$T = T_1 \epsilon^{-t/HZ} \quad \ldots\ldots\ldots\ldots \quad (5)$$

From (5) the thermal time constant (τ), defined as the time for the temperature to decay to $1-\epsilon^{-1}$ of its initial value, is seen to be HZ, the product of the heat capacity of the thermistor flake and the thermal impedance of the dielectric layer.

For small temperature changes, the detector resistance changes proportionally according to Equation (2). From the bolometer circuit of Figure 7 the signal voltage at the junction S is seen to be,

$$\Delta V = \Delta R V_{\alpha/2R}$$

Hence,

$$\Delta V = \frac{\alpha V_\alpha}{2} [\Delta T]$$

From (4),

$$\Delta V = \frac{\alpha\alpha}{2} PZV_\alpha$$

or finally the transient response of the bolometer bridge from (3) is,

$$\Delta V = \frac{\alpha}{2}\alpha V_\alpha \Delta P \epsilon^{-t/HZ} \text{ volts} \quad \ldots\ldots \quad (6)$$

By a similar simple analysis it can be shown that for periodically modulated radiation the responsivity $R(\omega)$ of the detector as a function of frequency becomes,

$$R(\omega) = \frac{\alpha}{2} \alpha V_a Z \left[1 + (\omega HZ)^2\right]^{-1/2} \text{ (volts/watt)} \quad (7)$$

How accurately these relationships describe the behavior of bolometers depends mostly upon the degree to which H and Z can be considered lumped constants. This matter has been treated in the literature [9] [10]. Ideally, the thermistor flake should have low heat capacity and high heat conductivity while the thermal barrier (Z) should have negligible heat capacity and low heat conductivity. To make an ideal thermal ground, the sink must have highest heat conductivity and heat capacity.

In Figure 11 is shown a family of idealized thermistor detectors formed by assigning four discrete values of thermal impedance to detectors 1 square millimeter in area and 10 microns in thickness. This kind of idealized behavior has been formalized by R. C. Jones [11] as characteristic of Class IIa detectors. It will be demonstrated in a subsequent paper that modern thermistor detectors closely approximate the characteristics of this ideal family. In Figure 11 all parameters are held constant except the thermal impedance Z which can be varied to control detector speed and responsivity.

(e) Noise

The ultimate sensitivity of all radiation detectors is limited by some kind of noise. In the case of thermistor detectors, limiting noise is thermal or Johnson noise [12]. Johnson noise depends only upon ohmic resistance, absolute temperature, and the bandwidth of the measuring circuitry. It can be exactly expressed in terms of these parameters. For example, the noise voltage produced by a 2-megohm (each thermistor element) detector operated at 300°K in a bandwidth of 10 cps is 0.4 microvolts rms.

For bolometers whose resistance is of the order of a few megohms there is, in addition to Johnson noise, a small amount of noise at low frequencies. In good thermistor bolometers this spurious noise lies below 30 cps. Its frequency distribution is not exactly known. Measurements are reported in the literature [13] indicating an inverse frequency relationship but these data are no longer considered to be representative of quiet thermistor detectors. In a noise bandwidth from 5-100 cps, good thermistor detectors operate at noise levels no more than 5-10% in excess of Johnson noise. In narrower bandwidths, say 10 cps, centered at frequencies from 50-200 cps, they show no noise other than that attributable to Johnson noise.

It is important to bring out the practical difficulties in achieving detector operation at theoretical noise levels. Preselected commercial vacuum tubes cannot be found with effective noise inputs much lower than theoretical

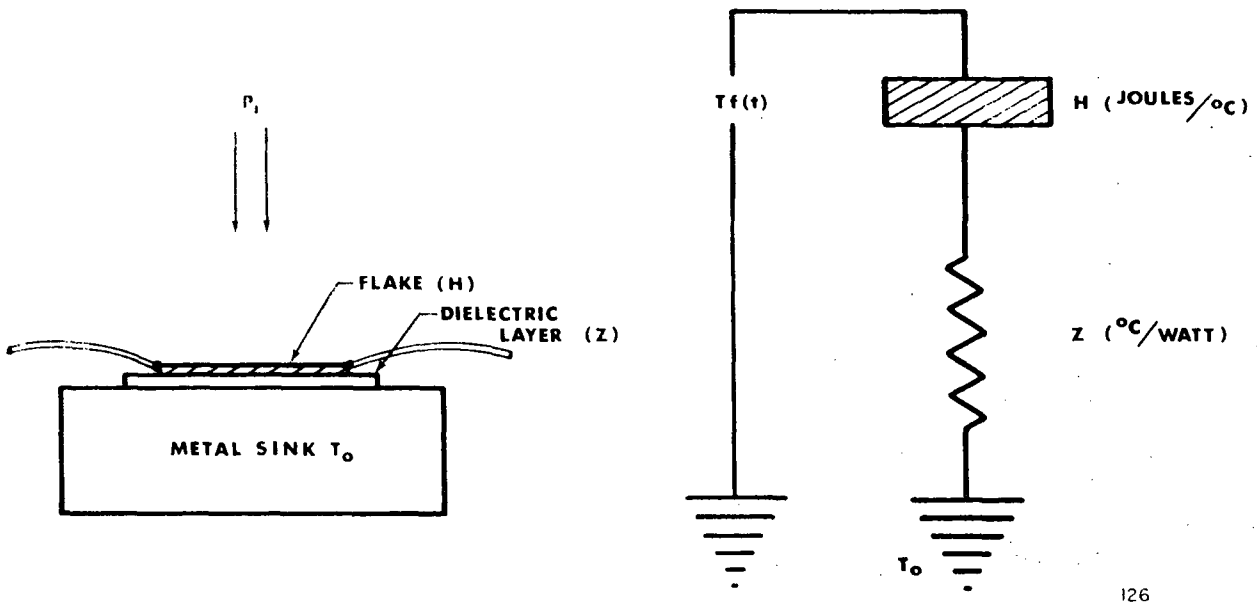

Figure 10 CONSTRUCTION AND EQUIVALENT THERMAL CIRCUIT OF THE SOLID-BACKED DETECTOR

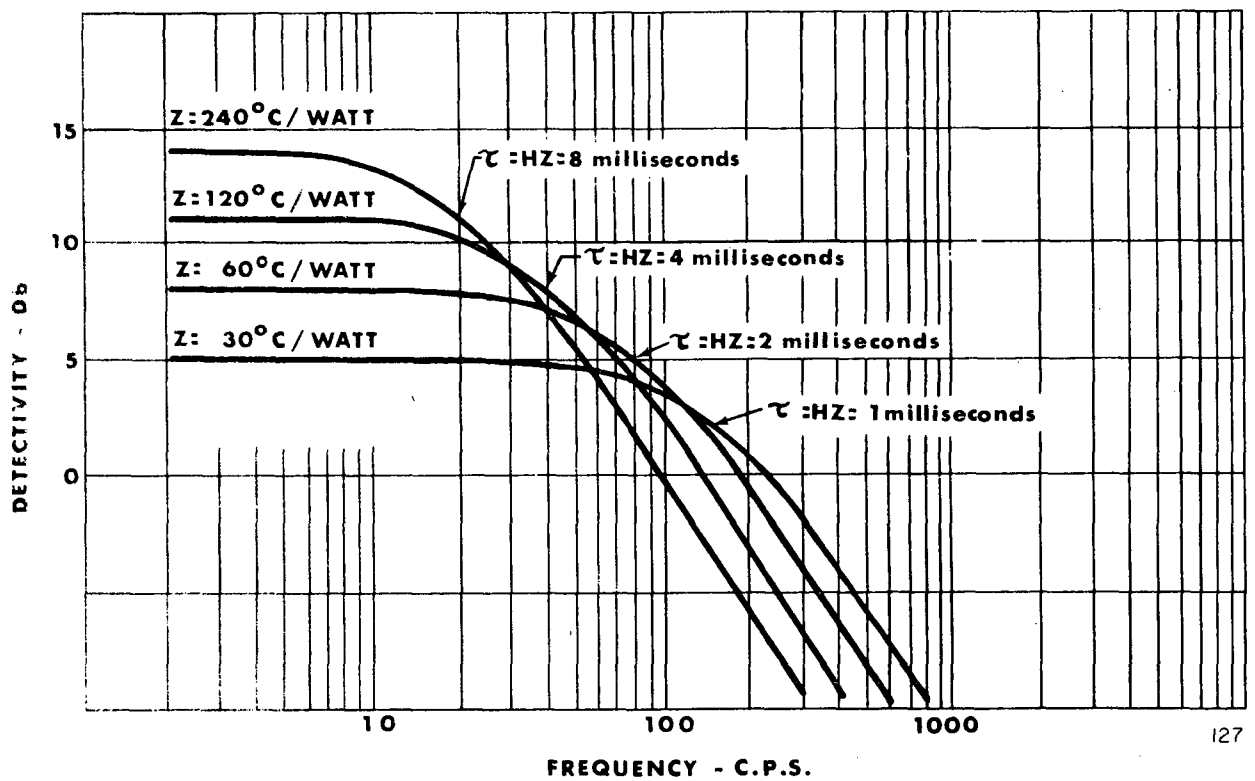

Figure 11 FAMILY OF IDEALIZED THERMISTOR DETECTORS SHOWING INFLUENCE OF THERMAL IMPEDANCE

Johnson noise of a 200,000 ohm resistor in the bandwidths of interest. Hence, for a one megohm detector (2 megohms each flake) the preamplifier will add 20-30% to the noise of the detector.

(f) Swish

There is a phenomenon known as "swish" associated with thermistor detectors. The term is apt because it refers to a signal generated by the detector due to the motion of air in the immediate vicinity of the thermistor surface. Because the thermistor flake operates at a temperature slightly above its surroundings, any convected air at the thermistor interface will carry away heat and hence cool it. If the thermistor flake is enclosed in a sealed capsule, spurious convection or pressure change effects are eliminated. If, however, the capsule is sealed at atmospheric pressure, convection can still occur if the bolometer is vibrated. Low frequency vibration in the plane of the thermistor element will give rise to output signals at the frequency of vibration. In practice, due to the low inertial mass of the air in bolometer capsules, only low frequency motions are troublesome, below about 20 cps.

To avoid entirely the swish phenomenon, bolometer capsules are evacuated. Hard vacuum is not required. Figure 12 shows a log-log plot of swish voltage as a function of capsule pressure. Substantially no swish exists below pressures of 20 millimeters of Hg. These data were taken for a 1/4" peak-to-peak sinusoidal vibration at 12 cps in the plane of the thermistor flake. At atmospheric pressure swish voltage is about 100 times detector noise under these severe vibration conditions.

(g) Internal Electric Discharge

In applications where low frequency vibrations are likely to occur, evacuation is obviously required. For reasons explained below, however, unless severe vibrations are encountered it may be advantageous to employ a sealed detector rather than one which has been evacuated. This is particularly true when the detector area is large and, as a result, the bias voltage also large. In Figure 13 is plotted the discharge potential in a bolometer capsule as a function of air pressure. These data are qualitatively in accord with Paashen's law which states that the "minimum discharge potential" is proportional to the product of gas pressure and interelectrode spacing. The minimum discharge potential for air is given in the literature [12] as 370 volts which is in good agreement with the experimental data shown in Figure 13. If the pressure in the bolometer capsule is maintained below 100 microns, no danger of electrical discharge exists up to potentials of 800 volts. In the pressure range from 0.2 millimeters to 30 millimeters of Hg, potentials above 400 volts can cause trouble. Good vacuum seals are achieved in bolometer capsules but pressure can increase with time due to slow outgassing of organic components involved in the construction of detectors.

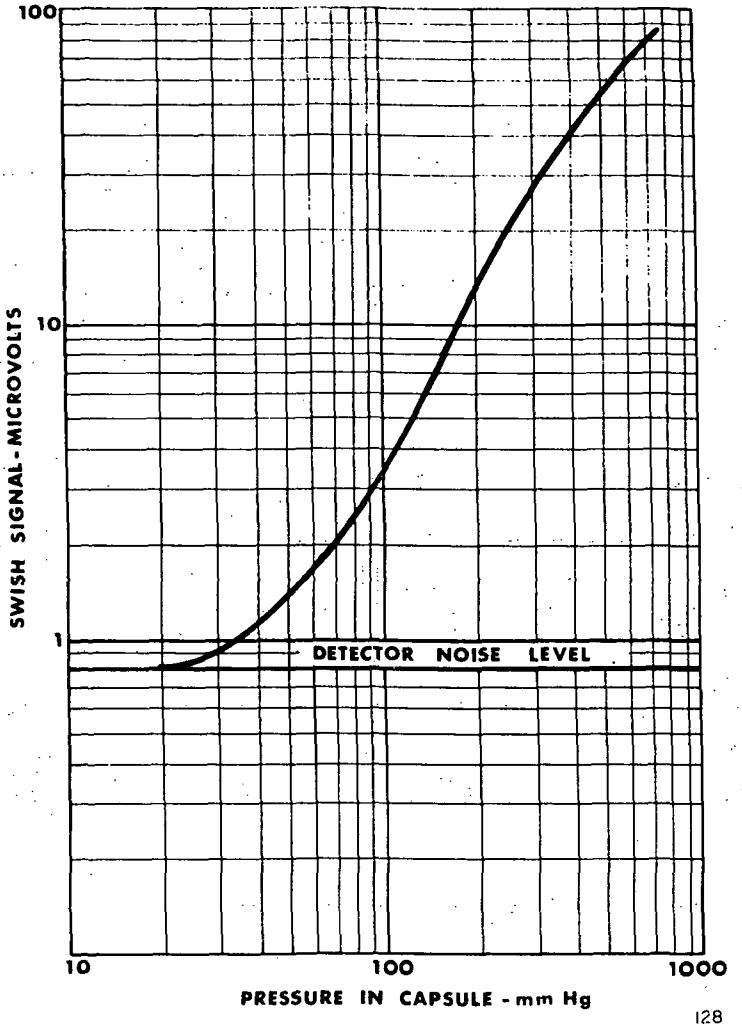

128

Figure 12 RELATIONSHIP OF SWISH VOLTAGE AND CAPSULE PRESSURE

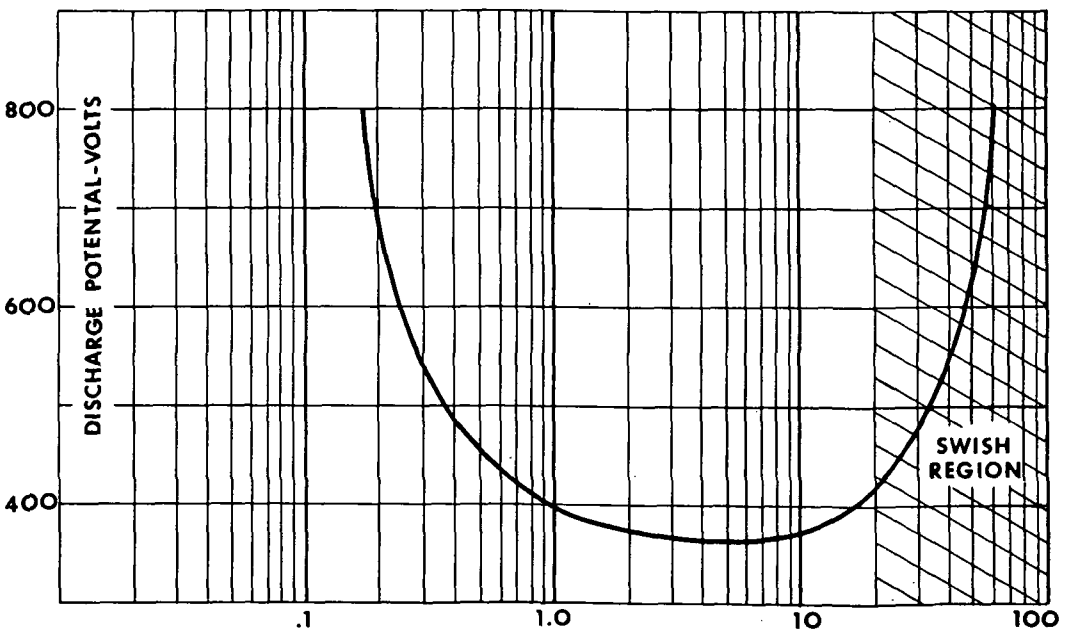

Figure 13 RELATIONSHIP OF DISCHARGE POTENTIAL AND CAPSULE PRESSURE

129

Hence, detectors encapsulated at one micron of Hg may in time, and depending on their temperature environment, rise in pressure and approach the discharge region. Obviously if the bias voltage does not exceed 360 volts, no electrical failure can occur. For large thermistors bias voltages may, however, exceed this value.

4. DETECTOR WINDOWS

Coated thermistor bolometer elements are substantially flat in spectral response from the ultraviolet to about 35 microns. For reasons explained above, however, the bolometer element must be completely sealed in a housing. This necessitates a window which limits to some extent the spectral range. A number of infrared optical materials are employed as windows, and can be chosen to exclude short wavelength radiation, long wavelength radiation, or to transmit a very wide spectrum. Window materials [14] are listed in Table III along with their transmission ranges and mean transmissivity.

TABLE III
DETECTOR WINDOW MATERIALS

MATERIAL	MEAN TRANSMITTANCE PERCENT	SHORT WAVE CUT-OFF MICRONS	LONG WAVE CUT-OFF MICRONS
Quartz	90	0.4	4.0
Sapphire	90	0.20	5.5
Barium Fluoride	93	0.17	12
Silver Chloride	80	2.0*	25
KRS-5	72	0.6	35
Germanium	45**	2.0	20

Note: 1-2 mm thickness

*With silver sulfide coating

**95% peak transmission with 1/4 λ antireflection coating.

5. AMBIENT TEMPERATURE EFFECTS

It is not always possible to use thermistor detectors and associated instrumentation at fixed ambient temperature. For absolute radiation measurements, therefore, it is important to consider how detector responsivity, noise, and detectivity are affected by changes in ambient temperature. In the following discussion it should be understood that ambient temperature refers to the temperature of the detector capsule and not necessarily ambient air temperature. This distinction is made because the bolometer capsule will, in general, be warmer than ambient air, moderate heating usually being produced by electronic components in the instrument or by exposure to radiant heating from sunlight.

(a) Responsivity

Two factors combine to produce responsivity change with ambient. One is the temperature coefficient of resistance, α , of the thermistor flake. The second involves impedance coupling between the detector and the preamplifier. The following relationship shows how responsivity is related to operational parameters.

For a fixed bias voltage, only α changes with temperature. The temperature referred to here, however, is the temperature of the thermistor flake, which in general is different from ambient. With no bias on the detector, the flake temperature is at the bolometer base temperature. Depending upon the bias voltage used, the flake temperature rises above ambient. Figure 14 shows the fractional temperature rise of the flake above the detector base plotted against fractional peak bias voltage. Figure 15 shows the flake temperature rise above the base at peak bias voltage as a function of the detector base temperature. For example, consider Material No. 2 at an ambient temperature of 25°C. From Figure 15 temperature rise at peak bias voltage is 31°C. From the hyperbolic curve of Figure 14, 60% of peak bias results in a temperature rise of 0.14 x 31°C = 4.3°C. Now consider this same detector with the same bias voltage but operating at a higher ambient temperature. The thermistor flake will have reduced resistance due to ambient change and further reduced resistance due to self-heating from increased current flow. From Equation (1),

$$R = R_o \epsilon^{\beta (1/T - 1/T_o)} \quad \ldots\ldots\ldots\ldots\ldots\ldots \quad (8)$$

R and R_o are the thermistor resistance, respectively, at absolute temperatures T and T_o (Kelvin). When voltage (V_B) is applied to the thermistor, equilibrium dictates that electrical power input must equal thermal power loss to the base,

$$\frac{V_B^2}{R} = \frac{\Delta T}{Z} \quad \ldots\ldots\ldots\ldots\ldots\ldots \quad (9)$$

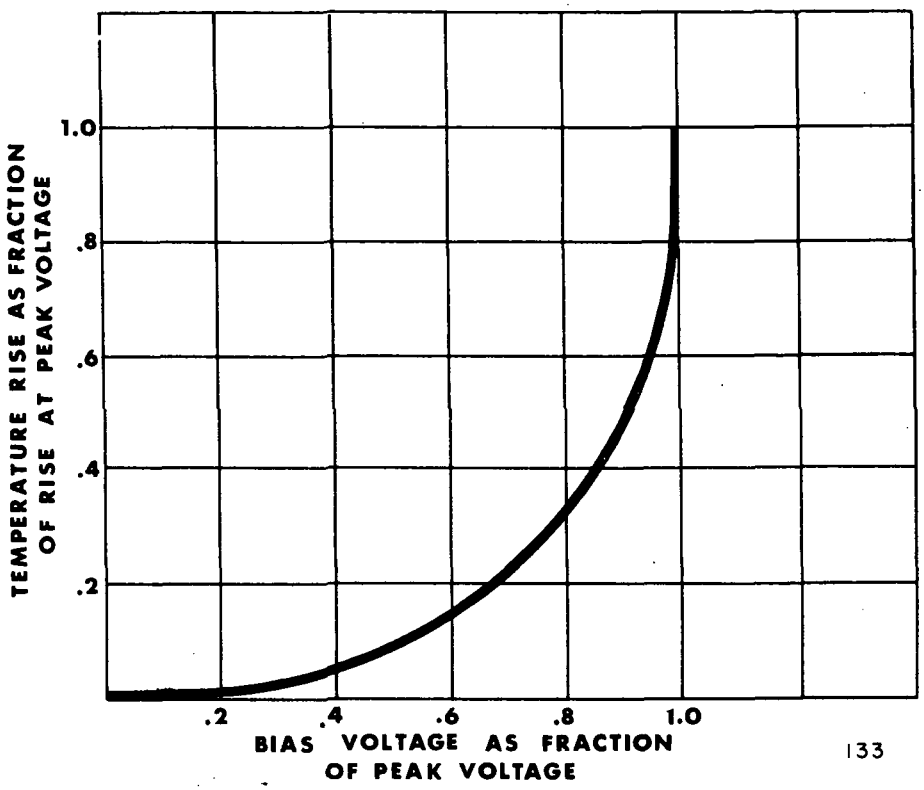

Figure 14 RELATIONSHIP OF FLAKE TEMPERATURE AND BIAS VOLTAGE

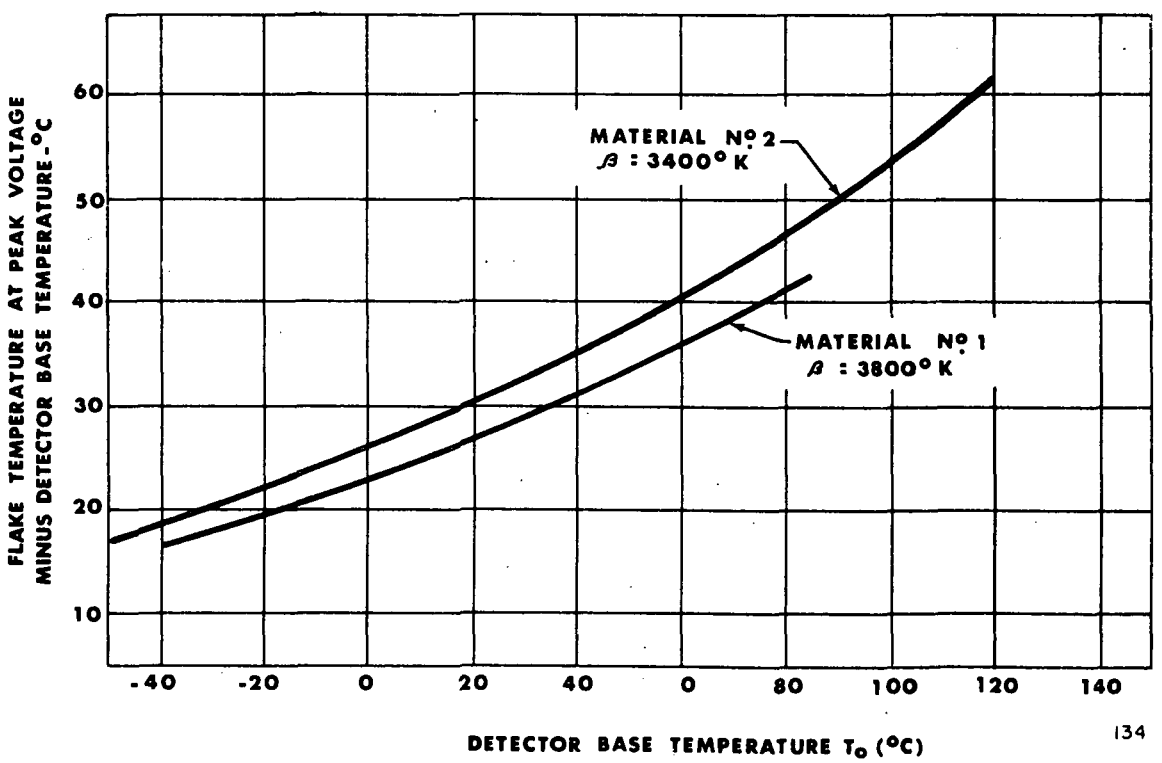

Figure 15 RELATIONSHIP OF FLAKE TEMPERATURE AND BASE TEMPERATURE

ΔT is the temperature differential between the thermistor and the base, and Z the thermal impedance as defined earlier. From Equations (8) and (9) one can deduce the resistance-temperature relationship at peak bias voltage, namely,

$$R_p = R_o \epsilon^{-T_p/T_o} \quad \ldots\ldots\ldots\ldots\ldots\ldots \quad (10)$$

R_p and R_o are the thermistor resistance with peak bias and with no bias respectively; T_p and T_o are absolute thermistor temperatures at these same conditions. To a good approximation $R_o/R_p = 3$ over a wide range of operating temperatures.

Returning to the numerical example cited above, assume the detector base temperature rises from 25°C to 60°C and the bias voltage is left unchanged. From (9) and (10) the ratio of peak voltages at two temperatures, using the approximation above, can be expressed as,

$$\frac{V_{p60}}{V_{p25}} = \left[\frac{R_{60}}{R_{25}} \times \frac{T_{60}}{T_{25}}\right] \quad \ldots\ldots\ldots\ldots\ldots\ldots \quad (11)$$

R_{60} and R_{25} are, respectively, the resistance of the thermistor at base temperatures of 60 and 25°C with no voltage on the detector. The resistance ratio can be found from (8). From Figure 15, ΔT_{25} and ΔT_{60} are, respectively, 31 and 41°C. This information and (11) yields $V_{p60}/V_{p25} = 0.64$. Hence, the detector at 60°C is operating at $\frac{0.60}{0.64} = 94\%$ of its peak voltage. With the aid of Figure 14 we can also establish the temperature of the thermistor flake under these conditions. The temperature rise of the thermistor above the base is approximately 0.6 x 41 = 25°C. Hence, the flake temperature is about 85°C.

Figure 16 shows relative responsivity as a function of temperature for the case where bias voltage is 60% of peak bias voltage at 25°C. Two curves are shown, one for the case where the preamplifier input impedance is 10 times the detector impedance at 25°C, and the other under conditions where the preamplifier impedance is substantially infinite compared to the detector impedance at all temperatures. For ambient temperatures above 25°C, resistance mismatch with the amplifier has small effect because detector impedance falls rapidly at the higher temperatures. For lower ambient temperatures, impedance mismatch with the amplifier begins to become serious due to rapid increase in detector impedance .

At 63°C the responsivity curve (2) in Figure 17 is shown to have an abrupt discontinuity. At this ambient temperature and under the operating conditions specified, the detector flakes will disintegrate due to excessive temperature rise. This critical run-away condition occurs instantly at peak bias voltage.

Figure 17 includes two other bias voltage examples, namely, for the

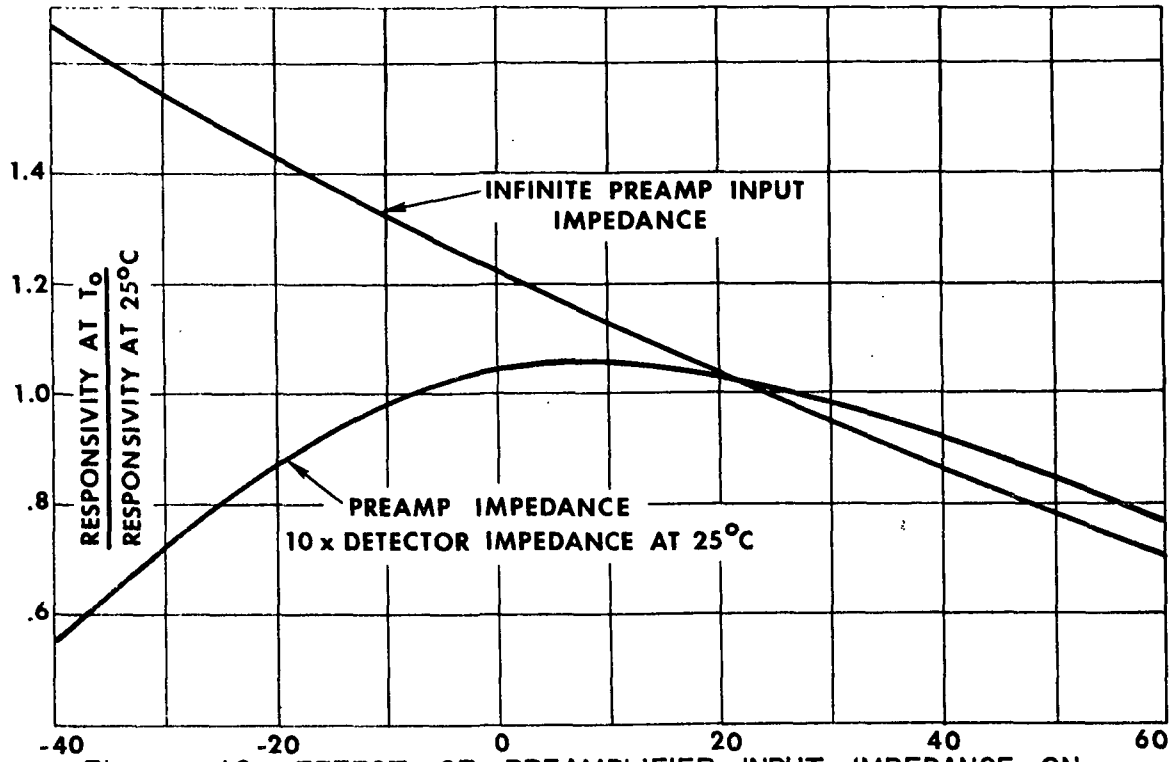

Figure 16 EFFECT OF PREAMPLIFIER INPUT IMPEDANCE ON BASE- TEMPERATURE CHARACTERISTIC

135

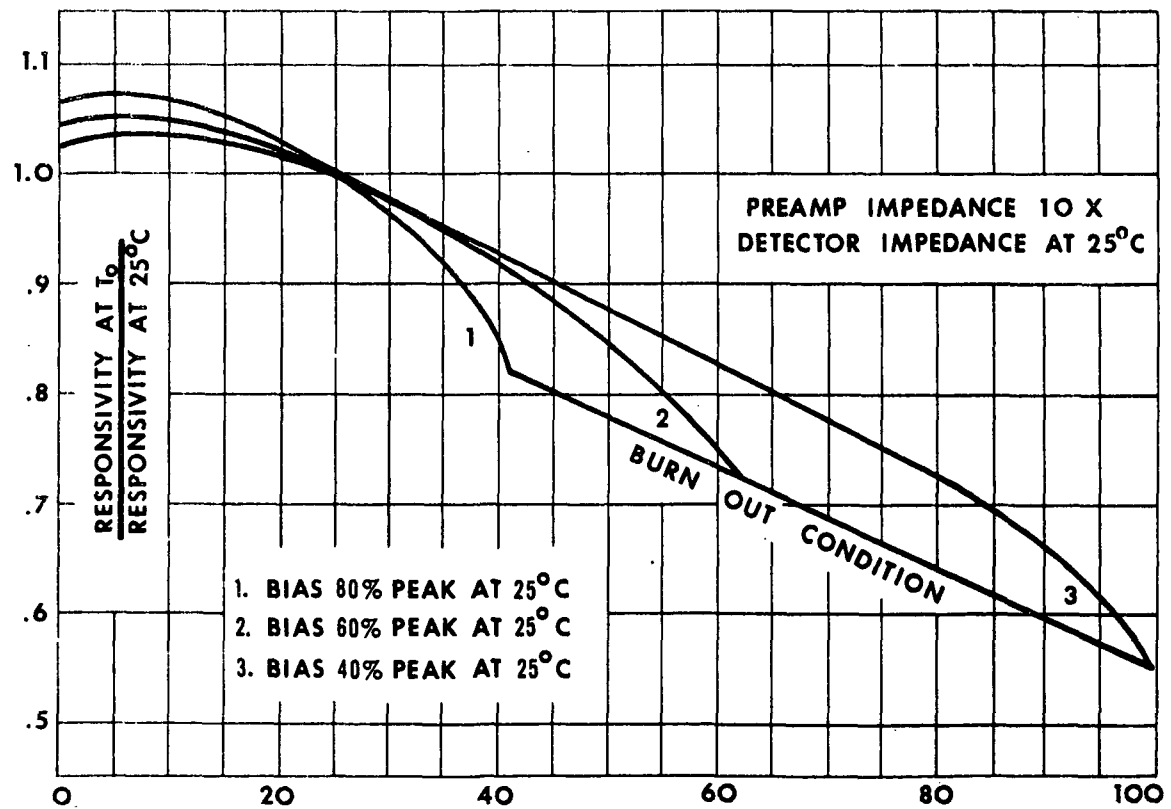

Figure 17 EFFECT OF BIAS VOLTAGE ON BASE TEMPERATURE CHARACTERISTIC

136

cases where bias voltage is 40% of peak at 25°C and 80% of peak at 25°C. Reducing the bias from 60% to 40% is seen to increase the useful ambient temperature range from 53°C to 100°C. Conversely, increasing to 80% bias reduces the upper ambient limit to about 42°C.

A few remarks are appropriate with respect to the shape of the responsivity vs. temperature graphs. Referring to curve 3 in Figure 17, responsivity reduces linearly at about 0.5%/°C up to almost 80°C and beyond falls off at an increasing rate to the burn-out point. Physically what is happening is that below 80°C the thermistor flake undergoes almost no self-heating and, hence, is substantially at ambient temperature. Beyond 80°C the thermistor flake rises rapidly above ambient, finally attaining a temperature just before burn-out of 153°C (refer to Figure 15). The higher biasing condition represented in curves 1 and 2 (Figure 17) exhibit shorter linear portions because self-heating is more readily induced as the detector base temperature rises above 25°C. It should be noted that flake temperatures in excess of 100°C produce degredation of organic coatings in physical contact with the flake.

BARNES ENGINEERING COMPANY

SOLID-BACKED THERMISTOR INFRARED DETECTOR

ESCRIPTION

ne solid-backed thermistor detector contains a matched pair of ermally-sensitive resistors (thermistors) that exhibit a large ange in electrical resistance when heated by exposure to radia-on from the infrared to the ultraviolet. The thermistors are in e form of small flakes cemented to a sapphire backing block. The tire assembly is mounted, in turn, in a metal capsule and her-etically sealed. This construction provides an accurately con-olled thermal impedance between the flakes, as well as a good ntrol of the detector time constant.

ne "active" flake is located in the center of the capsule and is ex-osed to the radiation to be detected. The compensating flake is cated off-center and is shielded from this outside radiation. Both akes are connected in a bridge circuit (Figure 5) providing the tive flake with compensation for resistance changes caused by nbient temperature variations.

n infrared transmitting window is normally installed to limit the tector's spectral response to the requirements of the application. his sealed assembly has the physical dimensions shown in Fig-e 2. Ruggedly constructed, the solid-backed thermistor detector resistant to vibration, shock, temperature variations, high hu-idity and other extreme environmental conditions found in de-nse, space and industrial applications.

andard detectors are available in a selection of flake sizes and e made of thermistor material with a choice of two resistivities. etails are shown in Table I. Although KRS-5 window material hich transmits in the 0.6 to 35 micron region is normally sup-ied as the standard window, a wide variety of alternate windows e available on special order. Some of these are listed in Table II.

gnificant performance characteristics include responsivity, fre-ency response, bias voltage requirements, noise and noise equiv-ent power characteristics. These are defined and illustrated in gures 3 through 7.

variety of special modifications are available. Alternate window aterials will be supplied as required by the application as will be ounts of special construction. When requested, detectors will be reconditioned with the required bias voltage for the desired num-r of hours. Relative spectral response curves over the range of 25 to 35 microns will also be made as requested.

PECIAL FEATURES

- No Need For Cooling; Operates At Room Temperature
- Compact, Rugged and Reliable
- Dynamic Range Of Over One Million To One
- Wide Selection of Sensitive Area Dimensions
- High and Low Impedances Available
- Large Choice of Window Materials

Figure 1

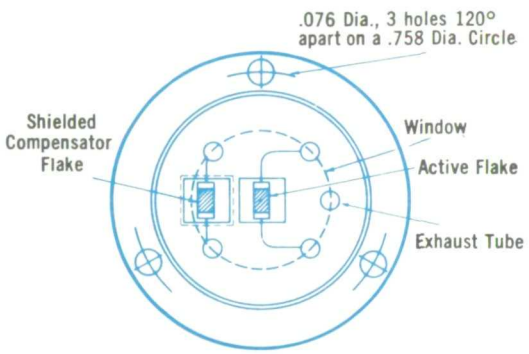

Top view of standard solid-backed detector

Figure 2

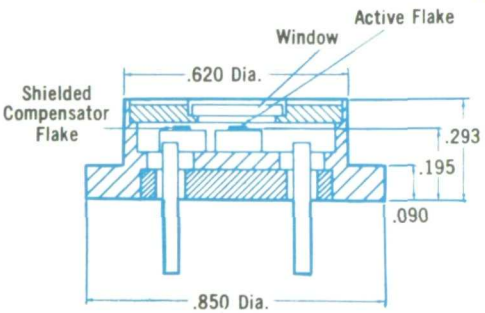

Side view details of standard solid-backed detector

Figure 3

Window Material	Useful Spectral Range (in microns)	Window Material	Useful Spectral Range (in microns)
KRS-5	0.6 — 35	Irtran-1	1 — 8
Barium-Fluoride	0.2 — 11	Irtran-2	2 — 14
Calcium Fluoride	0.2 — 12	Irtran-3	1 — 10
Fused quartz	0.3 — 3	Irtran-4	0.6 — 20
Germanium	2 — 20	Irtran-5	1 — 8
Sapphire	0.25 — 6	Irtran-6	—
Silicon	1 — 16	Indium Antimonide	8 — 25
Arsenic Trisulphide	0.6 — 13	Indium Antimonide and Arsenic Trisulphide	8 — 13

BARNES ENGINEERING COMPANY
30 Commerce Road / Stamford, Connecticut 06902 / Phone (203) 348-5381 / TWX 710-474-3367

TABLE II

	Flake Size** (millimeters)	Nominal Time Constant (milliseconds)	Material Type*
Small Square Flakes	0.1 x 0.1	1.2, 2.5 or 5.0	No. 1 or No. 2
	0.3 x 0.3		
	0.5 x 0.5		
Large Square Flakes	1.0 x 1.0	1.2, 2.5 or 5.0	No. 2
	1.5 x 1.5		No. 2
	2.0 x 2.0		No. 2
	2.5 x 2.5		No. 2
Rectangular Flakes	0.1 x 1.0	1.2, 2.5 or 5.0	No. 1 or No. 2
	0.2 x 2.0		
	0.3 x 3.0		
Rectangular Flakes	1.0 x 0.1	1.2, 2.5 or 5.0	No. 2
	2.0 x 0.2		
	3.0 x 0.3		

* Type No. 1 material is 2.5 megohms per square flake.
Type No. 2 material is 0.25 megohms per square flake.

Resistance of rectangular flakes is $\left(\frac{L}{W}\right)$ times the square flake resistance.

** For the dimensions listed, the first one (L) is the flake length between electrodes; the second one is the width (W).

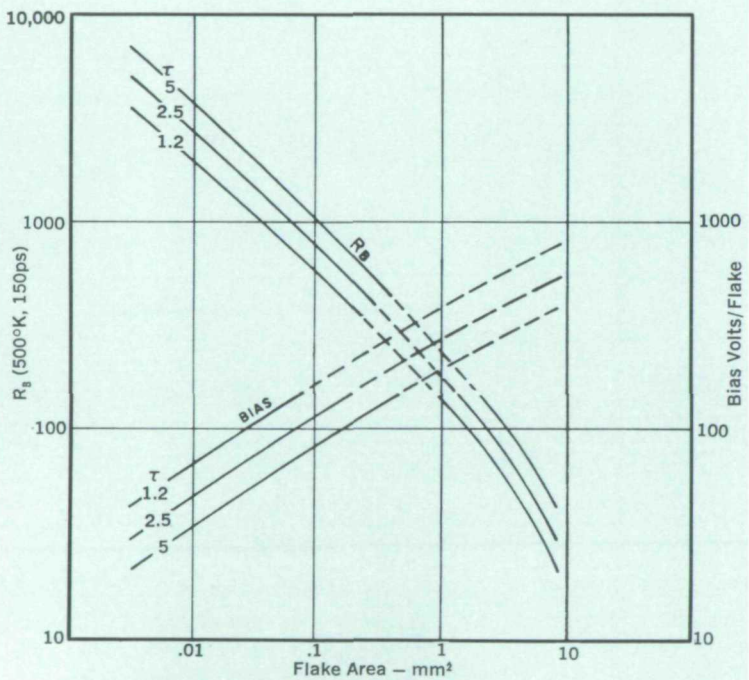

Responsivity and Bias
Square No. 1. Thermistors 2.5 Megohms. 25°C. **Figure 4**

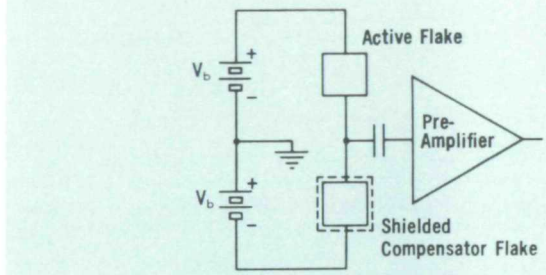

V_b = applied bias voltage per flake.

Conventional bridge circuit arrangement for biasing Thermistor Bolometer Detectors

Figure

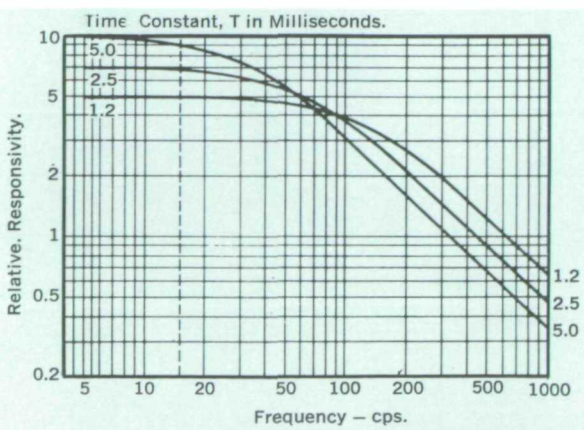

Frequency Response Characteristics.

Figure 6

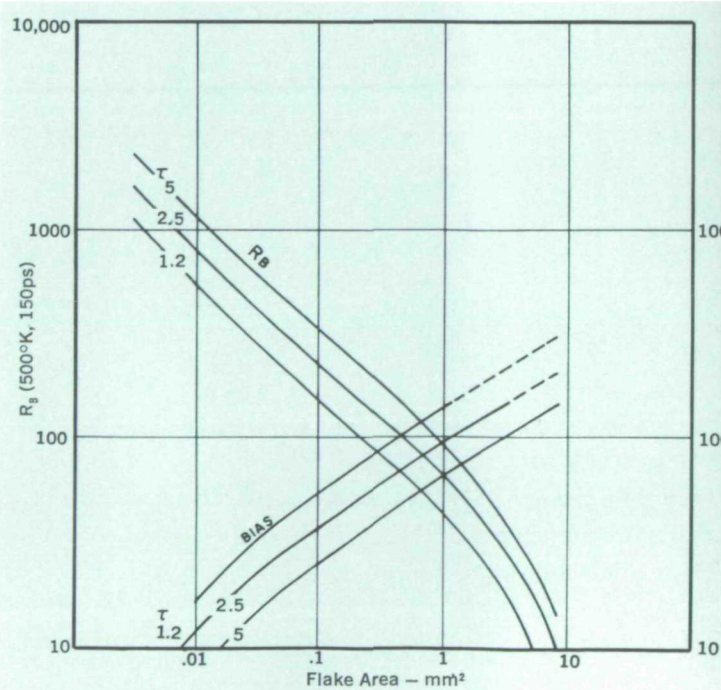

Responsivity and Bias
Square No. 2. Thermistors
250KΩ 25°C.

Figure

BULLETIN 2-102

BARNES ENGINEERING COMPANY
30 Commerce Road / Stamford, Connecticut 06902

IMMERSED THERMISTOR INFRARED DETECTOR

ESCRIPTION

ıe immersed thermistor infrared detector normally contains a ıtched pair of thermally-sensitive resistors (thermistors) that hibit a large change in electrical resistance when heated by frared radiation. The "active" flake is exposed to the radiation be detected, and the compensating flake is shielded from this tside radiation. Both flakes are connected in a bridge circuit 'igure 6) which provides an electrical output signal for amplifi- tion and processing and which compensates for resistance ange caused by ambient temperature variations.

contrast to the solid-backed thermistor bolometer described in ıllletin 2-101, the immersed detector has its active flake optically tached to an infrared transmitting lens having a high index of fraction. A germanium hemispheric lens is typically used for is purpose and the flake is located at the center of the hemi- here's plano surface. The compensating flake is usually mounted the detector base.

hen a germanium hemispherically immersed detector is used as replacement for a solid-backed detector in an optical system, the quired area of the immersed flake is one-sixteenth the area of e equivalent solid-backed flake, and a lower value of bias voltage required.

ɔmpared to a solid-backed flake of the same size, detectivity is ıproved by almost a factor of four. Further improvements can ually be realized by using a hyperhemispheric lens, but the prop- design and resulting detectivity gain depends on the particular tical system located in front of the detector.

ypical construction details of an immersed detector are shown in gure 2. The lens serves both as the optical element and the heat ık. Standard detectors are available with a selection of flake zes, thermistor materials and immersion lens sizes. See Table I.

ındamental performance characteristics such as responsivity, equency response and bias voltage requirements are illustrated Figures 3 through 8.

odifications and custom designs are available on special order. though the standard anti-reflection coating is 10 microns, coat- gs with other spectral responses can be obtained. Also detectors n be preconditioned with the required bias voltage for the rec- ımended number of hours. Relative spectral response curves can so be supplied. Custom-made detectors employing silicon, wedge- aped lenses and other special optical configurations are also ailable.

ECIAL FEATURES

- No Need For Cooling; Room Temperature Operation
- Compact, Rugged and Reliable
- Dynamic Range Of Over One Million To One
- Wide Selection Of Sensitive Area Dimensions
- High and Low Impedance Available

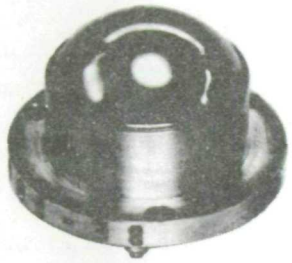

Figure 1

.325" Radius of Germanium Immersion Lens

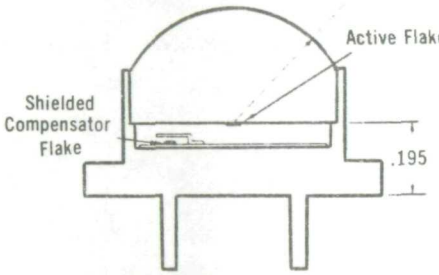

Standard Immersed Detector showing large size immersion lens used with larger flake sizes

Figure 2

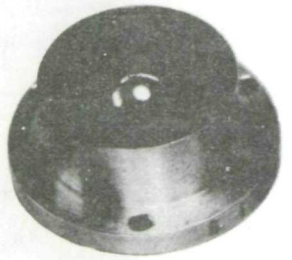

Figure 3

.140" Radius of Germanium Immersion Lens

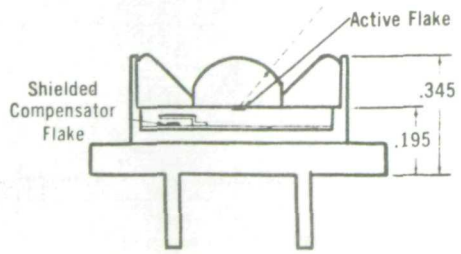

Standard Immersed Detector showing immersion lens used with small flake sizes

Figure 4

TABLE I

Lens Hemisphere Radius (inches)	Flake Size (millimeters)** (L) & (W)	Nominal Time Constant (milliseconds)	Material Type*
0.140	0.05 x 0.05	1.2 or 2.5	No. 1 or No. 2
0.140	0.075 x 0.075	1.2 or 2.5	No. 1 or No. 2
0.140	0.10 x 0.10	1.2 or 2.5	No. 2
0.140	0.15 x 0.15	2.5	No. 2
0.140	0.25 x 0.25	2.5	No. 2
0.140	0.30 x 0.30	2.5	No. 2
0.325	0.50 x 0.50	2.5	No. 2
0.325	0.1 x 1.0	2.5	No. 1 or No. 2

*Type No. 1 material is 2.5 megohms per square flake. Type No. 2 material is 0.25 megohms per square flake.

Resistance of rectangular flakes is $\left(\frac{L}{W}\right)$ times as large as the square-flake resistance.

** For the dimensions listed, the first one (L) is the length between electrodes; the second one (W) is the width.

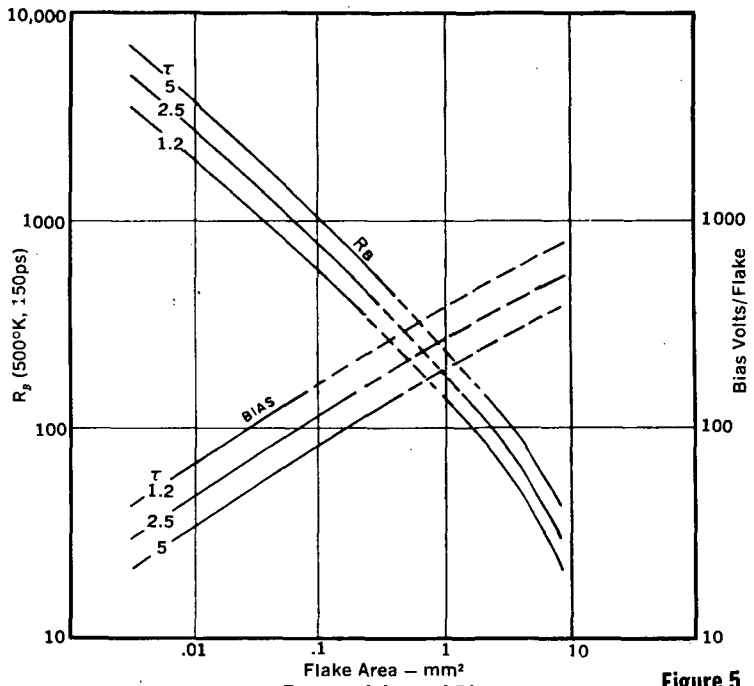

Responsivity and Bias (Note 1)
Square No. 1. Thermistors 2.5 Megohms. 25°C.

Figure 5

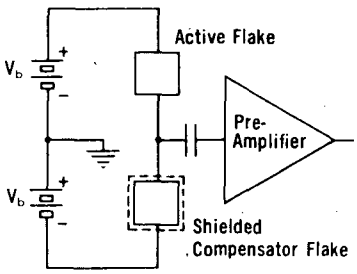

V_b = applied bias voltage per flake.

Conventional bridge circuit arrangement for biasing Thermistor Bolometer Detectors

Figure

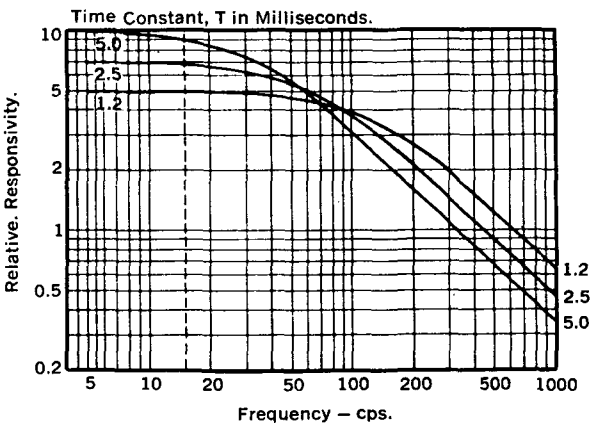

Frequency Response Characteristics.

Figure 7

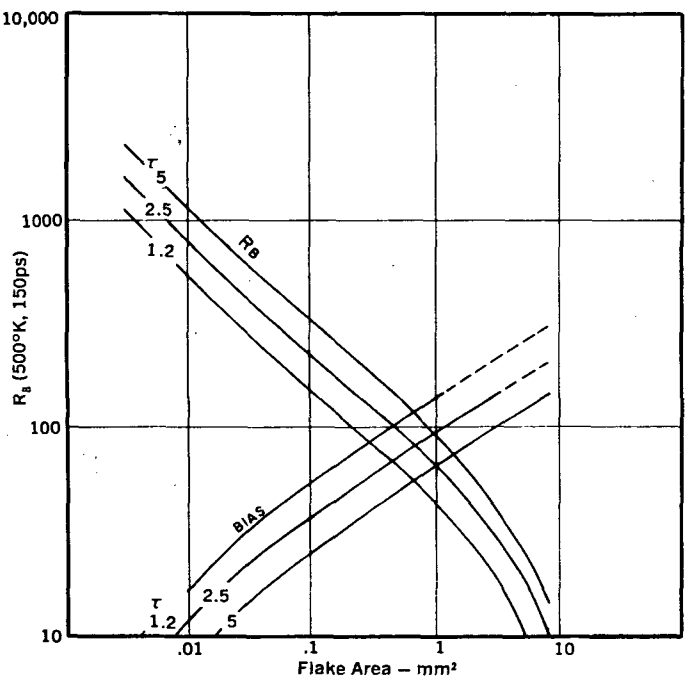

Responsivity and Bias (Note 1)
Square No. 2. Thermistors
250KΩ 25°C.

Figure

Note 1. Responsivity measured at the flake. Does not include lens gain.

APPENDIX C

CALCULATION OF DETECTOR NOISE

DETECTOR-PREAMPLIFIER NOISE CONSIDERATIONS (excerpted from Proposal P-1522.

The noise characteristic of a thermistor detector can be approximated by the curve sketched below in a solid line with three frequency regions including a flat (white) Johnson noise region (f_3 and greater), a region from f_2 to f_3 with a 1/f low frequency noise characteristic and a very low frequency region f_1 to f_2 in which noise appears to increase at a rate $1/f^2$.

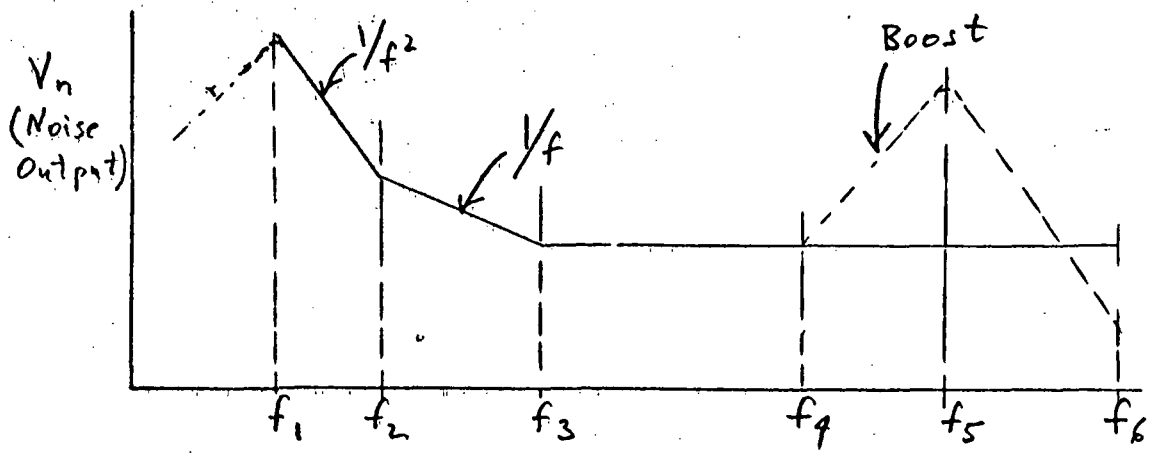

The preamplifier will have a frequency response that will roll off at very low frequencies and will include a boost network starting at f_4 where the detector frequency response begins to fall and up to f_5, the high frequency cut-off for the system (144 Hz, as specified). Beyond f_5 the amplifier provides a 12 db per octave roll off.

To determine the degradation in noise due to the inclusion of the low frequency excess noise and the boosted high frequency Johnson noise, we can develop an expression for spot noise as a function of frequency.

$$V_T^2 = V_n^2 \left[\frac{f_3}{f_2} \int_{f_1}^{f_2} \left(\frac{f_2}{f} \right)^2 df + \int_{f_2}^{f_3} \frac{f_3}{f} df + \int_{f_3}^{f_4} df \right.$$

$$\left. + \int_{f_4}^{f_5} \left(\frac{f}{f_4} \right)^2 df + \left(\frac{f_5}{f_4} \right)^2 \int_{f_5}^{f_6} \left(\frac{f_5}{f} \right)^4 df \right]$$

V_T = Total Noise

V_n = Johnson noise at the reference level

f_1 = 2.5 Hz as specified

f_2 = 5 Hz

f_3 = 50 Hz

f_4 = 60 Hz

f_5 = 144 Hz as specified high frequency corner

f_6 = 260 Hz

$$V_T^2 = V_n^2 \left[f_3 f_2 \left\{ \frac{-1}{f} \right\}_{f_1}^{f_2} + f_3 \left\{ \ln f \right\}_{f_2}^{f_3} + \left(f_4 - f_3 \right) \right.$$

$$\left. + \frac{1}{3f_4^2} \left\{ f^3 \right\}_{f_4}^{f_5} + \frac{f_5^6}{3f_4^2} \left\{ - \frac{1}{f^3} \right\}_{f_5}^{f_6} \right]$$

$$V_T^2 = V_n^2 \left[(50)(5) \left(\frac{1}{2.5} - \frac{1}{5} \right) + 50 \ln \frac{50}{5} + (60-50) \right.$$

$$\left. + \frac{1}{3(60)^2} (144^3 - 60^3) + \frac{144^6}{3(60)^2} \left(\frac{1}{144^3} - \frac{1}{260^3} \right) \right]$$

$$= V_n^2 \left[250 \ (.2) + 50 \ (2.3) + 10 + \left\{ \frac{144^3}{3(60)^2} - 20 \right\} \right.$$

$$\left. + \left\{ \frac{144^3}{3(60)^2} - \frac{144^5}{3(60)^2 (260)^3} \right\} \right]$$

$$= V_n^2 \left(50 + 115 + 10 + 256 + 222 \right)$$

$$= V_n^2 \left(653 \right)$$

Therefore:

$$\text{Loss} = \sqrt{\frac{653}{144}} = 2.1$$

This is the degradation factor to be expected as a result of the need for high frequency boosting and due to 1/f noise. The factor has been included in the calculation of system sensitivity.

We can calculate the noise expected at the preamplifier input. This will serve to indicate the amount of gain needed and sets the preamplifier noise limit. The Johnson noise will be:

$$V_n = \sqrt{4kTR\Delta f} = \sqrt{4KT \times 1.5 \times 10^5 \times 144}$$

where

R = resistance of bolometer bridge = 150 KΩ

Δf = bandwidth = 144 Hz

$V_n \approx .65\ \mu V$

With the degradation factor of 2.1 the total noise input will be 1.3μV. This value will be lower at high temperatures; at 80°C the resistance drops by about 6 and the noise by $\sqrt{6}$ or 2.5 X. Our experience in preamplifier design indicates that it will be possible to process signals and noise levels of this order without a significant degradation (less than 1 db noise increase).

Note: The frequency response in the ARPESH system, as built, is narrower than was planned in Proposal P-1522. Hence the revised calculations presented in Section 3.1.1 and Section 5.3.

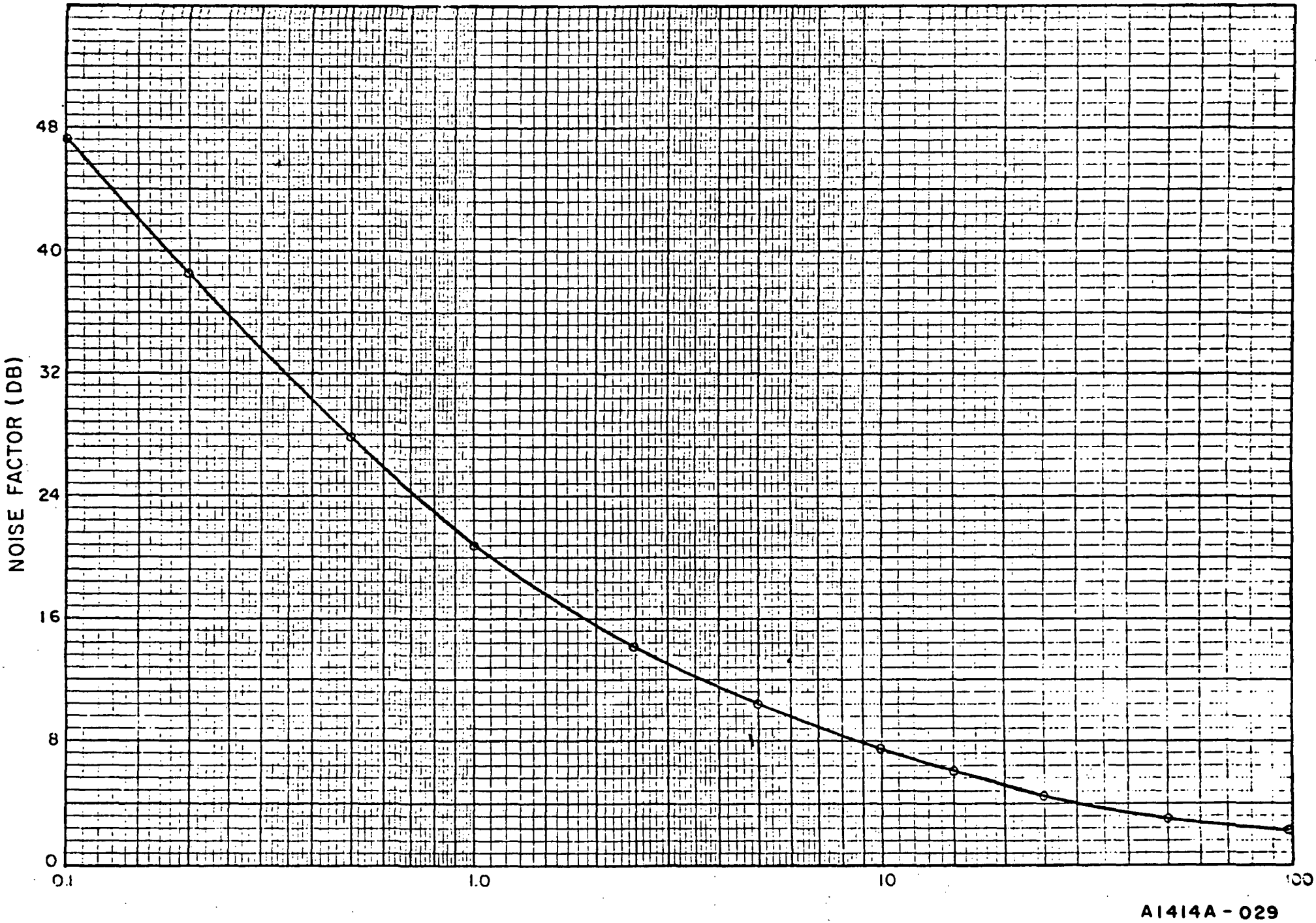

TYPICAL THERMISTOR NOISE